UNIVERSITY OF OKLAHOMA

GRADUATE COLLEGE

SEDIMENTOLOGICAL STUDY OF AN EARLY PLEISTOCENE UPLAND LAKE CORE, UNAWEEP CANYON, COLORADO

A THESIS

SUBMITTED TO THE GRADUATE FACULTY

In partial fulfillment of the requirements for the

Degree of

Master of Science

By

BRANSON HARRIS

Norman, Oklahoma

2023

SEDIMENTOLOGICAL STUDY OF AN EARLY PLEISTOCENE UPLAND LAKE CORE, UNAWEEP CANYON, COLORADO

A THESIS APPROVED FOR THE

SCHOOL OF GEOSCIENCES

BY THE COMMITTEE CONSISTING OF

Dr. Shannon Dulin, Chair

Dr. Gerilyn Soreghan

Dr. Michael Soreghan

ACKNOWLEDGEMENTS

I would like to thank the faculty and staff at the University of Oklahoma for providing their experience and support towards the completion of this project. I would also like to thank the National Science Foundation (Award Number:1849623) and the GSA Continental Scientific Drilling Division for providing funding to this project and future projects. Thank you to Dr. Shannon Dulin, Dr. Lynn Soreghan, and Dr. Mike Soreghan for your insight and patience. Additionally, I would like to thank Himes Drilling Co., Ray and Leon Moores of Moores Mining in Unaweep Canyon, Mt. Sopris Instruments, and our drilling supervisor Doug Schnurrenberger. A big thank you to Anders Noren and Brady Shannon at the CSDF at the University of Minnesota for assistance in logging the core. Thank you to Karen Valles and David Sanger for assistance in sampling, and to Steve Adams and Lily Pfeifer for helping to kill time during the drilling process.

TABLE OF CONTENTS

LIST OF FIGURES

ABSTRACT

The recent recovery of a core in Unaweep Canyon, Colorado, penetrated ~140 m of lacustrine sediment of what is here termed paleo-Lake Unaweep. The lake is inferred to have formed as a result of mass wasting that blocked the ancestral Gunnison River during the early Pleistocene, causing partial filling of Unaweep Canyon before the ancestral Gunnison River abandoned the canyon. This core has been correlated to previous core that also penetrated paleo-Lake Unaweep, and captures a sediment record that dates from ~1.4-1.3 Ma, enabling a glimpse of the Early Pleistocene before the mid-Pleistocene transition— a time interval rarely captured in an upland (or any) setting of the greater Rocky Mountains. The lacustrine section begins atop an interval of ~21 m of inferred ancestral Gunnison River gravels, and comprises a series of mass flows that, overall, decrease in thickness (2 to 60 cm) from the bottom to the top of the core. The entire lacustrine section exhibits an alternation of two intervals: one exhibiting an olive-gray color and containing siderite, and intervals exhibiting red and ochre colors, possibly recording climatic variations. The basal ~20 m consists of reddish-brown, graded (granules to fine sand) mass flows. Above this is a ~15 m interval of thinner (2-10 cm) and finer-grained mass flows exhibiting ochre colors with pink/white clay caps. Next is an olive-gray interval (~48 m) with mass flows exhibiting basal loading, convolute bedding, sand injections, and mud clasts with thin (<1 cm) clay caps. Siderite layers also occur locally in the olive gray interval. Above this, there is ~18.5 m of the same ochre-colored interval. The upper interval (~38.5 m) is also olive-gray and comprises 2-5 cm beds of upwardly fining, sandy clay. Macroscopic charcoal occurs commonly at the bases of event beds and in transitional units of the olive-gray interval but is absent from the intervals that exhibit an oxidized color. Many of the mass flows exhibit normal grading capped by silt, interpreted as partial turbidite sequences. Preliminary palynological results exhibit changes in pollen and spore assemblages that track the large-scale color variation observed, supporting the inference of a climate driver for these alternations. Analyses are ongoing to determine whether mass flows reflect autogenic (e.g., deltaic failure) events, or allogenic (e.g., flooding) events. The primary goal of this study is to utilize this recently recovered UDR1 core to understand the drainage history and the origin and evolution of this paleo-lake. These Quaternary paleo-lake sediments provide a continuous record of sedimentological processes within this unique upland lake that dates from before the Mid Pleistocene Transition. This study also provides new data points to help reconstruct a possible basement profile that mandates a remarkable shallowing of the gradient of the ancestral Gunnison River in westernmost Unaweep Canyon.

INTRODUCTION

The Ute tribe of Western Colorado aptly named Unaweep Canyon; the "canyon with two mouths." Unaweep Canyon is located in western Colorado near the town of Gateway and just south of Grand Junction. Overlain by Mesozoic strata, this canyon is situated on the Cenozoic Uncompahgre Plateau, overlying the Uncompahgre uplift-- one of several basement-cored uplifts associated with the formation of the Ancestral Rocky Mountains in the Late Paleozoic (Kluth and Coney, 1981). Two underfit creeks, East Creek and West Creek, drain in opposite directions from Unaweep Divide at 2135 m, to their respective outlet. Unaweep Canyon is lined by walls of Precambrian igneous and metamorphic basement topped with sedimentary strata from the Mesozoic, and the canyon floor is underlain by a thick sediment infill (Oesleby, 1978; Marra, 2008). Unaweep Canyon's size and shape are incompatible with the modern drainages, an observation that has led geologists to speculate about its origins and evolution (e.g., Cater, 1955; Hunt, 1956; Lohman, 1961; Cater, 1966; Hunt, 1969; Sinnock, 1978; Lohman, 1981; Cole and Young, 1983; Perry and Annis, 1990; Soreghan et al., 2007, 2008, 2015). Although East Creek and West Creek are the two rivers that currently occupy Unaweep Canyon, originating at Unaweep Divide, many have recognized that they could not have carved Unaweep Canyon due to their underfit discharge and erosion rates (e.g., Cole and Aslan, 2001).

In the Early Pleistocene, a single river flowed from the northeast to the southwest through Unaweep Canyon, and many speculate that this was the ancestral Gunnison River, with its headwaters in the San Juan Mountains and Black Canyon (Kaplan, 2006; Soreghan et al., 2007, 2008, 2015). The ancestral Gunnison then flowed through Whitewater, making its way west to merge with the Dolores River near the town of Gateway, Colorado. In this scenario, the ancestral

Gunnison River was dammed by a large mass-wasting event at the western mouth of Unaweep Canyon, resulting in the accumulation of an extensive lacustrine unit, now overlain by alluvium/colluvium (Kaplan, 2006; Soreghan et al., 2007, 2015). A National Science Foundation (NSF) funded drilling project recovered core from the Early Pleistocene "paleo-Lake Unaweep" and intercepted well-rounded cobbles and boulders, and fractured basement lithologies before drilling ceased. The Quaternary paleo-lake sediments provide a continuous record of sedimentological processes within this unique upland lake that dates from before the Mid-Pleistocene Transition. Utilizing the sedimentological record from the recently recovered core, we provide an interpretation of the paleo-lake's origin and evolution. This study also provides new data points to help constrain the slope of the underlying basement through Unaweep Canyon.

GEOLOGIC SETTING

The modern-day Uncompahgre Plateau, which contains Unaweep Canyon, is a northwest-trending monoclinal uplift that occupies a part of the region formerly occupied by the Late Paleozoic Uncompahgre uplift (Kluth and Coney, 1981). After the formation of the Ancestral Rocky Mountains, including the Uncompahgre uplift, the entire region subsided, accumulating significant thicknesses of Mesozoic strata. Tectonic uplift associated with the Laramide orogeny then began during the Late Cretaceous (Bird, 1998). After the Laramide orogeny, the Rockies remained relatively stable in the Late Cenozoic (Morgan and Swanberg, 1985; Pederson et al., 2002; Molnar, 2004), but the Colorado Plateau’s actual timing, elevation and mechanism of uplift remains debated (Hunt, 1956; Morgan and Swanberg, 1985; Pederson et al., 2002; Huntington et al., 2010; Liu and Gurnis, 2010; van Wijk et al., 2010). The Colorado Plateau has been connected with multiple uplift events from the Laramide to the Neogene, noted by incised canyons throughout the plateau.

Regarding the modern nearby drainages, the Gunnison River has its headwaters in the volcanic San Juan Mountains (see Figure 1 for location map). The north fork of the Gunnison River drains through the West Elk Mountains, then Black Canyon, and then through the Mancos Shale and Grand Valley, along the northeast edge of the Uncompahgre Plateau. The Dolores River also has its headwaters in the San Juan Mountains but flows along the southwestern edge of the Uncompahgre Plateau. The Colorado River passes through Grand Valley and then around the northern edge of the Uncompahgre Plateau.

The Gunnison River provenance signature is characterized by a relatively high amount of volcanic lithics compared to other rivers in the region. These volcanic lithics are described as "grayish intermediate volcanic, silicic volcanic, and shallow intrusive rocks originating from the Tertiary volcanics of the San Juan Mountains and Gunnison Uplift" (Cater, 1966, Aslan et al., 2005; Kaplan, 2006). The North Fork of the Gunnison River incorporates a small number of basalt clasts and other clasts originating from Tertiary laccoliths (Aslan et al., 2005; Kaplan, 2006). The Dolores River also has a relatively high amount of volcanic lithics, reflecting its origin in the San Juan Mountains, but does not drain basalt terrane like the North Fork of the Gunnison River (Lohman, 1961; Cater, 1966). The Colorado River, with a source farther north, traverses vesicular basalt and a small number of volcanic and porphyritic intrusive rock types (Cater, 1966; Aslan et al, 2005; Kaplan, 2006). Volcanic clasts of intermediate composition, and trace, non-vesicular basalts occur in ancient river gravels exposed at both Cactus Park (eastern Unaweep Canyon) and the western mouth of Unaweep Canyon, leading Kaplan (2006) to conclude that the primary canyon occupant was the ancestral Gunnison River. Paleocurrent data (Kaplan, 2006) from exposed gravels found at the western mouth of the canyon near Gateway, Colorado, also show a predominant south-southwest trend.

Utilizing regional incision rates of nearby Grand Mesa with an incision rate of 17 cm per 1,000 years (Cole and Aslan, 2001); the ancestral Gunnison River would have occupied Unaweep Canyon for at least 4.8 Ma with a time of abandonment at ~1.4 Ma (Balco et al., 2013). This implies that Unaweep Canyon was occupied by the Gunnison River from the Messinnian to the Early Pleistocene before eventually abandoning the canyon (Aslan et al., 2008). These data, together with the lack of field evidence for fresh scarps, refute the hypothesis of neotectonic uplift in the region (Lohman, 1961; Hunt, 1969; Perry and Annis, 1990; Noble et al., 2006; Schoepfer et al., 2007). For example, incision rates link the ancestral Gunnison River occupation to ~5.6 – 0.8 Ma (Marra, 2008), but fault motion on the Ute Creek Graben is too slow to account for the uplift, so the incision rates outpace the rates of epeirogenic uplift possible in the area (Aslan et al., 2008; Marra, 2008).

The ancestral Gunnison River, while occupying Unaweep Canyon, is thought to have been dammed by a mass-wasting event (~1.4 Ma) near the western mouth of Unaweep Canyon, precipitating deposition of an extensive lacustrine unit before the river ultimately abandoned the canyon (Marra, 2008; Soreghan et al., 2007, 2015). This lacustrine deposition, followed by alluvium/colluvium deposition, and headward erosion by East and West Creeks account for the creation of Unaweep Divide (Soreghan et al., 2015). The hypothesized mass-wasting event near the western mouth of Unaweep Canyon is not uncommon in high-relief regions as, for example, the paleo-lakes on the Dadu and Jinsha Rivers in China, the Ilanz paleo-lake in the Swiss Alps, and the Hunza and Gilgit River Valleys in Karakoram Himalaya all record similar processes that operated within larger and smaller catchments and magnitudes (Fort et al., 1989; Hewitt, 1998, 2001; Wassmer et al., 2004; Zhang et al., 2011; Chen et al., 2013; Wu et al., 2019; Klein et al., 2022). The recently recovered lacustrine sediment from the most recently drilled core, UDR1, and two other previously recovered cores, Massey #1 and #2, corroborate the existence of a major lake that filled Unaweep Canyon in the early Pleistocene (See Figure 2 for core locations).

Previous Work

Marra (2008) identified three distinct units of canyon fill from two cores, Massey #1 and #2. The first of two cores (Massey #1, drilled in 2004) is located at 38º 46.052 N 108º 48.861 W with an elevation of 1,993 msl (meters above sea level), and the second (Massey #2, drilled in 2006) was ~ 30 m southwest of the first (see Figure 2). The upper part of the Massey #1 core consisted predominantly of conglomerate composed of Mesozoic sandstone clasts and Precambrian basement clasts. Below this, lacustrine sandy clay prevailed, rich with macerated carbonaceous matter, insect fossils, wood fragments, and other organic material. Massey #1 also penetrated Calcisols situated between the (lower) sandy clay (lacustrine) and (upper) conglomeratic (alluvial fan) intervals, recording landscape stabilization up to 10^5 years (Marra, 2008). The lowest ~15 m of the Massey #1 core penetrated a diamictite, with Precambrian basement clasts suspended in a muddy matrix. Massey #1 did not penetrate deeper, owing to drilling problems, which prompted drilling of Massey #2 (in 2006). Massey #2 was destructively drilled to ~280 mbs (923’) depth and thereafter cored, recovering lacustrine clayey deposits until penetrating what appeared to be heavily fractured, crystalline basement at ~328 mbs (~1078’). However, a thin (~30 cm) granule conglomerate at ~337 mbs (~1105’) suggests that the inferred basement may have been a boulder. Drilling was halted at ~343 mbs (~1126’), after coring additional fractured basement lithologies.

Numerous geophysical methods have been employed to help infer the shape of the basement underlying the sedimentary fill in Unaweep Canyon, to help interpret the canyon's origins. The shape of Unaweep Canyon has been assessed in various locations via vertical electrical profiles by Oesleby (1978), gravity surveys by Davogustto et al. (2005), seismic refraction and reflection by Suarez-Rojas (2007), active seismic by Patterson et al. (2021), and passive seismic by Dangwal et al. (2023). Recent unpublished electrical resistivity data from the University of Oklahoma Bartell Field Camp was also used in attempting to locate the basement near the eastern and western ends of the canyon, but only the data collection in the eastern canyon is inferred to have imaged the sediment-basement interface (unpub. data, 2023). Previous studies have come to differing conclusions in regards to an inferred basement shape; some authors suggesting a “V” shaped cross-section indicative of fluvial incision (Oesleby, 1983) and others a “U” shaped cross section (Patterson et al., 2021), including an over-deepened section potentially attributable to glacial carving (Dangwal, 2023). Alternative interpretations for the origin of the canyon aside from the long-prevailing idea of Cenozoic fluvial incision (Cater, 1955; Hunt, 1956; Lohman, 1961; Cater, 1966; Hunt, 1969; Sinnock, 1978; Lohman, 1981; Perry and Annis, 1990) include Pleistocene glacial incision (Cole and Young, 1983) and a late Paleozoic glacial incision with a Cenozoic exhumation by Soreghan et al. (2007, 2008, 2015). The hypothesis of formation by late Paleozoic glaciation remains a viable -- albeit controversial -- mechanism, but Pleistocene glaciation is precluded by higher elevations of terminal moraines in similar latitudes of the Rocky Mountains (Pierce, 2003).

METHODS

In February of 2022, an NSF (National Science Foundation) project by the University of Oklahoma drilled the UDR1 core at 38.78076°N, 108.87059°W (elevation: 1,924.44 msl), to a depth of ~426 mbs (meters below surface), approximately 5 km west of the Massey #1 well (Figure 2). A transverse seismic line acquired along a N-S oriented dirt road in western Unaweep Canyon imaged a deep sediment fill (Patterson et al., 2021) that guided the location of the UDR1 wellsite (Figure 3). Drilling was destructive in the upper ~200 m, using a mud rotary drill head with no core recovery. Below this, the core was recovered in 1.524 m intervals using an HQ3 impregnated diamond bit and wireline core recovery. Cores were recovered in transparent plastic liners, cut to size, and capped. Core recovery, depth, and general lithologies were recorded on site. Recovery was ~80% within the lower olive-gray section of the cored interval (~305-257 mbs) and ~90% for the remainder of the cored section. We attribute this core loss to the difficult weather conditions at the time of drilling: An extreme cold snap caused freezing of parts of the drill rig and contributed to wash out resulting from circulating drilling fluids during down time.

The core was shipped to the CSDF (Continental Scientific Drilling Facility) at the University of Minnesota where it was split, imaged, and cataloged from the top of the core down to ~178 mbs. Individual 1.5 m cores were then corrected for depths using the IODP (Integrated Ocean Drilling Program) CSF-B depth scale standard to resolve any overlapping core recovery. Note that this depth correction was done by the author prior to the depth corrections applied by the CSDF, owing to timing pressures. This resulted in minor differences in depths reported for individual core sections between this thesis and the data archived on the CSDF website. However, such differences should amount to less than a few cm for any given core section.

Samples for smear slides, thin sections, magnetic mineralogy, palynology, and petrography were taken. Smear slides were prepared on site at the CSDF for use in identifying composition and (visual) grain size. Magnetic mineralogy samples were prepared for reflected light microscopy and vibrating sample magnetometry. Palynology samples (n = 35; ~50g each) were taken at intervals of ~4 m in dark mudstones to attain maximum palynological recovery. Exact sampling locations are noted within the full core log (See Appendix I). Sand samples (n = 34) were also collected, washed, and sieved (isolating the 0.125 mm - 0.701 mm fraction) for point counts of framework composition (provenance). Thin sections for provenance studies were stained for potassium feldspar, and 400 grains were counted per sample using both the traditional and Gazzi-Dickinson point counting methods (Ingersoll et al., 1984). Exact sampling locations are noted within the full core log (See Appendix I pp. 61-177).

Borehole logging was done by Mt. Sopris Instruments. Whole core ITRAX elemental, X-radiographic data, and magnetic susceptibility measurements were taken over the entire core length at the CSDF. All cores were scanned at 0.5 cm, 15 sec dwell time with the Cr tube without radiographs. Stratigraphic logs were made in Inkscape for visual representations of grain size, lithology, sedimentary structures, and biotic processes. These were observed from core photographs and smear slides. The core was then divided into separate facies based on differences in structures/bedding and grain sizes. The UDR1 core and all supplemental materials are archived at the CSDF.

RESULTS

We logged the UDR1 core from high-resolution photographs taken at the CSDF (Continental Scientific Drilling Facility) at the University of Minnesota. The total core length was ~226 m, with coring beginning at ~200 mbs and ending at ~426 mbs. This thesis focuses on the uppermost cored section (from ~200-340 mbs), comprising interbedded muds and sands, and subjacent loose gravels (~340-360 mbs). After analyzing the upper unit of the core, six facies and sub-facies were described and interpreted for environments of deposition.

Palynological samples were analyzed by G. Jiménez-Moreno (University of Grenada, Spain) and yielded several species of Pleistocene Rocky Mountain palynomorphs. These include *Artemisia* (aromatic shrubs and herbs known as Mugworts), *Picea* (coniferous evergreen trees), and *Pinus edulis* (Colorado Pinyon Pine).

Based on wireline logs, crystalline basement was picked at ~370 mbs, about 10 m below the lowest identified gravels. The interval from ~360-370 mbs was not the focus of this thesis, and remains under study. The subjacent ~56 m (See Appendix I for full core photos; basal slabbed section pp. 172-177) of core appears similar to the basement exposures within Unaweep Canyon and surrounding areas, and includes early Proterozoic (1.45 – 1.7 Ga) metamorphic lithologies including feldspathic gneiss, amphibole gneiss, amphibolite, porphyroblastic microcline gneiss, biotite-microcline gneiss, and quartzite, which is intruded by younger gneissic granodiorite, metadiorite, metagabbro, biotite granodiorite, porphyritic biotite quartz monzonite (Case, 1991). Mafic dikes are present in outcrops, particularly in the eastern canyon. This is consistent with observations from the basement section of the UDR1 core, which generally includes granitoid dikes (~1-20 cm) cutting through dark gray gneiss. However, hematite-stained fractures (~1-5 cm) occur throughout the section below the gravels. Macroscopically visible fractures are commonly filled with either a mosaic of quartz and plagioclase feldspar or a green, platy mineral (likely chlorite or epidote resulting from hydrothermal diagenesis operating within fractures) (Figure 4).

The gravels (~340-360 mbs) (See Appendix pp. 153-166) consist of loose, well-rounded clasts ranging from ~1 cm up to ~1 m in diameter. The larger clasts resemble the local Proterozoic basement, whereas the smaller (~1-5 cm) clasts consist of both Proterozoic basement and predominately andesitic volcanic clasts (Figure 5). The percentages of smaller, local basement clasts to rounded gravels are 70% basement and 30% rounded gravels. Of that 30%, one third are andesitic, attributable to the San Juan Tertiary volcanics. The andesite clasts are dark gray-black and very well rounded, ranging in size from 4-10 cm.

The upper ~ 140 m of core (See Appendix pp. 61-153 or summary figure on pp.59) consists primarily of repetitive, upwardly fining event beds. This part of the core can appear reddish brown, ochre, or olive gray in color. The base is reddish brown which gradually transitions to ochre around ~320 mbs. The ochre color persists to ~305 mbs where it transitions to olive gray. Core recovery is poor in this olive gray section. Ochre color sparsely occurs in ~1 m intervals throughout the olive gray section until ~257 mbs where the ochre color again predominates. The color returns to olive gray for the remainder of the core at ~238.5 mbs. Six distinct facies were identified within the lithologies of this section of the core (Figure 6). Facies are interpreted to represent changing depositional processes, as detailed below.

Facies 1/1a Description

Facies 1 (Figure 7a) is an upwardly fining sequence (~1-20 cm) in which the basal section is very fine sand or silt, which grades to clay (D-E Bouma Sequence). Facies 1a (Figure 7b) is a variant of Facies 1 in which bioturbation occurs within the clayey interval of the upwardly fining sequence. Bioturbation most commonly occurs at the very top of the facies, or at the transition from silt to clay. These facies occur primarily within the olive-gray colored intervals of the core.

Facies 1/1a Interpretation

Facies 1 is interpreted to record relatively distal deposition of turbulent flow or suspension sedimentation within the lake basin, i.e., background sedimentation. The slight fining apparent at the base of each of these thin intervals suggests settling from the tail (finest) part of a turbidity flow, followed by pelagic settling. Facies 1a is similar to Facies 1 but is bioturbated, further supporting the idea of suspension settling at the top that is then disturbed by organisms (and reflects syndepositional oxic conditions). The burrows are well preserved and undisturbed by overlying event beds, suggesting some quiescence between events.

Facies 2/2a Description

Facies 2 (Figure 8a) is an upwardly fining sequence (~1-50 cm) in which the basal grain size of the bed is fine to coarse sand and grades upward to clay (A-B-E Bouma Sequence). Sand grains are medium sorted with sub-angular shape. Much like Facies 1a, Facies 2a (Figure 8b) is a variant of Facies 2 in which bioturbation occurs at bed tops. These facies occur mainly throughout the olive-gray and ochre-colored sections of the core.

Facies 2/2a Interpretation

Facies 2 is interpreted to record the deposition of turbidity flows, but the coarser basal grain size signals either a more energetic flow or proximity to source relative to Facies 1.

Facies 3/3a Description

Facies 3 (Figure 9a) is an upwardly fining sequence (~1-25 cm) in which the basal grain size is very coarse sand to pebbles that grade to clay, and is very clean. This facies resembles an A-C-D-E Bouma sequence. Thicker occurrences of Facies 3 tend to include basement clasts (medium granules to very coarse granules) that float within the basal sandy sections of the upwardly fining sequence. Facies 3 exhibits poor sorting and angular grains. Facies 3a (Figure 9b) is bioturbated in similar areas to that of Facies 1a and Facies 2a. These facies occur primarily within the ochre and reddish-brown colored sections of the core.

Facies 3/3a Interpretation

Facies 3 is also interpreted as the products of high-density turbidites but, considering the increased grain size and basal thickness, it is most likely in a more energetic part of the lake system from either close to the canyon walls or the major axial input. The base of Facies 3 and 3a (bioturbated) comprises clasts from the local basement, suggesting the larger grains were inertia-driven and deposited by lateral flow (Mutti et al., 2003).

Facies 4 Description

Facies 4 (~2-15 cm) (Figure 10) consists of convolute beds composed of one or more upwardly fining sequences, like that of Facies 1-3. Facies 4 occurs within the olive-gray and ochre-colored sections of the core. This facies occurs randomly with respect to other facies and seems to be unrelated to other depositional processes.

Facies 4 Interpretation

Facies 4 is interpreted as syn- or post-depositional soft-sediment deformation. The convolute bedding implies slumping (Hovikoski et al., 2016), attributable to instability likely caused by rapid, water-charged deposition and/or deposition on a slope.

Facies 5 Description

Facies 5 (~1-5 cm) (Figure 11) consists of massive (unstructured) sand/gravel capped by clay/silt with no gradation between the grain sizes (A-E Bouma Sequence). Grains are medium sorted and subangular within the sand/gravel. Facies 5 occurs sparsely throughout the olive-gray colored sections of the core.

Facies 5 Interpretation

Facies 5 is interpreted as a slump failure in which pre-sorted sands from further up the subaqueous canyon walls succumb to gravity and settle out more distal to the canyon walls where they are then capped by pelagic sediment.

Facies 6 Description

Facies 6 (2-5 cm) (Figure 12) consists of a matrix of silt and clay with intercalated basement clasts (~1 cm) floating throughout. The facies is massive (structureless). Facies 6 is most common throughout the olive-gray colored sections of the core and occurs within other event beds.

Facies 6 Interpretation

Facies 6 is interpreted as a cohesive debrite– the deposition of locally sourced loose sediment catastrophically transported into the paleo-lake possibly in the wake of floods or fires. The clasts suspended within the matrix indicate rapid deposition with no sorting. These deposits are intercalated with both coarse- and fine-grained deposits.

General Sedimentological Trends

Load structures and flame structures are common throughout the core, in all facies and every color interval. Grain size and individual bed thicknesses generally decrease upward through the core, but also correlate with color intervals. Specifically, the reddish-brown (more oxidized) intervals of the core typically exhibit coarser grain sizes and thicker “beds” while the ochre (less oxidized) sections of the core comprise beds with medium grain sizes and thicknesses, and the olive gray (most reduced) sections contain the finest sediment and thinnest units. Facies 1 occurs commonly in very thinly bedded, upwardly fining stacks (3-15 cm) with individual bed thicknesses ~1 cm (Figure 13). This is interpreted as periods of stable lake levels with consistent background sedimentation.

Siderite beds (~1-4 cm) occur only within the olive gray intervals and commonly within Facies 1, 1a, 2, 2a, 3, and 3a (Figure 14). Manganese oxide dendrites are present throughout the ochre-colored sections of the core and in stacks of Facies 1, branching upwards from the base of fining upwards sequences (Figure 15). Both the siderite and the manganese oxide dendrites reflect post-depositional diagenesis (Potter and Rossman, 1979).

Provenance Data

Point counts of framework mineralogy from sands sampled throughout the core show distinct patterns that correlate with other factors (Figure 16). Total quartz within sands of the olive-gray (reduced) sections is > ~40% whereas it is typically < ~40% in the ochre and reddish-brown (oxidized) sections (Figure 17). There is a small but distinctive population of sand-sized grains that are perplexing; they consist of either quartz and plagioclase feldspar bound within a hematite matrix, or chert-like very fine-grained quartz+feldspar in grains that look like volcanic lithics, but are visually similar to fractured basement found below the gravel section. It is unclear how these should be classified. Here, we call them "clasts of fractured basement" (CFB). Sedimentary lithics within the gravels (~5%) and reddish-brown (~3%) sections of the core are predominately clastic and well-rounded with a clay matrix. Sedimentary lithics within the olive-gray (<1%) and ochre-colored (~2%) sections of the core are also well-rounded but have a calcite cementation. Amphibole occurs predominantly within the ochre-colored sections of the core (<1%) and in the very base of the reddish-brown section (9.75%), where black sands overlie the gravels (Figure 18).

DISCUSSION

The acquisition and study of the UDR1 core contextualizes and further improves our understanding of the sedimentological processes that occurred within paleo-Lake Unaweep.

The UDR1 cored section – from base to top—consists of fractured basement lithologies, rounded gravels from the (inferred) ancestral Gunnison River, owing to the presence of intermediate volcanics, and then sediment recording a paleo-Lake Unaweep. The UDR1 core, having been destructively drilled 200 m to 1,725 msl, did not preserve the top of the lake sediments where the Calcisols were identified within the Massey core at 1,829 msl (Marra, 2008). The lacustrine section of the UDR1 core is attributed to damming of the ancestral Gunnison River at the western mouth of Unaweep Canyon (Kaplan, 2006; Soreghan et al., 2007, 2015).

Color is not uniform throughout the core, suggesting a change in lake level, reduction/oxidation reactions, diagenesis, or some combination thereof. Charcoal is found predominantly within the olive-gray, dysoxic parts of the core (Figure 19). Bioturbation occurs within the upper portions of event beds in the olive-gray sections of the core suggesting a relatively stable environment with enough oxygen for burrowing. The burrows seen throughout the core are most similar to a *Mermia* ichnofacies (Buatois and Mángano, 1998).

The clasts of fractured basement found within the matrix of the ancestral Gunnison gravels are consistent with the observation of the thoroughly shattered and hematite-stained fractured basement and groundmass observed in the one thin section we have from the basement just below (~366 mbs) the gravel interval. These clasts are typically hematite stained (Figure 20). Once the mass wasting event at the western mouth of the canyon blocked the ancestral Gunnison River, sediment that once was flowing through the fluvial system lost velocity when hitting the water level of early paleo-Lake Unaweep. The loss in velocity via an increase in water depth resulted in deposition of sediment that is finer than that preserved before the mass-wasting event (gravels). High-density turbidites in the more energetic parts of the lake (Facies 3/3a and Facies 2/2a) are what predominately compose this interval of the lake's history, as the thickest event beds. A sharp increase in amphiboles (9.75%) at the base of the lacustrine section likely indicates localized sourcing from a mafic dike (Figure 18). Coarse-grained facies (Facies 2/2a and Facies 3/3a) became less common as the lake stabilized within the canyon, which is to be expected within a lake-fill sequence (Nelson 1967, Hewitt, 1998; Fawcitt, 2007; Staley et al., 2022). As the lake was stable, and considering there is no evidence of perennial streams entering the lake from transverse to the catchment (canyon sidewalls), we assume that most of the coarse-grained Facies 6 records mass wasting events. These events could be triggered by catastrophic overland flooding perhaps triggered in the wake of paleo-fires.

In recent years, rock slope failures in Cenozoic mountain belts ranging up to and larger than one million cubic meters have been identified by the hundreds (Hewitt et al., 2008). Catastrophic rock slope failures are classified by their large sizes, rapid speed, and very short durations (minutes) and can block entire valleys. They can form dams spanning hundreds of meters high and can create reservoirs in relatively brief time, determined by the catchment size and discharge of the river (Korup, 2004; Wassmer et al., 2004; Hewitt et al., 2008). In mountainous regions with rapid uplift and erosive rivers, these dams are very short lived (decades), but considering that the study area is relatively tectonically inactive, resistance to dam failure is high (Costa and Schuster, 1987). We interpret paleo-Lake Unaweep to have undergone a similar process by a landslide originating from a now scarred detachment zone near the western mouth (Figure 21). Using the elevation of the top of the scarp (2,375 msl) and a rough elevation of the basement at ~1,600 msl (about 450 m away from the top of the scarp laterally), we can infer that the angle of slope failure was ~ 35^{o}. Although this angle is within the expected range of an unconsolidated rock fall, this scarp is composed of highly fractured basement, in which pre-existing faults could have altered the angle at which the rock failed and created the dam. We suggest a rough estimate of the rockslide failure volume to be ~0.088 km^3 derived from the depth of the basement (~1,600 msl), height of the top of the scarp (2,375 msl), horizontal distance from the deepest section of the basement to the top of the scarp (~450 m), and the length of the scarp parallel to the valley (1,300 m). The area of the scarp to the other side of the valley at a spillover elevation of (~2,000 msl) to the depth of the basement is around ~270,500 m^3 which is well within the potential volume of the rockslide failure, including lateral accretion of the materials up and down slope at an angle of 35º.

We can assume that the materials of the rock slope failure were angular and had well distributed grain sizes to create a densely packed, consolidated dam necessary to create and maintain paleo-Lake Unaweep (Hewitt, 1998). A translational rockslide, lodging perpendicular to the axial stream, necessarily alters a drainage system at significant distances (tens of kilometers) upstream and for extended periods of geologic time or even irreversibly (Hewitt et al., 2008). This appears to have been the case in Unaweep Canyon, as the ancestral Gunnison River ultimately abandoned the canyon by diverting eastwards. In the Upper Indus basin (northern Pakistan), where more than 150 landslide dammed paleo-lakes have been identified up to 100 km long and 500-1,000 m deep (Hewitt, 1998, 2001; Hewitt et al., 2008), landslides often impound or alter river systems.

Initial investigation of palynological sample slides by G. Jîmenez (Univ Grenada, Spain) revealed pollen attributed to *Pinus edulis* (Pinyon pine), *Artemisia* (Sage), and *Picea* (Spruce) (Figure 22). *Artemisia*/*Picea* ratios have been used as a paleoclimate proxy to determine Rocky Mountain climate cycles in the past (Jiménez-Moreno et al., 2008; Jiménez-Moreno et at., 2011; Anderson et al., 2014; Jiménez-Moreno et al., 2021; Jiménez-Moreno et al., 2023). Utilizing *Pinus edulis*, a low elevation semi-arid tree, and *Artemisia*, an herbaceous shrub that resides primarily in sagebrush steppes, as warm climate indicators and *Picea*, a northern temperate high elevation tree, as a cool climate indicator, two cooling cycles appear within the core. The interpreted cool climates correlate with the ochre and reddish-brown sections of the core, with evidence of reworking. The length of the basal cooling cycle is unknown as much of the pollen in the reddish-brown section of the core is desiccated to the point of no meaningful identification. Alongside the correlation with color, the paleoclimate proxy from pollen data correlates with individual bed thickness and basal grain size (Figure 23).

As the vegetation belt of *Picea* fluctuated in elevation, tracking climate changes, the anchoring points for sediment within and around the canyon may have changed as well (Löbmann et al., 2020). Decreases in total precipitation would not only affect the vegetation of the surrounding area, but also lower the water level of paleo-Lake Unaweep. The vegetation changes from scrubland slopes to forests of *Pinus* would have altered the slope stability and led to coarser-grained material and more frequent event beds (Langbein and Schumm, 1958; Breshears et al., 2003; Staley et al., 2022). This is because a large tree like *Picea* has deep root structures that hold large boulders and pebbles, whereas sage brush like *Artemisia* can support and maintain slope stability of finer-grained sediment. This corroborates the changing grain size and bed thickness of the ochre colored, cold climate sections and the warmer, olive gray sections of the core but, the changing grain size could also reflect lateral changes in UDR1's proximity to sublacustrine sediment lobes within the canyon.

The changing vegetation and color within the core are necessarily correlated with the facies seen within these changes. Unaweep Canyon would have been undergoing morphing vegetation populations along its steep slopes, altering sedimentation rates as sediment anchoring plants entered and left the system. Within the reddish-brown and ochre-colored sections of the core, the coarser-grained facies recording more energetic processes (Facies 3/3a and 2/2a) predominate. Finer grained facies (Facies 1/1a) and cohesive debrites (Facies 6) are more common throughout the olive-gray colored sections. The facies correlations with color in the core are complementary to the interpretation that the lake system and sediment input is a result of both the (climatically induced) changes in vegetation and lateral changes in sedimentation (Figure 23).

The UDR1 core penetrated fractured basement lithologies; this thesis did not focus on the basement, so the elevation of the contact with intact basement remains interpretative until such work occurs. Nevertheless, combining the apparent elevations of outcrops of the ancestral Gunnison gravels, with borehole data of possible basement elevations reveal a paleo-gradient. The Massey #1 core did not penetrate the basement, so the basement is below this point (Figure 24). We created a depth profile from the base of the Gunnison gravels within the UDR1 core (1060 mbsl). The depth profile is also constrained by the elevation of Mesozoic strata and 0.8 Ma ancestral Gunnison gravels found at Cactus Park (east end of Unaweep Canyon). The slope from these two points, extended westward, is lower than where the gravels are exposed near the narrow section of the western mouth of the canyon (~1585 mbsl), but suggests the projected slope must be non-linear to relate to the Gunnison gravels (Figure 24).

If we assume an elevation of the dam spillover point from Soreghan et al. (2015) of ~1,950-1,975 msl, which is in the realm of possibility with the estimated size of the rockslide originating from the suggested western scarp, then paleo-Lake Unaweep could have reached a depth of ~360-385 m at its deepest point and reached as far east as Cactus Park. Using the modern Gunnison River discharge average of 7,452 km^3/day and a rough estimate of the volume of paleo-Lake Unaweep (max: 9,270 km^3, min: 3,474 km^3), the lake could essentially fill in a day or less. The maximum and minimum volume estimates of paleo-Lake Unaweep were calculated by forming polygons of constant elevation within the canyon at the highest and lowest possible bathymetric lines and, using their areas, we assumed a rough basement slope with an average of 200 meters depth (400 m at the west and 0 m at the east where basement is exposed). Even using magnitudes of lower discharge for the ancestral Gunnison River, the formation of paleo-Lake Unaweep would have happened very rapidly.

After paleo-Lake Unaweep filled with sediment, spillover occurred out of the western mouth (~1,950-1,975 msl). In the most quiescent parts of the paleo-lake (near the center), fine-grained sediment from very fine sand to clay formed rhythmic sequences, while in the more active sections of the lake system encroaching lobes of coarse sediment form turbidites.

Within the western interior of the canyon ~20 km west of Unaweep Divide, there is an area known as Unaweep Seep in which groundwater is perennial (Figure 25). The top of Unaweep Seep falls within the 1,820-1,840 m elevation range. Interestingly, Unaweep Seep is the largest and most biologically diverse wetland complex in the entire region (Doyle et al., 2002). Most notably, outside of a handful of places in Utah, it is the only location for a critically endangered butterfly, the Nokomis Fritillary (Doyle et al., 2002). Using the known top of the lacustrine succession from the Massey #1 core and extending that line westward, the top of Unaweep Seep falls at the same elevation as the top of the lake (Figure 24). Therefore, Unaweep Seep occurs at the exposed contact between the lower, finer-grained and presumably less permeable lacustrine section and upper, very coarse-grained and more porous and permeable alluvium/colluvium. This is further reinforced by recently collected geophysical electrical resistivity data from the University of Oklahoma Bartell Field Camp in which a saturated clay layer is seen at the surface of the seep where the alluvium/colluvium is eroded (Figure 26).

CONCLUSION

The UDR1 core is the deepest core preserving a continuous yet incomplete record of paleo-Lake Unaweep thus far. Because of this, we can study the origins and evolution of an upland lake in the Colorado Plateau during the Early Pleistocene better than before and provide a high-fidelity record that can help shed light on sedimentation and paleoclimate in this time and region. Paleo-Lake Unaweep was undergoing overall increased catchment stability over time with alternating vegetation changes associated with alternating warm/cold (interglacial/glacial) climates, occasional transverse sedimentation from the canyon walls, and paleo-fire triggered flooding events. We identified a scarp of adequate size to have dammed the ancestral Gunnison River and created paleo-Lake Unaweep. Rapid lacustrine sedimentation yields the opportunity to study the lithologies and landscape evolution of a landslide-induced paleo-lake and the sedimentological impacts of river incision and abandonment. Additionally, the elevation of an ancestral Gunnison gravels in the UDR1 core, together with outcrop gravels enables reconstruction of a possible basement profile that mandates a shallowing of the gradient of the ancestral Gunnison River in westernmost Unaweep Canyon.

BIBLIOGRAPHY

Anderson, R.S., Jimenez-Moreno, G., Ager, T., Porinchu, D., 2014. High-elevation paleoenvironmental change during MIS 6-4 in the central Rockies of Colorado as determined from pollen analysis. Quaternary Research 82, 542–552.

Aslan, A. et al., 2008. River incision histories of the Black Canyon of the Gunnison and Unaweep Canyon: Interplay between late Cenozoic tectonism, climate change, and drainage integration in the western Rocky Mountains, *in* Raynolds, R.G. ed., Roaming the Rocky Mountains and Environs: Geological Field Trips, Geological Society of America, v. 10, p. 0.

Aslan, A., Livaccari, R., Hood, W., Betton, C., and Garhart, A., 2005. Geological history of the Uncompahgre Plateau and Unaweep Canyon: Rocky Mountain Section Geological Society of America Field Trip Guidebook: Grand Junction, Colorado, Grand Junction Geological Society, p. 1–46.

Balco, G., Soreghan, G.S., Sweet, D.E., Marra, K.R., and Bierman, P.R., 2013. Cosmogenic-nuclide burial ages for Pleistocene sedimentary fill in Unaweep Canyon, Colorado, USA: Quaternary Geochronology, v. 18, p. 149–157.

Bird, P., 1998. Kinematic history of the Laramide orogeny in latitudes 35°–49°N, western United States: Tectonics, v. 17, p. 780–801.

Breshears, D.D., Whicker, J.J., Johansen, M.P., and Pinder, J.E., 2003. Wind and water erosion and transport in semi-arid shrubland, grassland and forest ecosystems: Quantifying dominance of horizontal wind-driven transport: Earth Surface Processes and Landforms, v. 28, p. 1189–1209.

Buatois, L.A., and Mángano, M.G., 1998. Trace fossil analysis of lacustrine facies and basins: Palaeogeography, Palaeoclimatology, Palaeoecology, v. 140, p. 367–382.

Case, J. E., 1991. Geologic map of the northwestern part of the Uncompahgre uplift, Grand County, Utah, and Mesa County, Colorado, with emphasis on Proterozoic rocks.

Cater, F.W., 1966. Age of the Uncompahgre Uplift and Unaweep Canyon, west-central Colorado: Geological Survey research 1966, p. C86–C92.

Cater, F.W., Jr., 1955. Geology of the Gateway Quadrangle, U.S. Geological Survey Quadrangle Map GQ-55.

Chen, J., Dai, F., Lv, T., and Cui, Z., 2013. Holocene landslide-dammed lake deposits in the Upper Jinsha River, SE Tibetan Plateau and their ages: Quaternary International, v. 298, p. 107–113.

Cole, R.D., and Young, R.G., 1983. Evidence for glaciations in Unaweep Canyon, Mesa County, Colorado, in Averett, W.R., ed., Northern Paradox basin—Uncompahgre uplift field trip guidebook: Grand Junction, Colorado, Grand Junction Geological Society, p. 73–80.

Cole, R., Aslan, A., 2001. Late Cenozoic erosional evolution of Grand Mesa, western Colorado: *Geological Society of America Abstracts with Programs* , v. 33, no. 5, p. A–22.

Costa, J.E., and Schuster, R.L., 1987. The formation and failure of natural dams: Open-File Report. Report 87–392.

Dangwal, D., Behm, M., Chen, X., and Soreghan, G.S., 2023. Imaging an Enigmatic Paleovalley with Passive Seismic Methods (Unaweep Canyon, Colorado, United States): The Seismic Record, v. 3, p. 116–124.

Davogustto, O.E., Young, R.A., Johnson, R.A. and Soreghan, G.S., 2005. A gravity survey in western Unaweep Canyon: looking for the bedrock boundary and its shape: Geological Society of America, Rocky Mountain Section, 57th Annual Meeting, Abstracts with Programs, v. 37, no. 6, p. 35.

Doyle, G., Rocchio, J., Culver, D.R., and Colorado Natural Heritage Program, P., 2002. Survey of seeps and springs within the Bureau of Land Management's Grand Junction Field Office Management Area (Mesa County, CO).

Fawcett, P.J., et al., 2007. Two middle Pleistocene glacial-interglacial cycles from the Valle Grande, Jemez Mountains, northern New Mexico, in Kues, B.S., Kelley, S.A., and Lueth, V.W., eds., Geology of the Jemez Mountains Region II: 58th Fall Field Conference Guidebook: Socorro, New Mexico, New Mexico Geological Society, p. 499.

Fort, M., Burbank, D.W., and Freytet, P., 1989. Lacustrine sedimentation in a semiarid alpine setting: An example from Ladakh, northwestern Himalaya: Quaternary Research, v. 31, p. 332–350.

Hewitt, K., 1998. Catastrophic landslides and their effects on the Upper Indus streams, Karakoram Himalaya, northern Pakistan: Geomorphology, v. 26, p. 47–80.

Hewitt, K., 2001. Catastrophic rockslides and the geomorphology of the Hunza and Gilgit River Valleys, Karakoram Himalaya: Erdkunde, v. 55, p. 72–93.

Hewitt, K., Clague, J.J., and Orwin, J.F., 2008. Legacies of catastrophic rock slope failures in mountain landscapes: Earth-Science Reviews, v. 87, p. 1–38.

Hood, W.C., 2009. An exhumed late Paleozoic Canyon in the Rocky Mountains: A discussion: Journal of Geology, v. 117, p. 210–214.

Hovikoski, J. et al., 2016. Density-Flow Deposition In A Fresh-Water Lacustrine Rift Basin, Paleogene Bach Long Vi Graben, Vietnam: Journal of Sedimentary Research, v. 86, p. 982–1007.

Hunt, C. B. 1956. Cenozoic geology of the Colorado Plateau. U.S. Geol. Surv. Prof. Pap. 279.

Hunt, C.B., 1969. Geologic history of the Colorado River: Chapter C in *The Colorado River region and John Wesley Powell (Professional Paper 669)*: U.S. Government Printing Office 669–C, 59–130 p.

Huntington, K.W., Wernicke, B.P., and Eiler, J.M., 2010. Influence of climate change and uplift on Colorado Plateau paleotemperatures from carbonate clumped isotope thermometry: Tectonics, v. 29.

Ingersoll, R.V., Bullard, T.F., Ford, R.L., Grimm, J.P., Pickle, J.D., and Sares, S.W., 1984. The effect of grain size on detrital modes: a test of the Gazzi-Dickinson point-counting method: Journal of Sedimentary Research, v. 54, p. 103–116.

Jiménez-Moreno, G., Anderson, R.S., Atudorei, V., and Toney, J.L., 2011. A high-resolution record of climate, vegetation, and fire in the mixed conifer forest of northern Colorado, USA: GSA Bulletin, v. 123, p. 240–254.

Jiménez-Moreno, G., Anderson, R.S., and Shinker, J.J., 2021. ENSO, sun and megadroughts in SW USA during the last 11,000 years: Earth and Planetary Science Letters, v. 576, p. 117217.

Jiménez-Moreno, G., Anderson, R.S., Markgraf, V., Staley, S.E., and Fawcett, P.J., 2023. Environmental and climate evolution in the Southwest USA since the last interglacial deduced from the pollen record from Stoneman lake, Arizona: Quaternary Science Reviews, v. 300, p. 107883.

Jiménez-Moreno, G., Fawcett, P.J., and Anderson, R.S., 2008. Millennial- and centennial-scale vegetation and climate changes during the late Pleistocene and Holocene from northern New Mexico (USA). Quaternary Science Reviews 27: 1442–1452.

Kaplan, S.A., 2006. Revealing Unaweep Canyon: The Late Cenozoic Exhumation History of Unaweep Canyon as Recorded by Gravels in Gateway, Colorado: M.S. Thesis, University of Oklahoma 52 p.

Klein, B., Puzrin, A.M., Stoecklin, A., and Kopf, A., 2022. Basin Sediments Geometry and Strength as Controls for Post-Failure Emplacement Style of Alpine Sub-Lacustrine Landslides: Journal of Geophysical Research: Solid Earth, v. 127.

Kluth, C.F., and Coney, P.J., 1981. Plate tectonics of the Ancestral Rocky Mountains: Geology, v. 9, p. 10–15.

Korup, O., 2004. Landslide-induced river channel avulsions in mountain catchments of southwest New Zealand: Geomorphology, v. 63, p. 57–80.

Langbein, W.B., and Schumm, S.A., 1958. Yield of sediment in relation to mean annual precipitation: Eos (Transactions, American Geophysical Union), v. 39, p. 1076–1084.

Leonard, E.M., 1984. Late Pleistocene Equilibrium-Line Altitudes and Modern Snow Accumulation Patterns, San Juan Mountains, Colorado, U.S.A.: Arctic and Alpine Research, v. 16, p. 65–76.

Liu, L., and Gurnis, M., 2010. Dynamic subsidence and uplift of the Colorado Plateau: Geology, v. 38, p. 663–666.

Löbmann, M.T., Geitner, C., Wellstein, C., and Zerbe, S., 2020. The influence of herbaceous vegetation on slope stability – A review: Earth-Science Reviews, v. 209.

Lohman, S.W., 1961. Abandonment of Unaweep Canyon, Mesa County, Colorado, by capture of the Colorado and Gunnison Rivers, U.S. Geological Survey Professional Paper 424, p. B144-B146.

Lohman, S.W., 1981. Ancient drainage changes in and south of Unaweep Canyon, southwestern Colorado, *in* Western Slope (Western Colorado), New Mexico Geological Society, p. 137–144.

Mack, G.H., James, W.C., and Monger, H.C., 1993. Classification of paleosols: GSA Bulletin, v. 105, p. 129–136.

Marra, K.R., 2008. Late Cenozoic Geomorphic and Climatic Evolution of the Northeastern Colorado Plateau as Recorded by Plio-Pleistocene Sediment Fill in Unaweep Canyon, Colorado: M.S. Thesis, University of Oklahoma 160 p.

Molnar, P., 2004. LATE CENOZOIC INCREASE IN ACCUMULATION RATES OF TERRESTRIAL SEDIMENT: How Might Climate Change Have Affected Erosion Rates? Annual Review of Earth and Planetary Sciences, v. 32, p. 67–89.

Morgan, P., and Swanberg, C.A., 1985, On the Cenozoic uplift and tectonic stability of the Colorado Plateau: Journal of Geodynamics, v. 3, p. 39–63.

Mutti, E., Tinterri, R., Benevelli, G., Biase, D. di, and Cavanna, G., 2003. Deltaic, mixed and turbidite sedimentation of ancient foreland basins: Marine and Petroleum Geology, v. 20, p. 733–755.

Nelson, C.H., 1967. Sediments of Crater Lake, Oregon: Geological Society of America Bulletin, v. 78, p. 833–848.

Noble, J.R., Bock, D., Benage, M., Martin, S., Crompton, O., Schoepfer, S.D., Cole, R.D., 2006. Comparative geomorphology of Unaweep Canyon and the Black Canyon of the Gunnison, western Colorado: *Geological Society of America Abstracts with Programs*, v. 38, no. 7, p. 61.

Oesleby, T.W., 1978. Uplift and deformation of the Uncompahgre Plateau: Evidence from fill thickness in Unaweep Canyon, west-central Colorado: M.S. Thesis, University of Colorado, Boulder, 122 p.

Oesleby, T.W., 1983. Geophysical Measurement of Valley Fill Thickness Unaweep Canyon, West Central Colorado: p. 2.

Patterson, A., Behm, M., Chwatal, W., Flores‐Orozco, A., Wang, Y., and Soreghan, G.S., 2021. Seismic Reflection and Electrical Resistivity Imaging Support Pre‐Quaternary Glaciation in the Rocky Mountains (Unaweep Canyon, Colorado): Geophysical Research Letters, v. 48.

Pederson, J.L., Mackley, R.D., and Eddleman, J.L., 2002. Colorado Plateau uplift and erosion evaluated using GIS: GSA Today, v. 12, p. 4.

Perry, T. W., IV, and Annis, D. R. 1990. Pleistocene history of the Gunnison R. in Unaweep Canyon, Colorado and implications for Colorado Plateau uplift. Cordilleran Section Geol. Soc. Am. Abstr. Program 22, 3: 75.

Pierce, K.L., 2003, Pleistocene glaciations of the Rocky Mountains, in Developments in Quaternary Sciences, Elsevier, The Quaternary Period in the United States, v. 1, p. 63–76.

Potter, R.M. and Rossman, G.R. 1979. The mineralogy of manganese dendrites and coatings. *American Mineralogist* 64: 1219-1226.

Richmond, G.M., 1965. Quaternary stratigraphy of the Durango area, San. Juan Mountains, Colorado: U.S. Geological Survey, Professional Paper. 525–C, p.

Schoepfer, S.D., Martin, S., Benage, M., Bock, D., Noble, J.R., Crompton, O., Cole, R.D., 2007. Quaternary abandonment and sedimentary fill history of Cactus Park and Unaweep Canyon, Uncompahgre Plateau, Colorado: *Geological Society of America Abstracts with Programs* , v. 39, no. 6, p. 307.

Sinnock, S., 1978. Geomorphology of the Uncompahgre Plateau and Grand Valley, western Colorado: Ph.D. Dissertation, Purdue University, 201 p.

Soreghan, G.S., Soreghan, M.J., Poulsen, C.J., Young, R.A., Eble, C.F., Sweet, D.E., and Davogustto, O.C., 2008. Anomalous cold in the Pangaean tropics: Geology, v. 36, p. 659–662.

Soreghan, G.S., Sweet, D.E., Marra, K.R., Eble, C.F., Soreghan, M.J., Elmore, R.D., Kaplan, S.A., and Blum, M.D., 2007. An exhumed Late Paleozoic canyon in the rocky mountains: Journal of Geology, v. 115, p. 473–481.

Soreghan, G.S., Sweet, D.E., Thomson, S.N., Kaplan, S.A., Marra, K.R., Balco, G., and Eccles, T.M., 2015. Geology of Unaweep Canyon and its role in the drainage evolution of the northern Colorado Plateau: Geosphere, v. 11, p. 320–341.

Staley, S., Fawcett, P., Anderson, R. & Jiménez-Moreno, Gonzalo, 2022. Early Pleistocene–to–present paleoclimate archive for the American Southwest from Stoneman Lake, Arizona, USA. GSA Bulletin. 134.

Suarez-Rojas, Y., 2007. Acquisition, Processing, and Modeling of Shallow Seismic Refraction and Reflection Profiles: Unaweep Canyon, Colorado: M.S. Thesis, University of Oklahoma, 135 p.

van Wijk, J.W., Baldridge, W.S., van Hunen, J., Goes, S., Aster, R., Coblentz, D.D., Grand, S.P., and Ni, J., 2010. Small-scale convection at the edge of the Colorado Plateau: Implications for topography, magmatism, and evolution of Proterozoic lithosphere: Geology, v. 38, p. 611–614.

Wassmer, P., Schneider, J.L., Pollet, N., and Schmitter-Voirin, C., 2004. Effects of the internal structure of a rock–avalanche dam on the drainage mechanism of its impoundment, Flims sturzstrom and Ilanz paleo-lake, Swiss Alps: Geomorphology, v. 61, p. 3–17.

Wu, L.Z., Deng, H., Huang, R.Q., Zhang, L.M., Guo, X.G., and Zhou, Y., 2019. Evolution of lakes created by landslide dams and the role of dam erosion: A case study of the Jiajun landslide on the Dadu River, China: Quaternary International, v. 503, p. 41–50.

Zhang, Y., Zhao, X., Lan, H., and Xiong, T., 2011. A Pleistocene landslide-dammed lake, Jinsha River, Yunnan, China: Quaternary International, v. 233, p. 72–80.

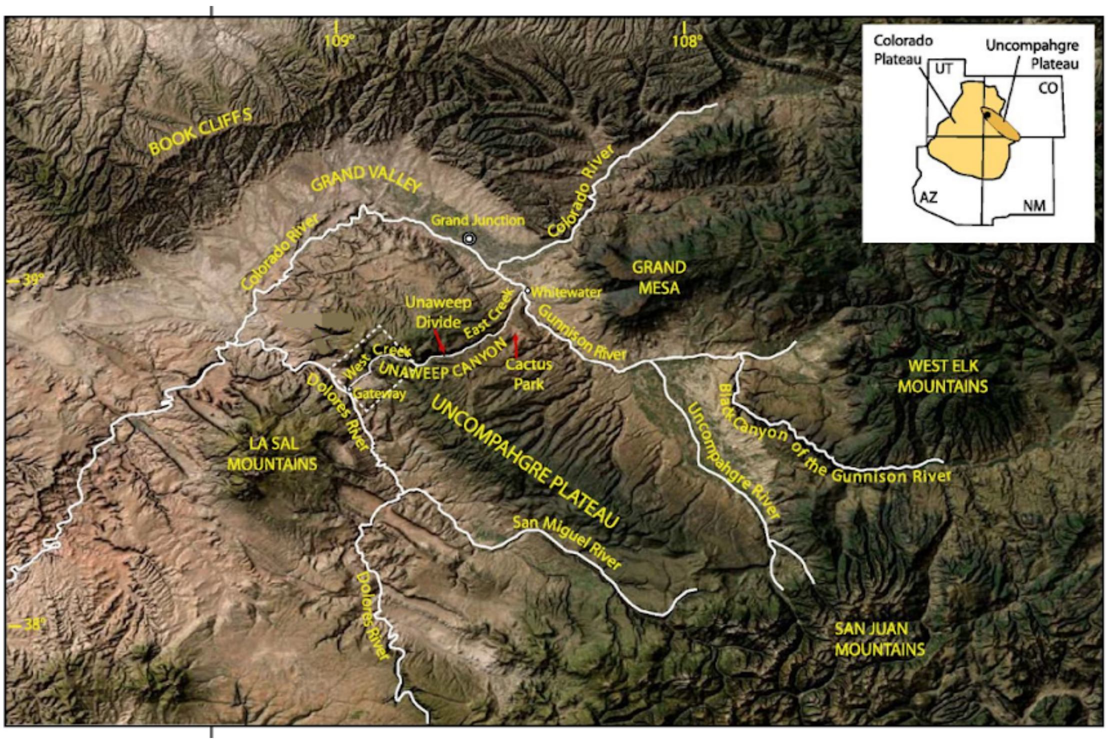

Figure 1: Map showing modern surrounding stream drainages of the Uncompahgre Plateau, along with structural and geologic provinces. (modified from Soreghan et al., 2015)

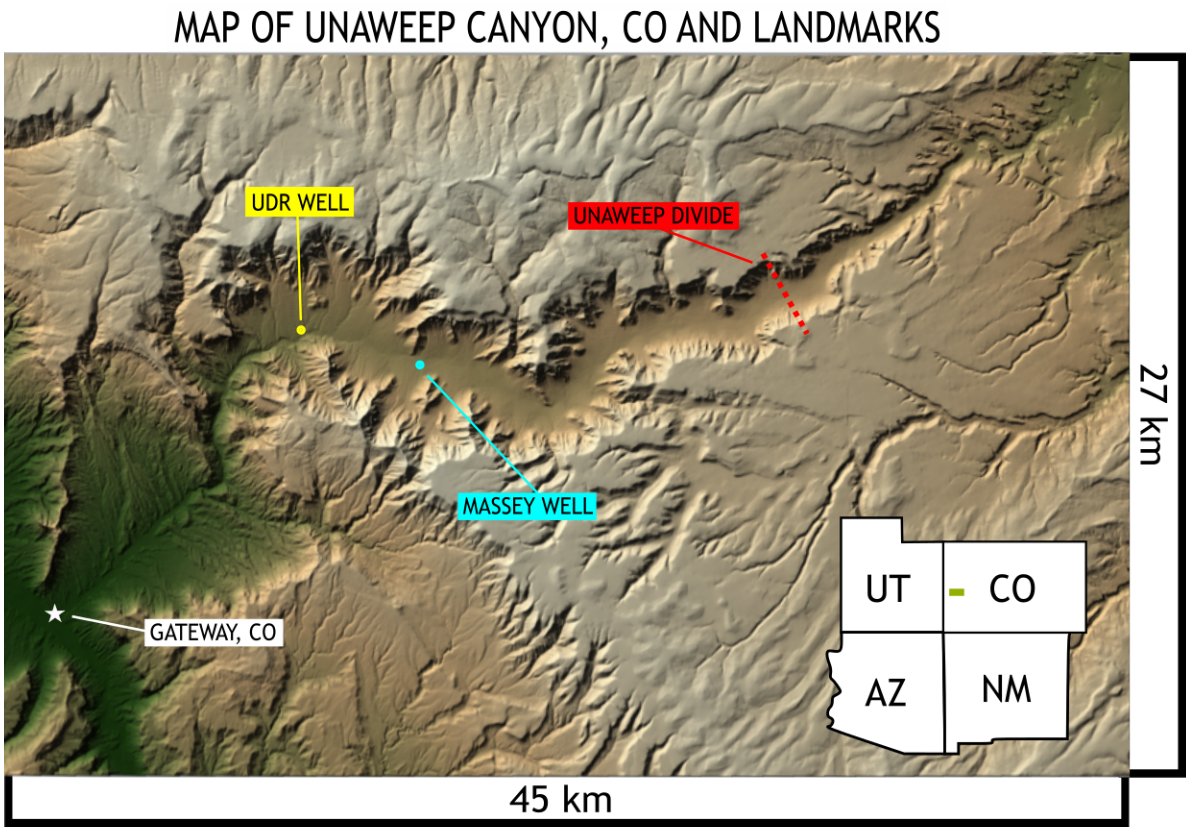

Figure 2: Map of Unaweep Canyon, CO and cores drilled within the area.

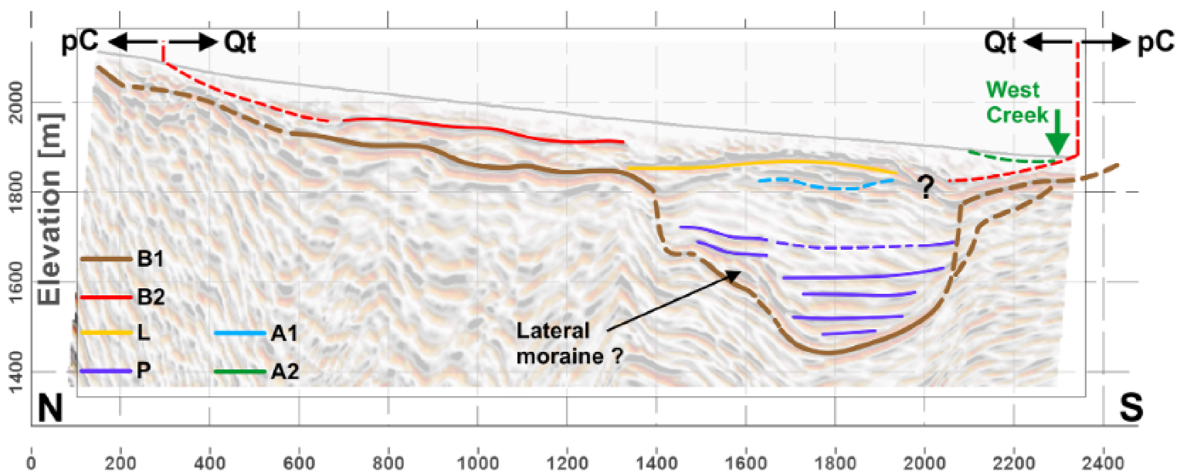

Figure 3: Seismic data and interpreted lines of changing lithology within a transecting line across Unaweep Canyon. (Patterson et al., 2021)

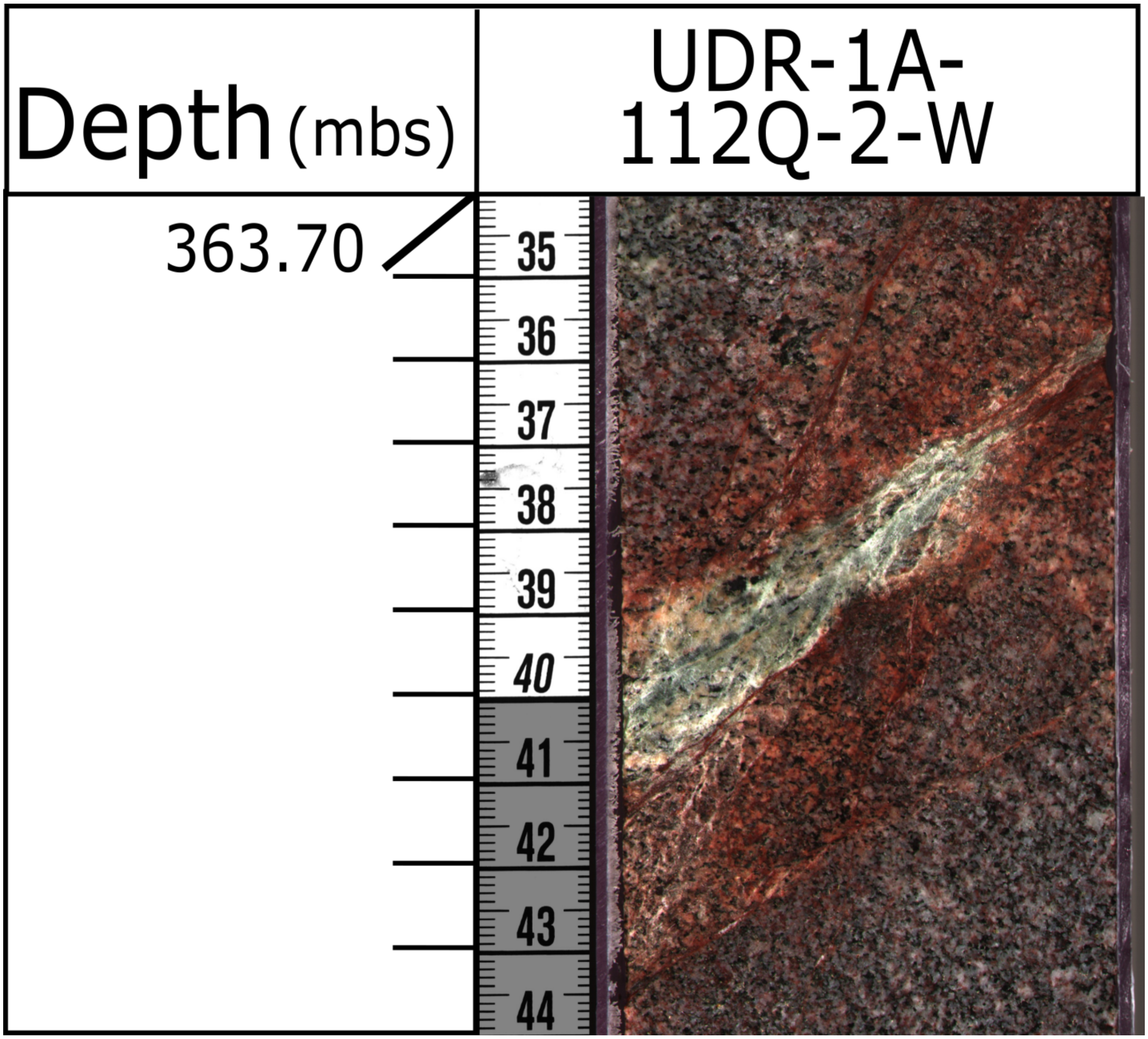

Figure 4:Hematite-stained fractures filled with a green, platy mineral. The green, platy mineral is most likely chloride or epidote resulting from hydrothermal diagenesis occurring within fractures.

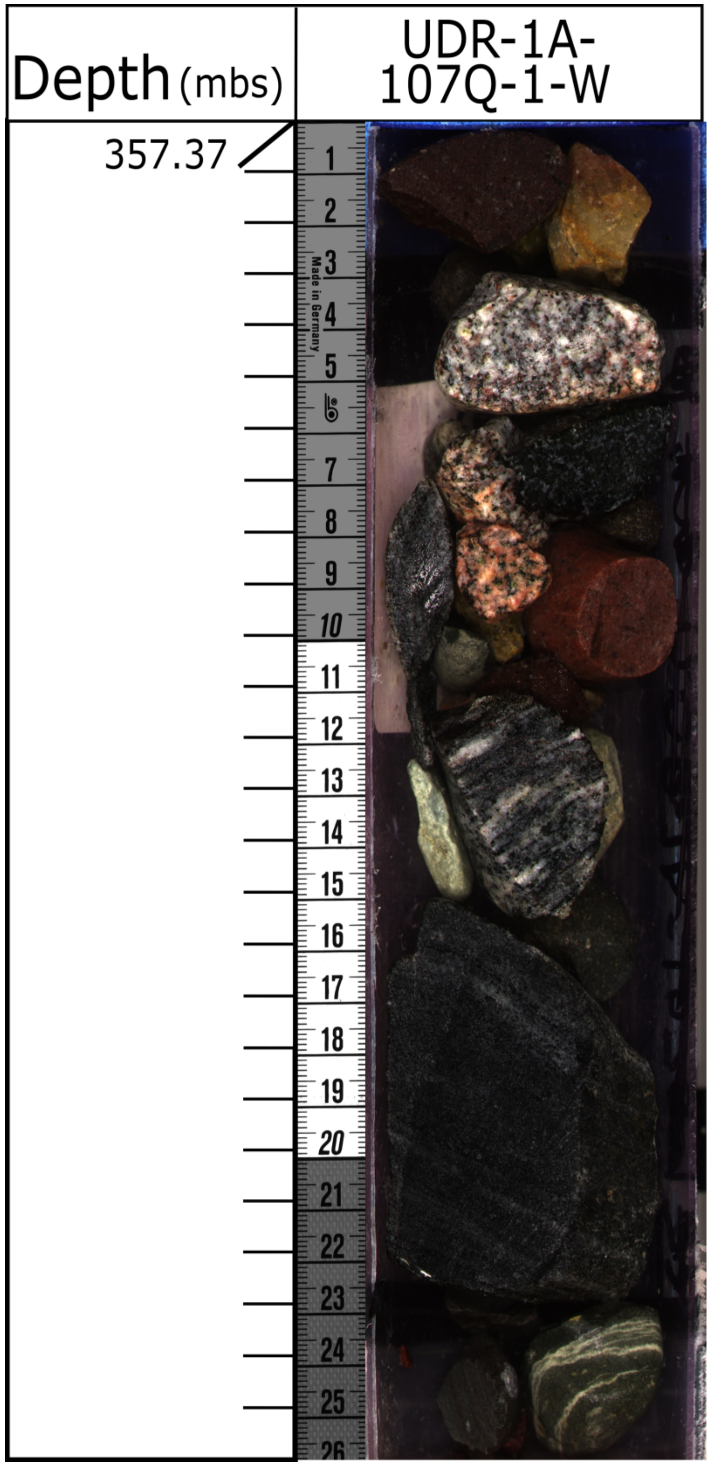

Figure 5: Section of the (inferred) ancestral Gunnison Gravels showing various (mostly basement) lithologies. The presence of intermediate volcanics (andesite) leads to the interpretation of these gravels originating from the Gunnison River.

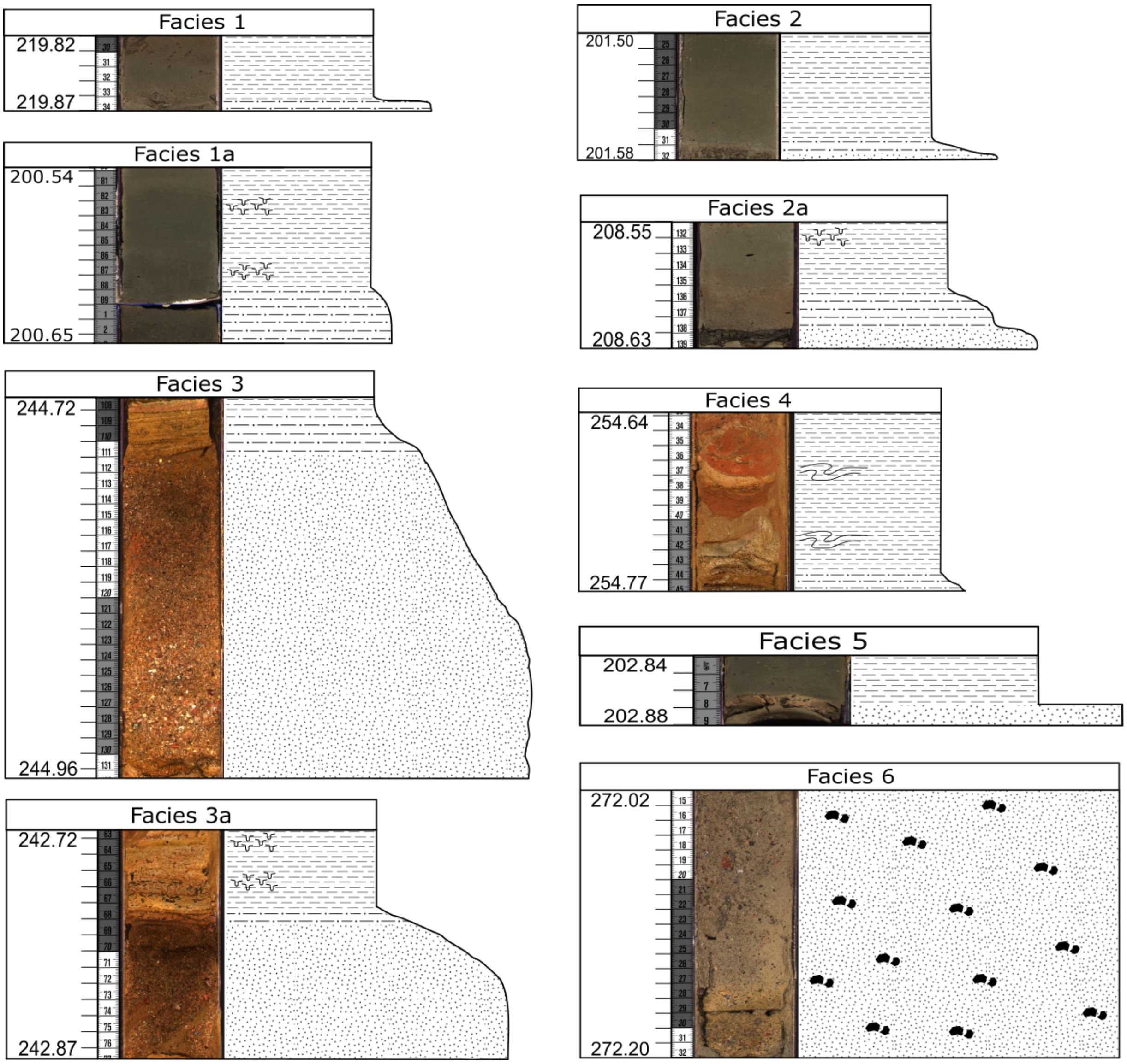

Figure 6: Facies identified within the UDR1 core.

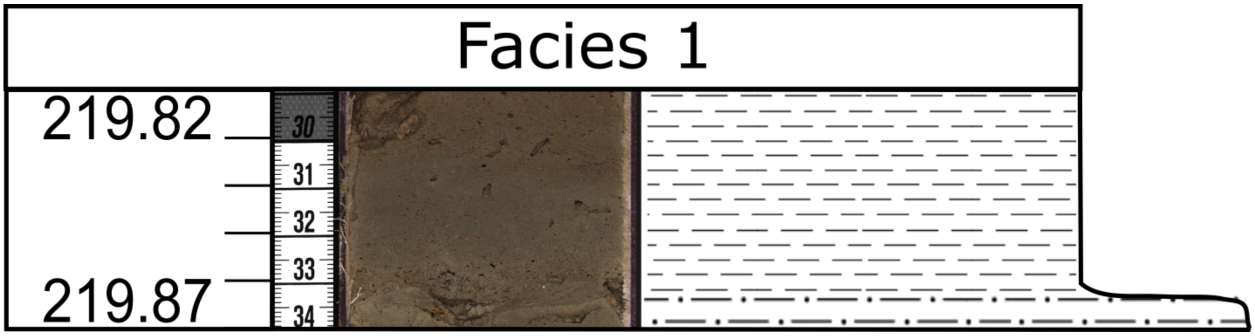

Figure 7a: Facies 1. A fining upwards sequence (~1-20 cm) in which the basal section of the bed is very fine sand or silt, which grades to clay.

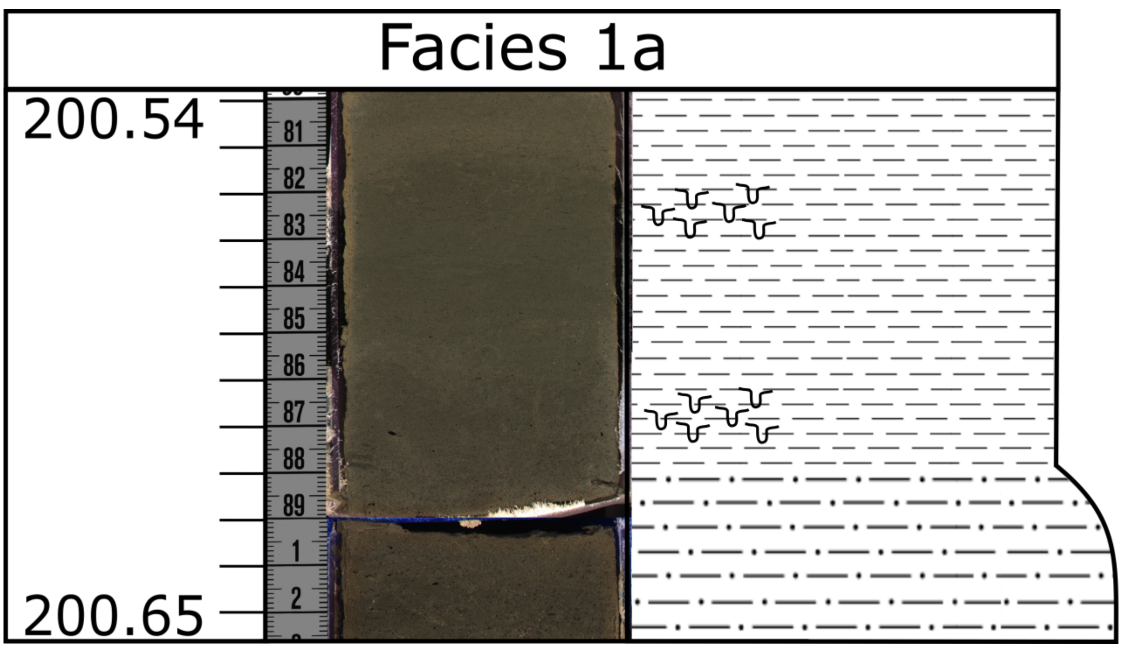

Figure 7b: Facies 1a. A variant of Facies 1 in which bioturbation occurs within the clayey interval of the fining upwards sequence. Bioturbation most commonly occurs at the very top of the facies, or at the point of changing grain size from silt to clay.

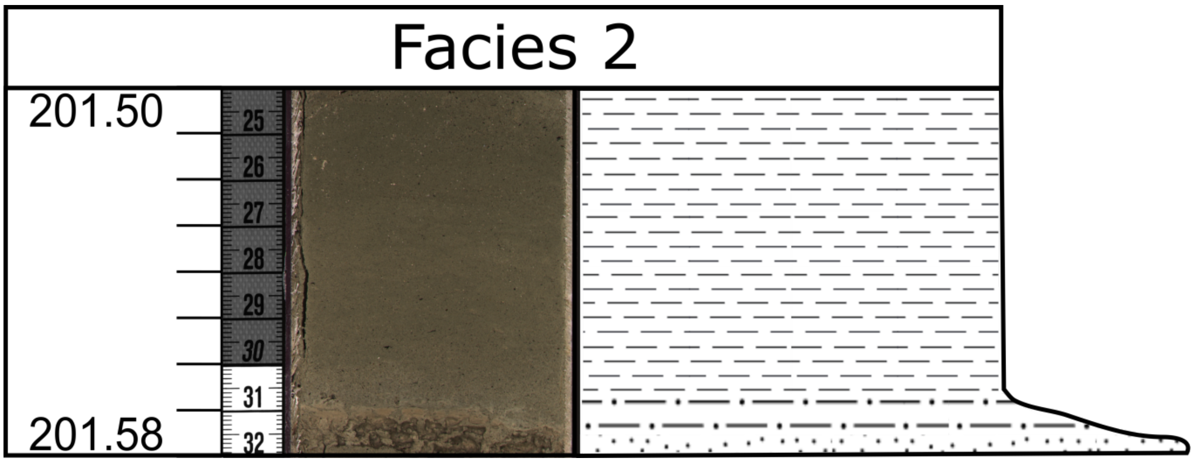

Figure 8a: Facies 2. A fining upwards sequence (~1-50 cm) in which the basal grain size of the bed is between fine sand and coarse sand and grades to clay. The grains are medium sorted with sub angular shape.

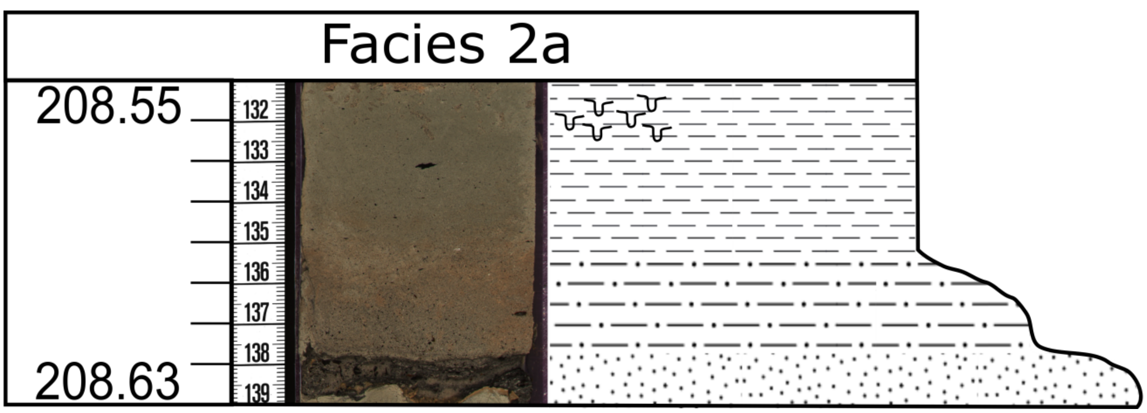

Figure 8b: Facies 2a. A variant of Facies 2 in which bioturbation occurs in places similar to Facies 1a.

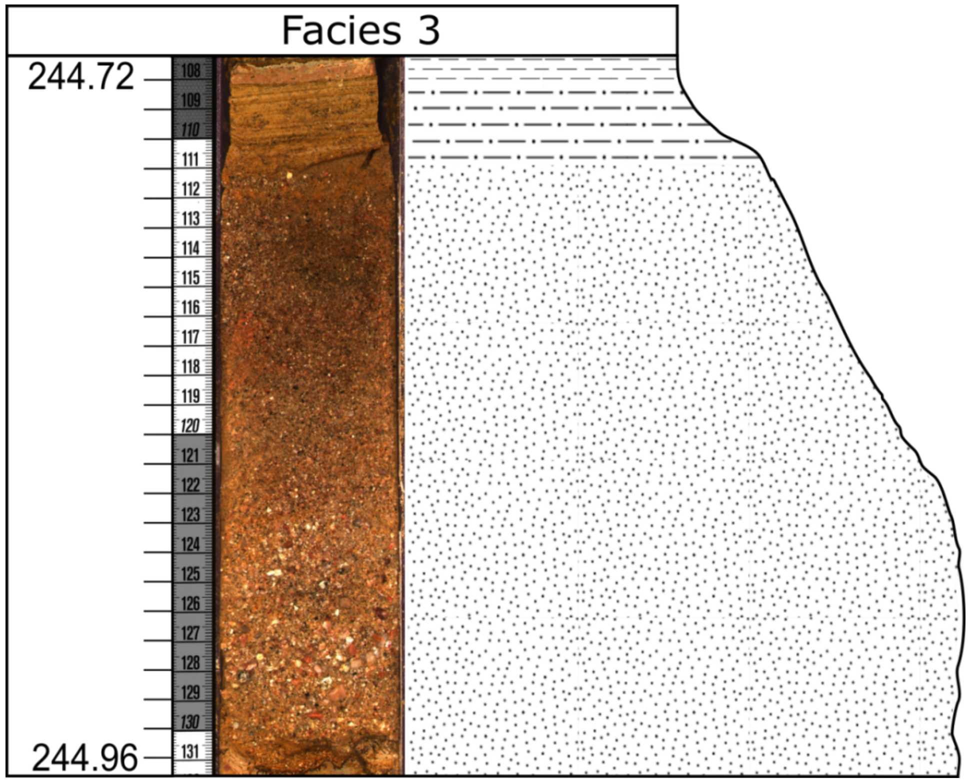

Figure 9a: Facies 3. A fining upwards sequence (~1-25 cm) in which the basal grain size of the bed is at least very coarse sand and up to pebble sized. This bed then grades to clay. Larger successions of Facies 3 tend to have floating basement clasts within the basal sandy sections of the fining upwards sequence. Facies 3 has poor sorting and angular grains.

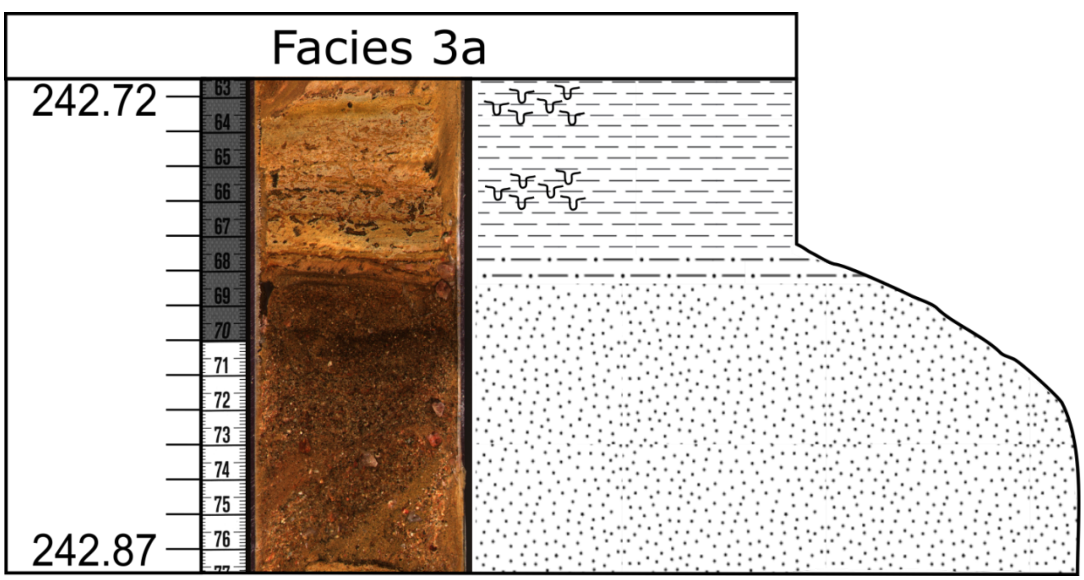

Figure 9b: Facies 3a. A variant of Facies 3 which is bioturbated in similar areas to that of Facies 1a and Facies 2a.

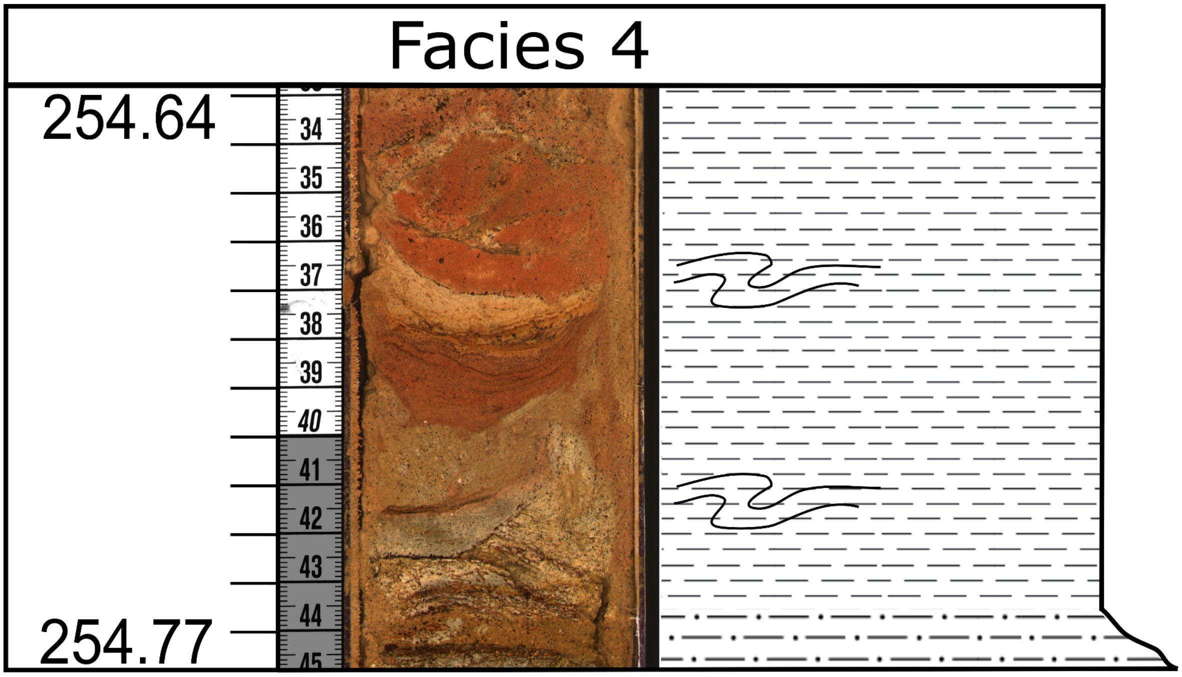

Figure 10: Facies 4 (~2-15 cm). These convolute beds are composed of one or more fining upwards sequences, like that of Facies 1-3.Facies 4 is interpreted as syn or post-depositional movement of beds. The convolute bedding exhibited within the facies is attributable to a slump fold.

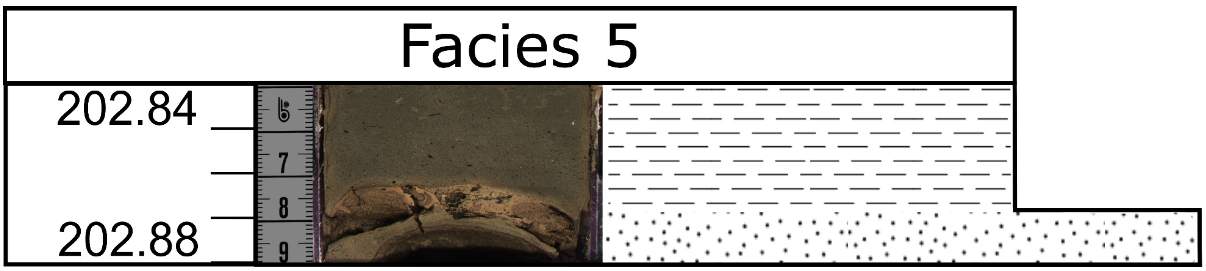

Figure 11: Facies 5 (~1-5 cm). Massive beds of sand/gravel topped by clay/silt with no gradation between the grain sizes (A-E Bouma Sequence). Grains are medium sorted and subangular within the sand/gravel. Facies 5 is interpreted as a slump failure or channel deposits.

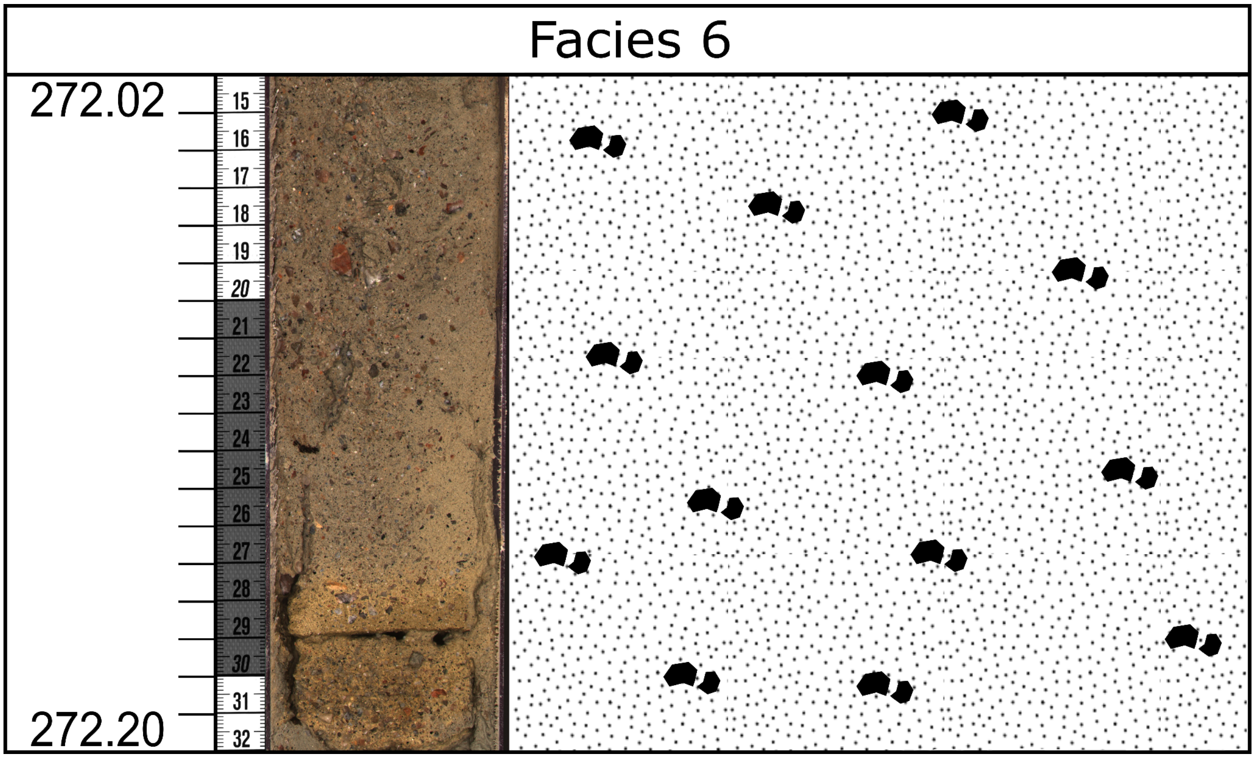

Figure 12: Facies 6 (2-5 cm). A matrix of silt and clay with basement clasts (~1 cm) floating throughout. This facies has no structure. Facies 6 is interpreted as the deposition of locally sourced gruss.

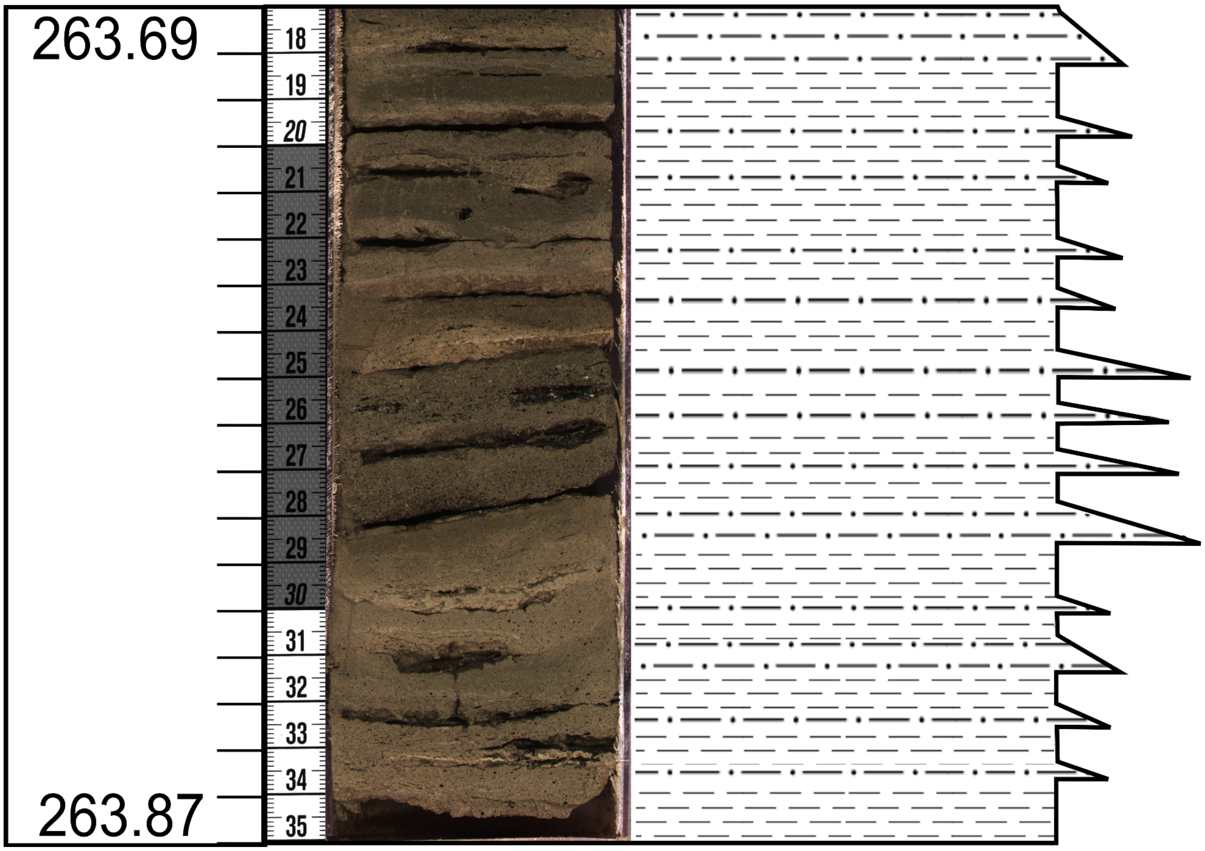

Figure 13: Very thinly bedded, upwardly fining stacks (3-15 cm) of Facies 1 with individual bed thicknesses around 1 cm (Figure 18). This facies association is most common throughout the ochre-colored sections of the core and rarely within the olive-gray colored sections of the core. Continuous stacks of Facies 1 indicate a period in which sediments settle out and an occasional seasonal flush were the primary sediment input in this part of the paleo-lake for an extended period of time.

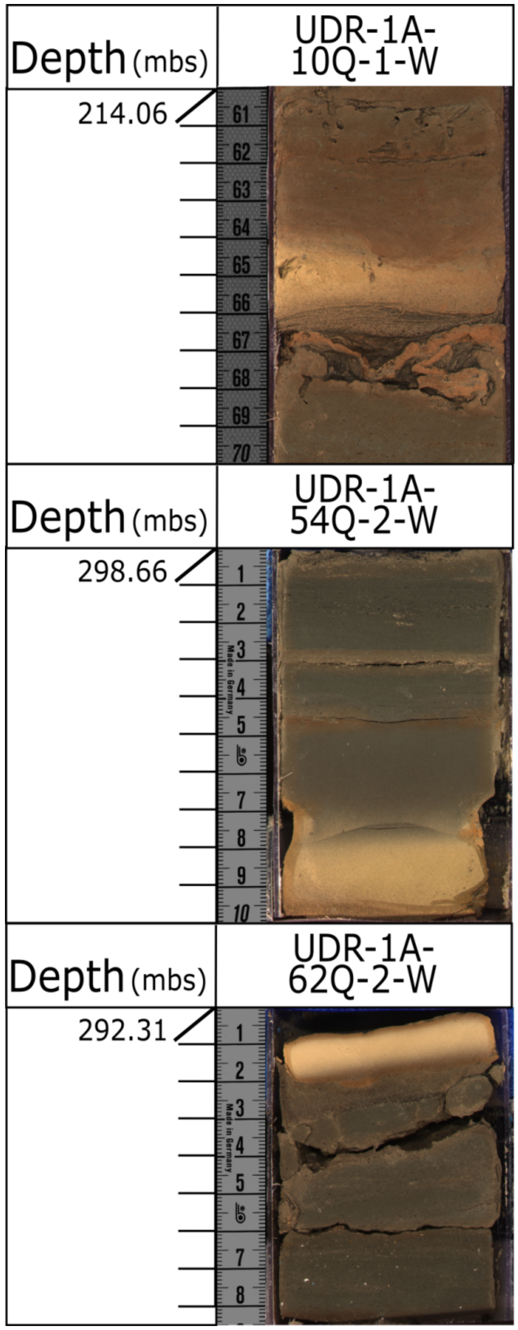

Figure 14: In situ siderite beds (~1-4 cm, white/yellow layers). Evidence of reduced environments in the olive-gray sections of the core. They occur in non-determinate facies and at any part of a facies sequence.

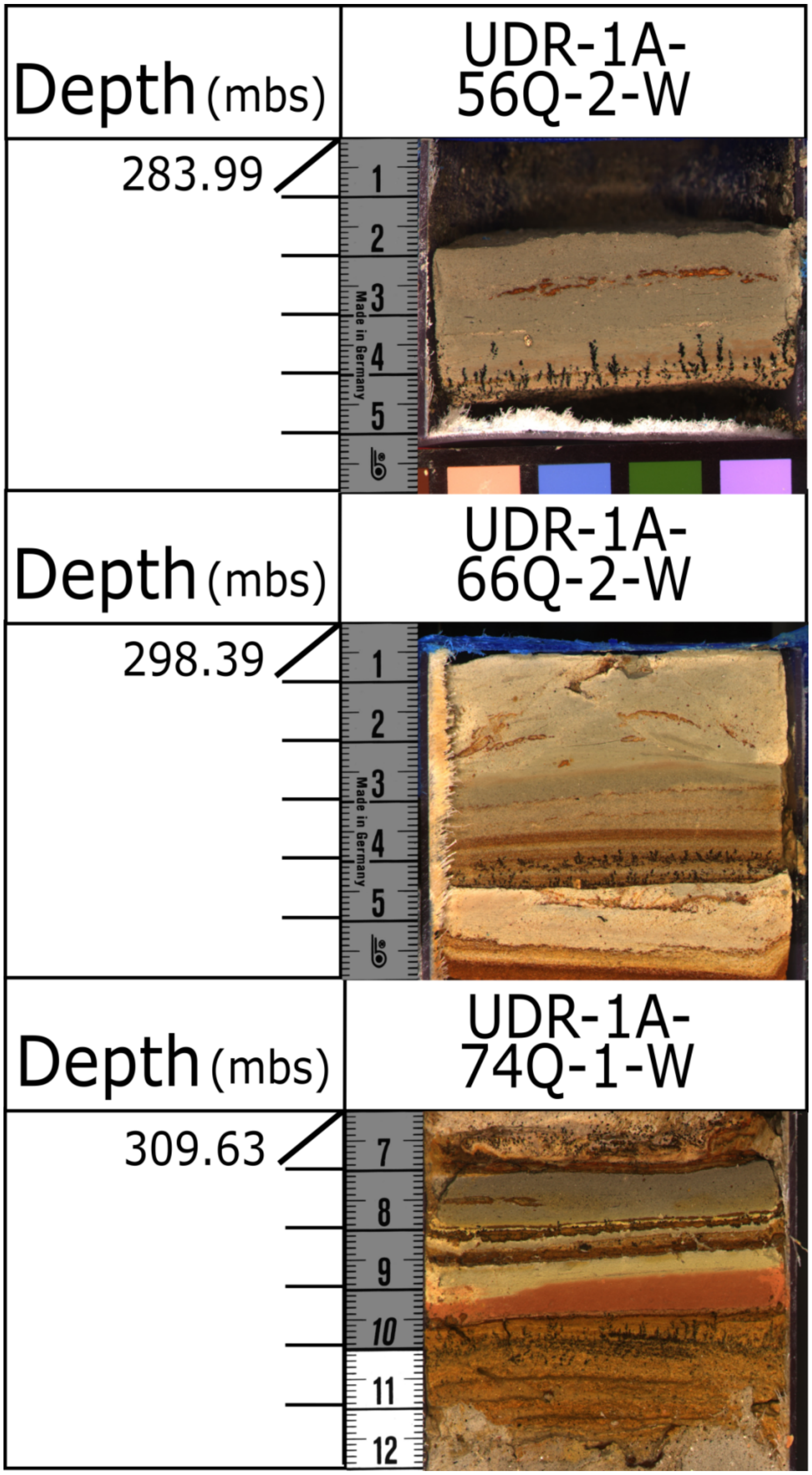

Figure 15: Manganese oxide dendrites in stacks of Facies 1. Evidence of diagenesis within the ochre sections of the core following fluid pattern.

Sample	Depth (m)	Qm	Qo	Q2-3	Q4^{+}	Qs	Qr	Ls (Qr)	Lp (Qr)	Cht	Km	Kr	Ls (Kr)	Lp (Kr)	Pm	Pr	Ls (Pr)	Lp (Pr)	M	Ls	Lv	Lp	Lm	A	H	O
UDR 2Q-1 103 cm	202.29	181	16	7	6	0	14	5	9	0	54	8	3	5	83	12	7	5	1	3	0	9	0	5	1	0
UDR 7Q-1 61 cm	209.5	144	11	9	3	0	20	15	5	0	52	6	6	0	93	8	6	2	33	6	0	6	0	4	5	0
UDR 10Q-2 8.5 cm	214.38	216	8	10	5	0	27	19	8	0	40	9	6	3	47	8	3	5	12	7	0	7	0	3	1	0
UDR 13Q-1 108 cm	219.09	209	8	12	3	0	21	6	15	0	40	3	1	2	59	11	2	9	15	7	0	11	0	1	0	0
UDR 18Q-1 22 cm	225.74	90	6	6	3	0	24	7	17	0	46	8	3	5	125	24	8	16	41	9	0	2	0	7	9	0
UDR 24Q-1 26 cm	234.75	135	7	8	2	0	12	2	10	0	40	2	1	1	121	19	18	1	36	1	0	5	0	4	8	0
UDR 27Q-1 118 cm	240.27	90	5	6	3	0	12	1	11	0	47	4	0	4	175	19	0	19	19	3	0	4	0	4	9	0
UDR 32Q-1 53 cm	247.3	74	6	4	2	0	39	9	30	0	37	12	0	12	148	31	1	30	38	0	0	0	0	4	5	0
UDR 34Q-1 78 cm	250.76	71	0	6	3	0	38	7	31	0	37	7	2	5	169	25	1	24	24	2	0	4	0	2	12	0
UDR 37Q-1 101.5 cm	255.32	61	0	1	3	0	36	10	26	0	12	8	0	8	157	40	1	39	50	7	0	2	0	6	17	0
UDR 39Q-1 27 cm	257.81	192	3	7	0	0	9	4	5	0	99	3	0	3	61	2	0	2	13	1	0	2	0	0	8	0
UDR 45Q-1 55 cm	266.84	263	8	5	4	0	9	2	7	0	65	1	0	1	37	2	0	2	4	0	0	1	0	0	1	0
UDR 49Q-1 27 cm	272.16	201	6	3	1	0	13	5	8	0	61	5	2	3	69	8	0	8	9	16	0	0	0	1	7	0
UDR 54Q-1 77 cm	280.31	190	0	0	0	0	29	0	29	0	70	13	0	13	69	7	0	7	12	2	0	5	0	2	1	0
UDR 57Q-1 28 cm	284.57	138	0	6	7	0	11	2	9	0	115	5	0	5	56	13	0	13	9	31	0	5	0	0	4	0
UDR 62Q-1 16 cm	291.68	193	0	0	0	0	46	0	46	0	72	12	0	12	58	3	0	3	1	11	0	0	0	1	3	0
UDR 68Q-1 122 cm	301.64	234	0	5	2	0	5	0	5	0	59	4	0	4	65	2	0	2	16	4	0	0	0	0	4	0
UDR 69Q-1 107 cm	303.01	111	0	0	0	0	41	0	41	0	37	11	0	11	136	28	0	28	17	2	0	12	0	3	2	0
UDR 72Q-1 51 cm	307.03	141	0	2	0	0	15	0	15	0	62	6	0	6	148	9	0	9	2	3	0	0	0	0	12	0
UDR 74Q-1 105 cm	310.61	108	0	0	0	0	25	0	25	0	28	5	0	5	162	27	0	27	32	0	0	4	0	9	0	0
UDR 75Q-1 127 cm	312.36	102	0	0	0	0	1	0	1	0	39	0	0	0	155	3	0	3	87	0	0	0	0	0	13	0
UDR 77Q-1 134 cm	315.48	182	0	1	1	0	18	0	18	0	85	16	0	16	77	12	0	12	4	0	0	3	0	1	0	0
UDR 81Q-2 5 cm	321.46	144	0	5	1	0	7	0	7	0	140	4	0	4	73	3	0	3	15	8	0	0	0	0	0	0
UDR 82Q-1 25 cm	321.83	91	0	2	0	0	22	0	22	0	24	9	0	9	211	26	0	26	2	0	0	4	0	7	2	0
UDR 84Q-2 101 cm	325.82	184	0	0	2	0	4	1	3	0	120	6	0	6	48	3	0	3	20	7	0	1	0	0	5	0
UDR 88Q-2 50 cm	331.65	174	0	2	0	0	10	0	10	0	85	11	0	11	79	12	0	12	7	13	0	6	0	1	0	0
UDR 90Q-1 71 cm	334.56	233	0	2	2	0	4	0	4	0	77	5	0	5	40	0	0	0	27	4	0	0	0	0	6	0
UDR 91Q-1 94 cm	336.42	132	0	0	2	0	7	0	7	0	56	8	0	8	122	8	0	8	53	1	0	3	0	6	2	0
UDR 93Q-1 37 cm	338.9	80	0	0	0	0	10	0	10	0	13	1	0	1	141	5	0	5	75	0	0	4	0	56	15	0
UDR 93Q-1 75.5 cm	339.28	121	0	1	0	0	9	0	9	0	34	2	0	2	93	12	0	12	67	24	0	3	0	28	6	0
UDR 93Q-1 141 cm	339.95	85	0	0	0	0	11	0	11	0	17	0	0	0	170	9	0	9	43	0	0	5	0	39	21	0
UDR 93Q-1 149 cm	340.02	148	0	0	0	0	15	0	15	0	101	21	0	21	70	17	0	17	17	2	0	2	0	5	2	0
UDR 99Q-1 10.5 cm	345.22	162	0	0	0	0	23	0	23	0	82	12	0	12	89	6	0	6	1	21	0	0	0	0	4	0
UDR 99Q-1 49 cm	345.66	59	0	0	0	0	35	1	34	0	49	11	0	11	119	25	1	24	54	15	0	26	0	4	3	0

Figure 16: Point count data from UDR1 core.

Figure 17: Point count percentages of total quartz throughout the UDR1 core. Quartz in a rock fragment as well as monocrystalline quartz were included.

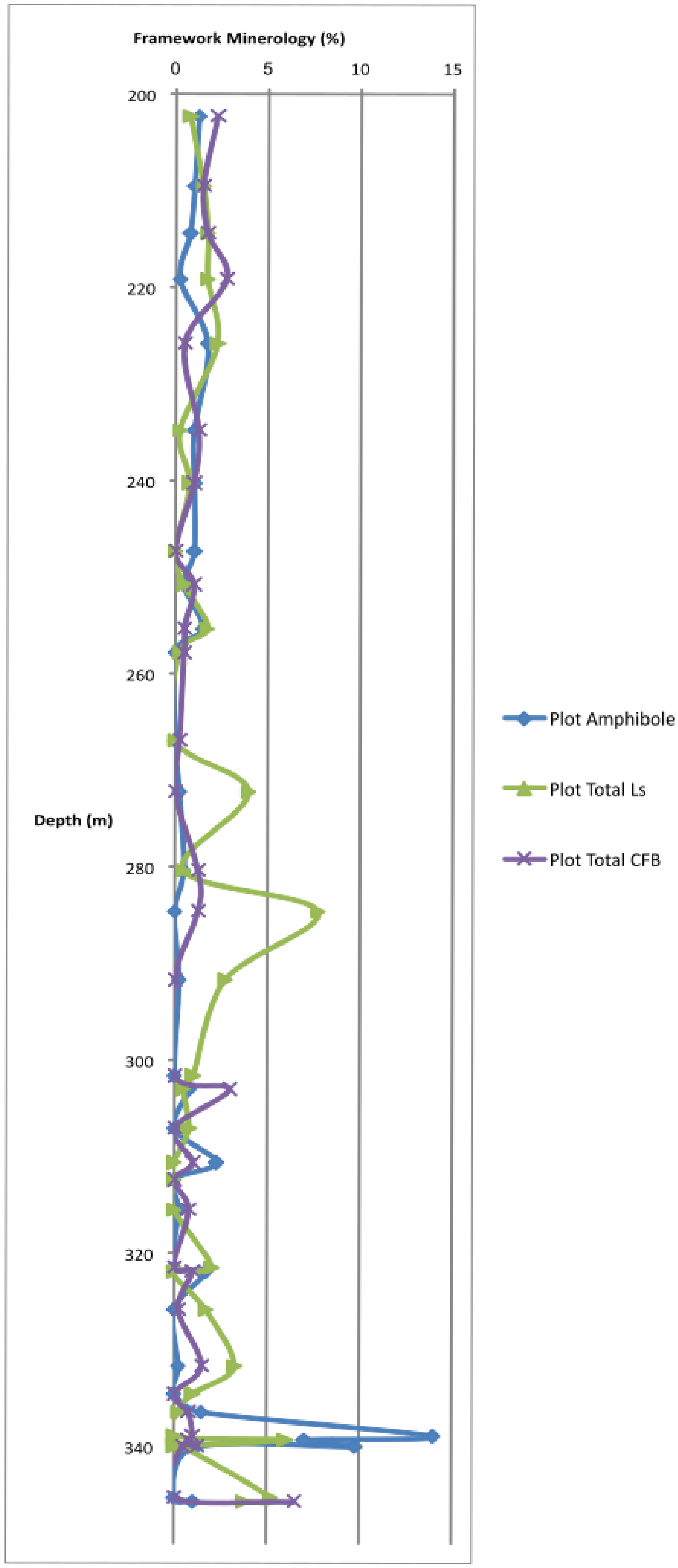

Figure 18: Point count data percentages of clasts of fractured basement (CFB), sedimentary lithics, and amphibole throughout the UDR1 core.

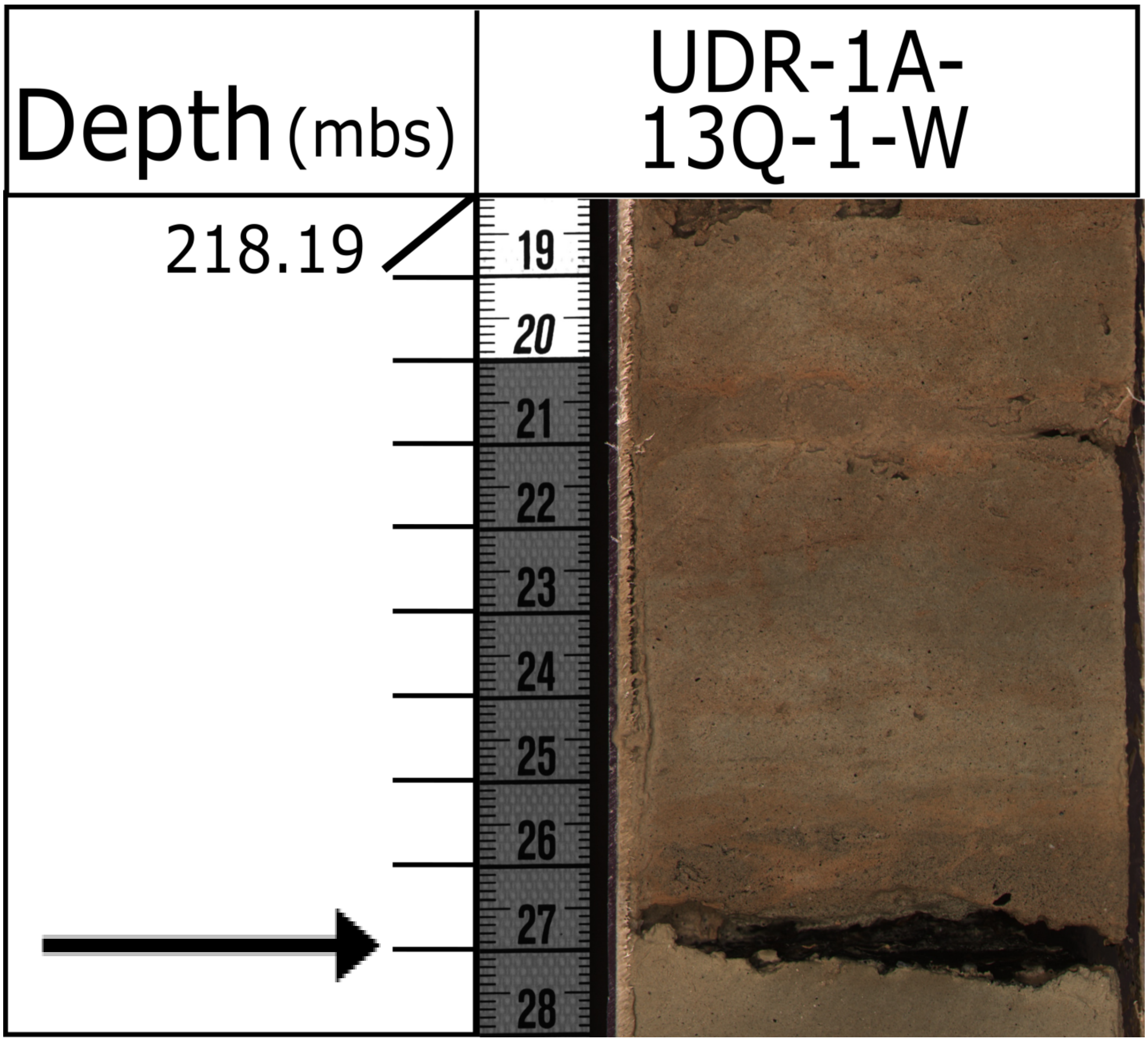

Figure 19: Charcoal shown by arrows, found within the basal sections of fining-upward, medium to coarse grained sand sequences.

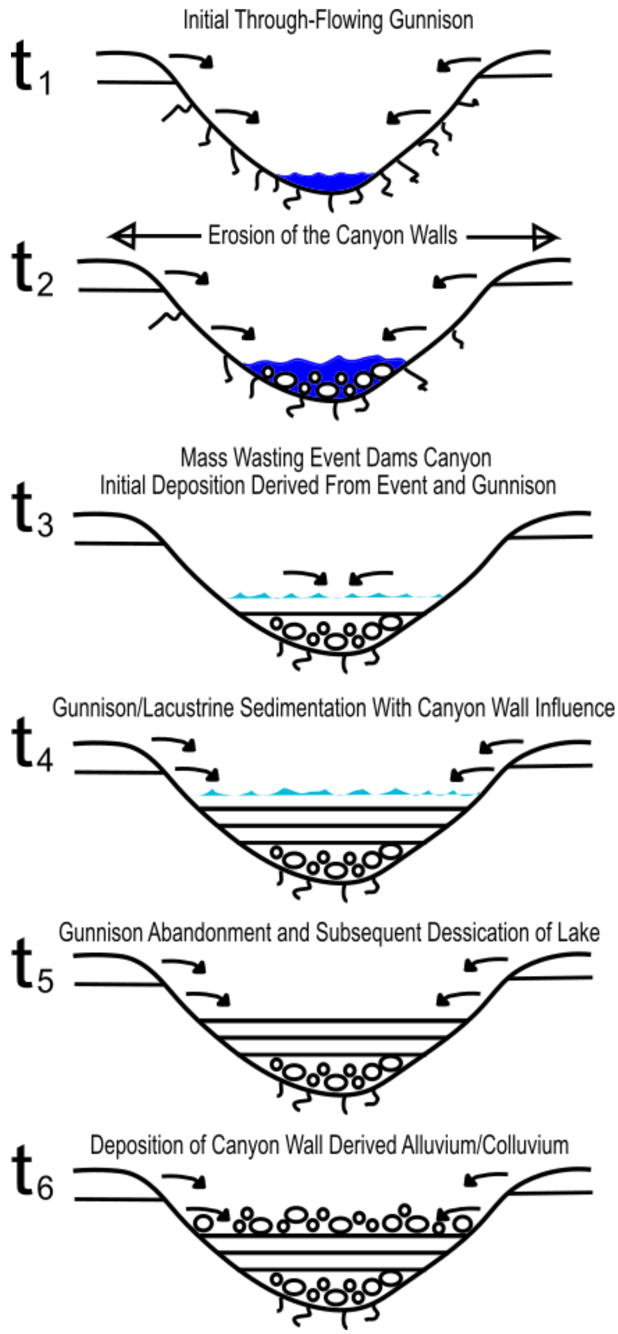

Figure 20: Model of the mode of deposition within the canyon. As the ancestral Gunnison River continues to flow, it deposits gravels within the channel, as well as continued input from the canyon walls (t_2). The canyon becomes blocked by the mass wasting event, and deposition is now mixed with axial ancestral Gunnison River deposits and transverse sediment input from the canyon walls (t_3). The ancestral Gunnison River abandons Unaweep Canyon (t_4), and the lake is subaerially exposed before the dam failure (t_5). Predominant sedimentation is now input from the canyon walls (t_6).

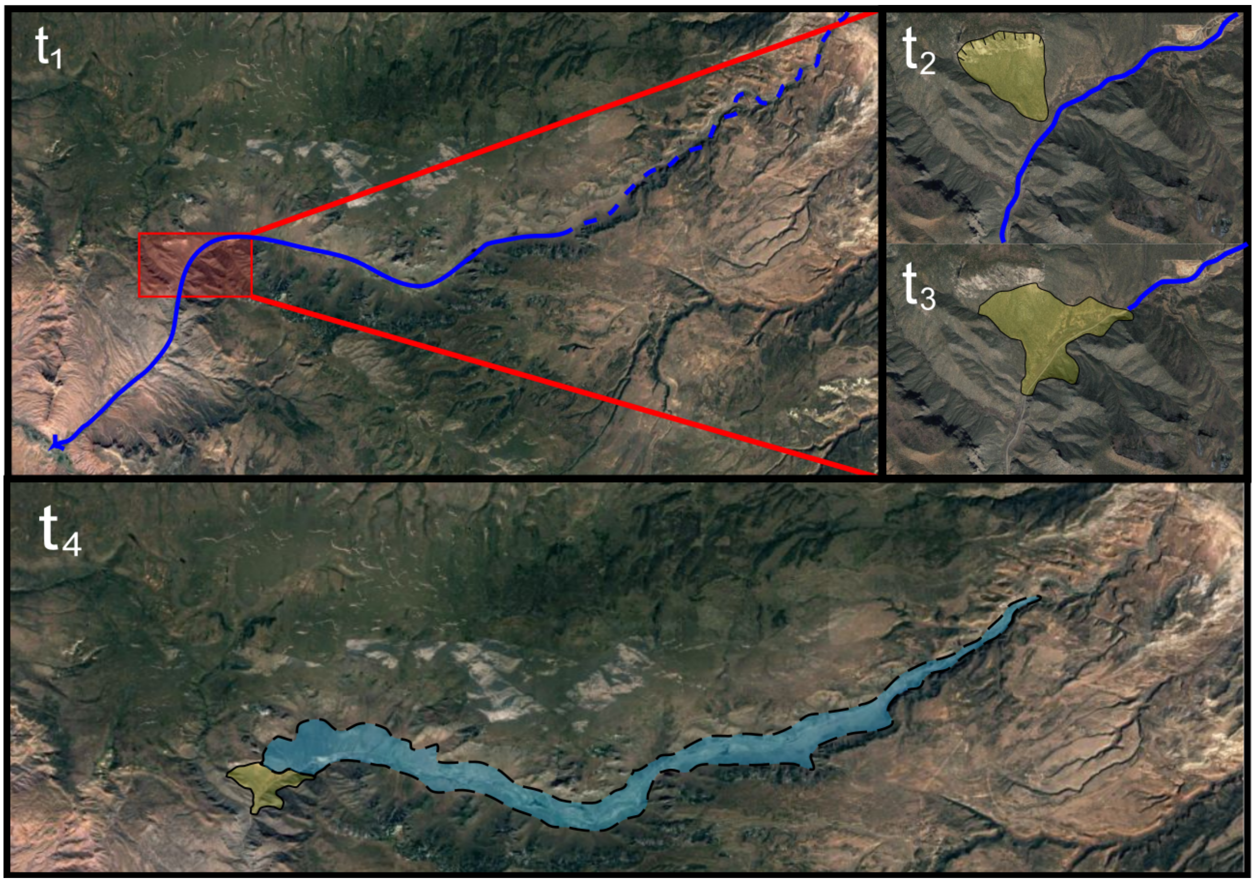

Figure 21: Evolution through time (earliest, t_1, to latest, t_6) of the ancestral Gunnison River, blocking of the canyon, and fill up of paleo-Lake Unaweep. Navy blue line is the ancestral Gunnison River, light blue polygon is paleo-Lake Unaweep, and the yellow polygon is the scarp and subsequent mass-wasting event at the westernmost section of Unaweep Canyon.

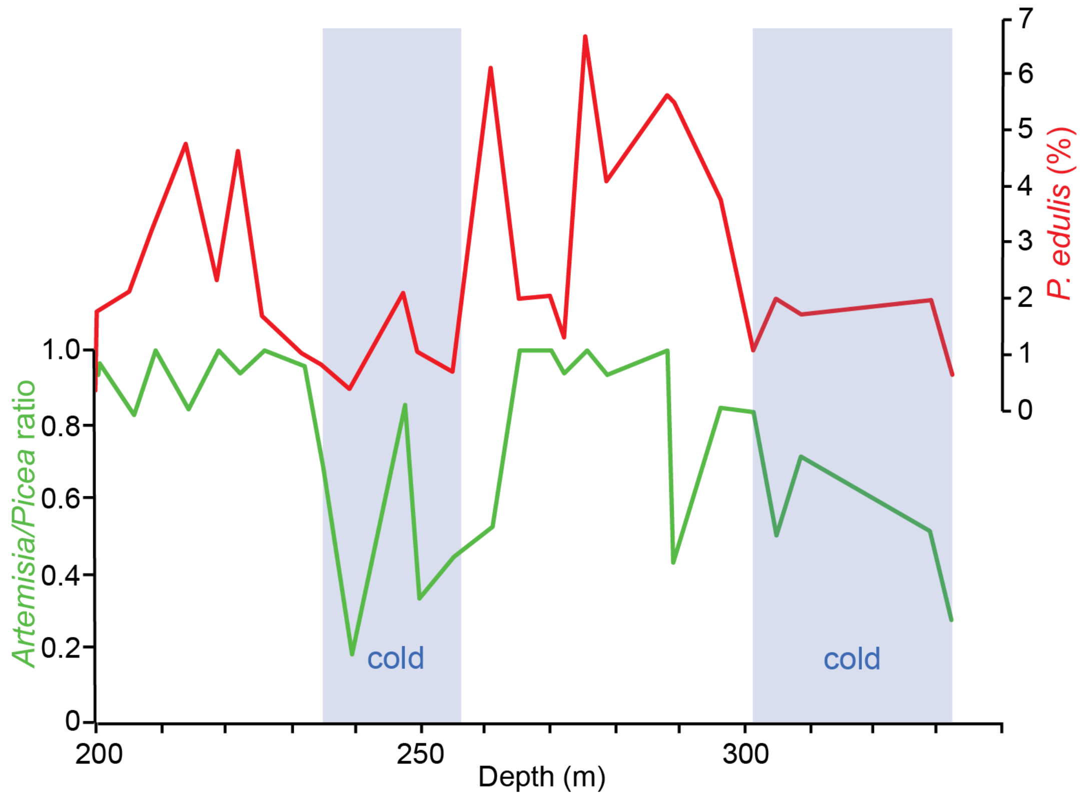

Figure 22: Chart showing warm/cold climate cycles from pollen data within the UDR1 core (from G. Jiménez-Moreno). *Artemisia*/*Picea* ratio shows changing vegetation belt due to climate, and *P. edulis* percentage further supports the suggested cycles.

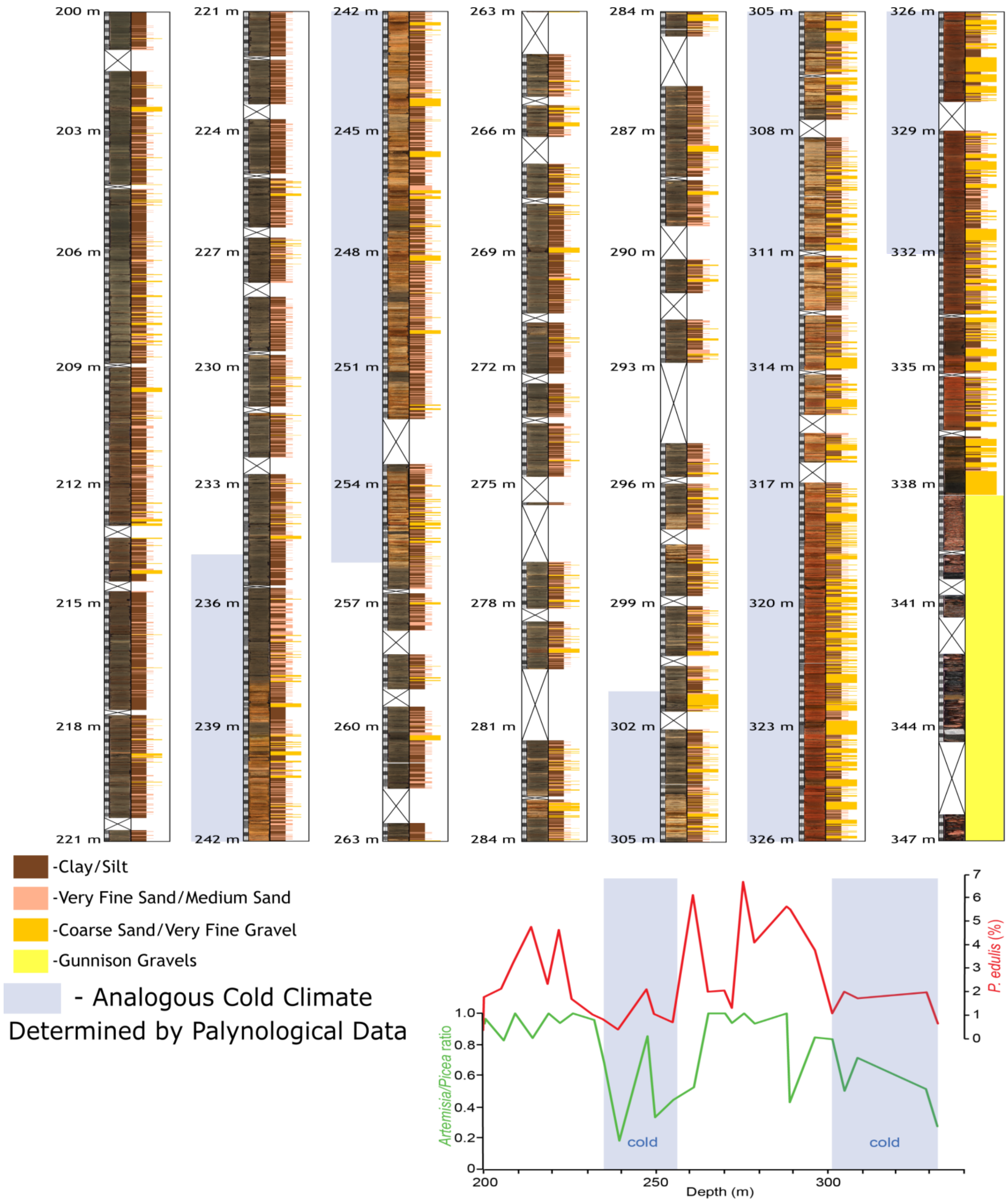

Figure 23: UDR1 condensed complete core with color-coordinated grain size indicators to the right of the core photos. Trends in grain size and bed thickness can be seen at this scale. The core column depths are colored gray and correlate to the colder conditions identified from the preliminary pollen analysis.

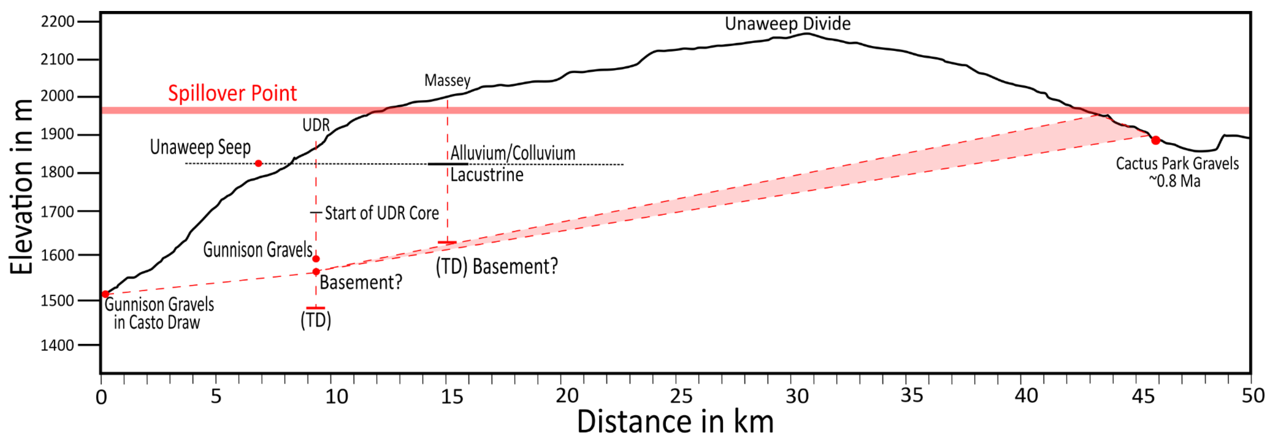

Figure 24: Elevation profile along modern Unaweep Canyon. The UDR1 and Massey #1 wells are shown as vertical red lines. The ancestral Gunnison Gravel location at Cactus Park is younger than the gravels exposed at the western mouth of Unaweep Canyon. The red dashed lines show a possible profile representing the assumed grade of the ancestral Gunnison River through Unaweep Canyon. This line does not align with the Gunnison Gravels at the western end of the canyon.

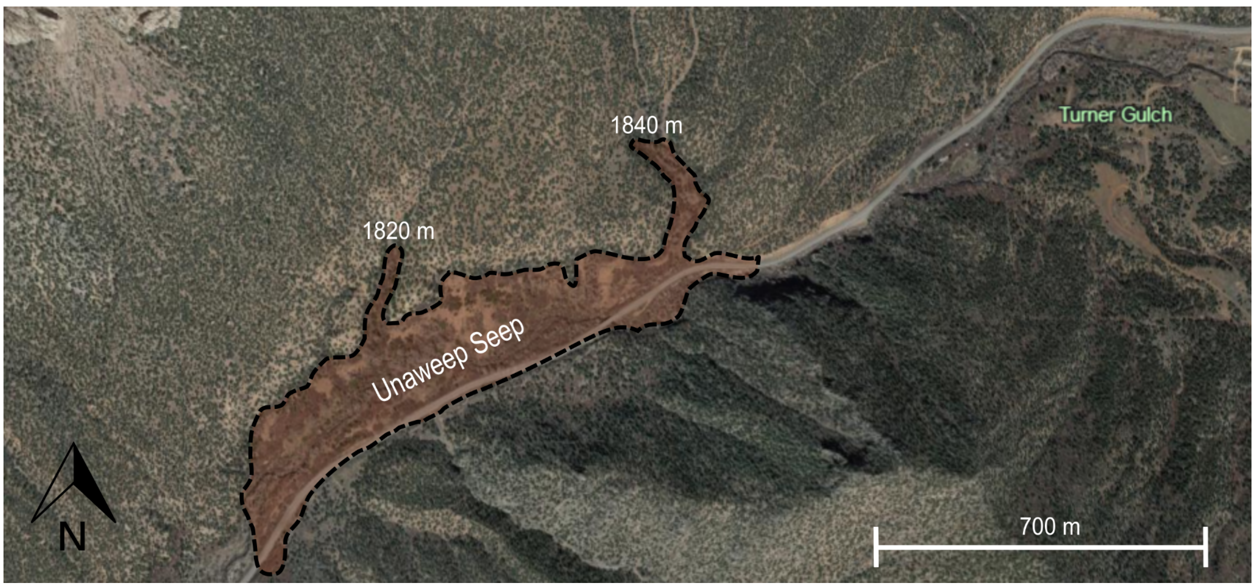

Figure 25: Map of Unaweep Seep near Turner Gulch in Unaweep Canyon.

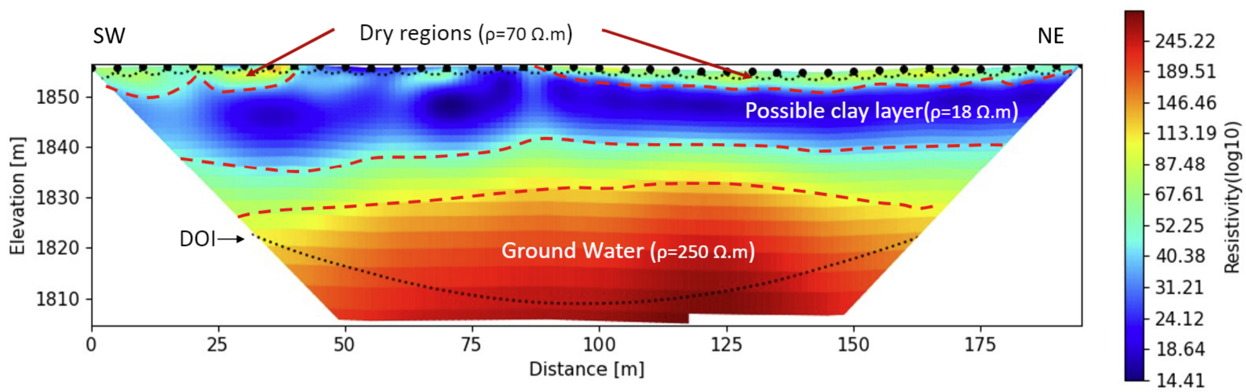

Figure 26:Electrical resistivity data at Unaweep Seep in Unaweep Canyon. Data notes groundwater is interacting with the surface at this locality.

APPENDIX I

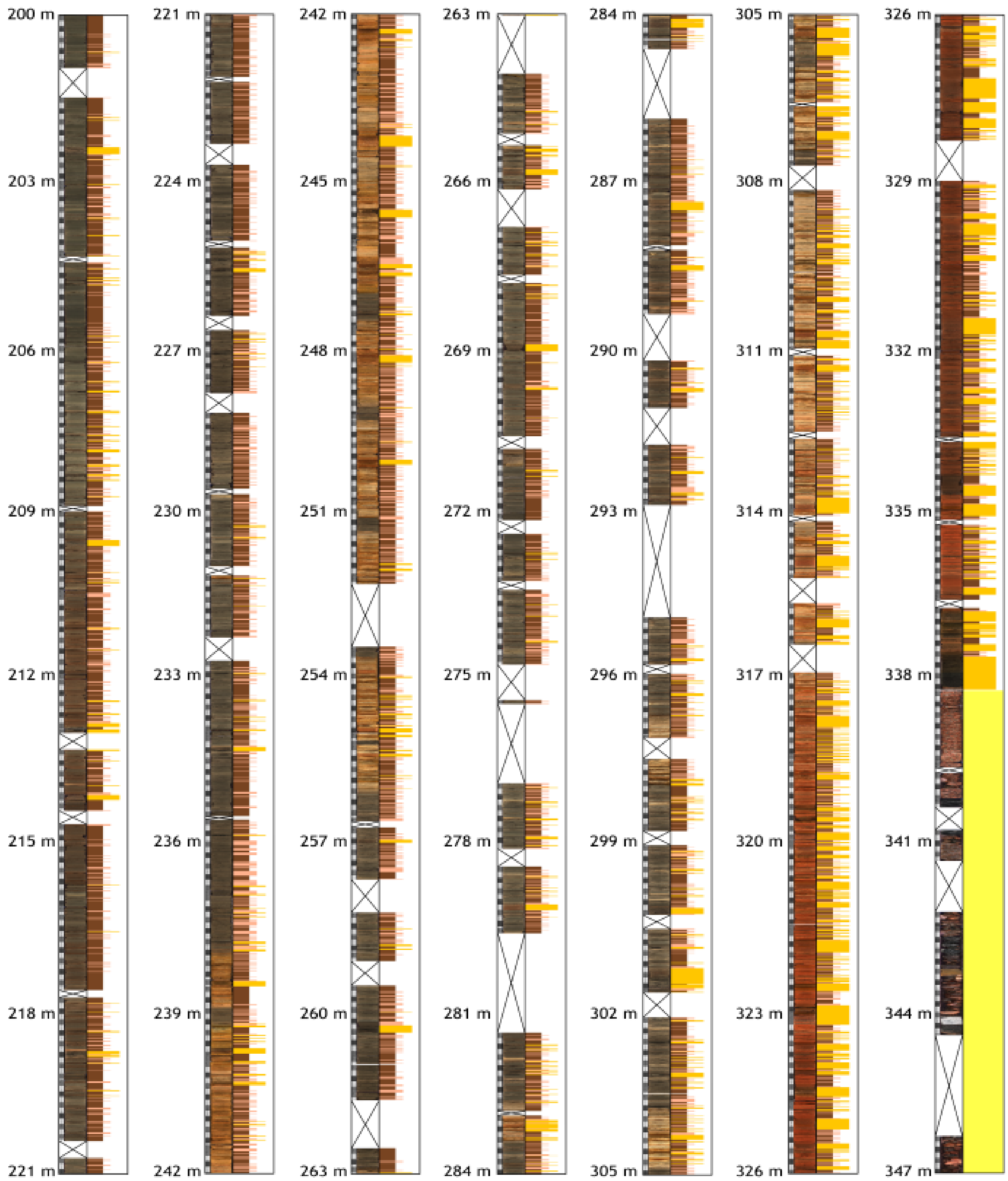
200 m
203 m
206 m
209 m
212 m
215 m
218 m
221 m
221 m
224 m
227 m
230 m
233 m
236 m
239 m
242 m
242 m
245 m
248 m
251 m
254 m
257 m
260 m
263 m
263 m
266 m
269 m
272 m
275 m
278 m
281 m
284 m
284 m
287 m
290 m
293 m
296 m
299 m
302 m
305 m
305 m
308 m
311 m
314 m
317 m
320 m
323 m
326 m
326 m
329 m
332 m
335 m
338 m
341 m
344 m
347 m

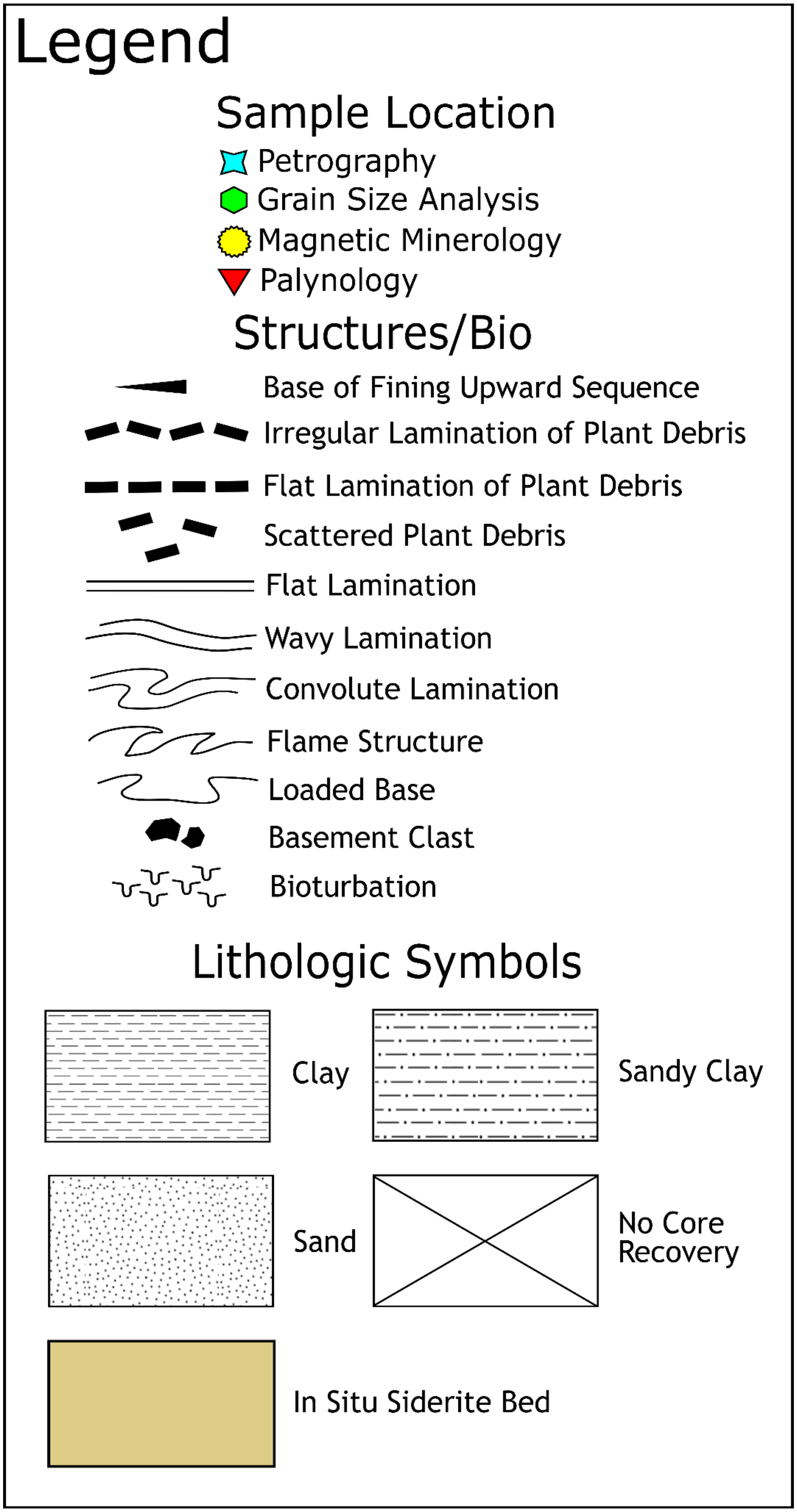
Legend
Sample Location
Petrography
Grain Size Analysis
Magnetic Minerology
Palynology
Structures/Bio
Base of Fining Upward Sequence
Irregular Lamination of Plant Debris
Flat Lamination of Plant Debris
Scattered Plant Debris
Flat Lamination
Wavy Lamination
Convolute Lamination
Flame Structure
Loaded Base
Basement Clast
Bioturbation
Lithologic Symbols
Clay
Sandy Clay
Sand
No Core Recovery
In Situ Siderite Bed

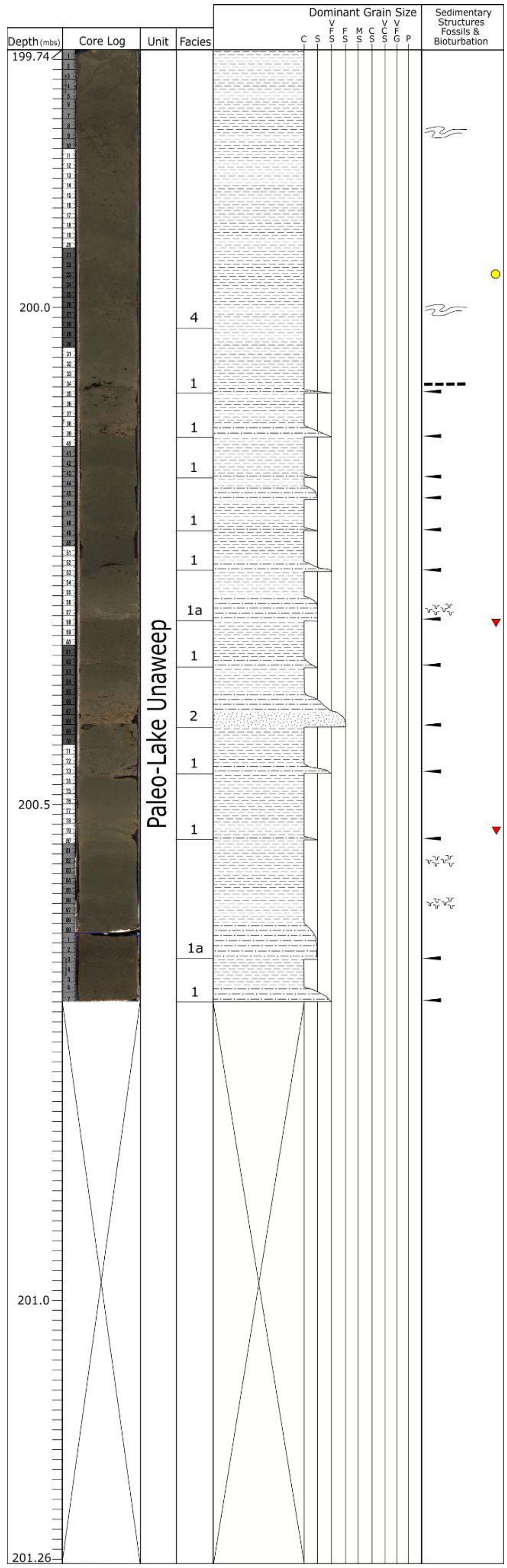
Depth (mbs)
Core Log
Unit
Facies
Dominant Grain Size
C S VFS FS MS CS VCS VFG P
Sedimentary Structures Fossils & Bioturbation
199.74
200.0
200.5
201.0
201.26
Paleo-Lake Unaweep
4
1
1
1
1
1
1a
1
2
1
1
1a
1

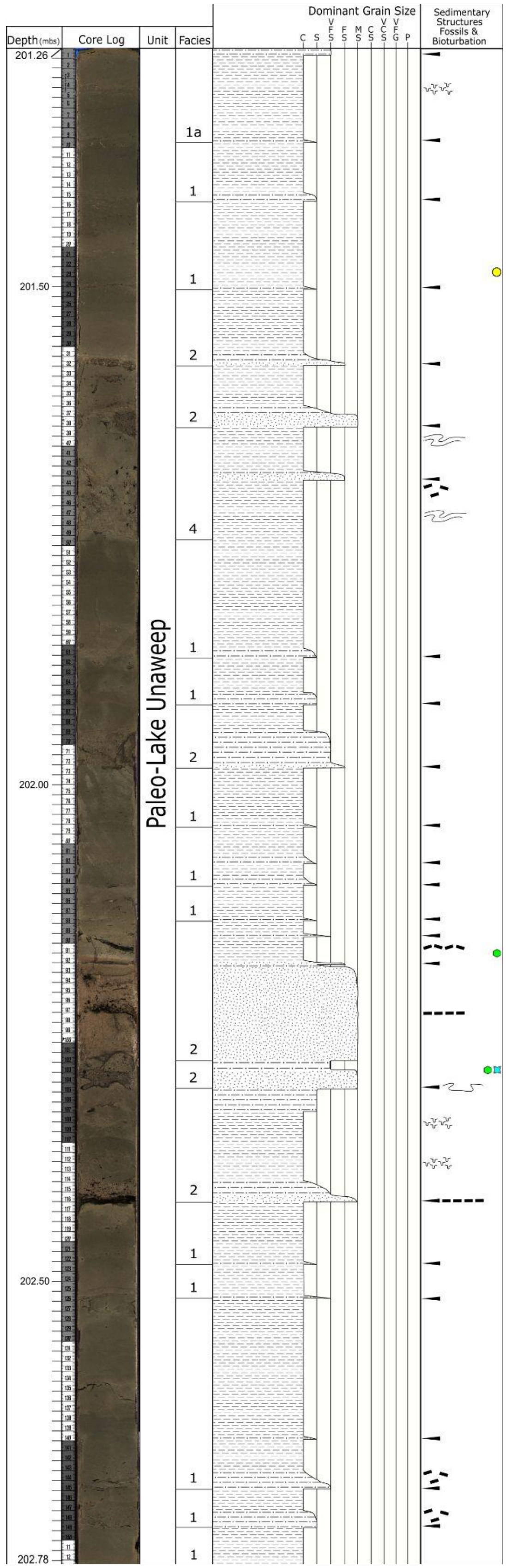

Depth (mbs)
Core Log
Unit
Facies
Dominant Grain Size
C S VFS FS MS CS VCS VFG P
Sedimentary Structures Fossils & Bioturbation
201.26
201.50
202.00
202.50
202.78
Paleo-Lake Unaweep
1a
1
1
2
2
4
1
1
2
1
1
1
2
2
2
1
1
1
1
1

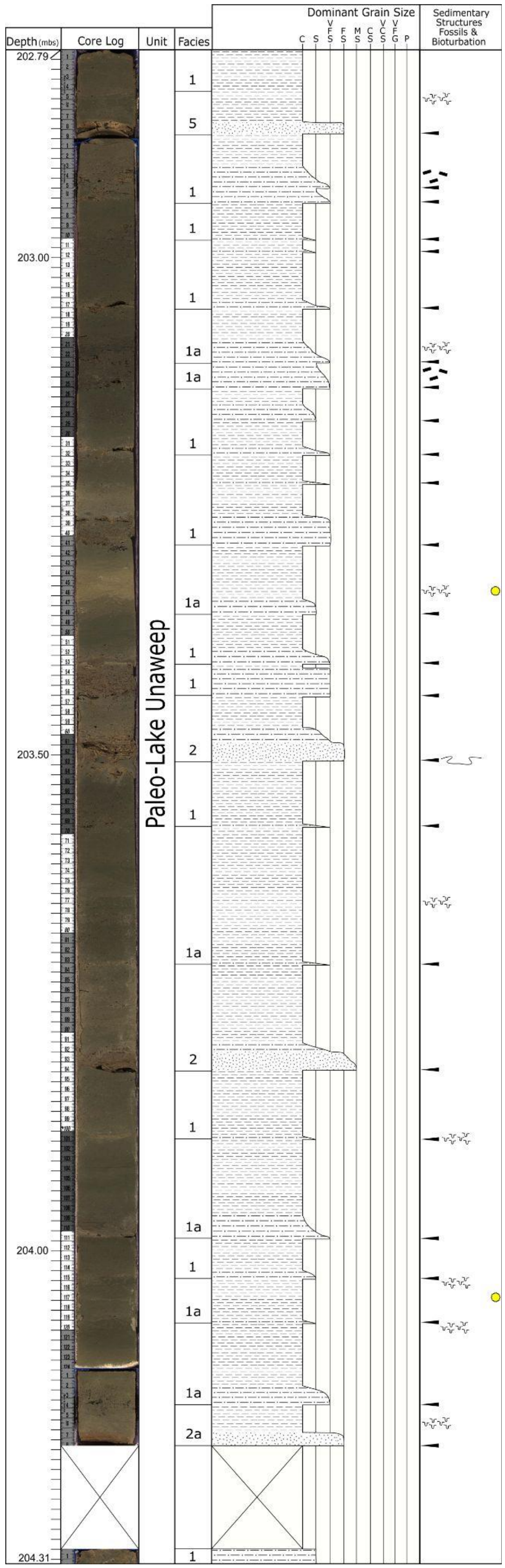
Depth (mbs)
Core Log
Unit
Facies
Dominant Grain Size
C S VFS FS MS CS VCS VFG P
Sedimentary Structures Fossils & Bioturbation
202.79
203.00
203.50
204.00
204.31
Paleo-Lake Unaweep
1
5
1
1
1
1a
1a
1
1
1a
1
1
2
1
1a
2
1
1a
1
1a
1a
2a
1

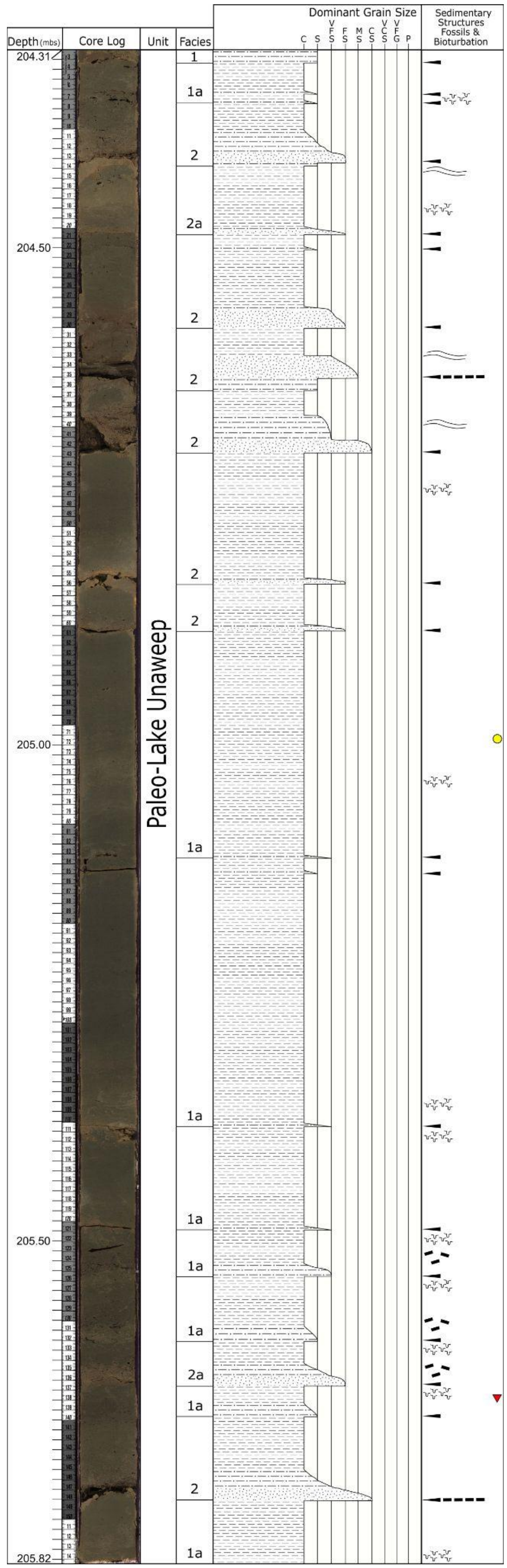
Depth (mbs)
Core Log
Unit
Facies
Dominant Grain Size
C S VFS FS MS CS VCS VFG P
Sedimentary Structures Fossils & Bioturbation
204.31
204.50
205.00
205.50
205.82
Paleo-Lake Unaweep
1
1a
2
2a
2
2
2
2
2
1a
1a
1a
1a
1a
2a
1a
2
1a

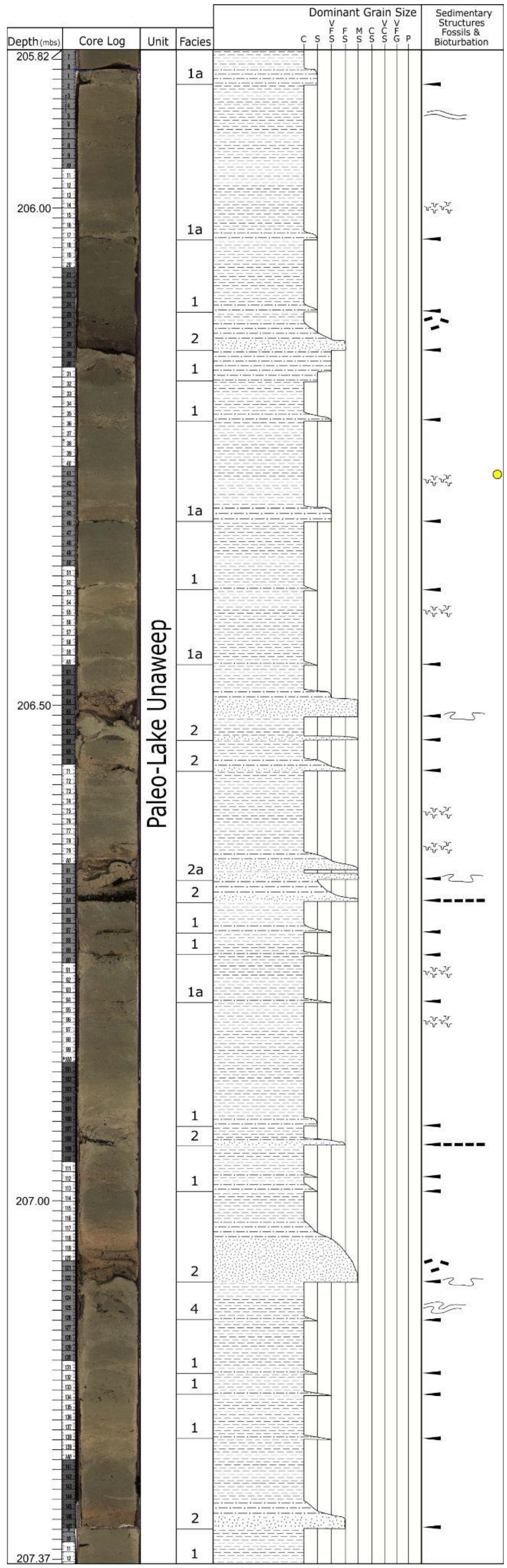
Depth (mbs)
Core Log
Unit
Facies
Dominant Grain Size
C S VFS FS MS CS VCS VFG P
Sedimentary Structures Fossils & Bioturbation
205.82
206.00
206.50
207.00
207.37
Paleo-Lake Unaweep
1a
1a
1
2
1
1
1a
1
1a
2
2
2a
2
1
1
1a
1
2
1
2
4
1
1
1
2
1

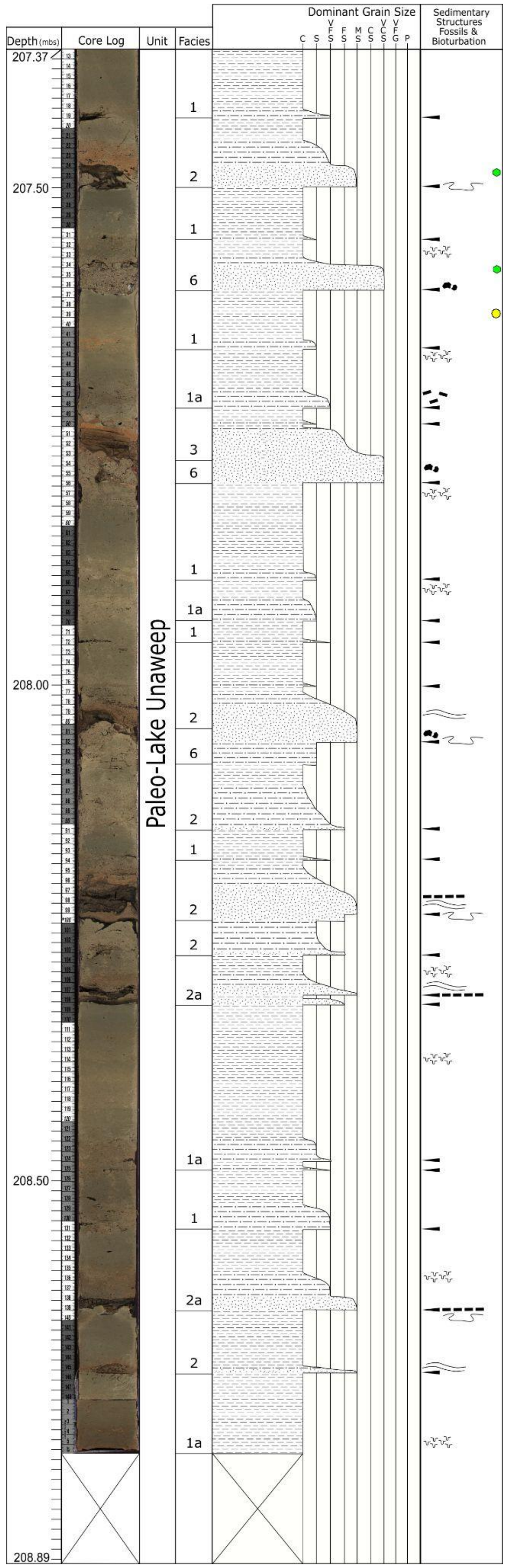
Depth (mbs)
Core Log
Unit
Facies
Dominant Grain Size
C S VFS FS MS CS VCS VFG P
Sedimentary Structures Fossils & Bioturbation
207.37
207.50
208.00
208.50
208.89
Paleo-Lake Unaweep
1
2
1
6
1
1a
3
6
1
1a
1
2
6
2
1
2
2
2a
1a
1
2a
2
1a

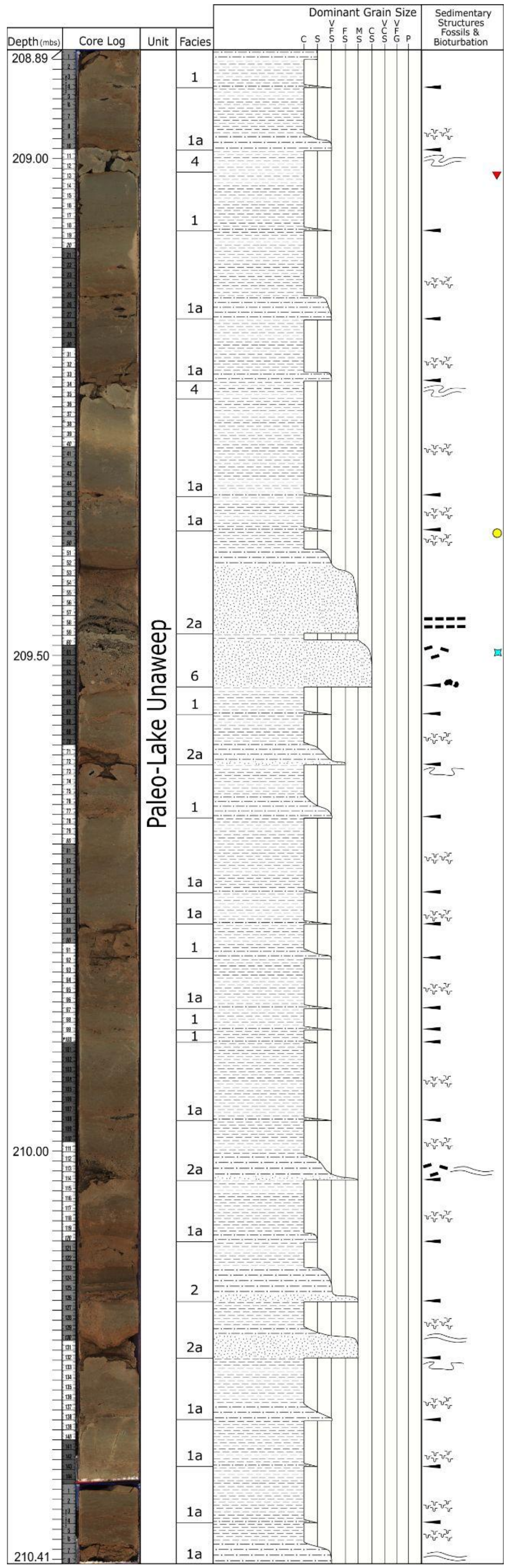

Depth (mbs)
Core Log
Unit
Facies
Dominant Grain Size
C S VFS FS MS CS VCS VFG P
Sedimentary Structures Fossils & Bioturbation
208.89
209.00
209.50
210.00
210.41
Paleo-Lake Unaweep
1
1a
4
1
1a
1a
4
1a
1a
2a
6
1
2a
1
1a
1a
1
1a
1
1
1a
2a
1a
2
2a
1a
1a
1a
1a

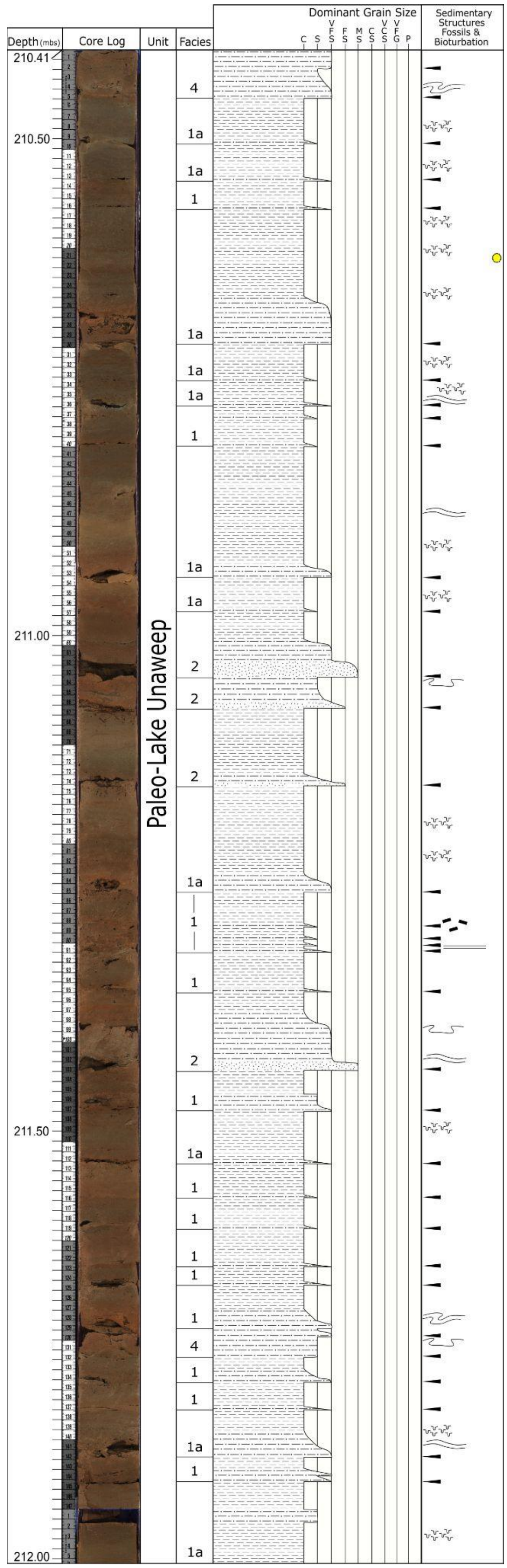
Depth (mbs)
Core Log
Unit
Facies
Dominant Grain Size
C S VFS FS MS CS VCS VFG P
Sedimentary Structures Fossils & Bioturbation
210.41
210.50
211.00
211.50
212.00
Paleo-Lake Unaweep
4
1a
1a
1
1a
1a
1a
1
1a
1a
2
2
2
1a
1
1
2
1
1a
1
1
1
1
1
4
1
1
1a
1
1a

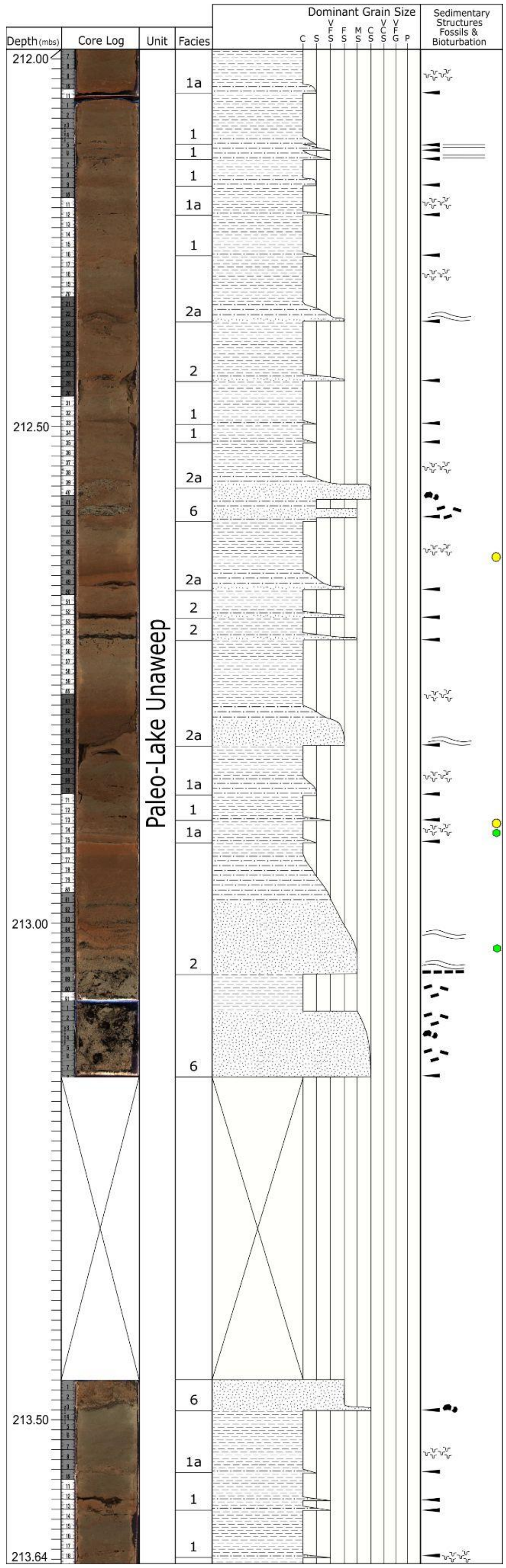
Depth (mbs)
Core Log
Unit
Facies
Dominant Grain Size
C S VFS FS MS CS VCS VFG P
Sedimentary Structures Fossils & Bioturbation
212.00
212.50
213.00
213.50
213.64
Paleo-Lake Unaweep
1a
1
1
1
1a
1
2a
2
1
1
2a
6
2a
2
2
2a
1a
1
1a
2
6
6
1a
1
1

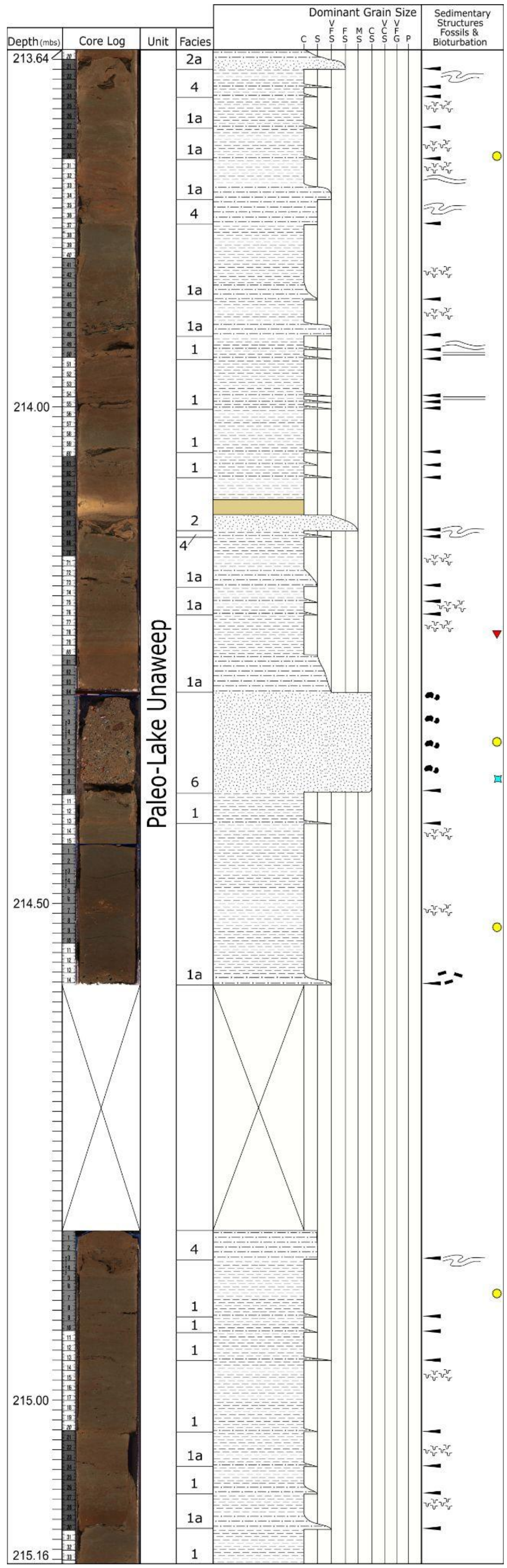

Depth (mbs)
Core Log
Unit
Facies
Dominant Grain Size
C S VFS FS MS CS VCS VFG P
Sedimentary Structures Fossils & Bioturbation
213.64
214.00
214.50
215.00
215.16
Paleo-Lake Unaweep
2a
4
1a
1a
1a
4
1a
1a
1
1
1
1
2
4
1a
1a
1a
6
1
1a
4
1
1
1
1
1a
1
1a
1

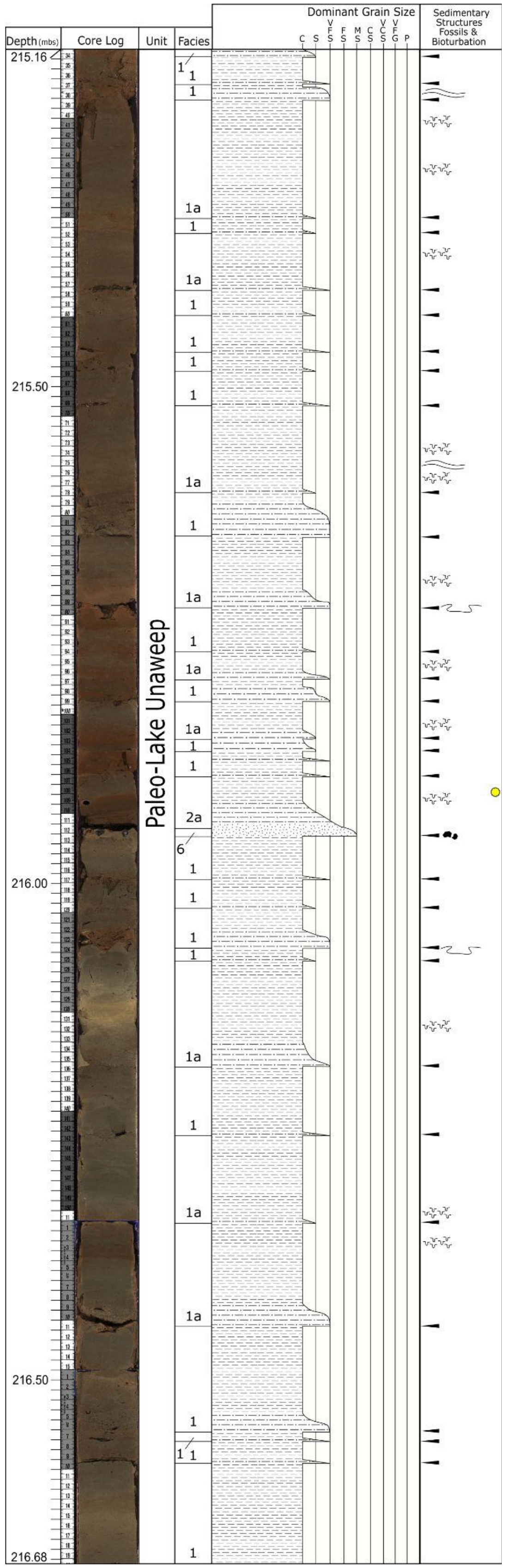
Depth (mbs)
Core Log
Unit
Facies
Dominant Grain Size
C S VFS FS MS CS VCS VFG P
Sedimentary Structures Fossils & Bioturbation
215.16
215.50
216.00
216.50
216.68
Paleo-Lake Unaweep
1a
2a
6
1

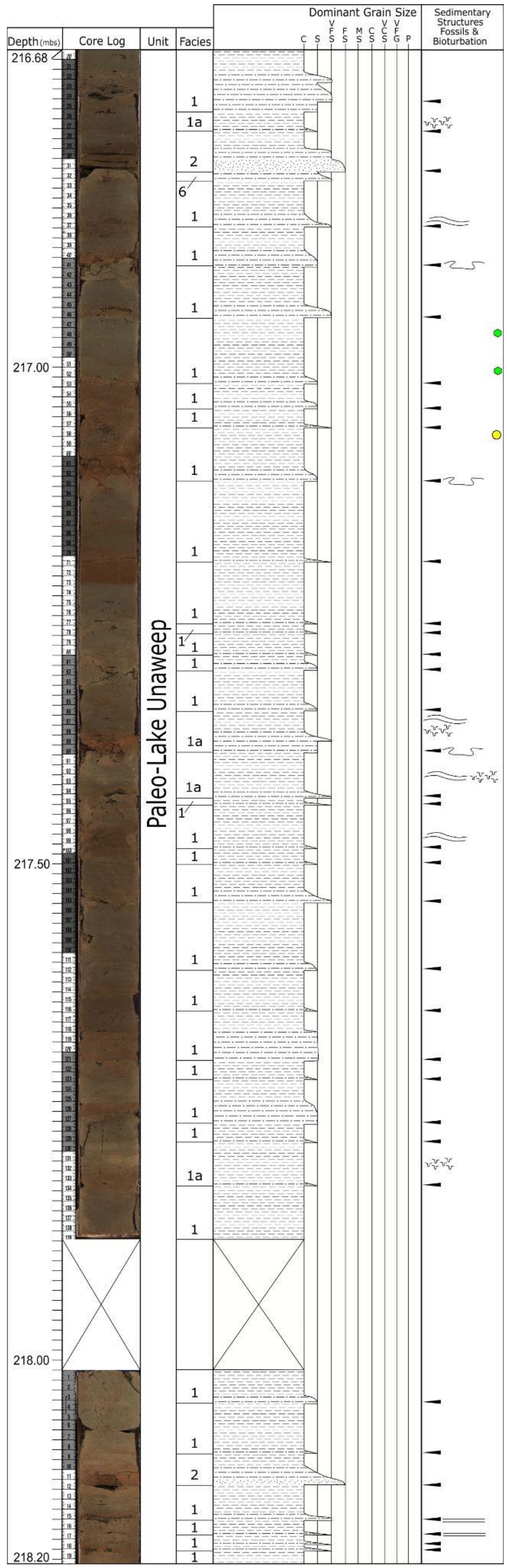
Depth (mbs)
Core Log
Unit
Facies
Dominant Grain Size
C S VFS FS MS CS VCS VFG P
Sedimentary Structures Fossils & Bioturbation
216.68
217.00
217.50
218.00
218.20
Paleo-Lake Unaweep

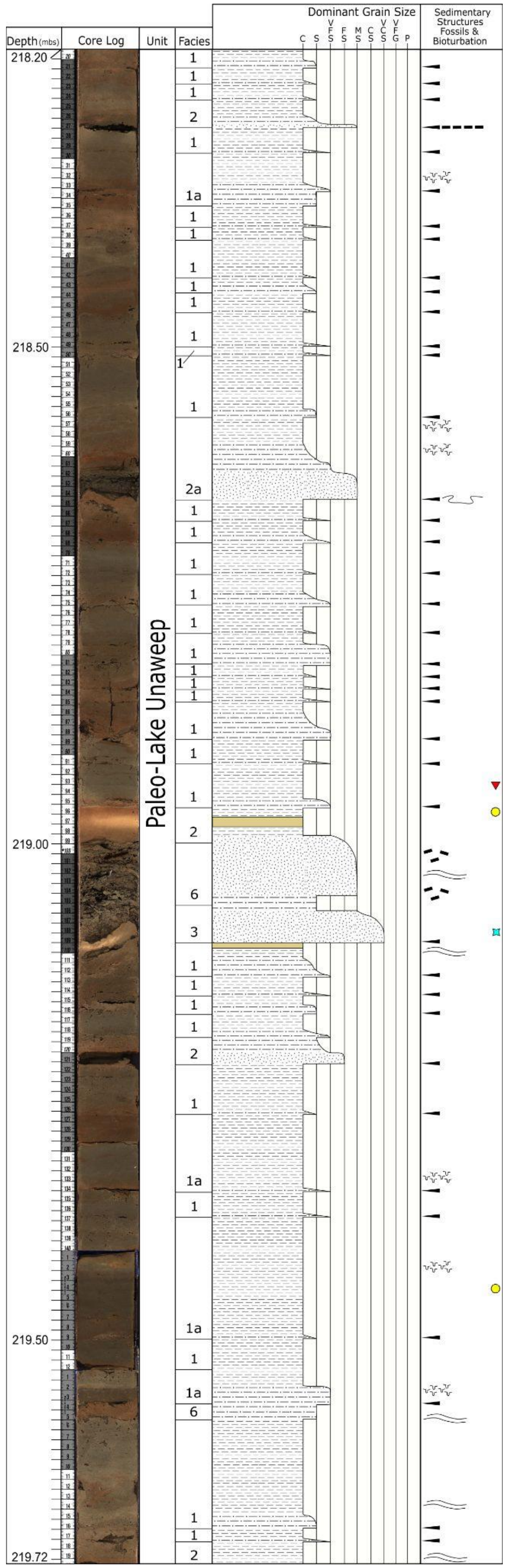
Depth (mbs)
Core Log
Unit
Facies
Dominant Grain Size
C S VFS FS MS CS VCS VFG P
Sedimentary Structures Fossils & Bioturbation
218.20
218.50
219.00
219.50
219.72
Paleo-Lake Unaweep
1
1
1
2
1
1a
1
1
1
1
1
1
1
1
2a
1
1
1
1
1
1
1
1
1
1
1
1
2
6
3
1
1
1
1
2
1
1a
1
1a
1
1a
6
1
1
2

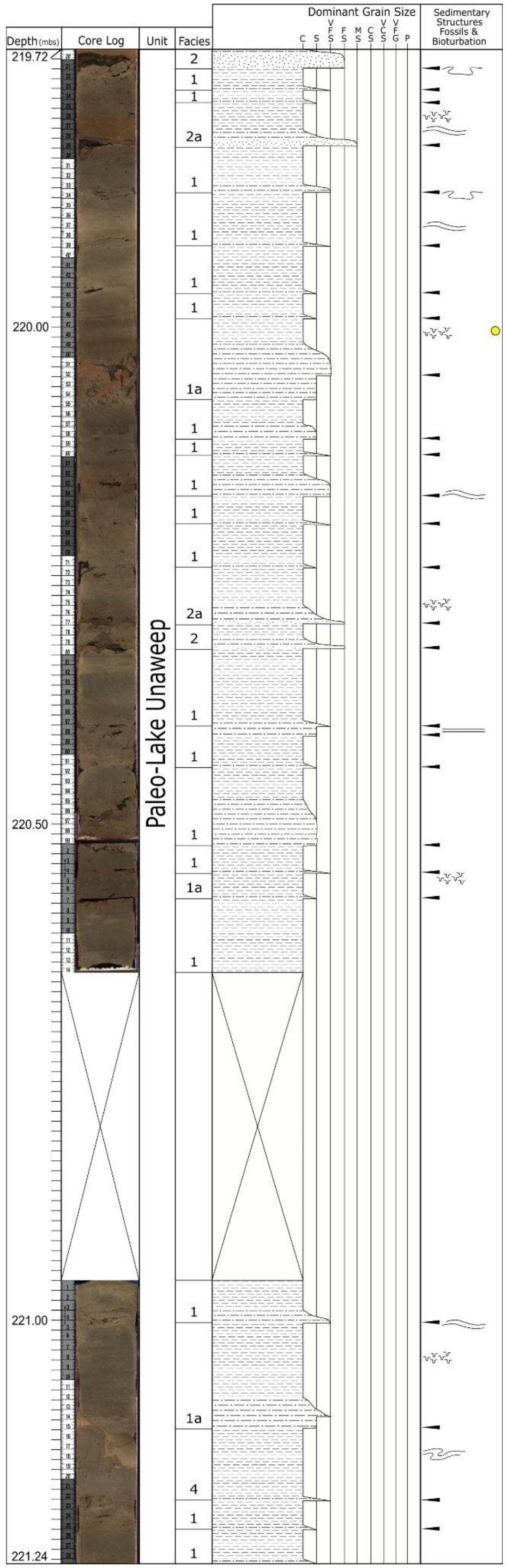

Depth (mbs)
Core Log
Unit
Facies
Dominant Grain Size
C S VFS FS MS CS VCS VFG P
Sedimentary Structures Fossils & Bioturbation
219.72
220.00
220.50
221.00
221.24
Paleo-Lake Unaweep
2
1
1
2a
1
1
1
1
1a
1
1
1
1
1
2a
2
1
1
1
1
1a
1
1
1a
4
1
1

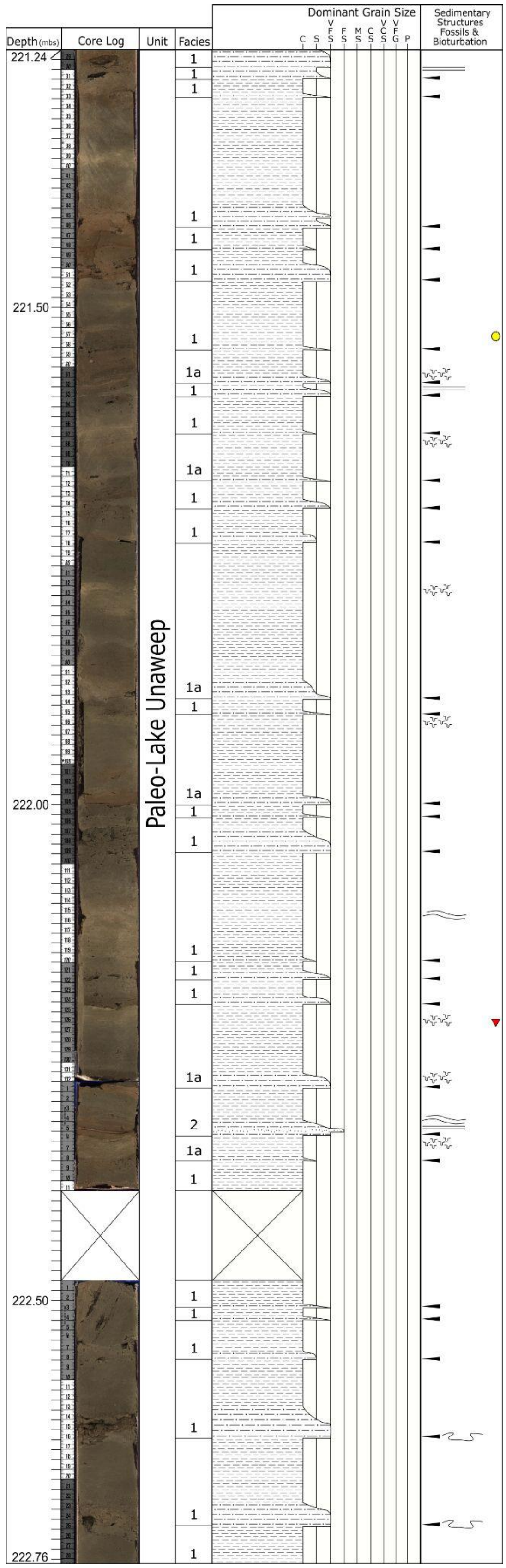
Depth (mbs)
Core Log
Unit
Facies
Dominant Grain Size
C S VFS FS MS CS VCS VFG P
Sedimentary Structures Fossils & Bioturbation
221.24
221.50
222.00
222.50
222.76
Paleo-Lake Unaweep
1
1a
2

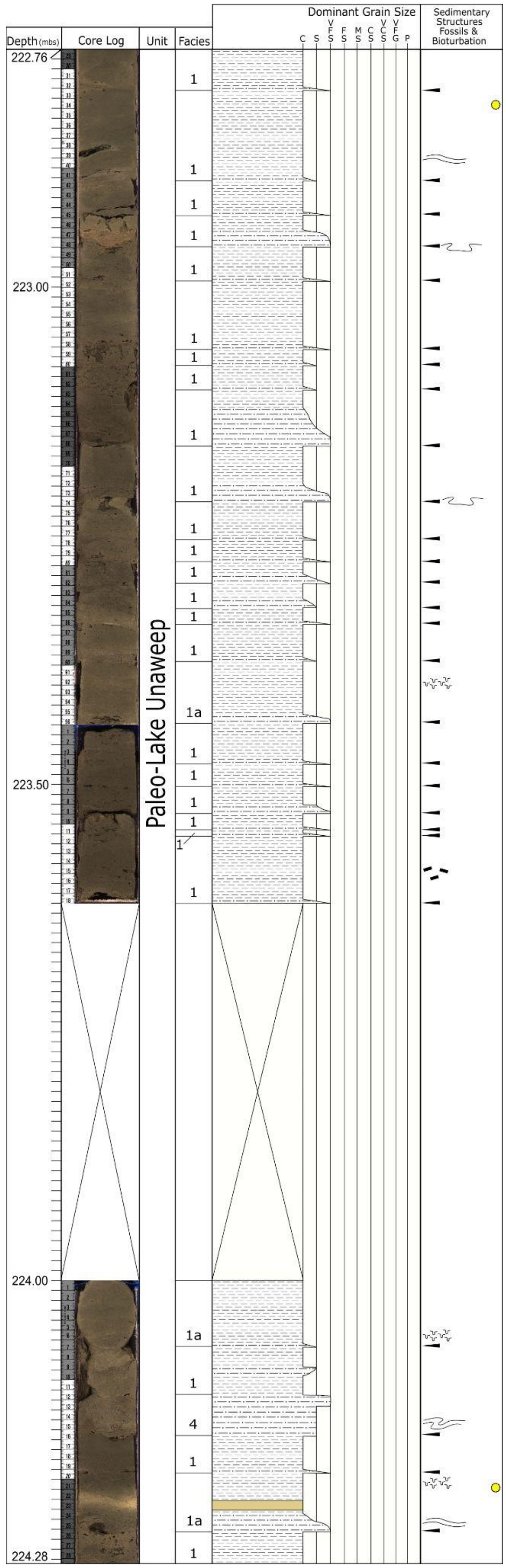
Depth (mbs)
Core Log
Unit
Facies
Dominant Grain Size
C S VFS FS MS CS VCS VFG P
Sedimentary Structures Fossils & Bioturbation
222.76
223.00
223.50
224.00
224.28
Paleo-Lake Unaweep
1
1a
4

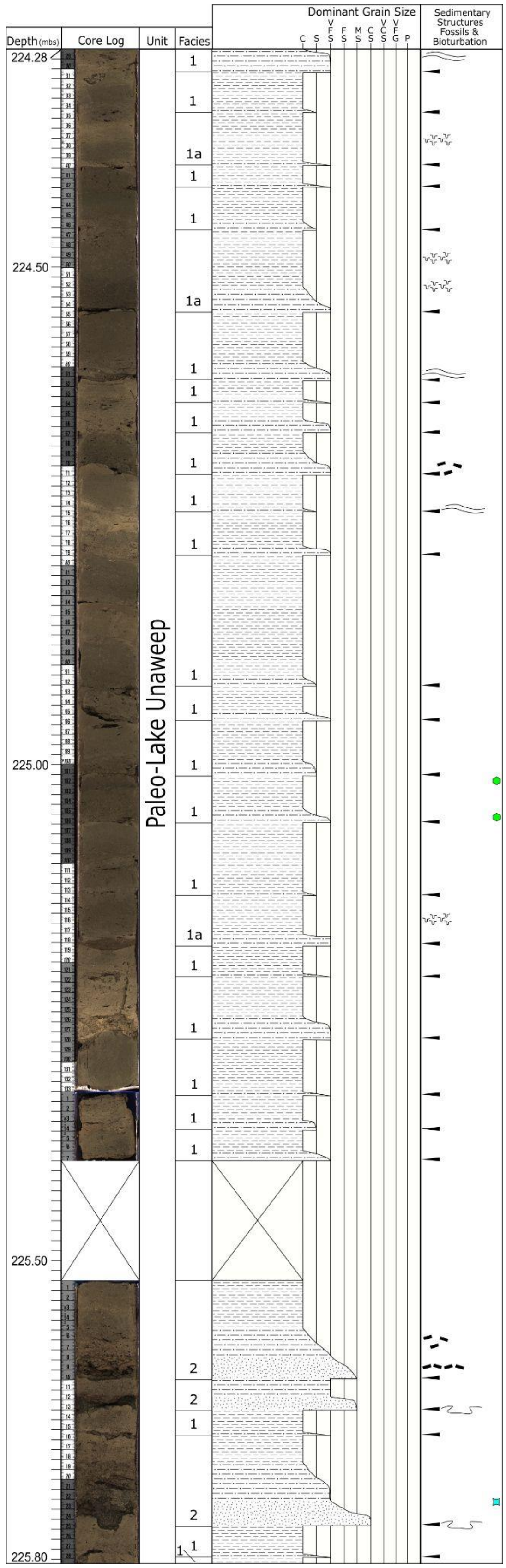

Depth (mbs)
Core Log
Unit
Facies
Dominant Grain Size
C S VFS FS MS CS VCS VFG P
Sedimentary Structures Fossils & Bioturbation
224.28
224.50
225.00
225.50
225.80
Paleo-Lake Unaweep
1
1
1a
1
1
1a
1
1
1
1
1
1
1
1
1
1
1
1a
1
1
1
1
1
2
2
1
2
1

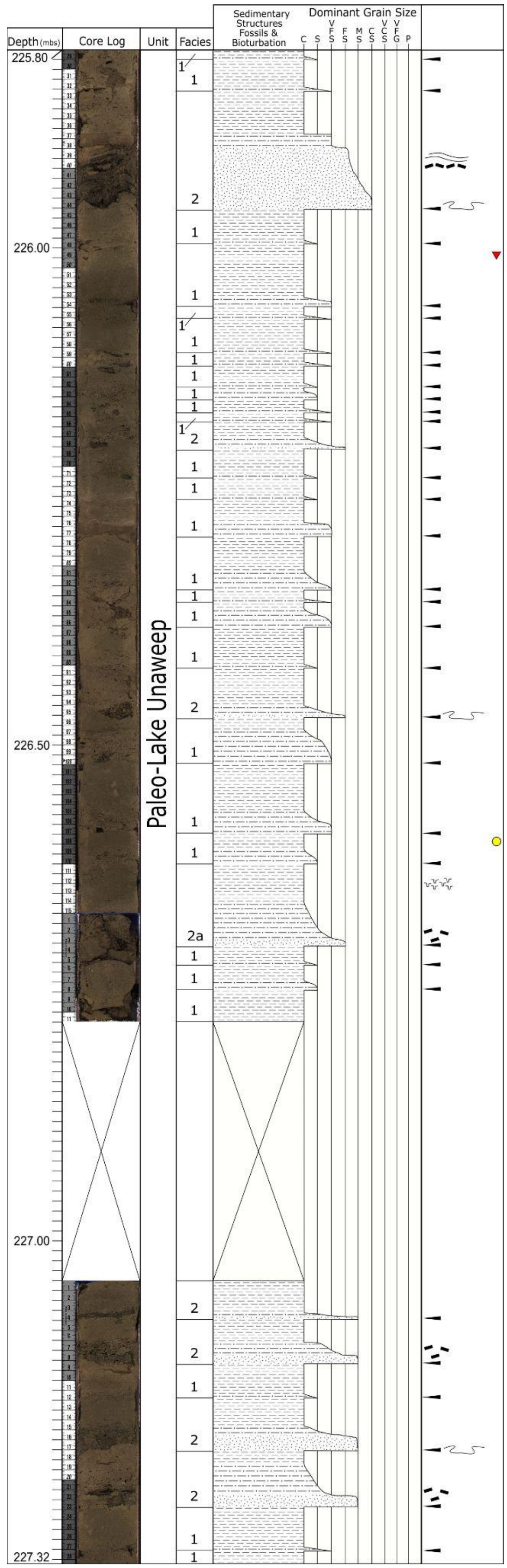
Depth (mbs)
Core Log
Unit
Facies
Sedimentary Structures Fossils & Bioturbation
Dominant Grain Size
C S VFS FS MS CS VCS VFG P
225.80
226.00
226.50
227.00
227.32
Paleo-Lake Unaweep
1
2
2a

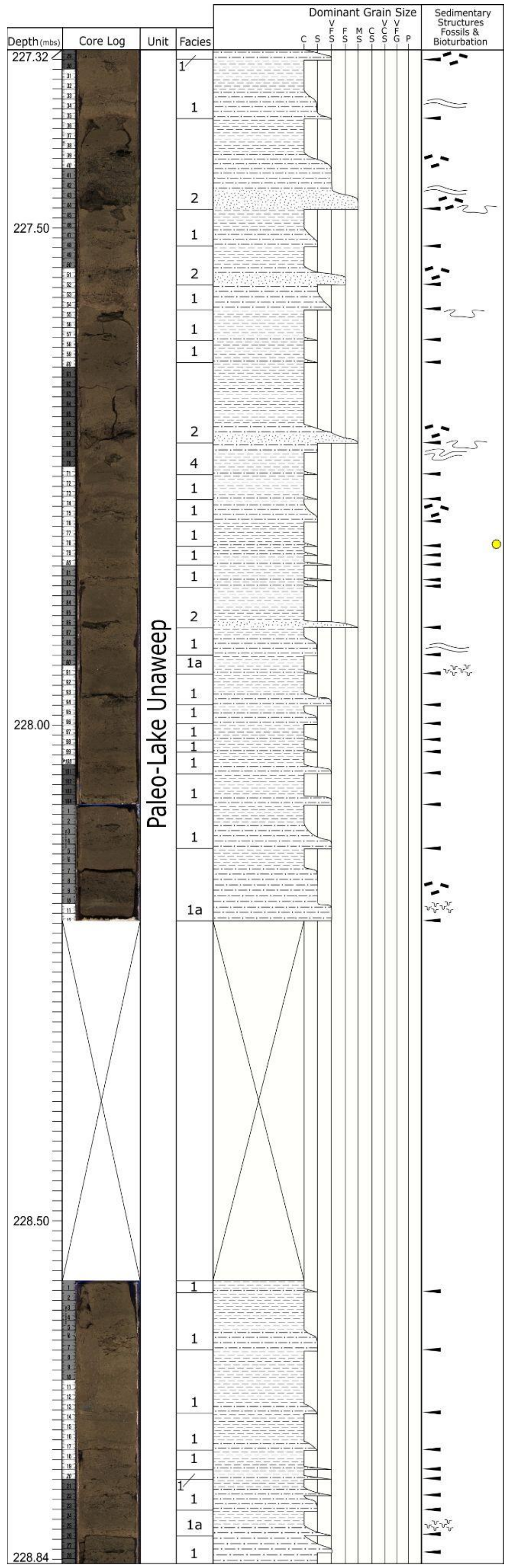
Depth (mbs)
Core Log
Unit
Facies
Dominant Grain Size
C S VFS FS MS CS VCS VFG P
Sedimentary Structures Fossils & Bioturbation
227.32
227.50
228.00
228.50
228.84
Paleo-Lake Unaweep

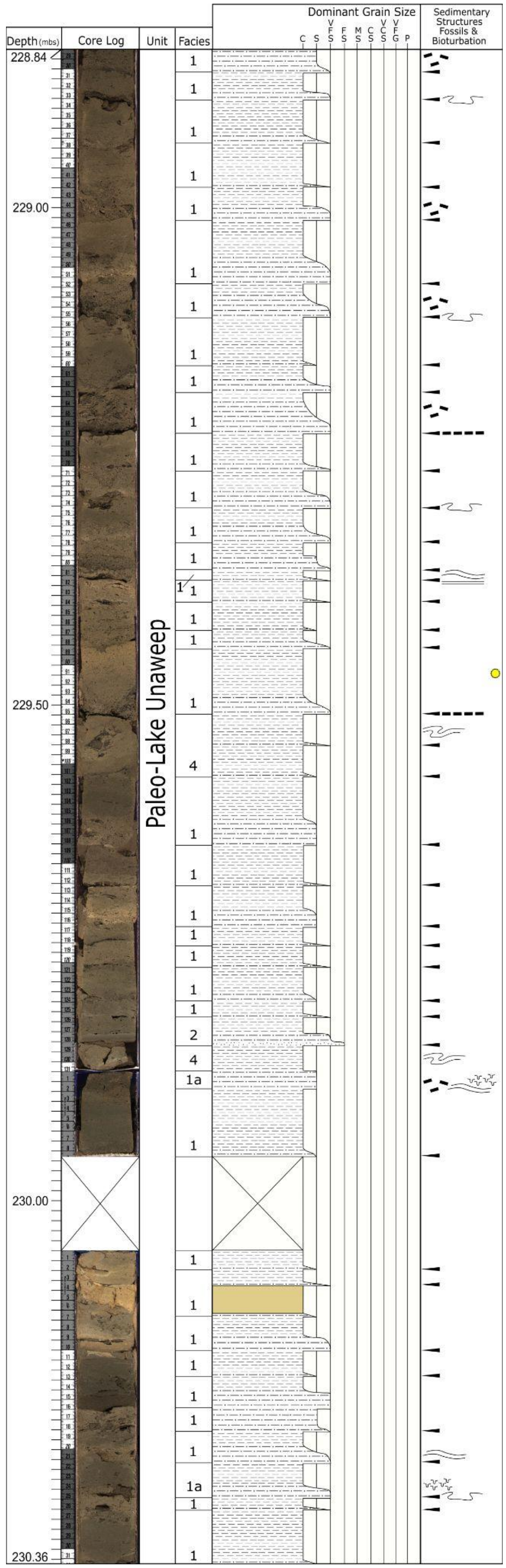

Depth (mbs)
Core Log
Unit
Facies
Dominant Grain Size
C S VFS FS MS CS VCS VFG P
Sedimentary Structures Fossils & Bioturbation
228.84
229.00
229.50
230.00
230.36
Paleo-Lake Unaweep
1
4
2
1a

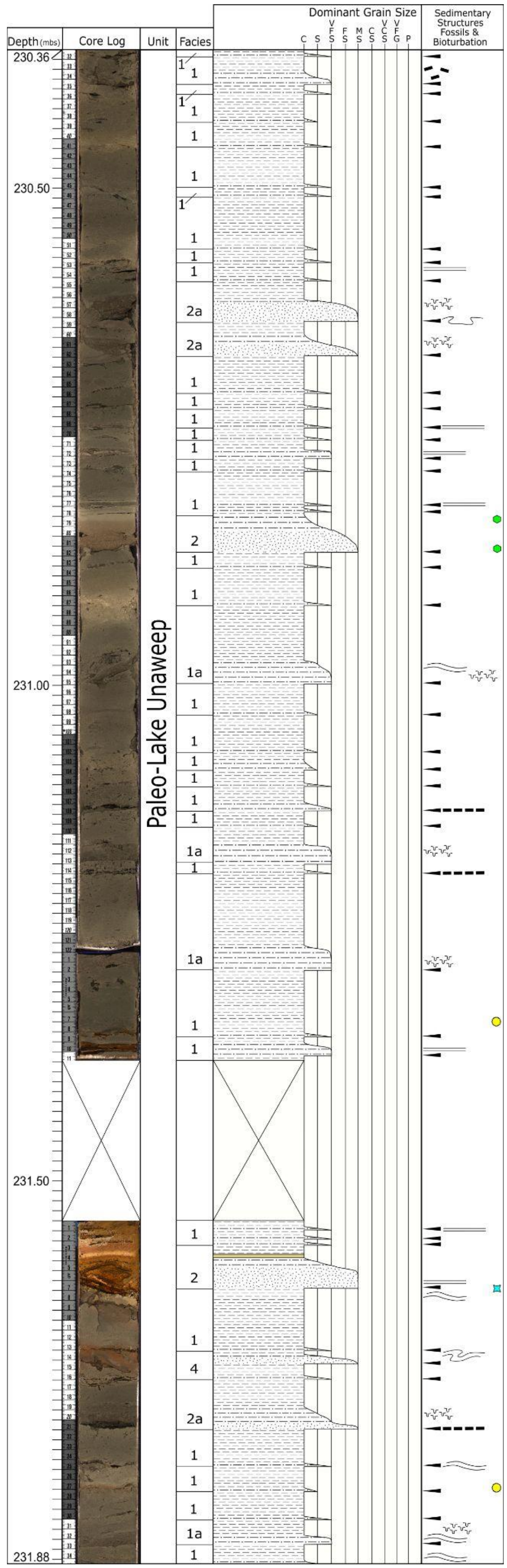
Depth (mbs)
Core Log
Unit
Facies
Dominant Grain Size
C S VFS FS MS CS VCS VFG P
Sedimentary Structures Fossils & Bioturbation
230.36
230.50
231.00
231.50
231.88
Paleo-Lake Unaweep
1
2a
2
1a
4

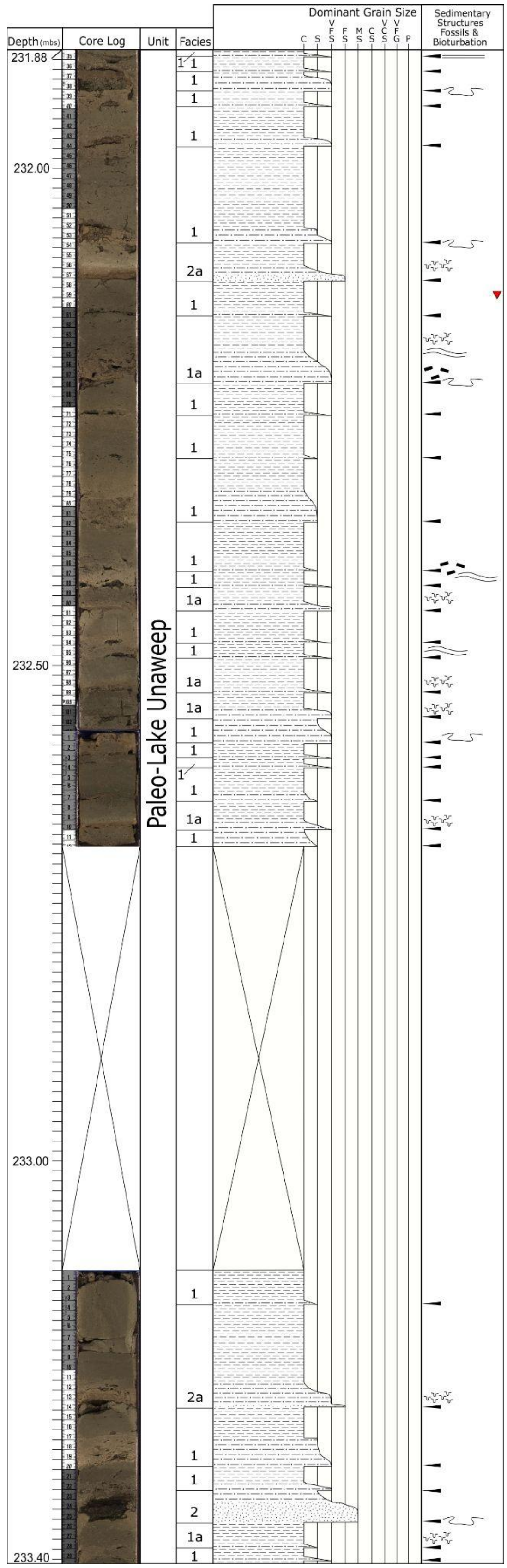
Depth (mbs)
Core Log
Unit
Facies
Dominant Grain Size
C S VFS FS MS CS VCS VFG P
Sedimentary Structures Fossils & Bioturbation
231.88
232.00
232.50
233.00
233.40
Paleo-Lake Unaweep
1a
2a
2

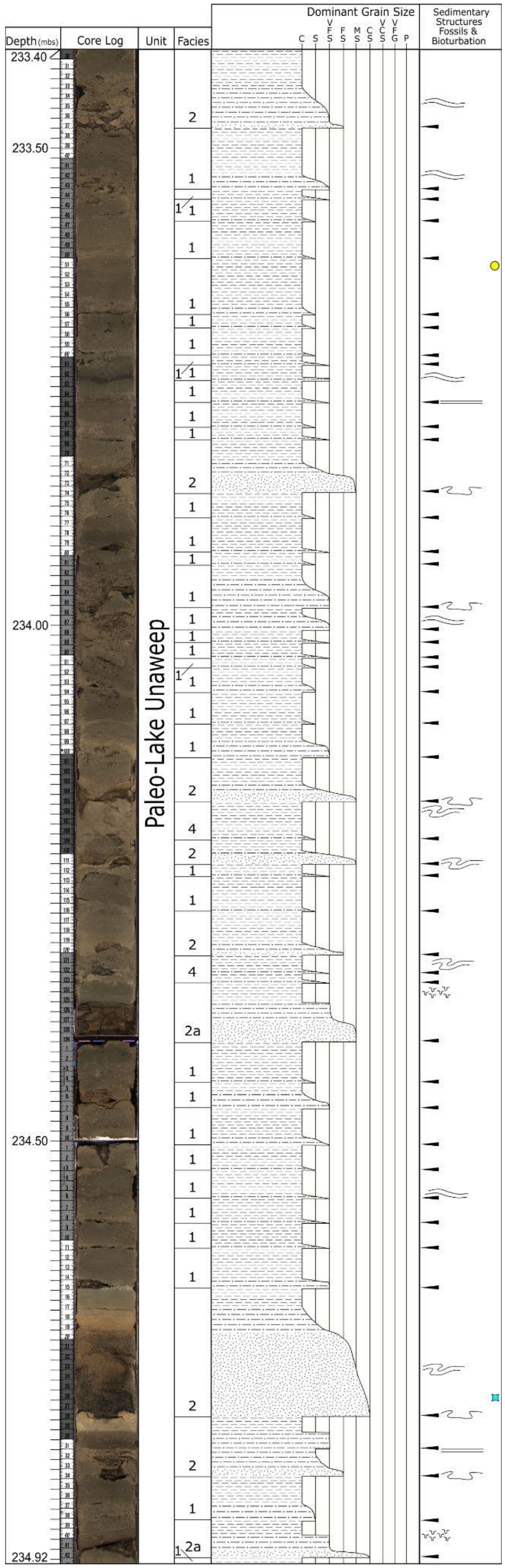
Depth (mbs)
Core Log
Unit
Facies
Dominant Grain Size
C S VFS FS MS CS VCS VFG P
Sedimentary Structures Fossils & Bioturbation
233.40
233.50
234.00
234.50
234.92
Paleo-Lake Unaweep
2
1
1
1
1
1
1
1
1
1
1
1
2
1
1
1
1
1
1
1
1
1
1
2
4
2
1
1
2
4
2a
1
1
1
1
1
1
1
1
2
2
1
2a

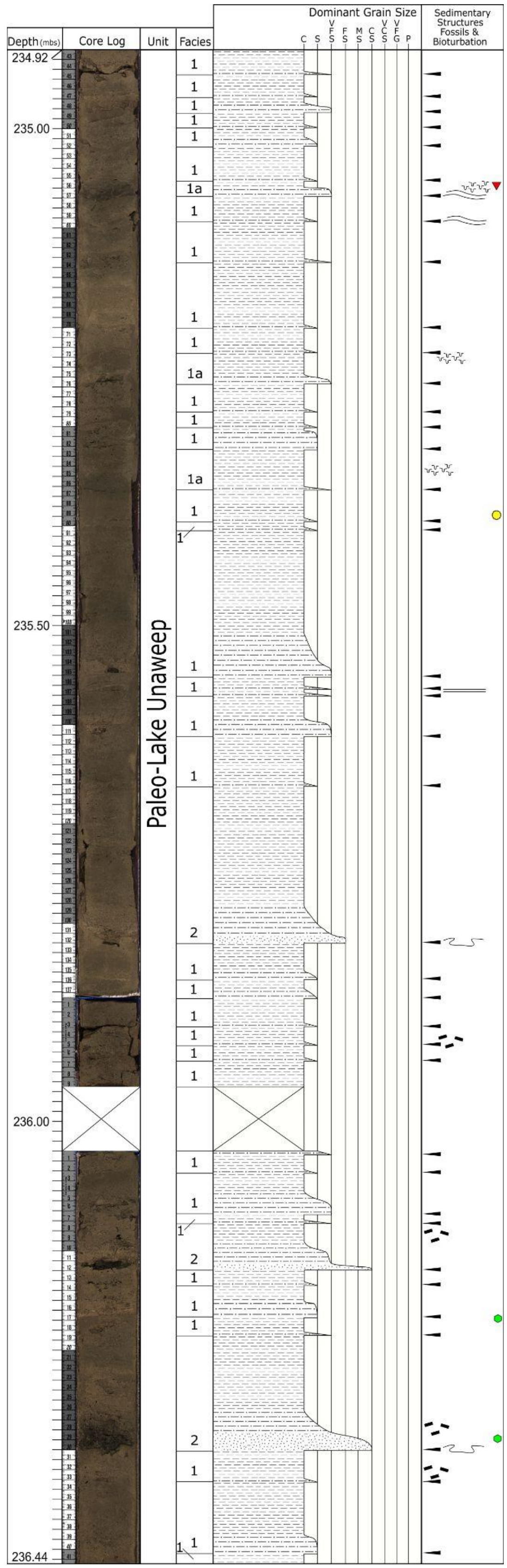

Depth (mbs)
Core Log
Unit
Facies
Dominant Grain Size
C S VFS FS MS CS VCS VFG P
Sedimentary Structures Fossils & Bioturbation
234.92
235.00
235.50
236.00
236.44
Paleo-Lake Unaweep

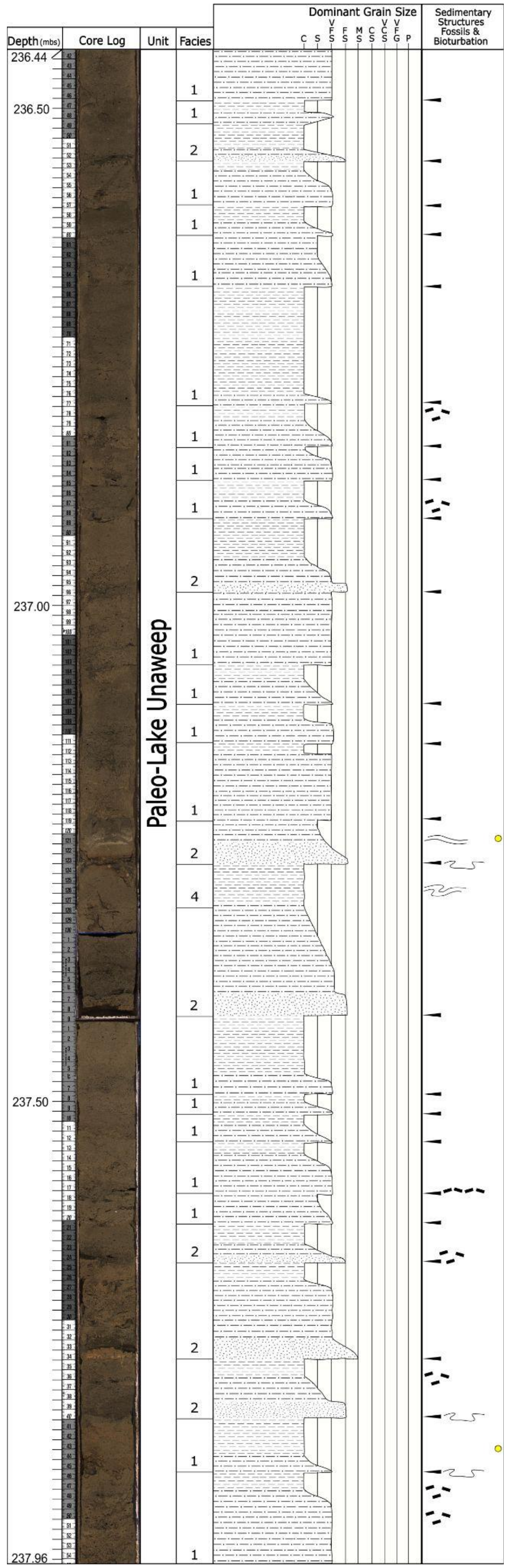
Depth (mbs)
Core Log
Unit
Facies
Dominant Grain Size
C S VFS FS MS CS VCS VFG P
Sedimentary Structures Fossils & Bioturbation
236.44
236.50
237.00
237.50
237.96
Paleo-Lake Unaweep
1
1
2
1
1
1
1
1
1
1
2
1
1
1
1
2
4
2
1
1
1
1
1
2
2
2
1
1

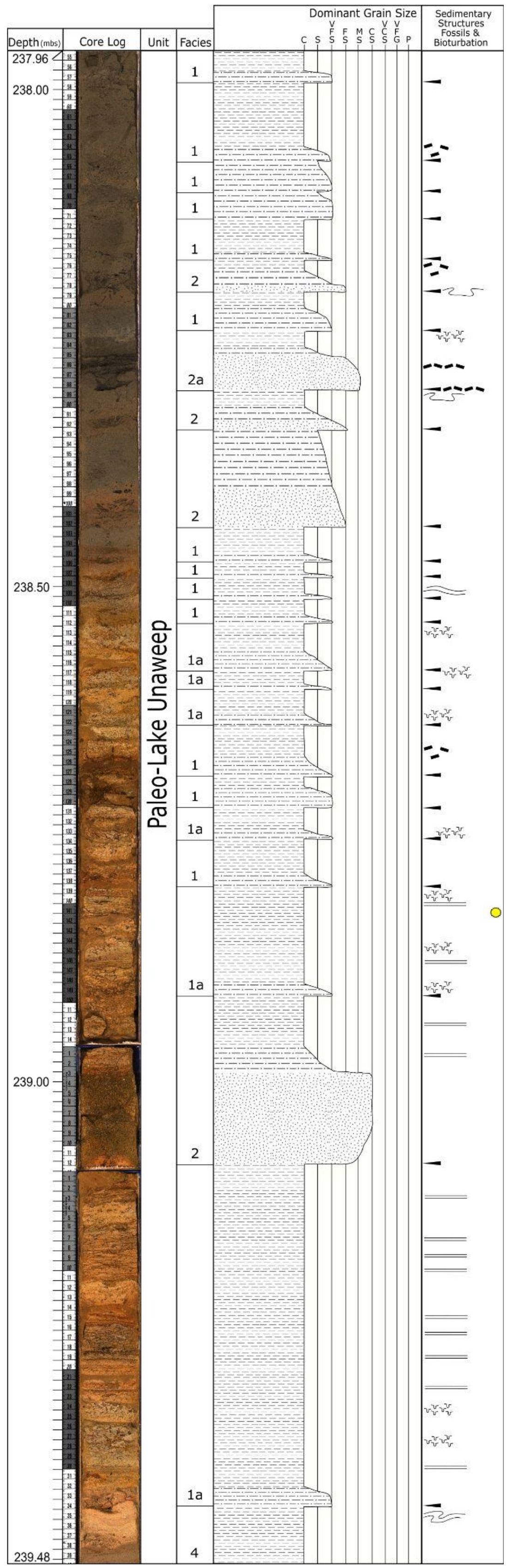
Depth (mbs)
Core Log
Unit
Facies
Dominant Grain Size
C S VFS FS MS CS VCS VFG P
Sedimentary Structures Fossils & Bioturbation
237.96
238.00
238.50
239.00
239.48
Paleo-Lake Unaweep
1
1
1
1
1
2
1
2a
2
2
1
1
1
1
1a
1a
1a
1
1
1a
1
1a
2
1a
4

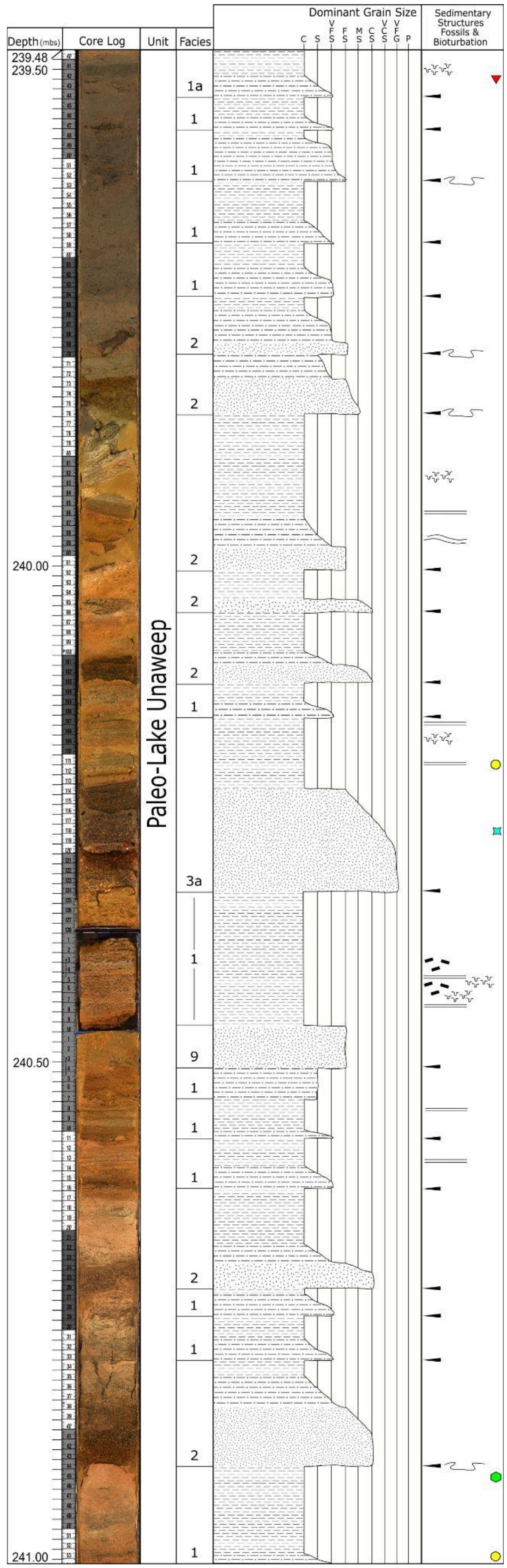
Depth (mbs)
Core Log
Unit
Facies
Dominant Grain Size
C S VFS FS MS CS VCS VFG P
Sedimentary Structures Fossils & Bioturbation
239.48
239.50
240.00
240.50
241.00
Paleo-Lake Unaweep
1a
1
1
1
1
2
2
2
2
2
1
3a
1
9
1
1
1
2
1
1
2
1

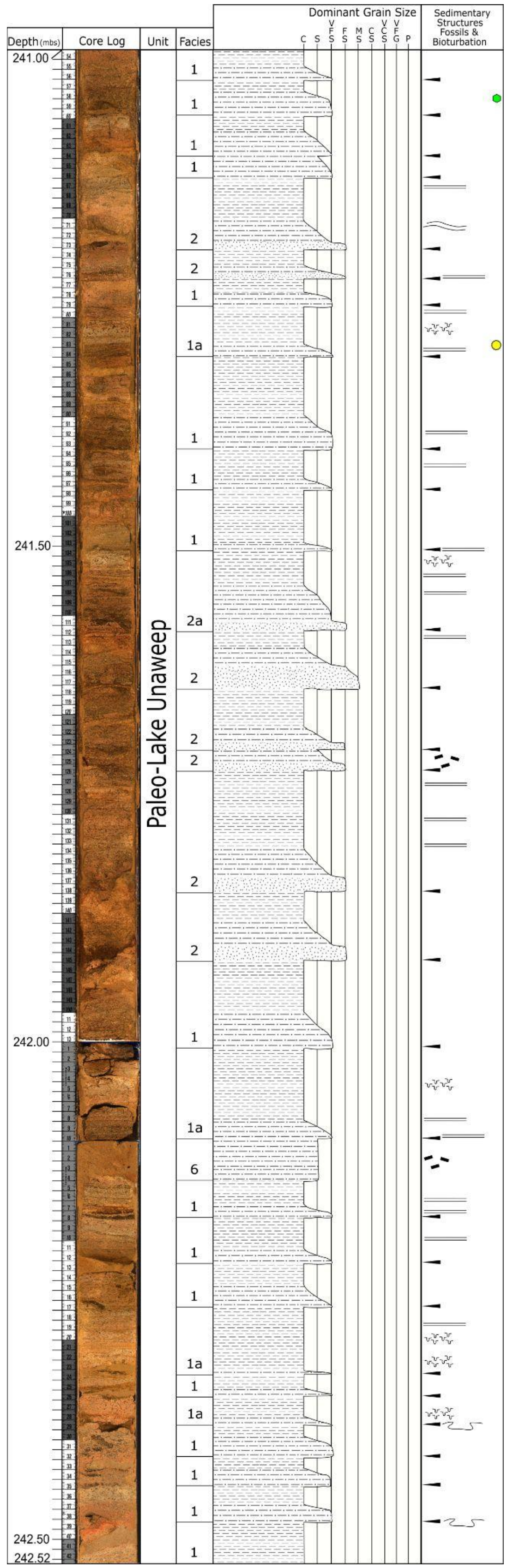
Depth (mbs)
Core Log
Unit
Facies
Dominant Grain Size
C S VFS FS MS CS VCS VFG P
Sedimentary Structures Fossils & Bioturbation
241.00
241.50
242.00
242.50
242.52
Paleo-Lake Unaweep
1
1
1
1
2
2
1
1a
1
1
1
2a
2
2
2
2
2
1
1a
6
1
1
1
1a
1
1a
1
1
1
1

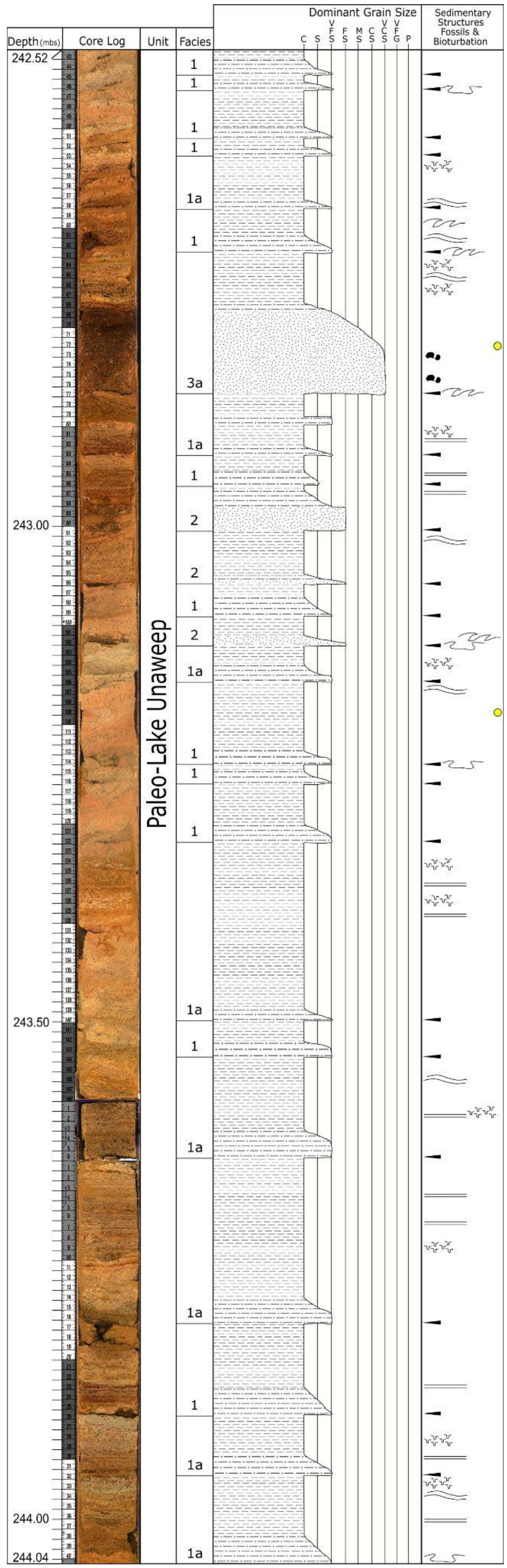
Depth (mbs)
Core Log
Unit
Facies
Dominant Grain Size
C S VFS FS MS CS VCS VFG P
Sedimentary Structures Fossils & Bioturbation
242.52
243.00
243.50
244.00
244.04
Paleo-Lake Unaweep
1
1
1
1
1a
1
3a
1a
1
2
2
1
2
1a
1
1
1
1a
1
1a
1a
1
1a
1a

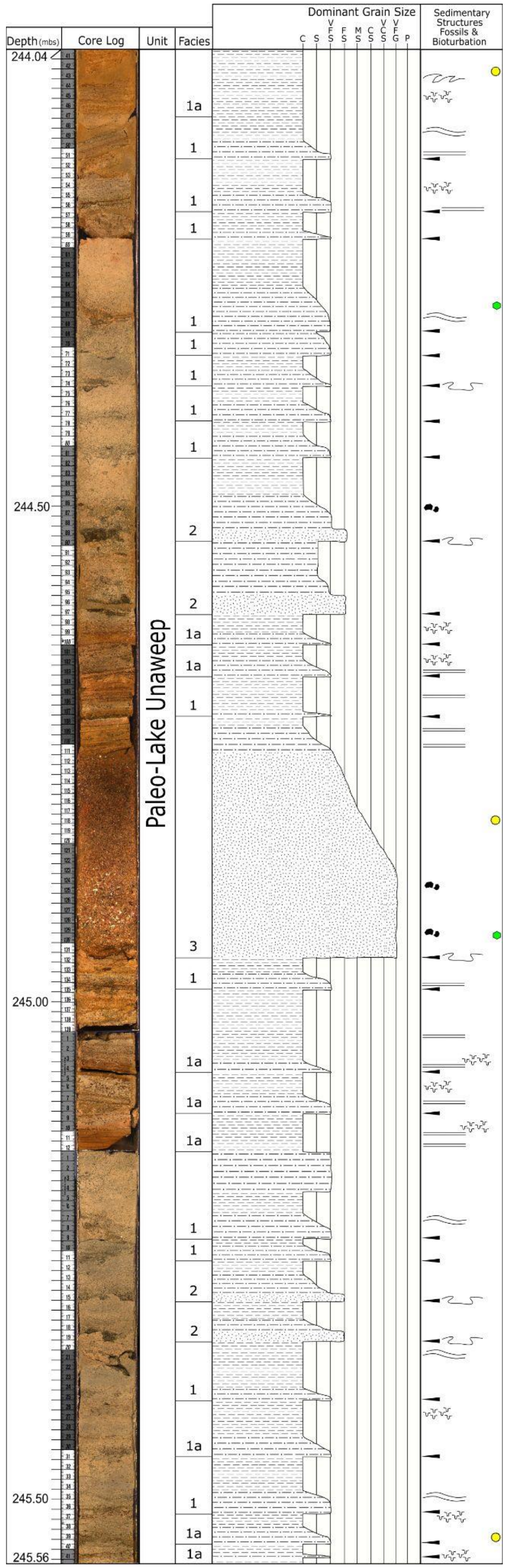
Depth (mbs)
Core Log
Unit
Facies
Dominant Grain Size
C S VFS FS MS CS VCS VFG P
Sedimentary Structures Fossils & Bioturbation
244.04
244.50
245.00
245.50
245.56
Paleo-Lake Unaweep
1a
1
1
1
1
1
1
1
1
2
2
1a
1a
1
3
1
1a
1a
1a
1
1
2
2
1
1a
1
1a
1a

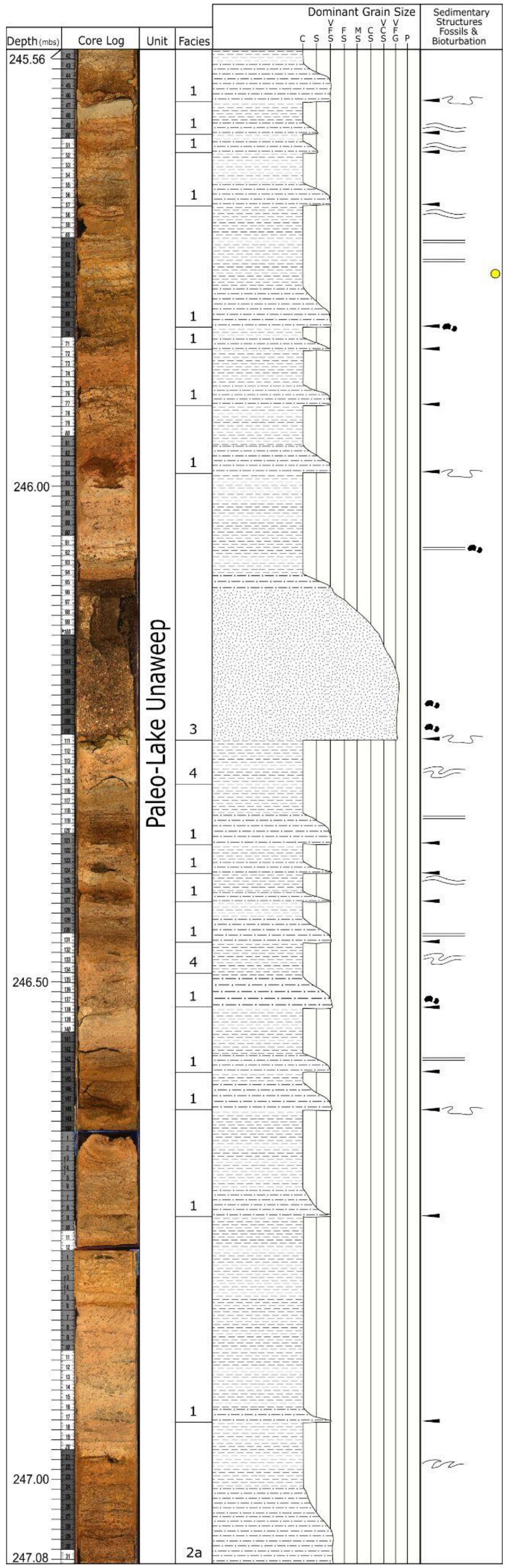
Depth (mbs)
Core Log
Unit
Facies
Dominant Grain Size
C S VFS FS MS CS VCS VFG P
Sedimentary Structures Fossils & Bioturbation
245.56
246.00
246.50
247.00
247.08
Paleo-Lake Unaweep
1
1
1
1
1
1
1
1
3
4
1
1
1
1
4
1
1
1
1
1
2a

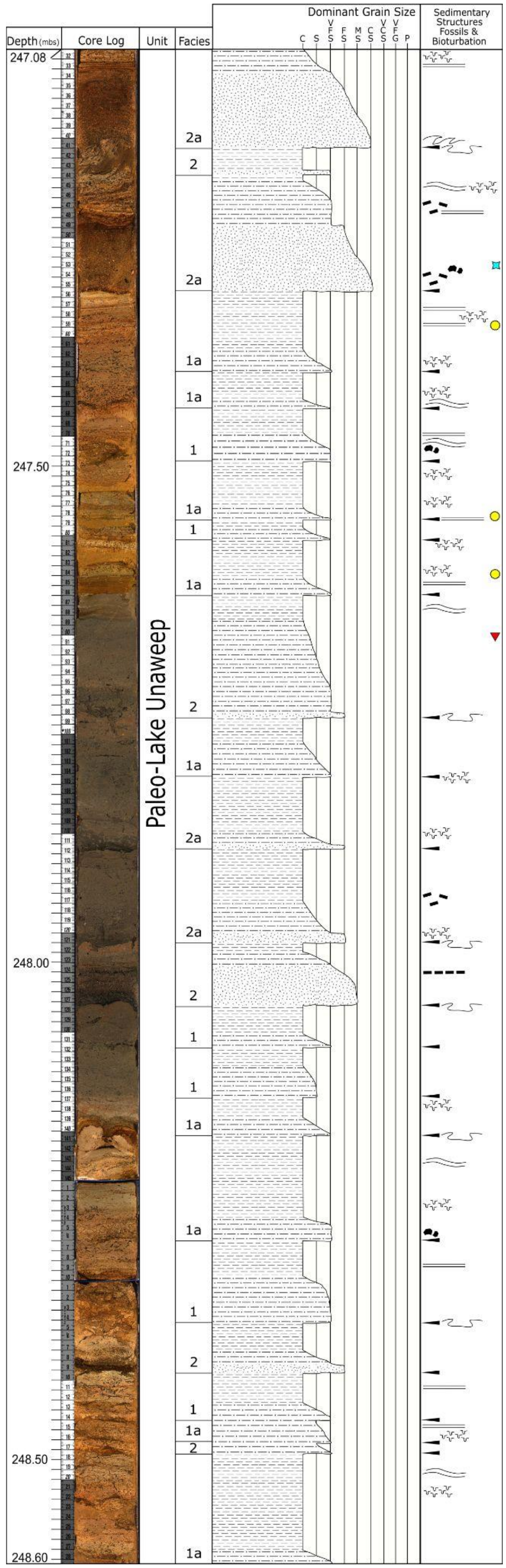
Depth (mbs)
Core Log
Unit
Facies
Dominant Grain Size
C S VFS FS MS CS VCS VFG P
Sedimentary Structures Fossils & Bioturbation
247.08
247.50
248.00
248.50
248.60
Paleo-Lake Unaweep
2a
2
2a
1a
1a
1
1a
1
1a
2
1a
2a
2a
2
1
1
1a
1a
1
2
1
1a
2
1a

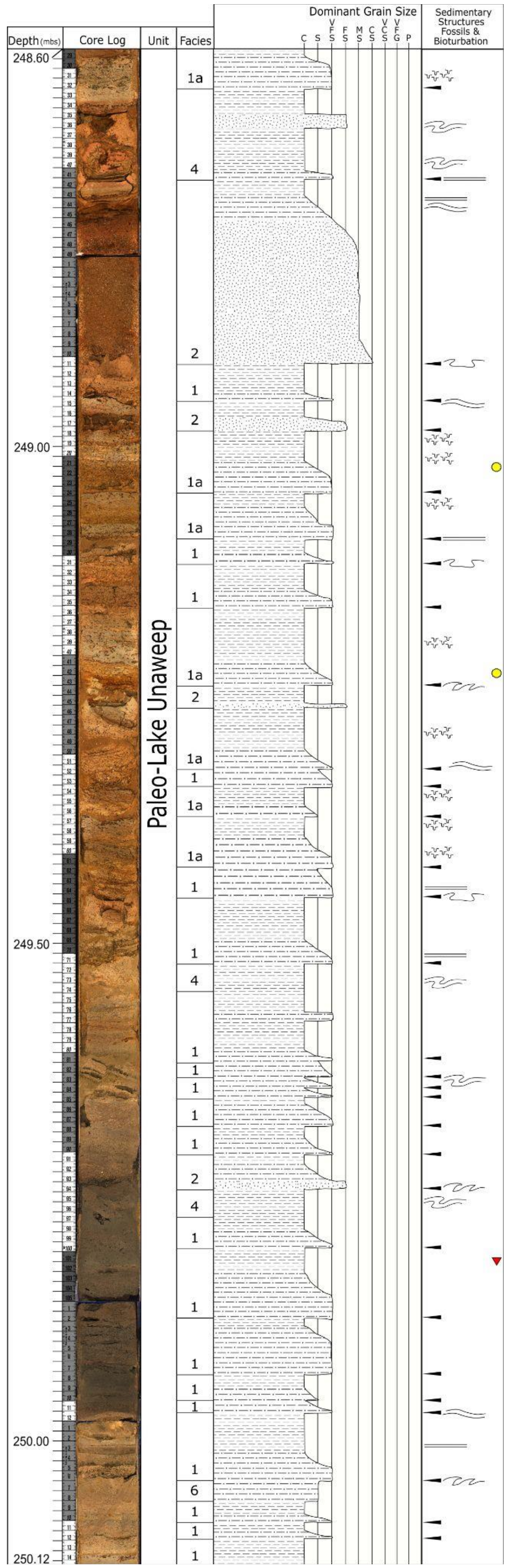
Depth (mbs)
Core Log
Unit
Facies
Dominant Grain Size
C S VFS FS MS CS VCS VFG P
Sedimentary Structures Fossils & Bioturbation
248.60
249.00
249.50
250.00
250.12
Paleo-Lake Unaweep
1a
4
2
1
2
1a
1a
1
1
1a
2
1a
1
1a
1a
1
1
4
1
1
1
1
1
2
4
1
1
1
1
1
1
6
1
1
1

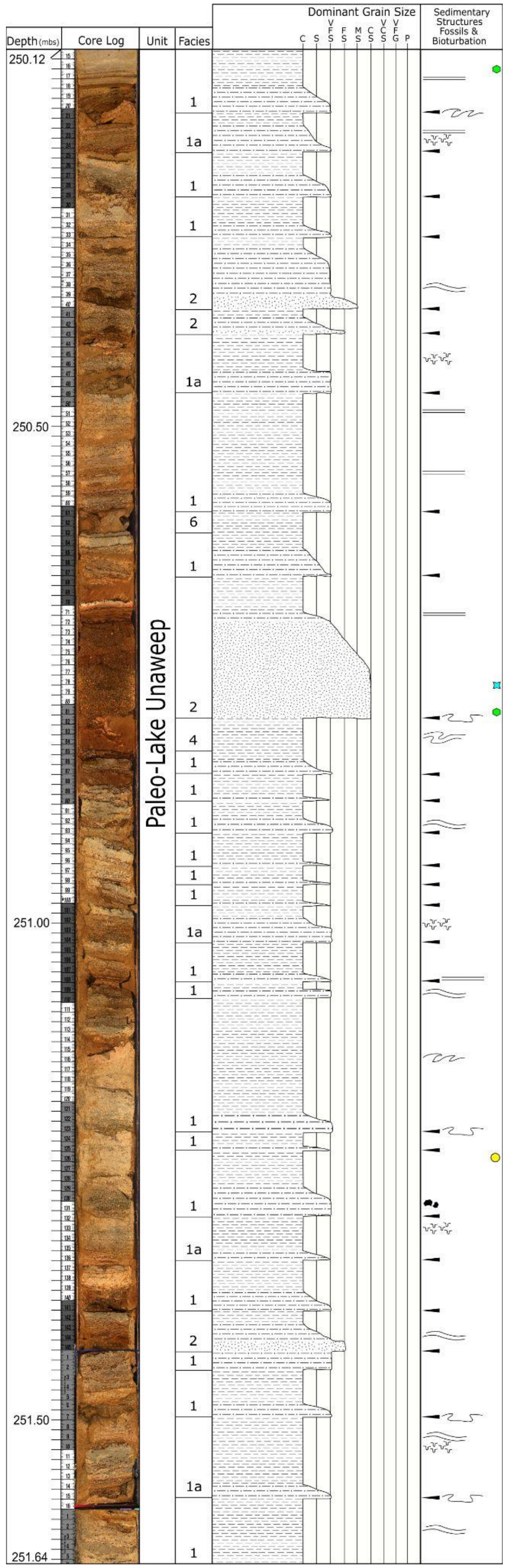

Depth (mbs)
Core Log
Unit
Facies
Dominant Grain Size
C S VFS FS MS CS VCS VFG P
Sedimentary Structures Fossils & Bioturbation
250.12
250.50
251.00
251.50
251.64
Paleo-Lake Unaweep
1
1a
1
1
2
2
1a
1
6
1
2
4
1
1
1
1
1
1
1a
1
1
1
1
1
1a
1
2
1
1
1a
1

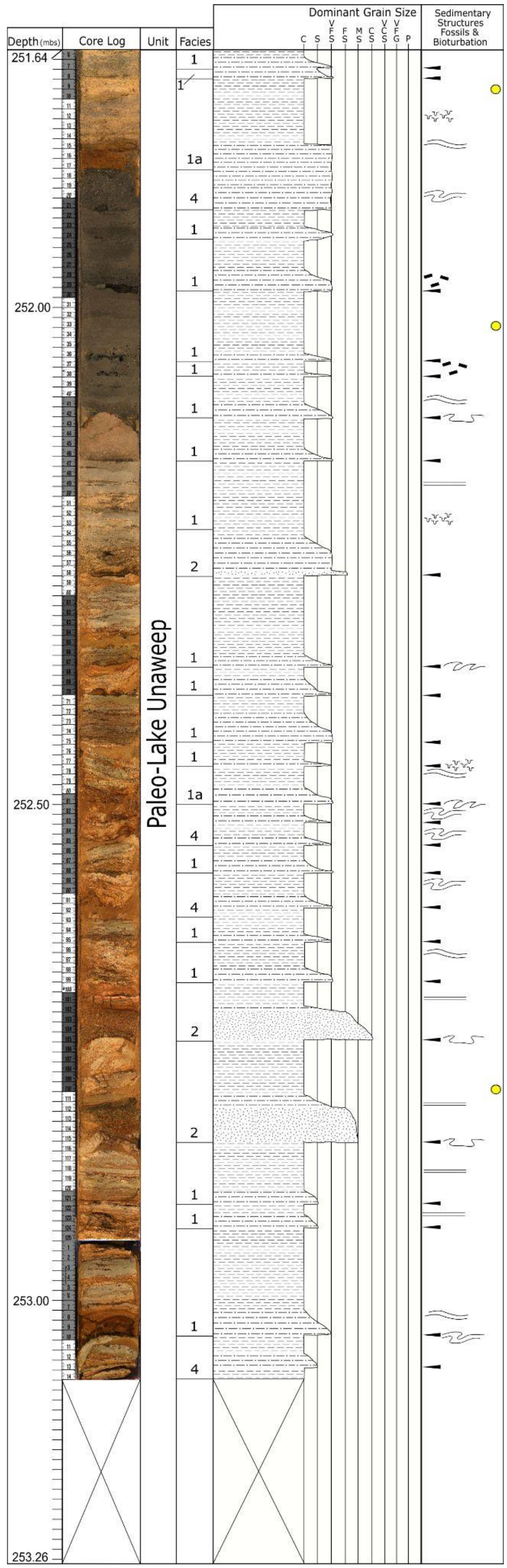

Depth (mbs)
Core Log
Unit
Facies
Dominant Grain Size
C S VFS FS MS CS VCS VFG P
Sedimentary Structures Fossils & Bioturbation
251.64
252.00
252.50
253.00
253.26
Paleo-Lake Unaweep
1
1
1a
4
1
1
1
1
1
1
1
2
1
1
1
1
1a
4
1
4
1
1
2
2
1
1
1
4

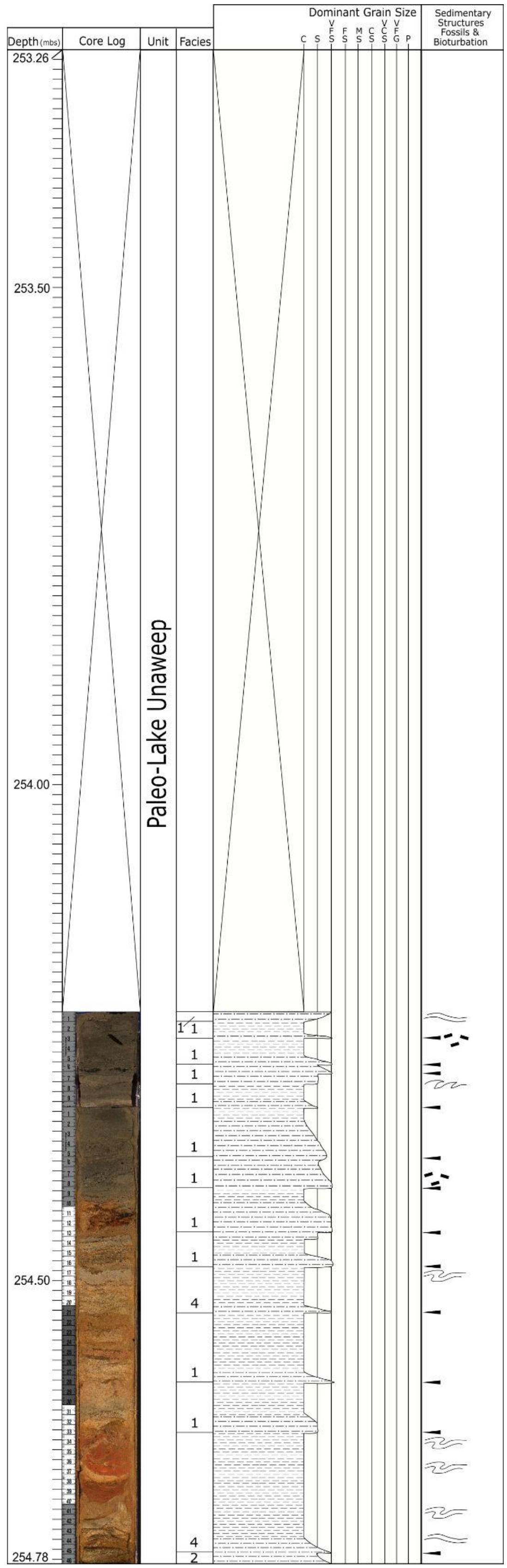
Depth (mbs)
Core Log
Unit
Facies
Dominant Grain Size
C S VFS FS MS CS VCS VFG P
Sedimentary Structures Fossils & Bioturbation
253.26
253.50
254.00
254.50
254.78
Paleo-Lake Unaweep
1
1
1
1
1
1
1
1
1
4
1
1
4
2

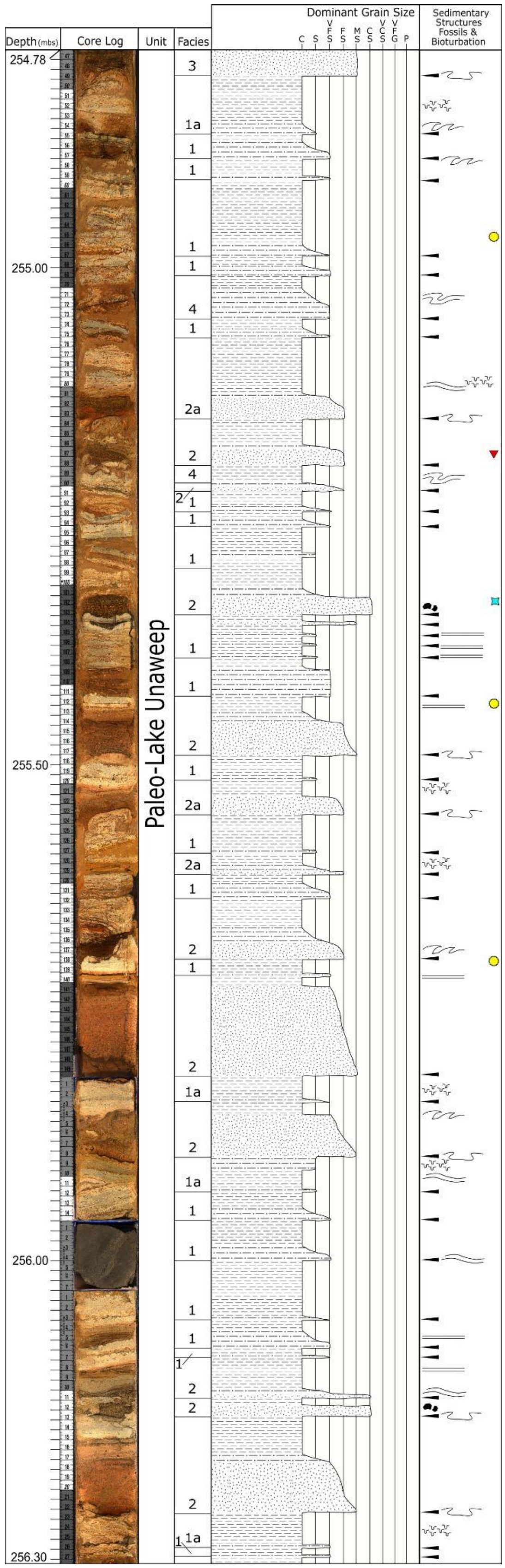
Depth (mbs)
Core Log
Unit
Facies
Dominant Grain Size
C S VFS FS MS CS VCS VFG P
Sedimentary Structures Fossils & Bioturbation
254.78
255.00
255.50
256.00
256.30
Paleo-Lake Unaweep

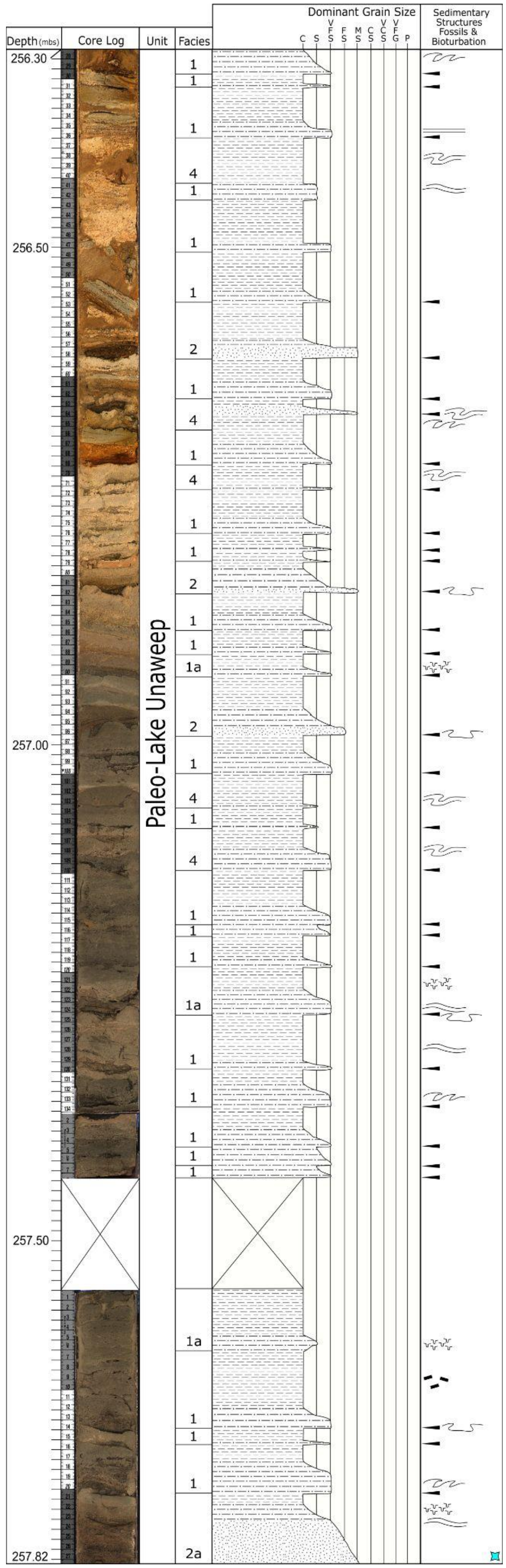

Depth (mbs)
Core Log
Unit
Facies
Dominant Grain Size
C S VFS FS MS CS VCS VFG P
Sedimentary Structures Fossils & Bioturbation
256.30
256.50
257.00
257.50
257.82
Paleo-Lake Unaweep
1
1
1
4
1
1
1
2
1
4
1
4
1
1
2
1
1
1a
2
1
4
1
4
1
1
1
1a
1
1
1
1
1
1a
1
1
1
2a

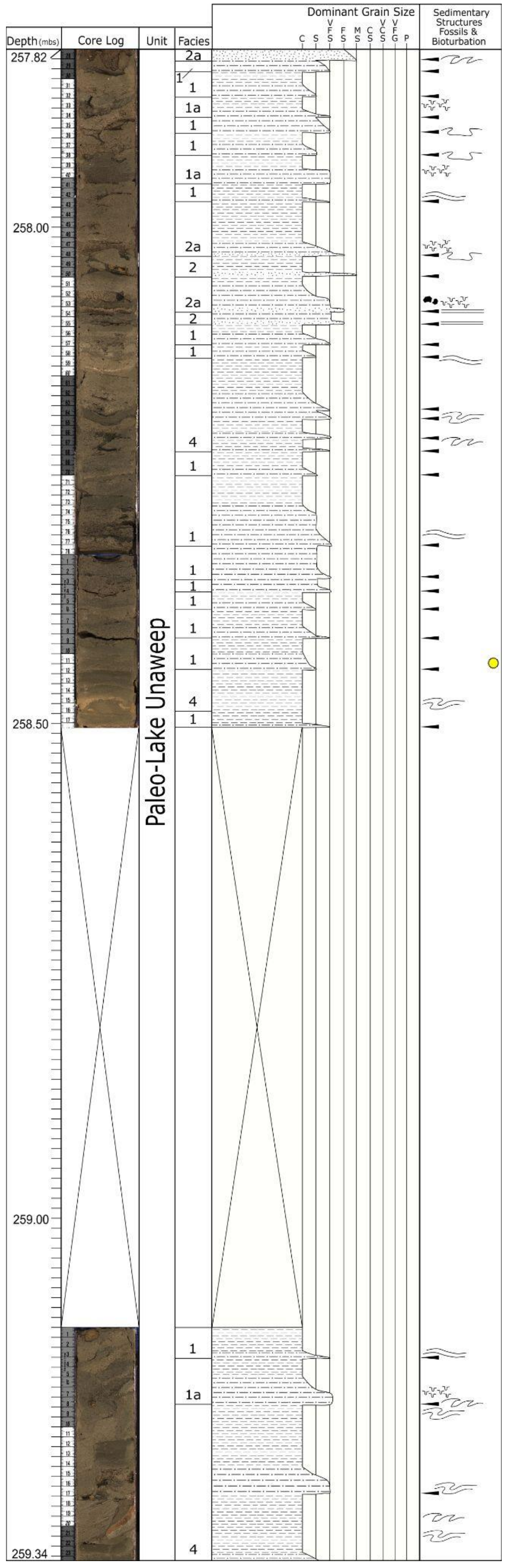

Depth (mbs)
Core Log
Unit
Facies
Dominant Grain Size
C S VFS FS MS CS VCS VFG P
Sedimentary Structures Fossils & Bioturbation
257.82
258.00
258.50
259.00
259.34
Paleo-Lake Unaweep
2a
1
1
1a
1
1
1a
1
2a
2
2a
2
1
1
4
1
1
1
1
1
1
1
4
1
1
1a
4

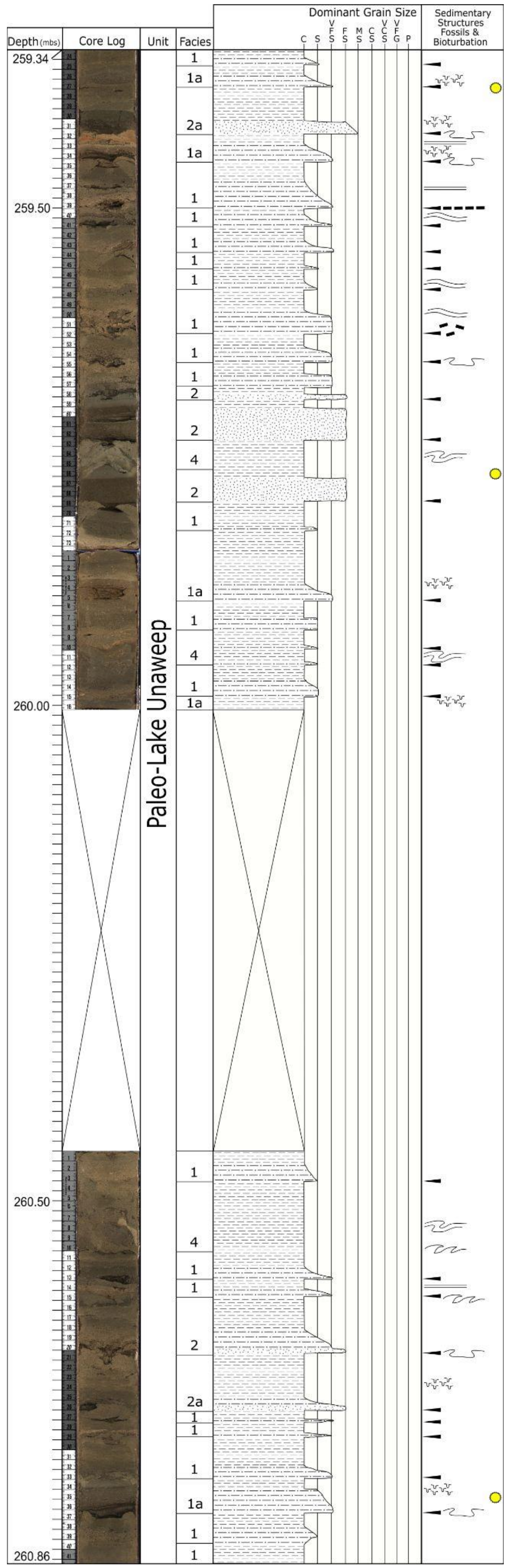
Depth (mbs)
Core Log
Unit
Facies
Dominant Grain Size
C S VFS FS MS CS VCS VFG P
Sedimentary Structures Fossils & Bioturbation
259.34
259.50
260.00
260.50
260.86
Paleo-Lake Unaweep
1
1a
2a
1a
1
1
1
1
1
1
1
1
2
2
4
2
1
1a
1
4
1
1a
1
4
1
1
2
2a
1
1
1
1a
1
1

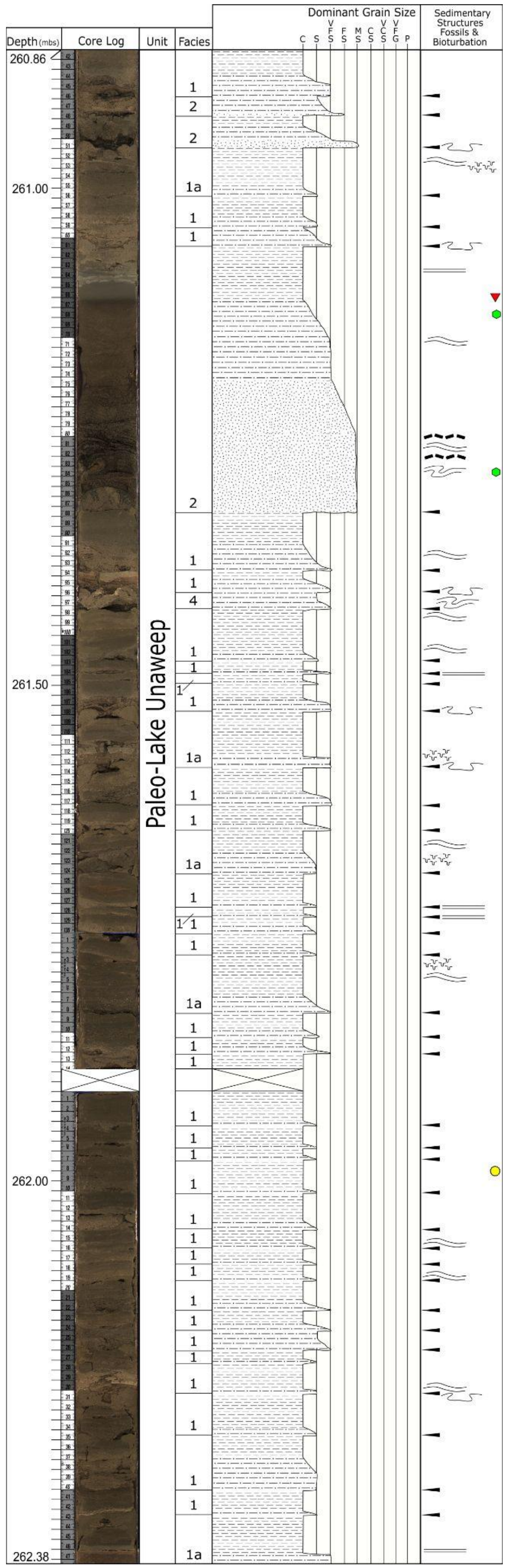
Depth (mbs)
Core Log
Unit
Facies
Dominant Grain Size
C S VFS FS MS CS VCS VFG P
Sedimentary Structures Fossils & Bioturbation
260.86
261.00
261.50
262.00
262.38
Paleo-Lake Unaweep
1
2
2
1a
1
1
2
1
1
4
1
1
1
1
1a
1
1
1a
1
1
1
1a
1
1
1
1
1
1
1
1
1
1
1
1
1
1
1
1
1
1
1
1a

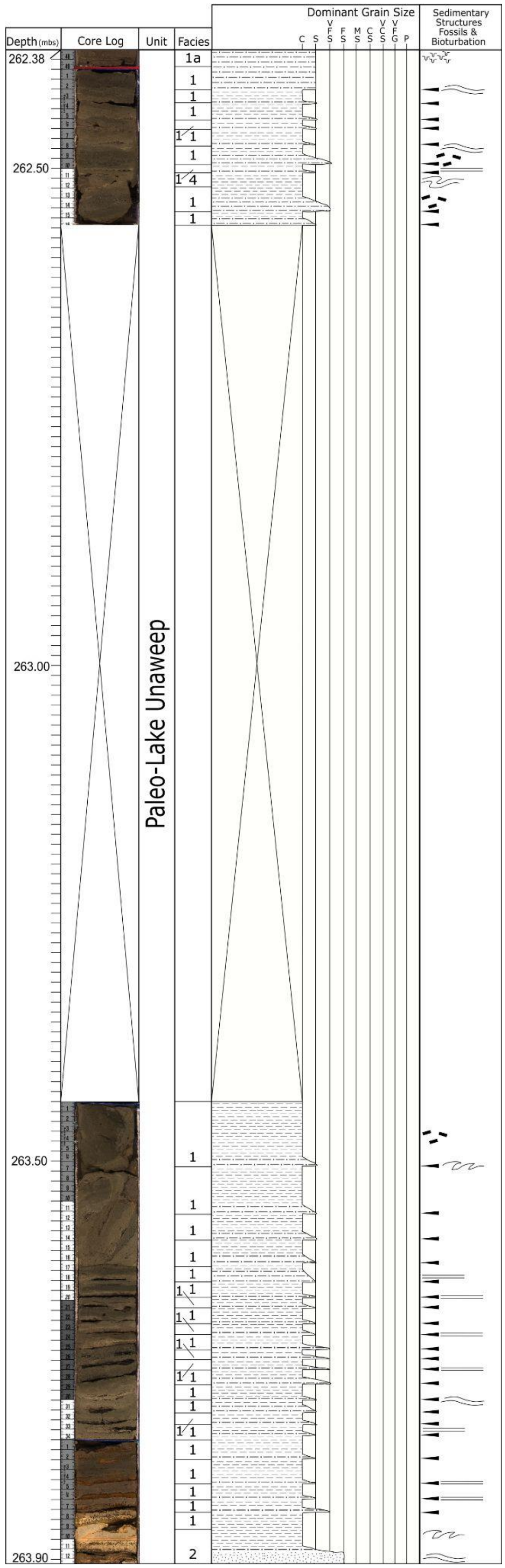
Depth (mbs)
Core Log
Unit
Facies
Dominant Grain Size
C S VFS FS MS CS VCS VFG P
Sedimentary Structures Fossils & Bioturbation
262.38
262.50
263.00
263.50
263.90
Paleo-Lake Unaweep
1a
1
4
2

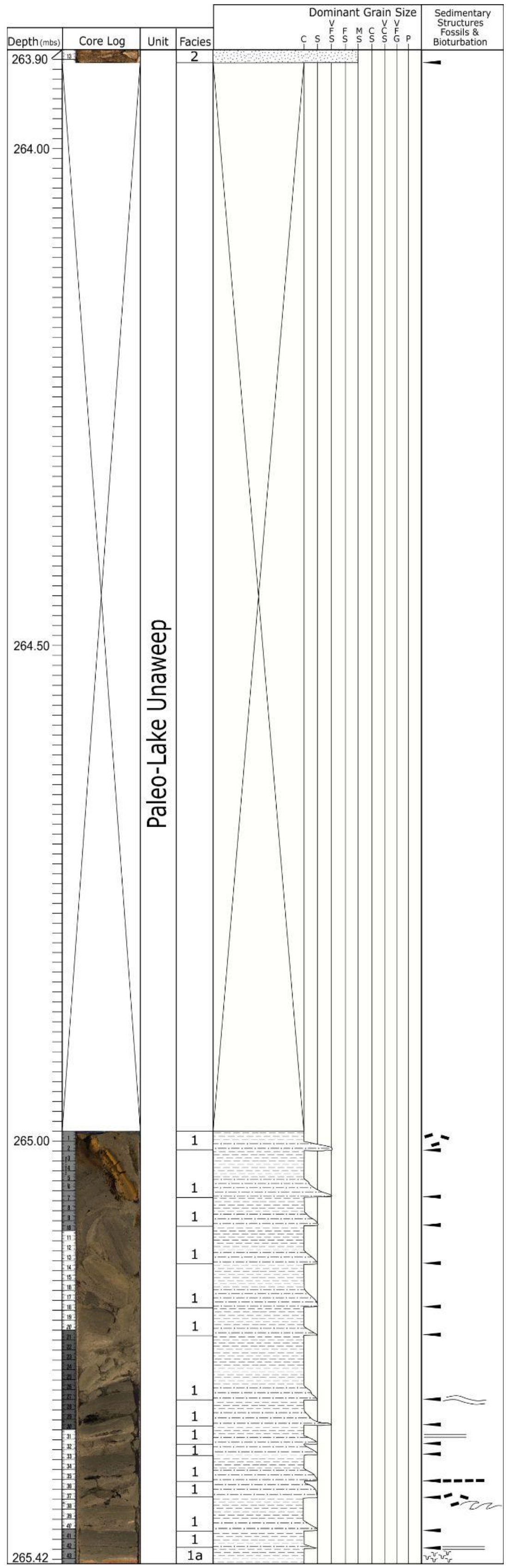
Depth (mbs)
Core Log
Unit
Facies
Dominant Grain Size
C S VFS FS MS CS VCS VFG P
Sedimentary Structures Fossils & Bioturbation
263.90
264.00
264.50
265.00
265.42
Paleo-Lake Unaweep
2
1
1a

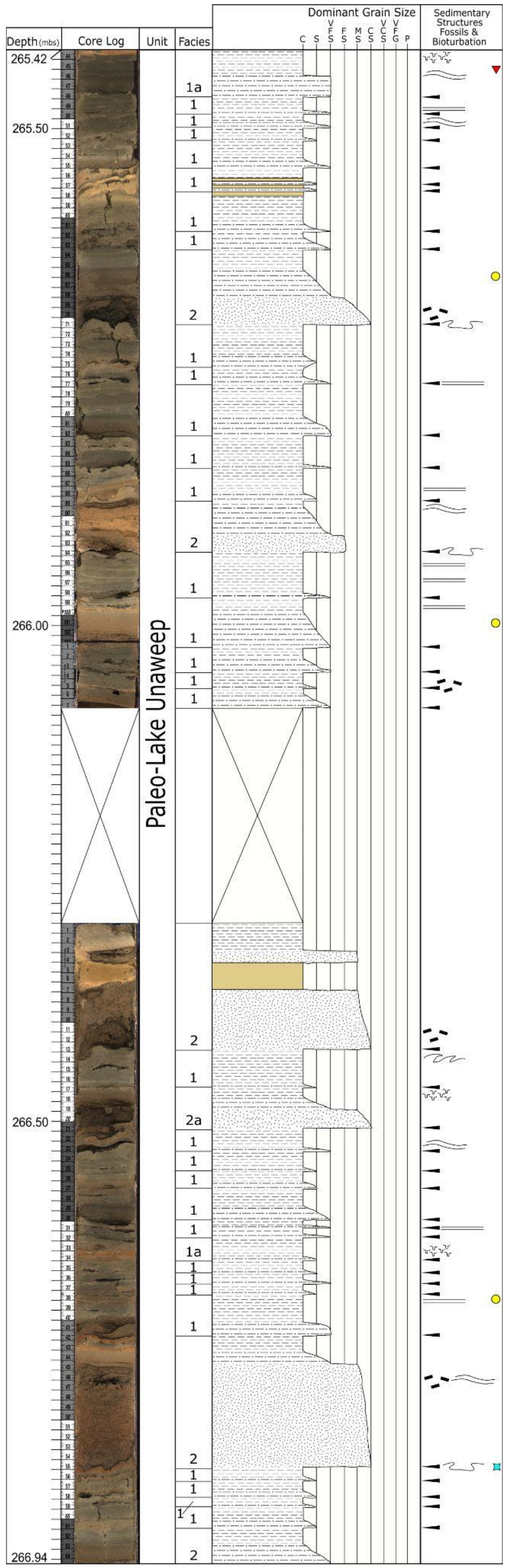
Depth (mbs)
Core Log
Unit
Facies
Dominant Grain Size
C S VFS FS MS CS VCS VFG P
Sedimentary Structures Fossils & Bioturbation
265.42
265.50
266.00
266.50
266.94
Paleo-Lake Unaweep
1a
1
2
2a

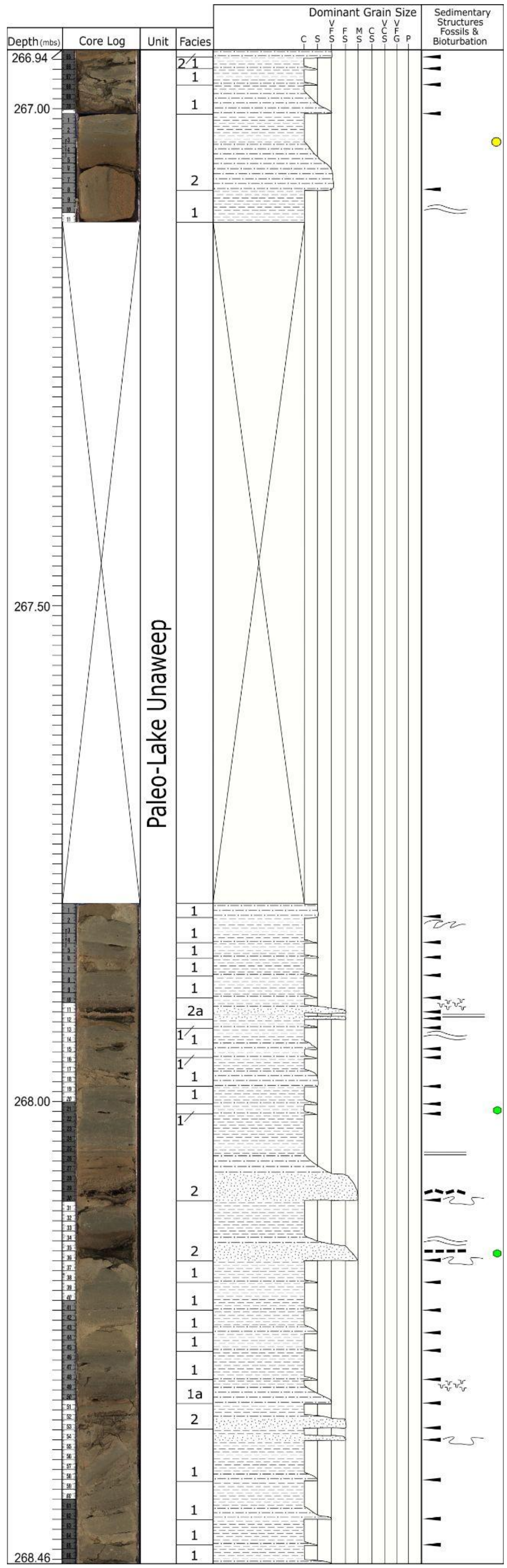
Depth (mbs)
Core Log
Unit
Facies
Dominant Grain Size
C S VFS FS MS CS VCS VFG P
Sedimentary Structures Fossils & Bioturbation
266.94
267.00
267.50
268.00
268.46
Paleo-Lake Unaweep
2
1
1
1
2
1
1
1
1
1
1
2a
1
1
1
1
1
1
2
2
1
1
1
1
1
1a
2
1
1
1
1

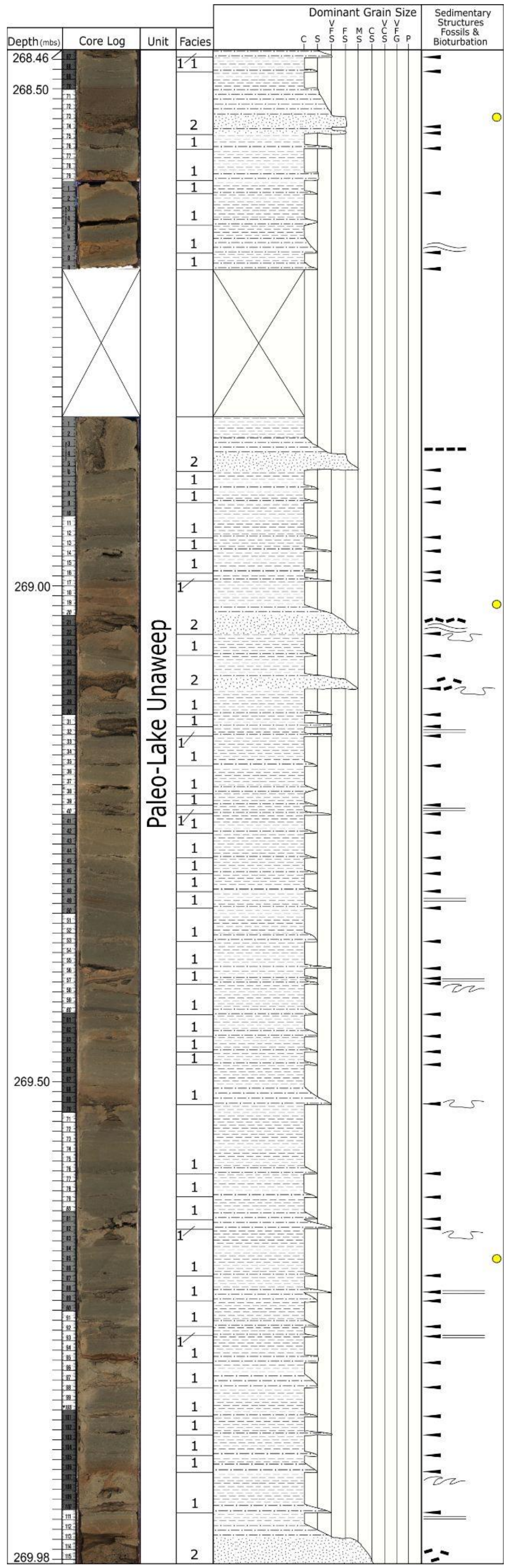

Depth (mbs)
Core Log
Unit
Facies
Dominant Grain Size
C S VFS FS MS CS VCS VFG P
Sedimentary Structures Fossils & Bioturbation
268.46
268.50
269.00
269.50
269.98
Paleo-Lake Unaweep

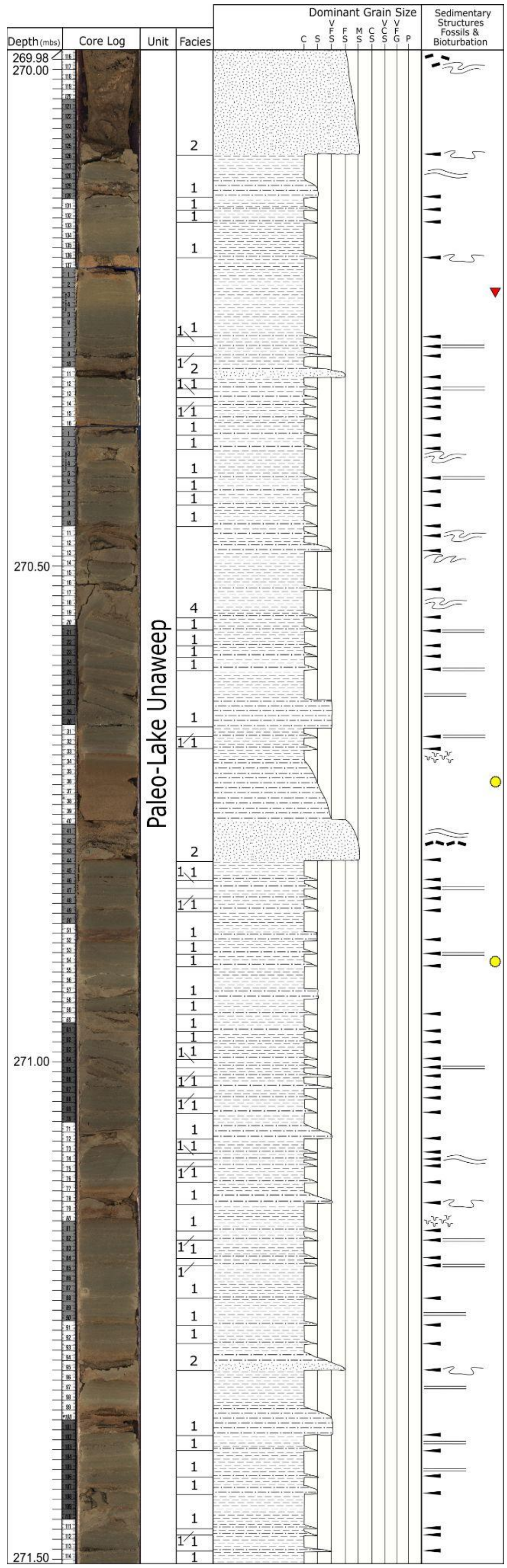

Depth (mbs)
Core Log
Unit
Facies
Dominant Grain Size
C S VFS FS MS CS VCS VFG P
Sedimentary Structures Fossils & Bioturbation
269.98
270.00
270.50
271.00
271.50
Paleo-Lake Unaweep

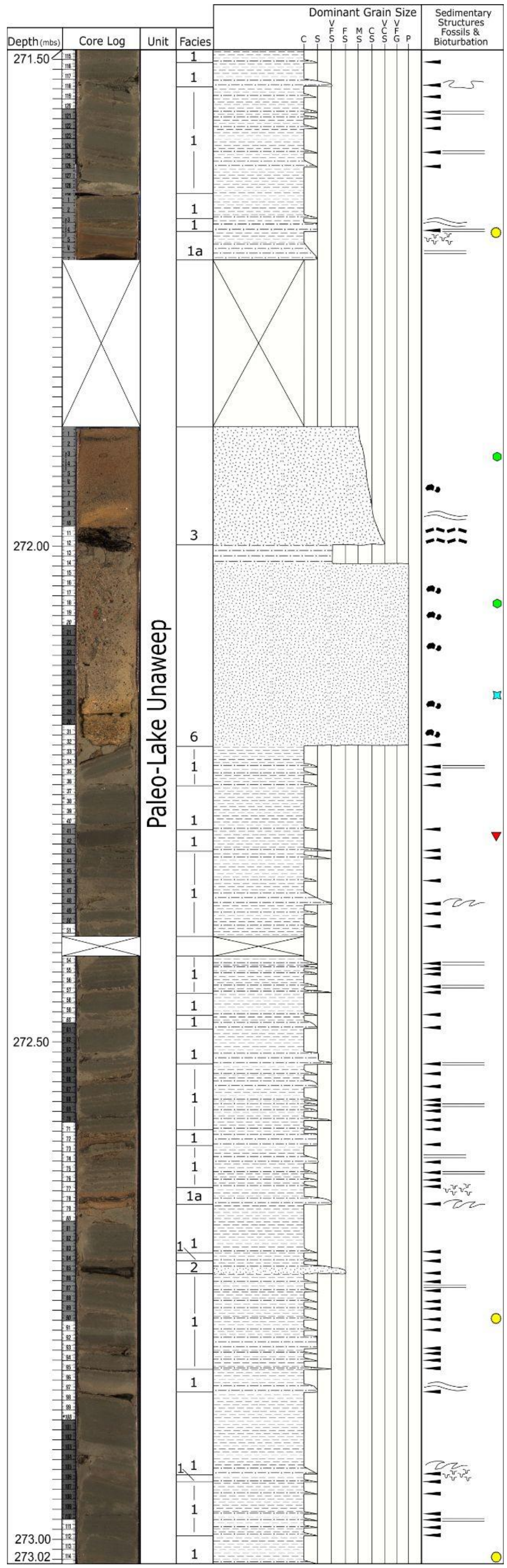
Depth (mbs)
Core Log
Unit
Facies
Dominant Grain Size
C S VFS FS MS CS VCS VFG P
Sedimentary Structures Fossils & Bioturbation
271.50
272.00
272.50
273.00
273.02
Paleo-Lake Unaweep
1a
3
6
2

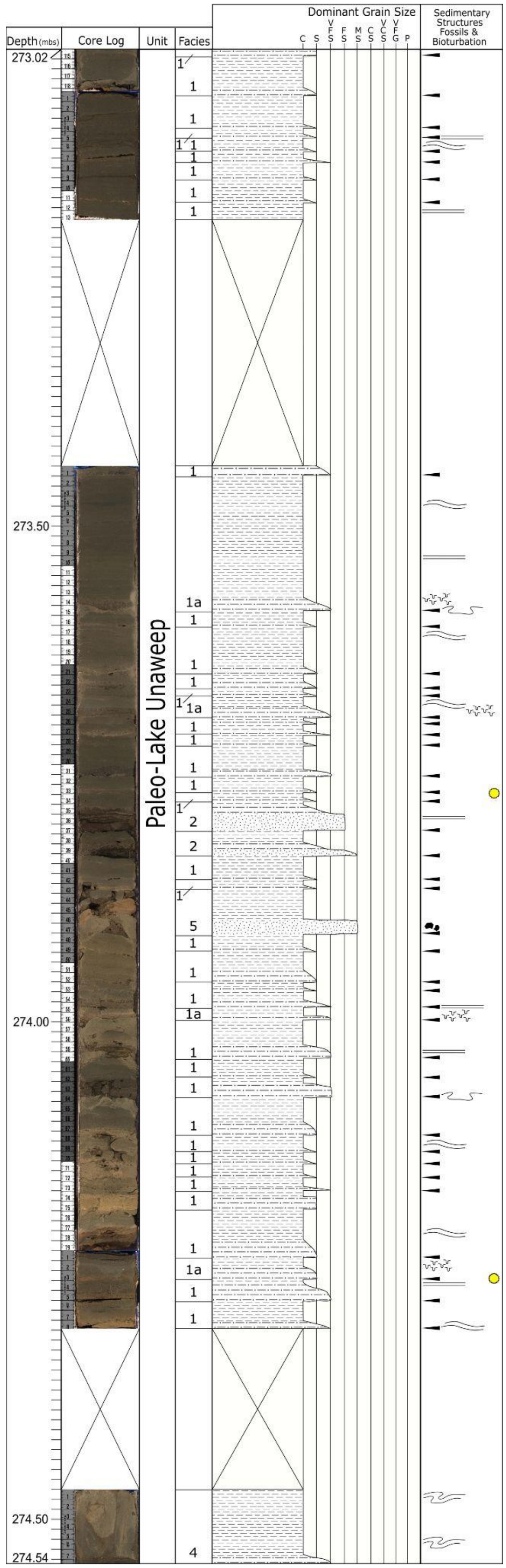

Depth (mbs)
Core Log
Unit
Facies
Dominant Grain Size
C S VFS FS MS CS VCS VFG P
Sedimentary Structures Fossils & Bioturbation
273.02
273.50
274.00
274.50
274.54
Paleo-Lake Unaweep

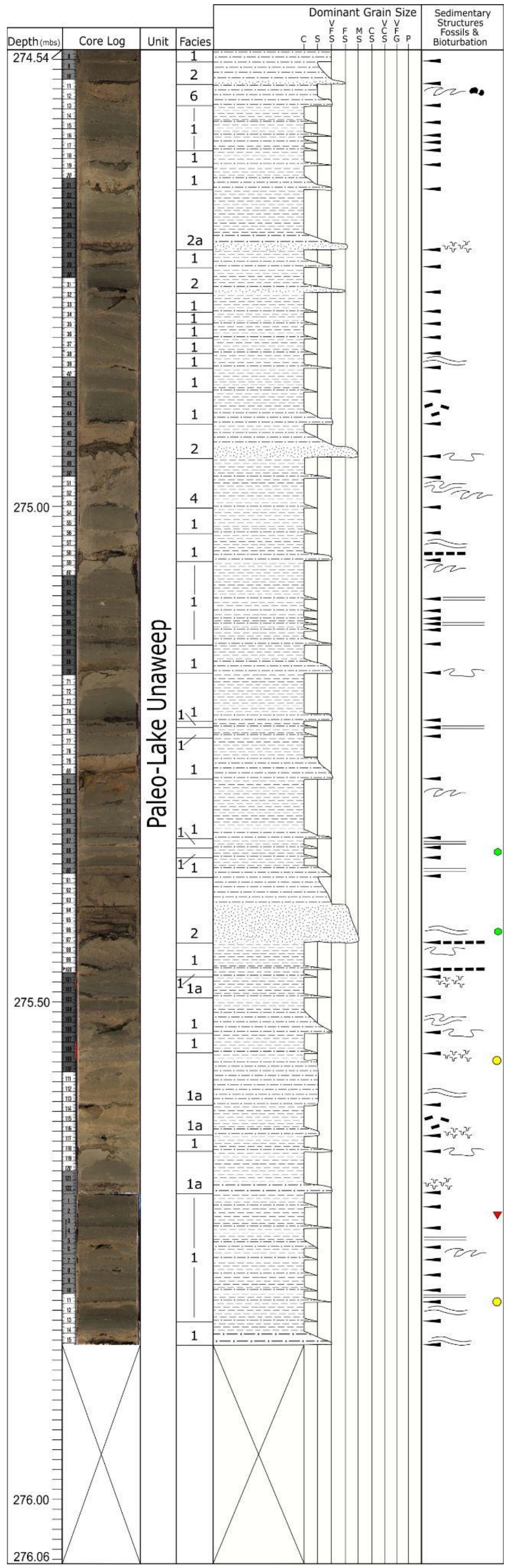
Depth (mbs)
Core Log
Unit
Facies
Dominant Grain Size
C S VFS FS MS CS VCS VFG P
Sedimentary Structures Fossils & Bioturbation
274.54
275.00
275.50
276.00
276.06
Paleo-Lake Unaweep

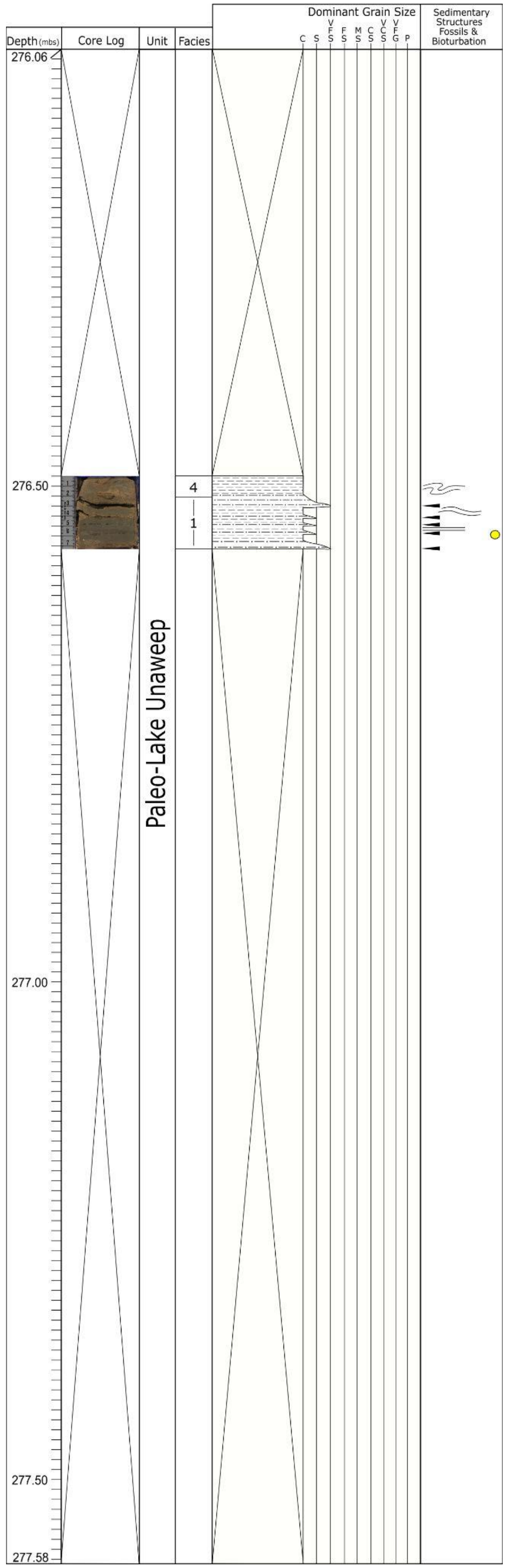

Depth (mbs)
Core Log
Unit
Facies
Dominant Grain Size
C S VFS FS MS CS VCS VFG P
Sedimentary Structures Fossils & Bioturbation
276.06
276.50
277.00
277.50
277.58
Paleo-Lake Unaweep
4
1

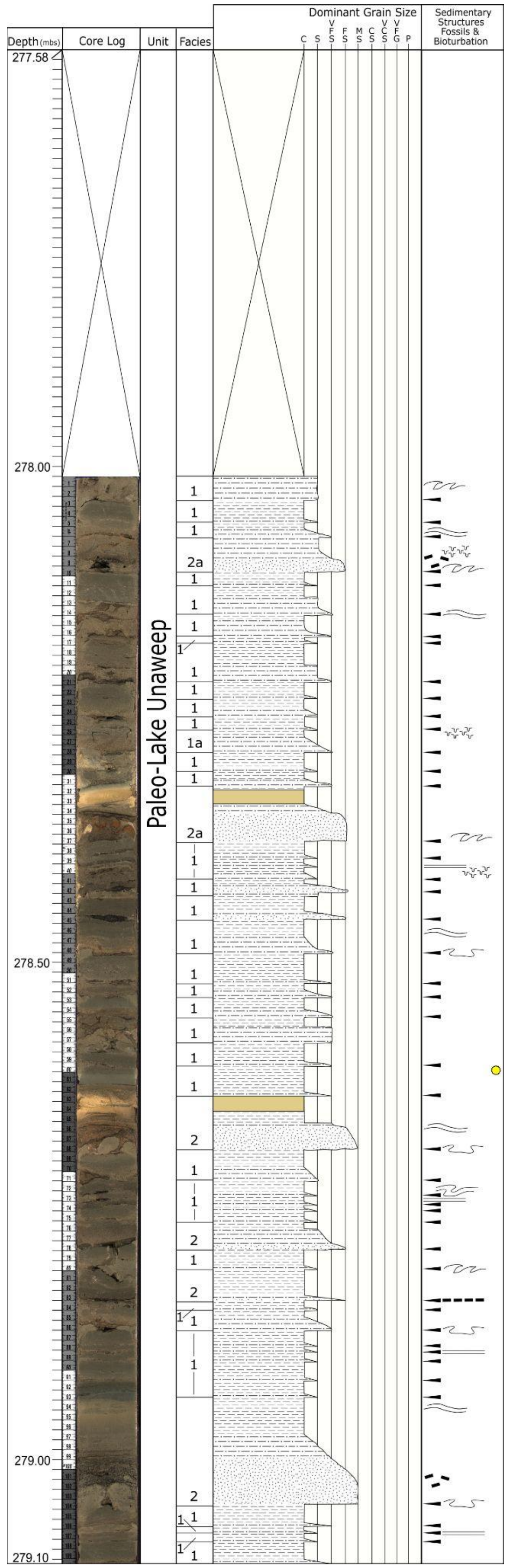
Depth (mbs)
Core Log
Unit
Facies
Dominant Grain Size
C S VFS FS MS CS VCS VFG P
Sedimentary Structures Fossils & Bioturbation
277.58
278.00
278.50
279.00
279.10
Paleo-Lake Unaweep
1
2a
1a
2

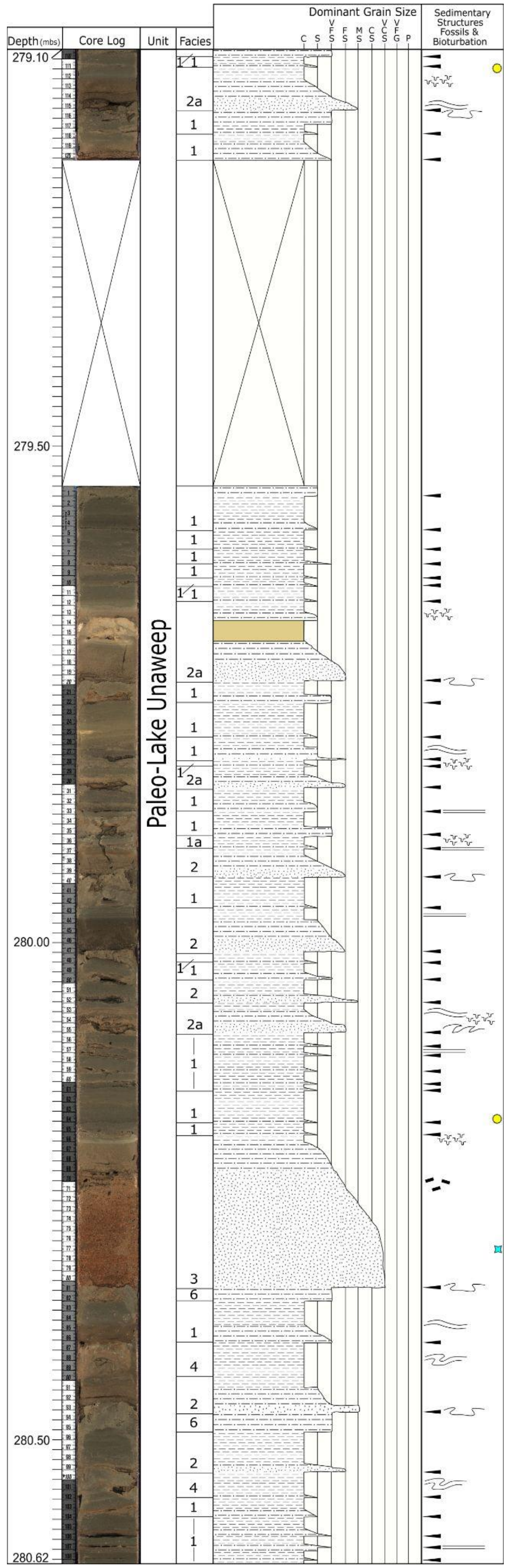

Depth (mbs)
Core Log
Unit
Facies
Dominant Grain Size
C S VFS FS MS CS VCS VFG P
Sedimentary Structures Fossils & Bioturbation
279.10
279.50
280.00
280.50
280.62
Paleo-Lake Unaweep

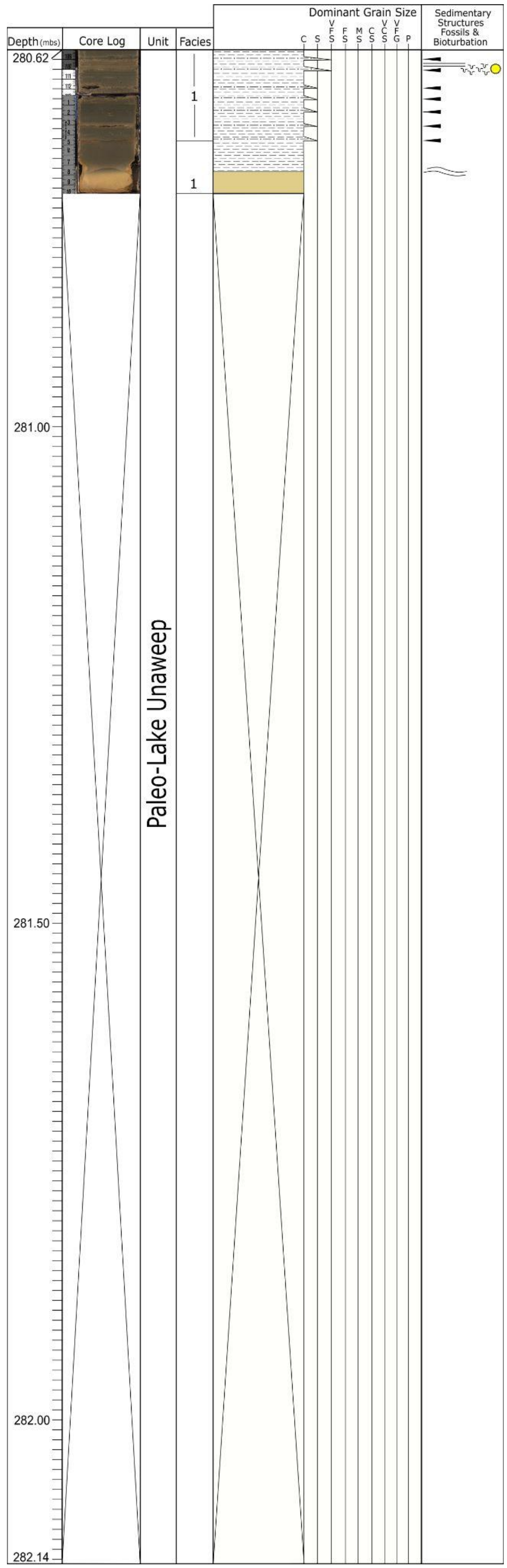
Depth (mbs)
Core Log
Unit
Facies
Dominant Grain Size
C S VFS FS MS CS VCS VFG P
Sedimentary Structures Fossils & Bioturbation
280.62
281.00
281.50
282.00
282.14
Paleo-Lake Unaweep
1
1

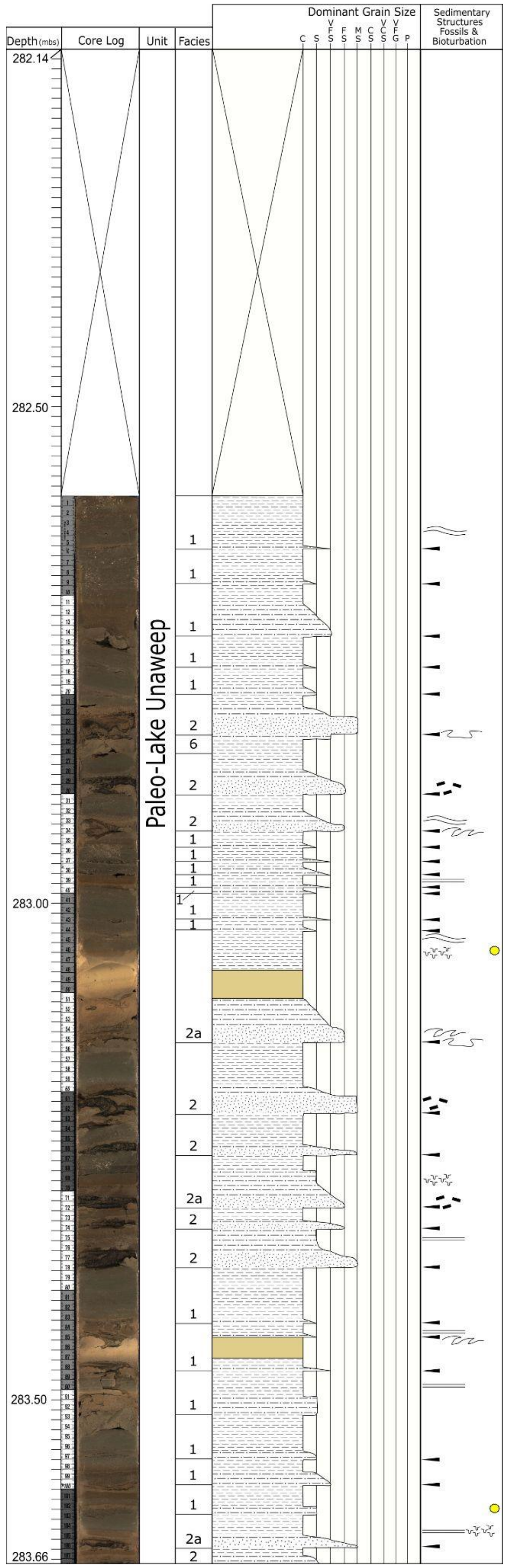
Depth (mbs)
Core Log
Unit
Facies
Dominant Grain Size
C S VFS FS MS CS VCS VFG P
Sedimentary Structures Fossils & Bioturbation
282.14
282.50
283.00
283.50
283.66
Paleo-Lake Unaweep
1
1
1
1
1
2
6
2
2
1
1
1
1
1
1
1
2a
2
2
2a
2
2
1
1
1
1
1
1
2a
2

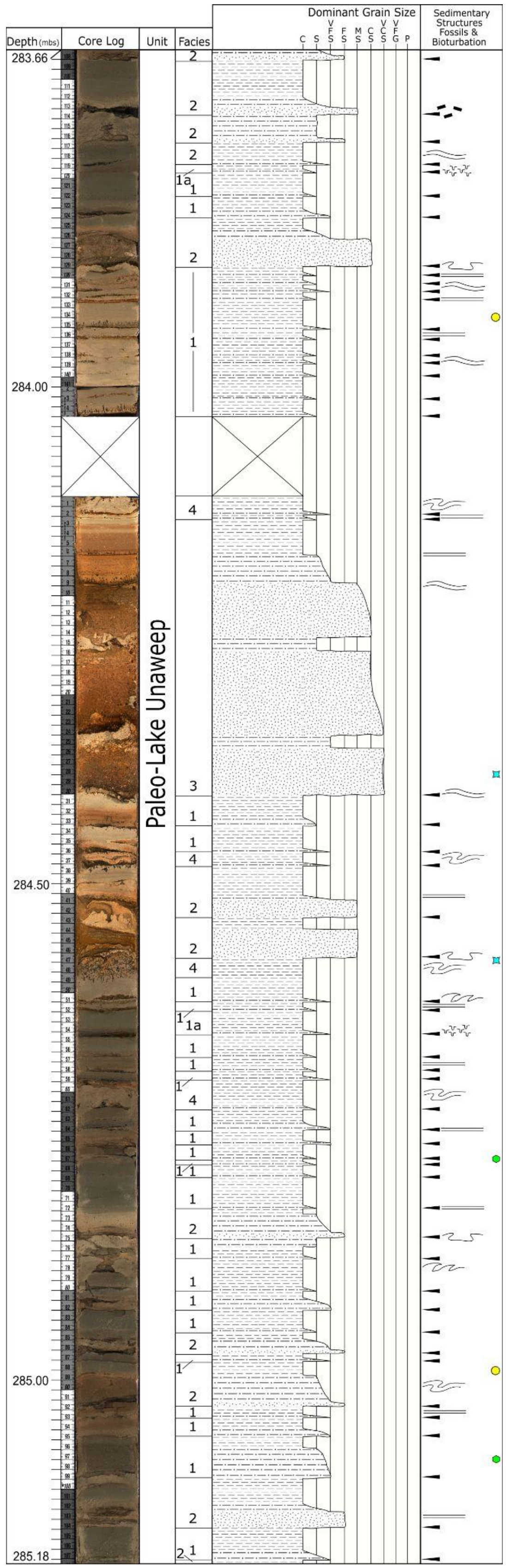
Depth (mbs)
Core Log
Unit
Facies
Dominant Grain Size
C S VFS FS MS CS VCS VFG P
Sedimentary Structures Fossils & Bioturbation
283.66
284.00
284.50
285.00
285.18
Paleo-Lake Unaweep

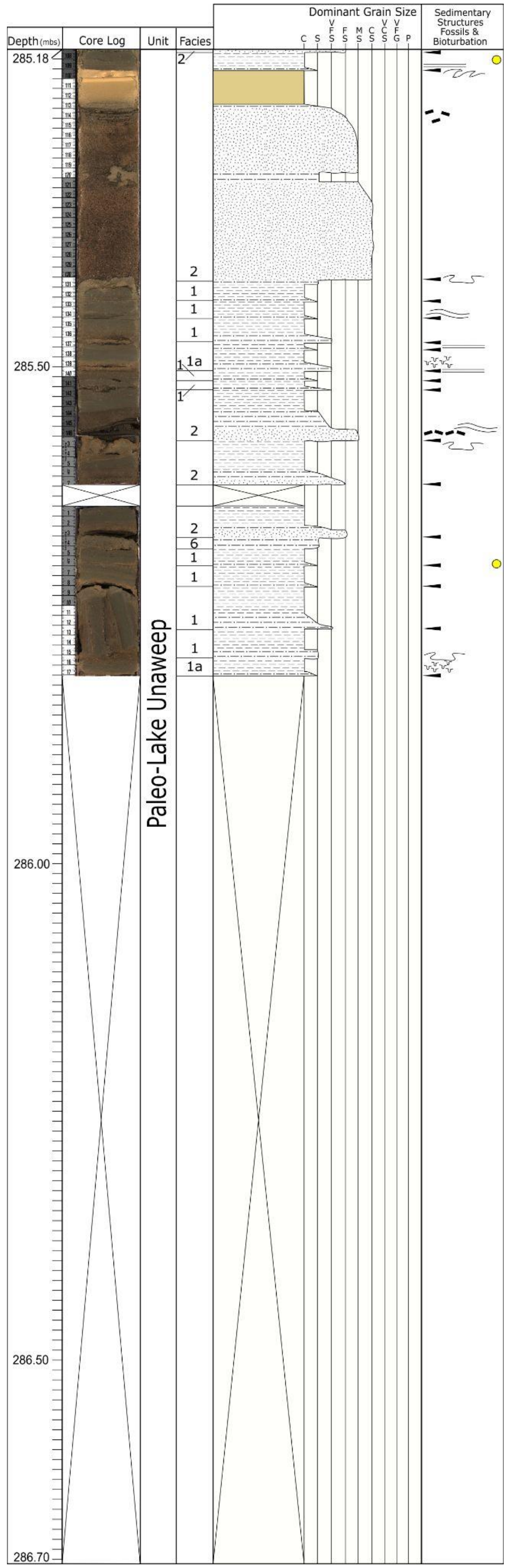
Depth (mbs)
Core Log
Unit
Facies
Dominant Grain Size
C S VFS FS MS CS VCS VFG P
Sedimentary Structures Fossils & Bioturbation
285.18
285.50
286.00
286.50
286.70
Paleo-Lake Unaweep

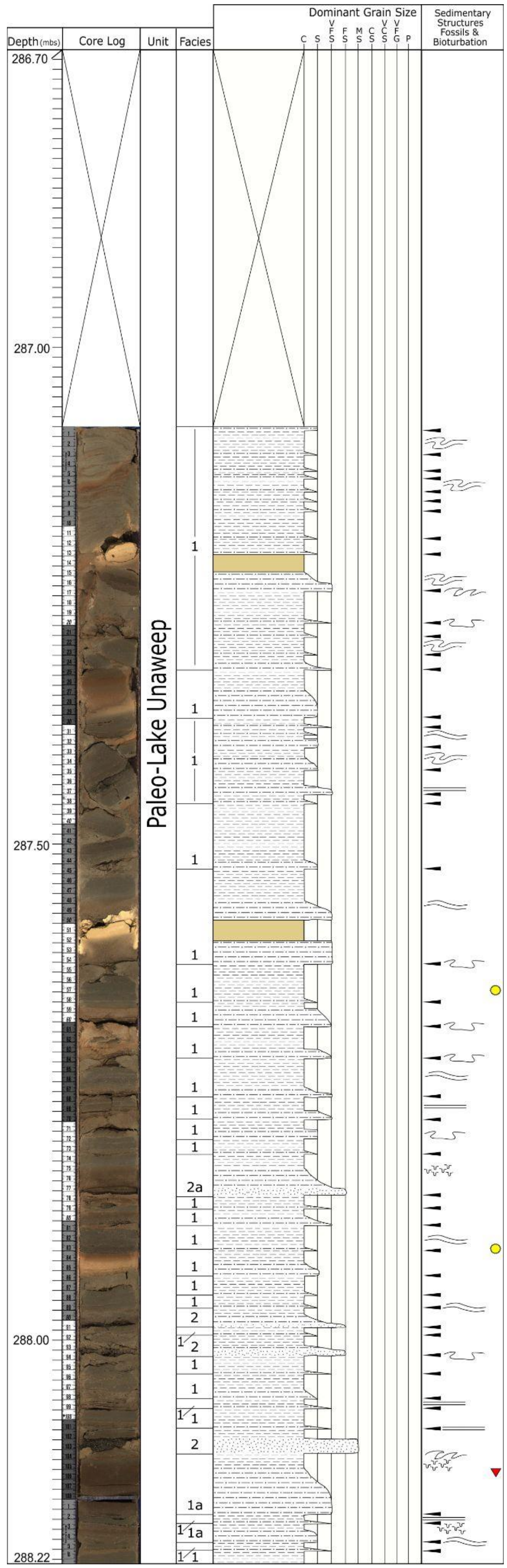
Depth (mbs)
Core Log
Unit
Facies
Dominant Grain Size
C S VFS FS MS CS VCS VFG P
Sedimentary Structures Fossils & Bioturbation
286.70
287.00
287.50
288.00
288.22
Paleo-Lake Unaweep
1
1
1
1
1
1
1
1
1
1
1
2a
1
1
1
1
1
1
2
1/2
1
1
1/1
2
1a
1/1a
1/1

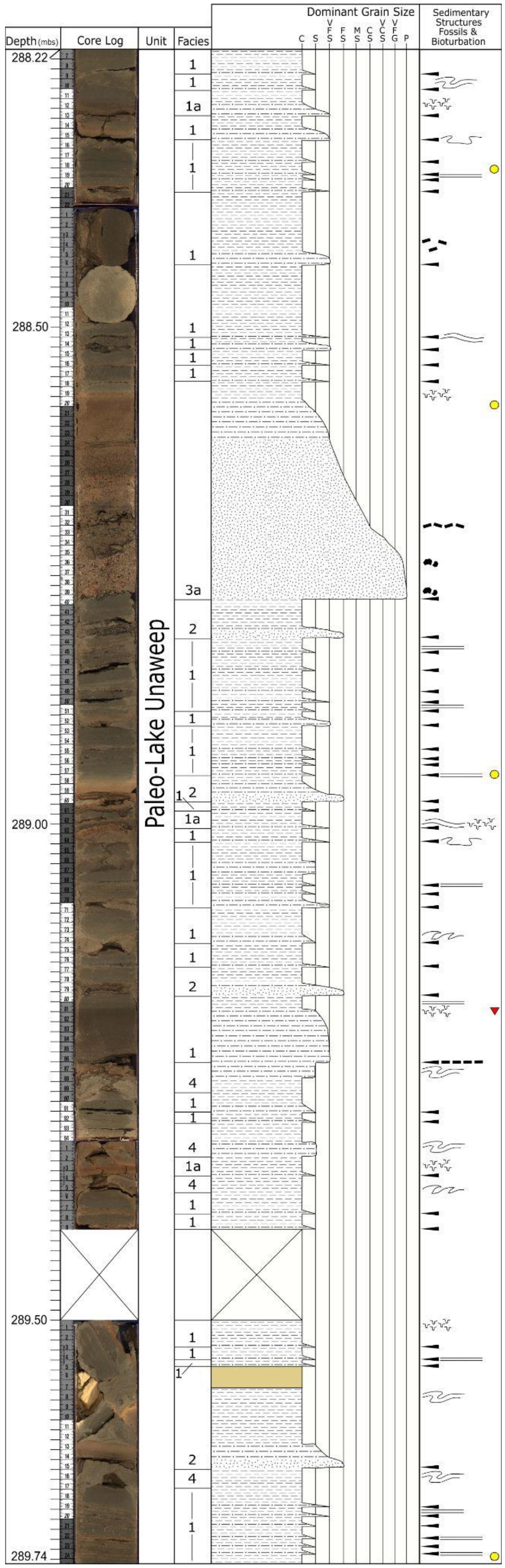

Depth (mbs)
Core Log
Unit
Facies
Dominant Grain Size
C S VFS FS MS CS VCS VFG P
Sedimentary Structures Fossils & Bioturbation
288.22
288.50
289.00
289.50
289.74
Paleo-Lake Unaweep
1
1
1a
1
1
1
1
1
1
1
3a
2
1
1
1
1
2
1a
1
1
1
1
2
1
4
1
1
4
1a
4
1
1
1
1
1
2
4
1

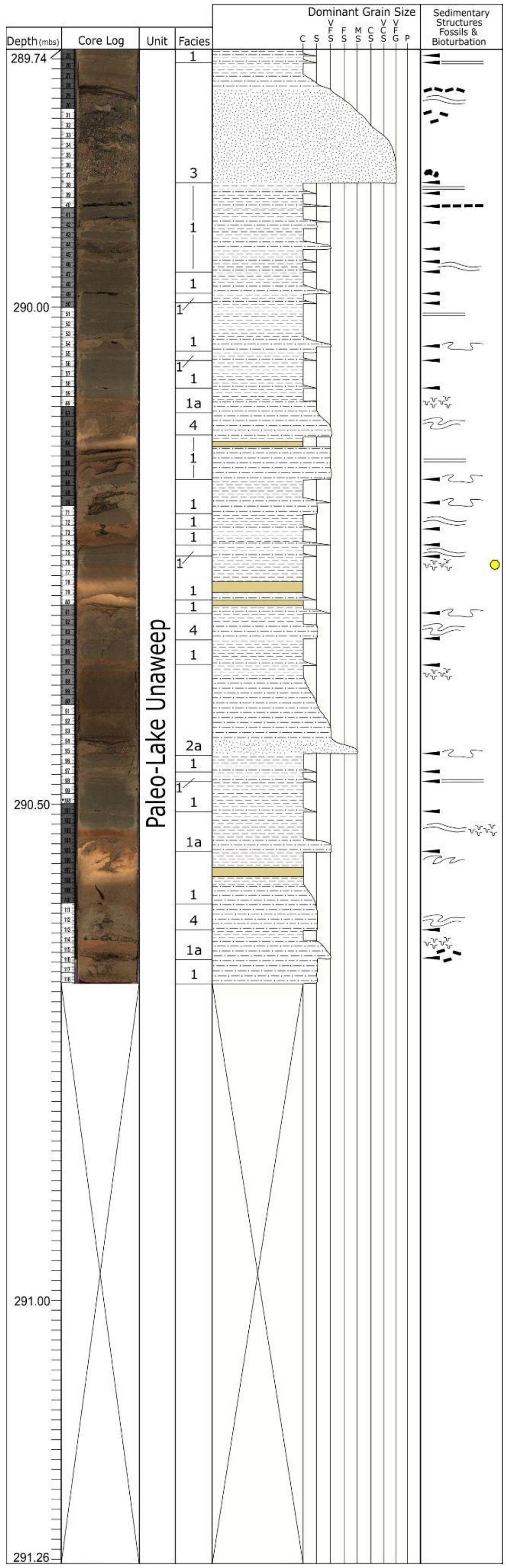
Depth (mbs)
Core Log
Unit
Facies
Dominant Grain Size
C S VFS FS MS CS VCS VFG P
Sedimentary Structures Fossils & Bioturbation
289.74
290.00
290.50
291.00
291.26
Paleo-Lake Unaweep
1
3
1
1
1
1
1
1a
4
1
1
1
1
1
1
4
1
2a
1
1
1a
1
4
1a
1

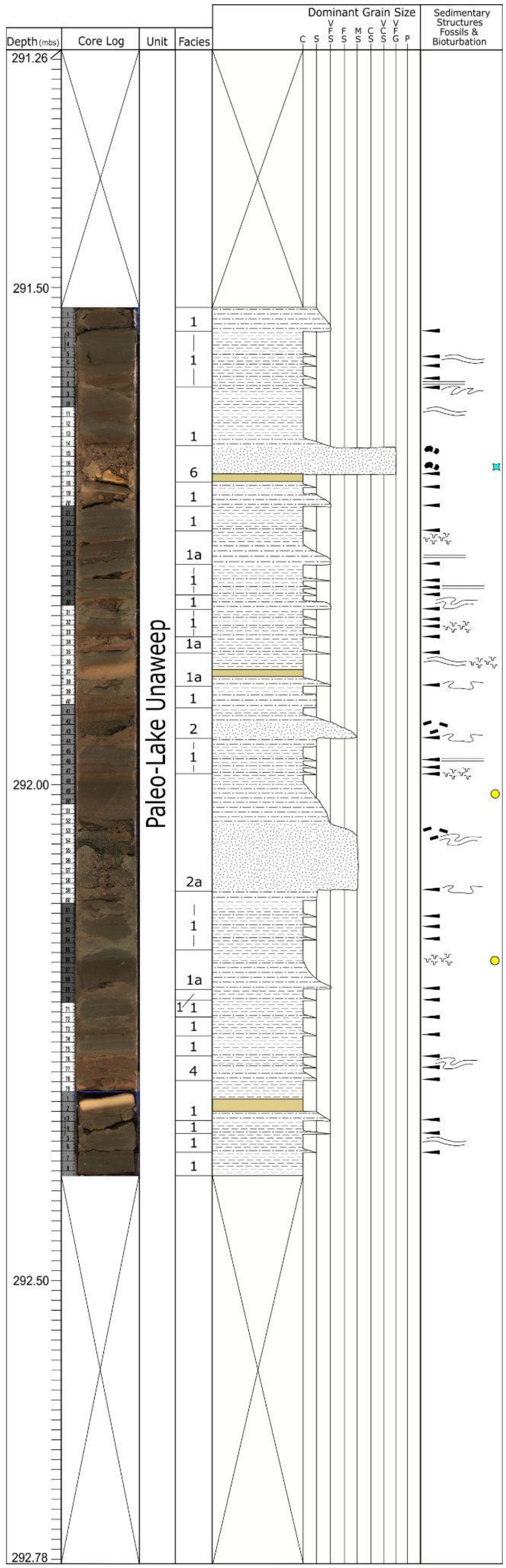
Depth (mbs)
Core Log
Unit
Facies
Dominant Grain Size
C S VFS FS MS CS VCS VFG P
Sedimentary Structures Fossils & Bioturbation
291.26
291.50
292.00
292.50
292.78
Paleo-Lake Unaweep
1
1
1
6
1
1
1a
1
1
1
1a
1a
1
2
1
2a
1
1a
1
1
1
4
1
1
1
1

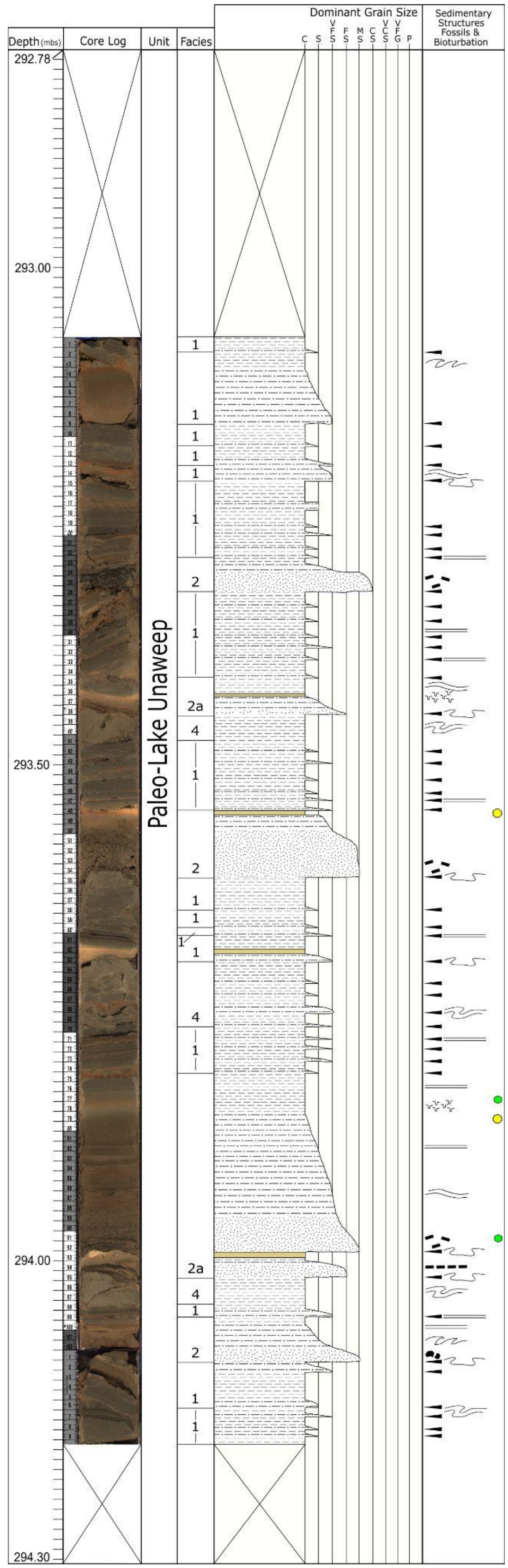
Depth (mbs)
Core Log
Unit
Facies
Dominant Grain Size
C S VFS FS MS CS VCS VFG P
Sedimentary Structures Fossils & Bioturbation
292.78
293.00
293.50
294.00
294.30
Paleo-Lake Unaweep
1
2
2a
4

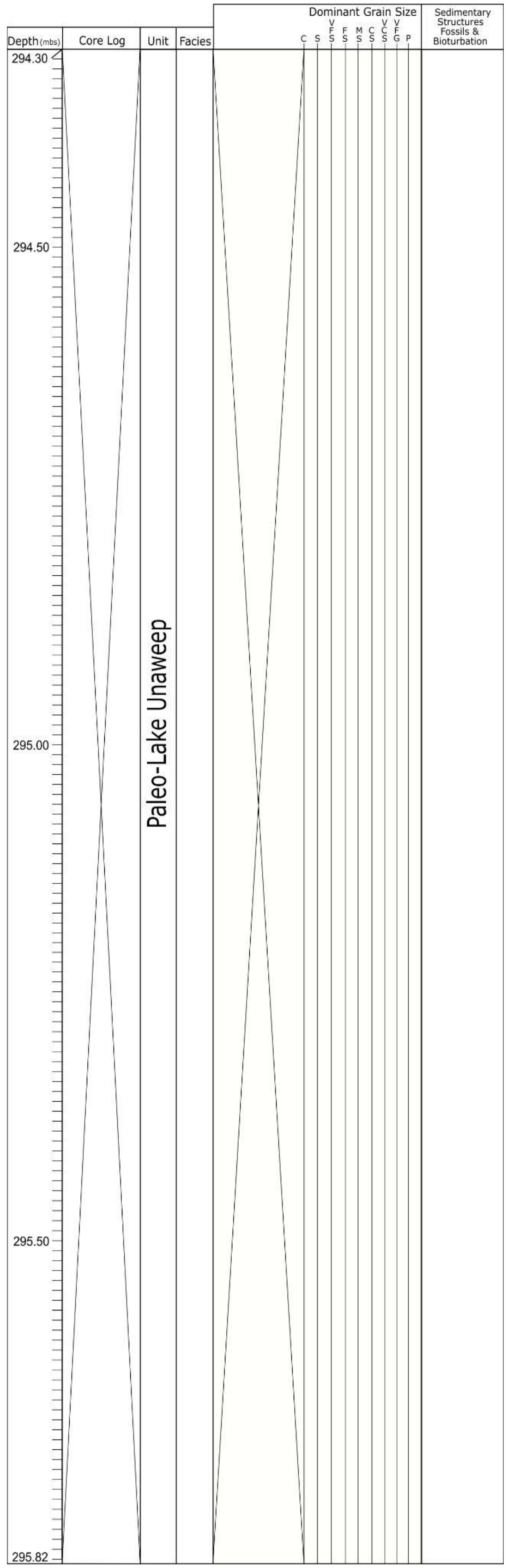
Depth (mbs)
Core Log
Unit
Facies
Dominant Grain Size
C S VFS FS MS CS VCS VFG P
Sedimentary Structures Fossils & Bioturbation
294.30
294.50
295.00
295.50
295.82
Paleo-Lake Unaweep

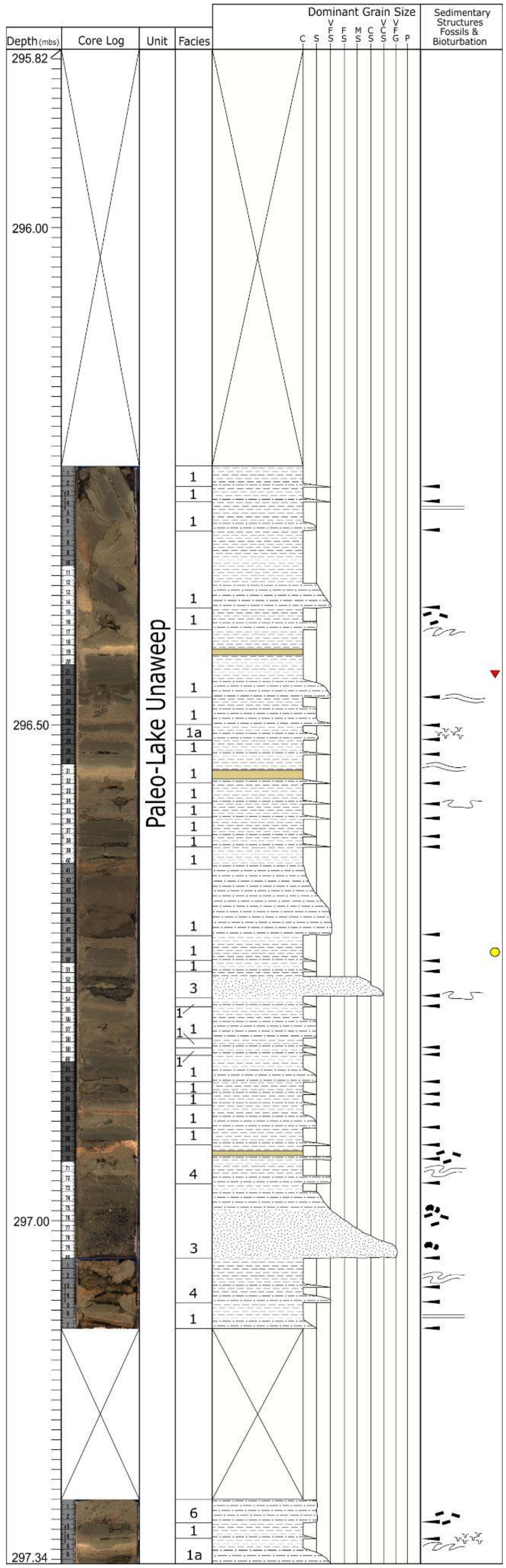

Depth (mbs)
Core Log
Unit
Facies
Dominant Grain Size
C S VFS FS MS CS VCS VFG P
Sedimentary Structures Fossils & Bioturbation
295.82
296.00
296.50
297.00
297.34
Paleo-Lake Unaweep

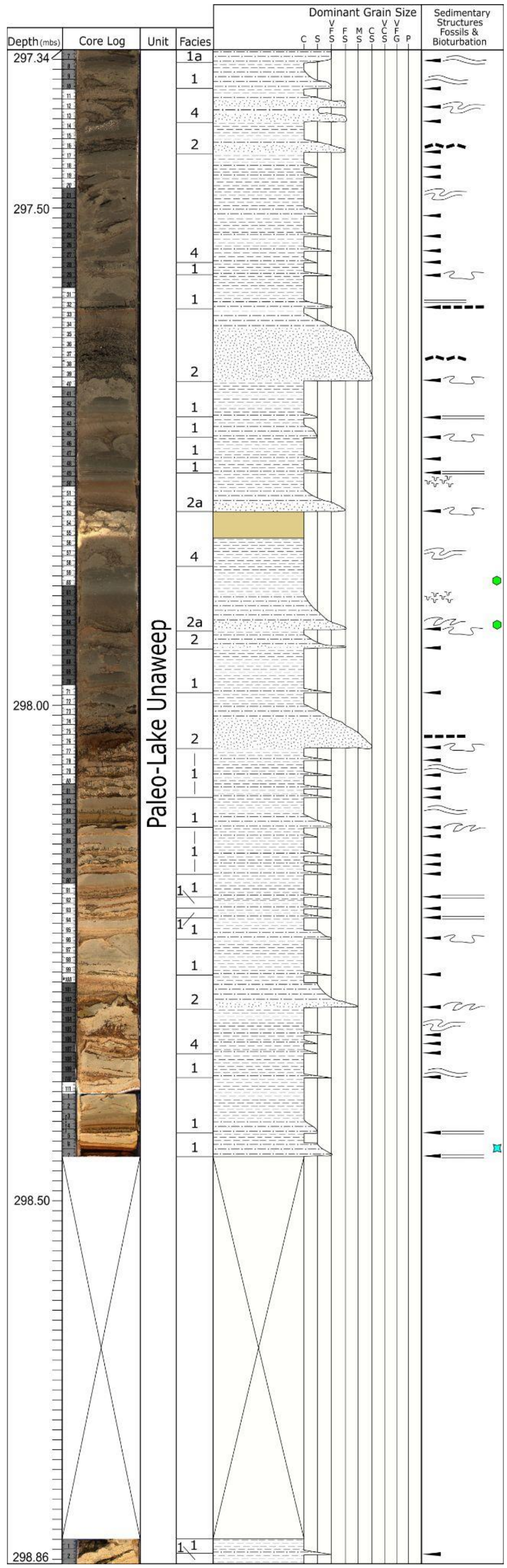

Depth (mbs)
Core Log
Unit
Facies
Dominant Grain Size
C S VFS FS MS CS VCS VFG P
Sedimentary Structures Fossils & Bioturbation
297.34
297.50
298.00
298.50
298.86
Paleo-Lake Unaweep
1a
1
4
2
4
1
1
2
1
1
1
1
2a
4
2a
2
1
2
1
1
1
1
1
1
2
4
1
1
1
1

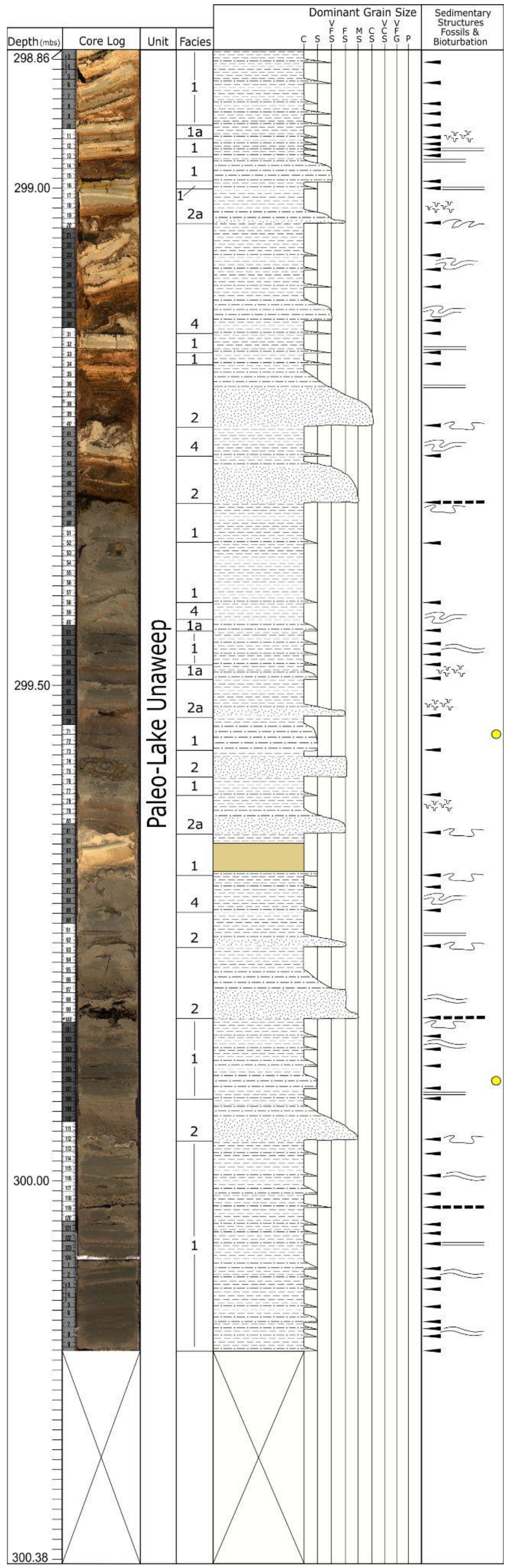
Depth (mbs)
Core Log
Unit
Facies
Dominant Grain Size
C S VFS FS MS CS VCS VFG P
Sedimentary Structures Fossils & Bioturbation
298.86
299.00
299.50
300.00
300.38
Paleo-Lake Unaweep
1
1a
1
1
1
2a
4
1
1
2
4
2
1
1
4
1a
1
1a
2a
1
2
1
2a
1
4
2
2
1
2
1

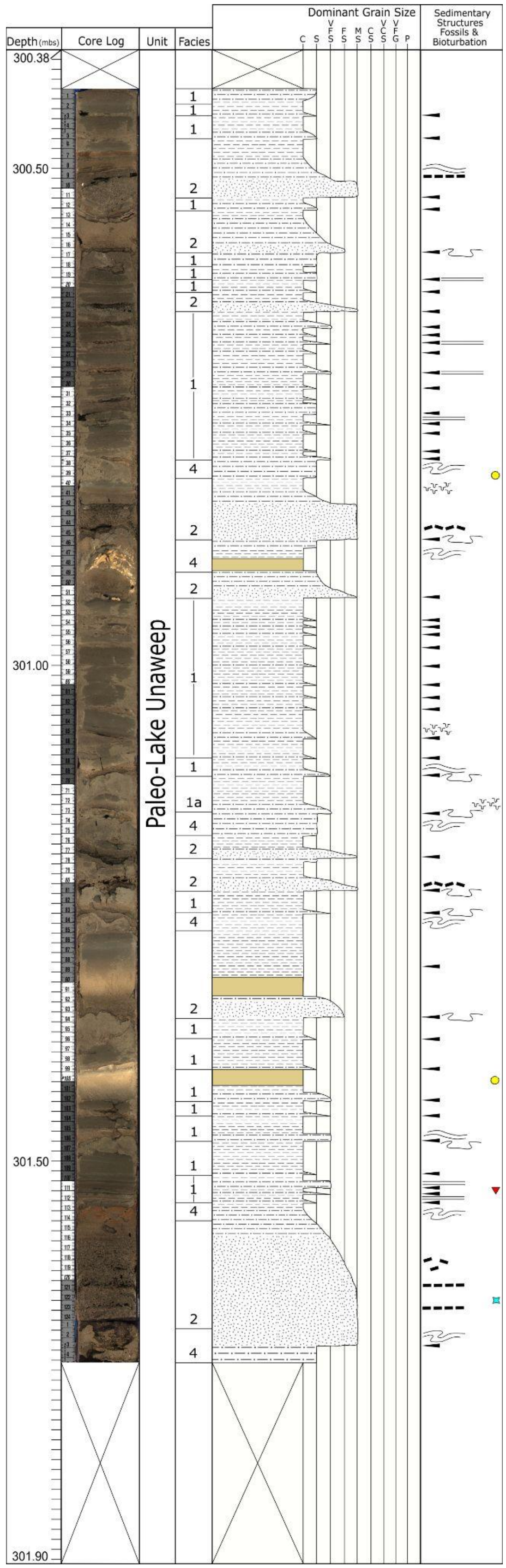
Depth (mbs)
Core Log
Unit
Facies
Dominant Grain Size
C S VFS FS MS CS VCS VFG P
Sedimentary Structures Fossils & Bioturbation
300.38
300.50
301.00
301.50
301.90
Paleo-Lake Unaweep
1a

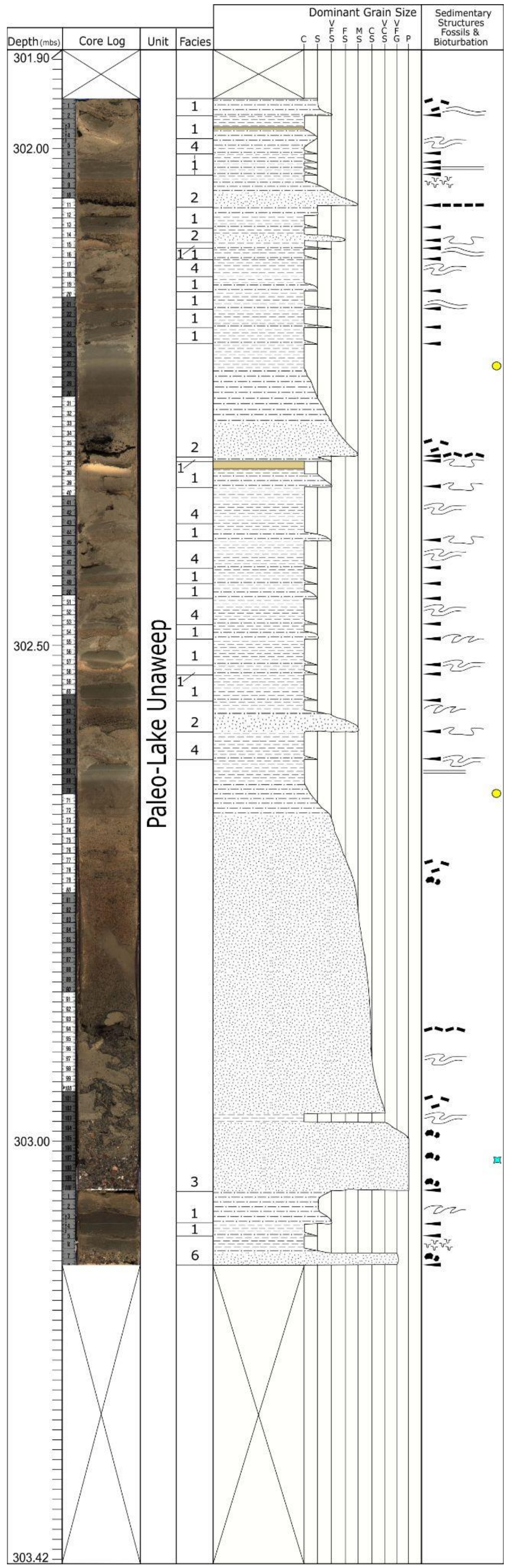
Depth (mbs)
Core Log
Unit
Facies
Dominant Grain Size
C S VFS FS MS CS VCS VFG P
Sedimentary Structures Fossils & Bioturbation
301.90
302.00
302.50
303.00
303.42
Paleo-Lake Unaweep

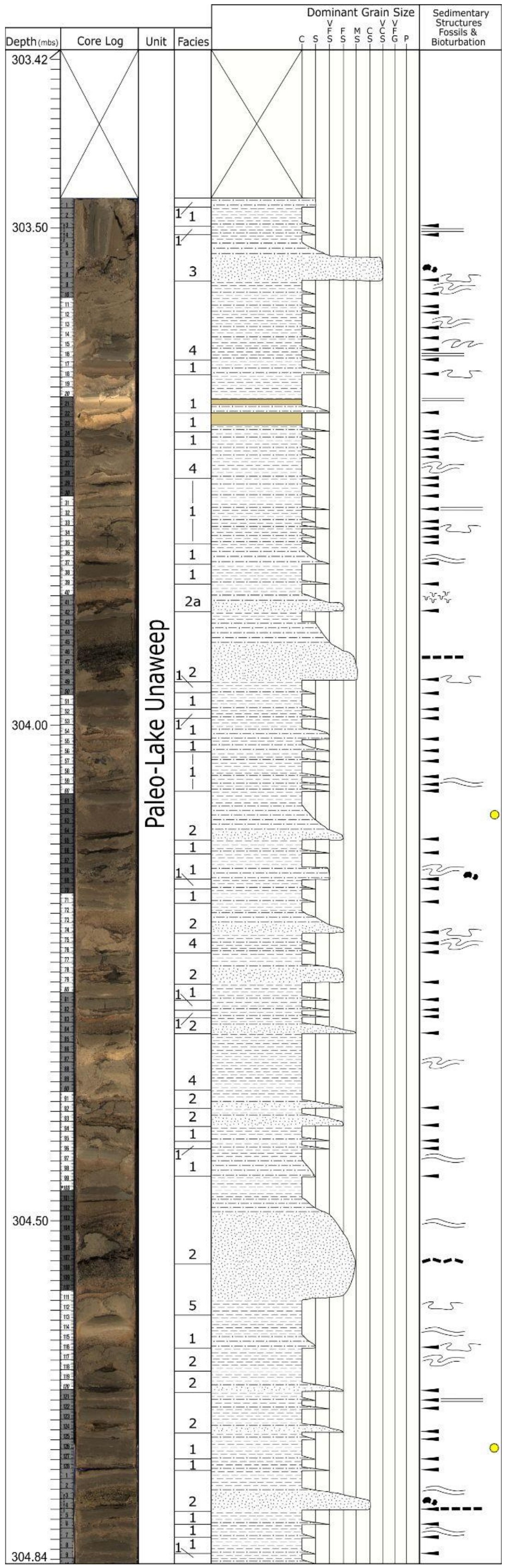

Depth (mbs)
Core Log
Unit
Facies
Dominant Grain Size
C S VFS FS MS CS VCS VFG P
Sedimentary Structures Fossils & Bioturbation
303.42
303.50
304.00
304.50
304.84
Paleo-Lake Unaweep

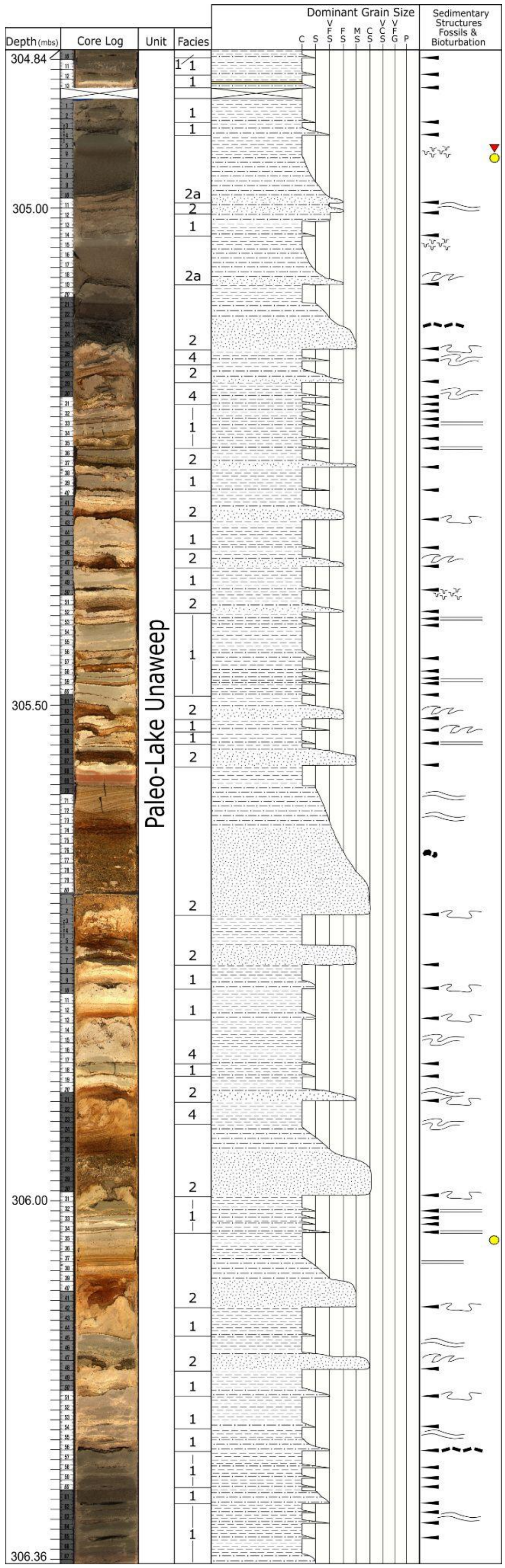

Depth (mbs)
Core Log
Unit
Facies
Dominant Grain Size
C S VFS FS MS CS VCS VFG P
Sedimentary Structures Fossils & Bioturbation
304.84
305.00
305.50
306.00
306.36
Paleo-Lake Unaweep

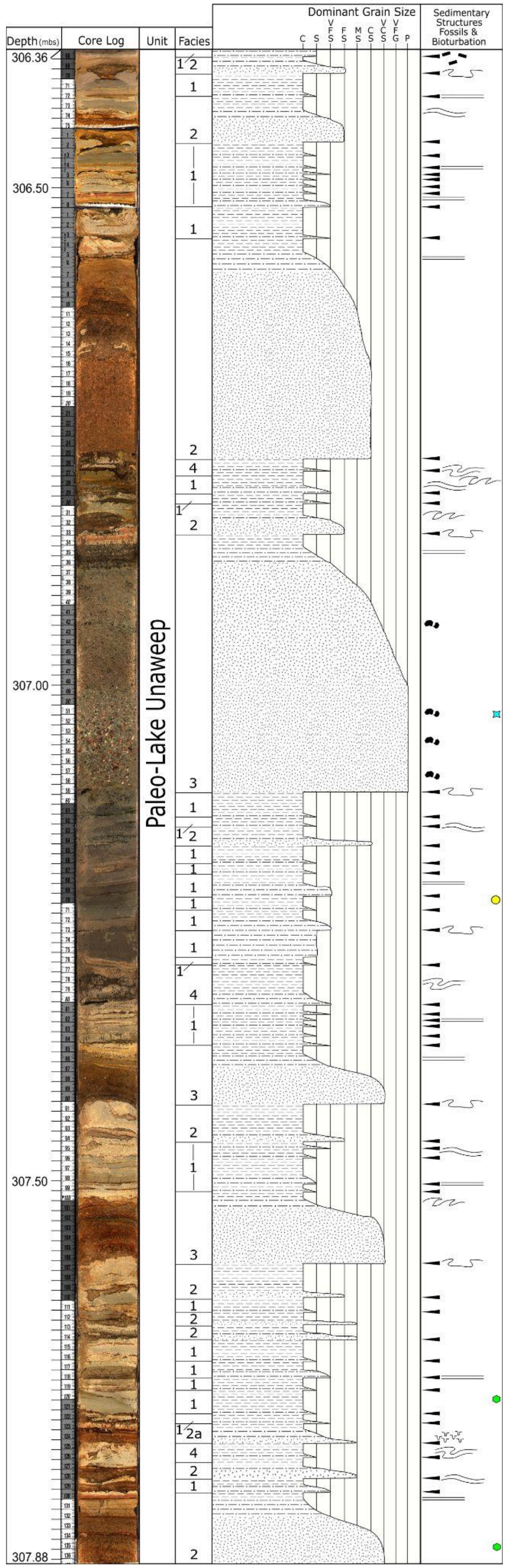
Depth (mbs)
Core Log
Unit
Facies
Dominant Grain Size
C S VFS FS MS CS VCS VFG P
Sedimentary Structures Fossils & Bioturbation
306.36
306.50
307.00
307.50
307.88
Paleo-Lake Unaweep

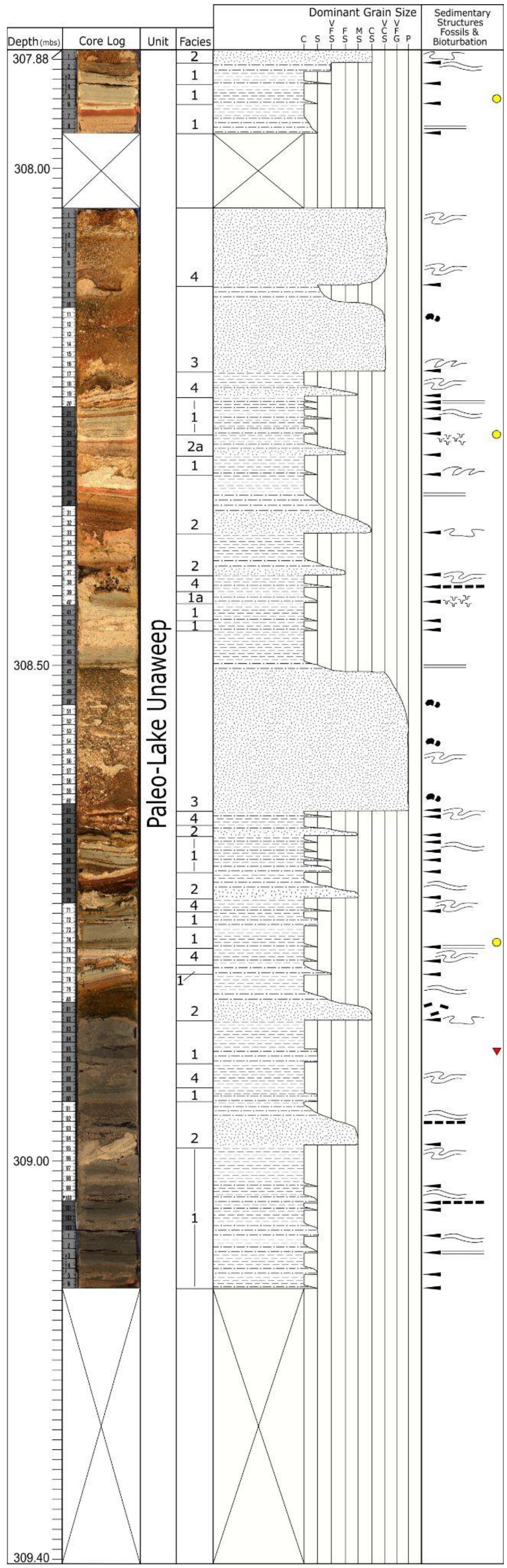

Depth (mbs)
Core Log
Unit
Facies
Dominant Grain Size
C S VFS FS MS CS VCS VFG P
Sedimentary Structures Fossils & Bioturbation
307.88
308.00
308.50
309.00
309.40
Paleo-Lake Unaweep
2
1
1
1
4
3
4
1
2a
1
2
2
4
1a
1
1
3
4
2
1
2
4
1
1
4
1
2
1
4
1
2
1

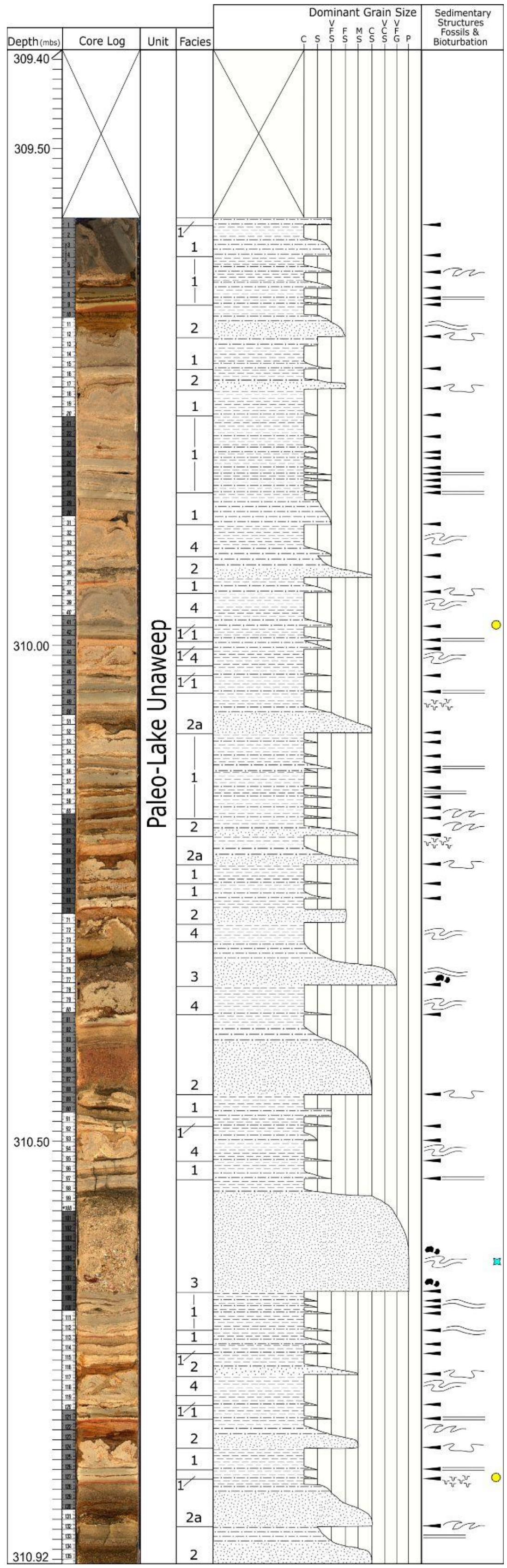

Depth (mbs)
Core Log
Unit
Facies
Dominant Grain Size
C S VFS FS MS CS VCS VFG P
Sedimentary Structures Fossils & Bioturbation
309.40
309.50
310.00
310.50
310.92
Paleo-Lake Unaweep

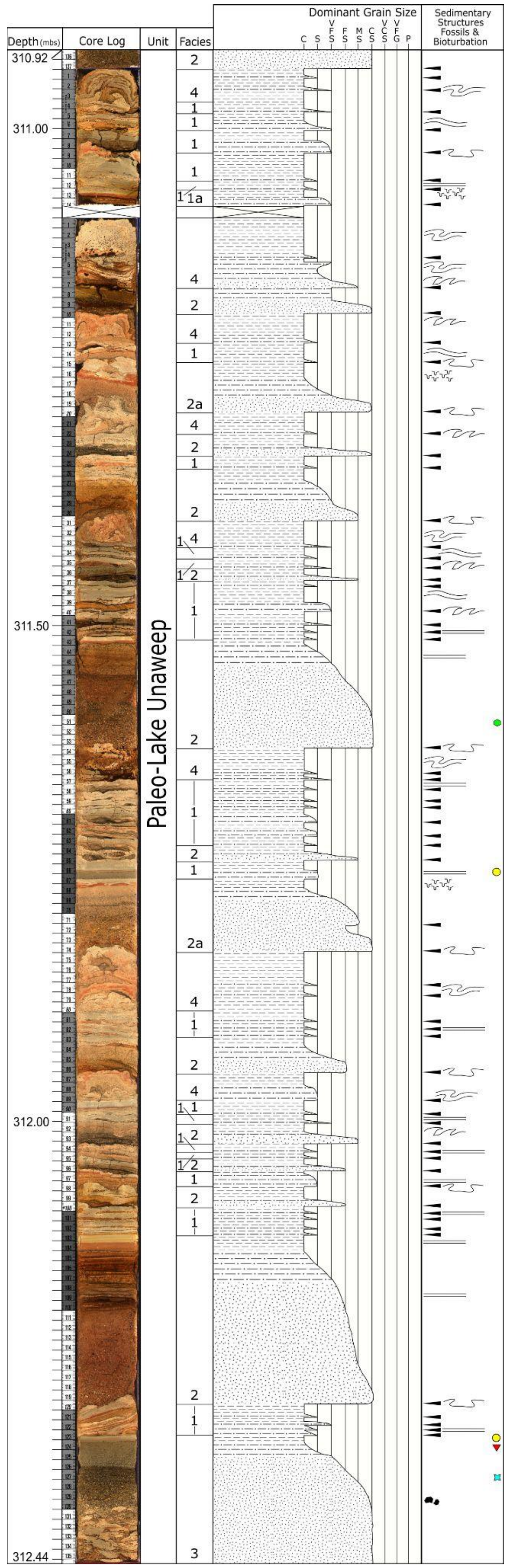
Depth (mbs)
Core Log
Unit
Facies
Dominant Grain Size
C S VFS FS MS CS VCS VFG P
Sedimentary Structures Fossils & Bioturbation
310.92
311.00
311.50
312.00
312.44
Paleo-Lake Unaweep

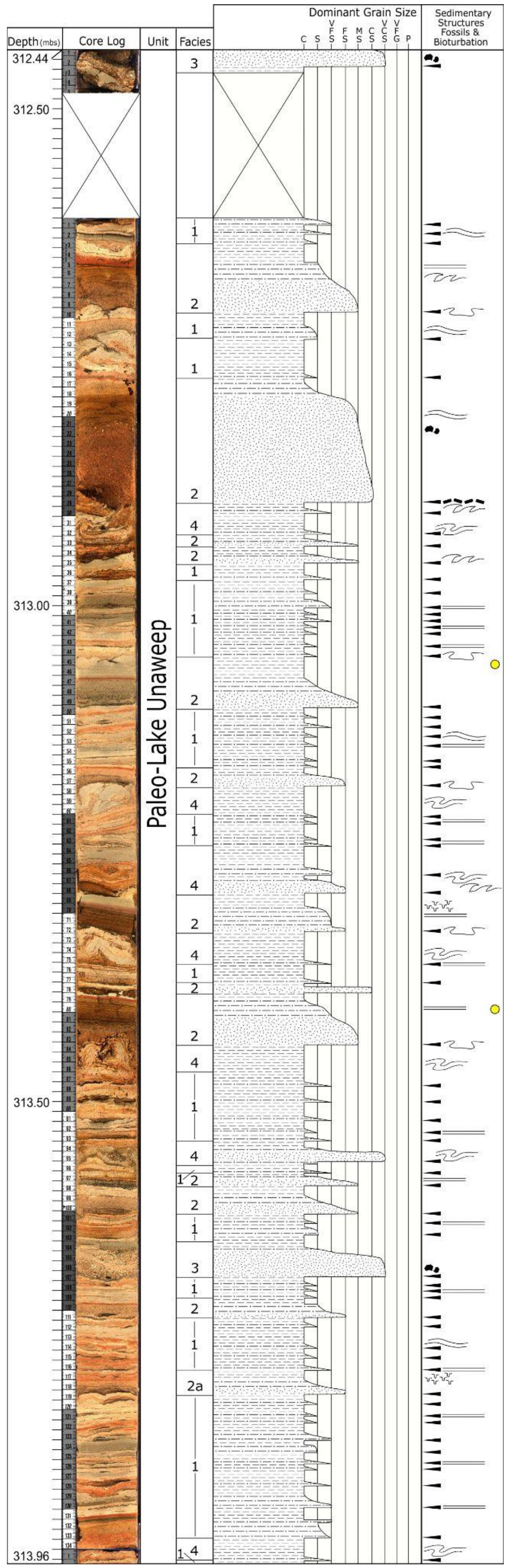
Depth (mbs)
Core Log
Unit
Facies
Dominant Grain Size
C S VFS FS MS CS VCS VFG P
Sedimentary Structures Fossils & Bioturbation
312.44
312.50
313.00
313.50
313.96
Paleo-Lake Unaweep

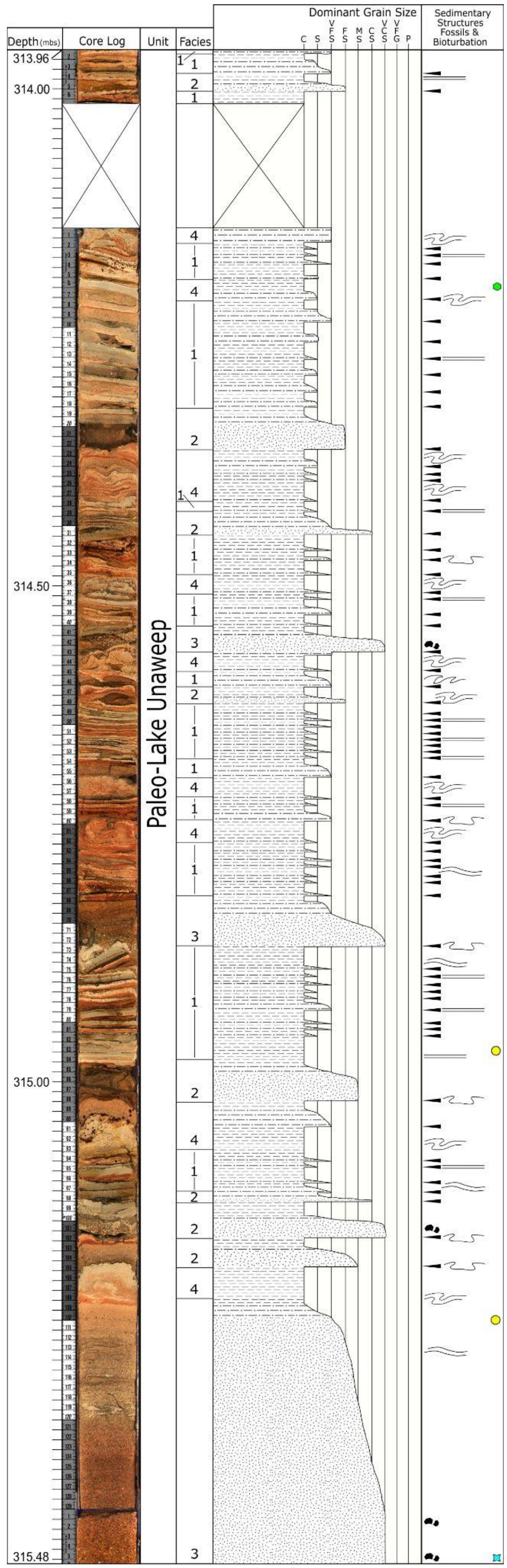
Depth (mbs)
Core Log
Unit
Facies
Dominant Grain Size
C S VFS FS MS CS VCS VFG P
Sedimentary Structures Fossils & Bioturbation
313.96
314.00
314.50
315.00
315.48
Paleo-Lake Unaweep

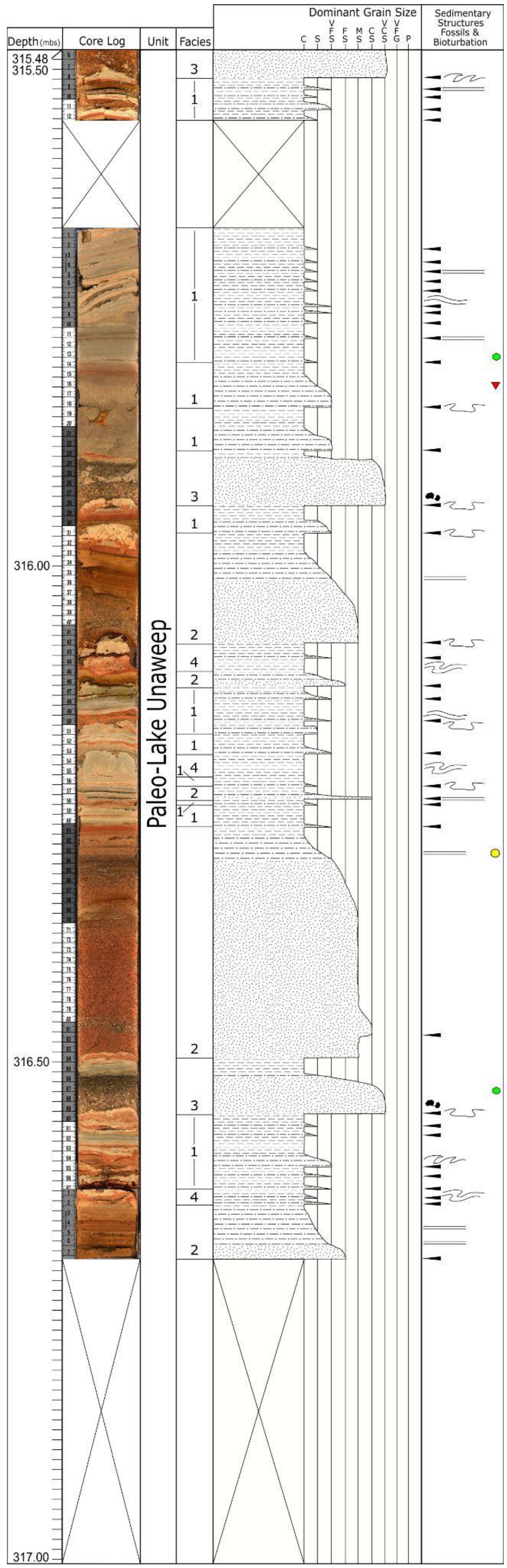
Depth (mbs)
Core Log
Unit
Facies
Dominant Grain Size
C S VFS FS MS CS VCS VFG P
Sedimentary Structures Fossils & Bioturbation
315.48
315.50
316.00
316.50
317.00
Paleo-Lake Unaweep

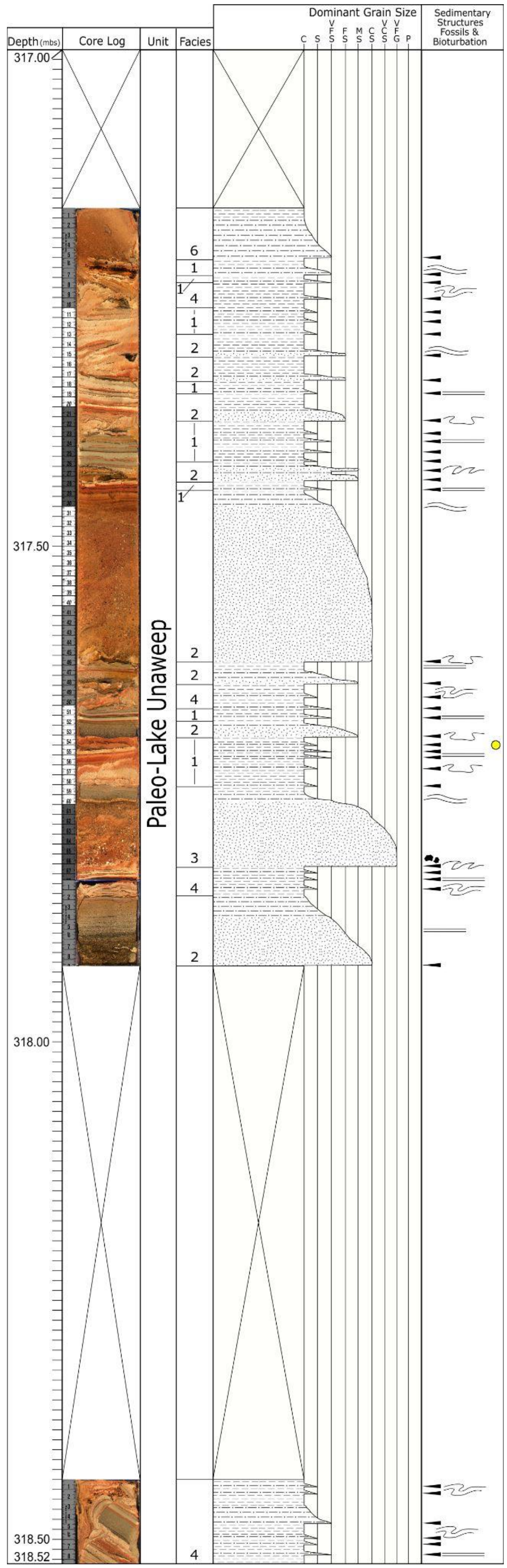
Depth (mbs)
Core Log
Unit
Facies
Dominant Grain Size
C S VFS FS MS CS VCS VFG P
Sedimentary Structures Fossils & Bioturbation
317.00
317.50
318.00
318.50
318.52
Paleo-Lake Unaweep
6
1
1
4
1
2
2
1
2
1
2
1
2
2
4
1
2
1
3
4
2
4

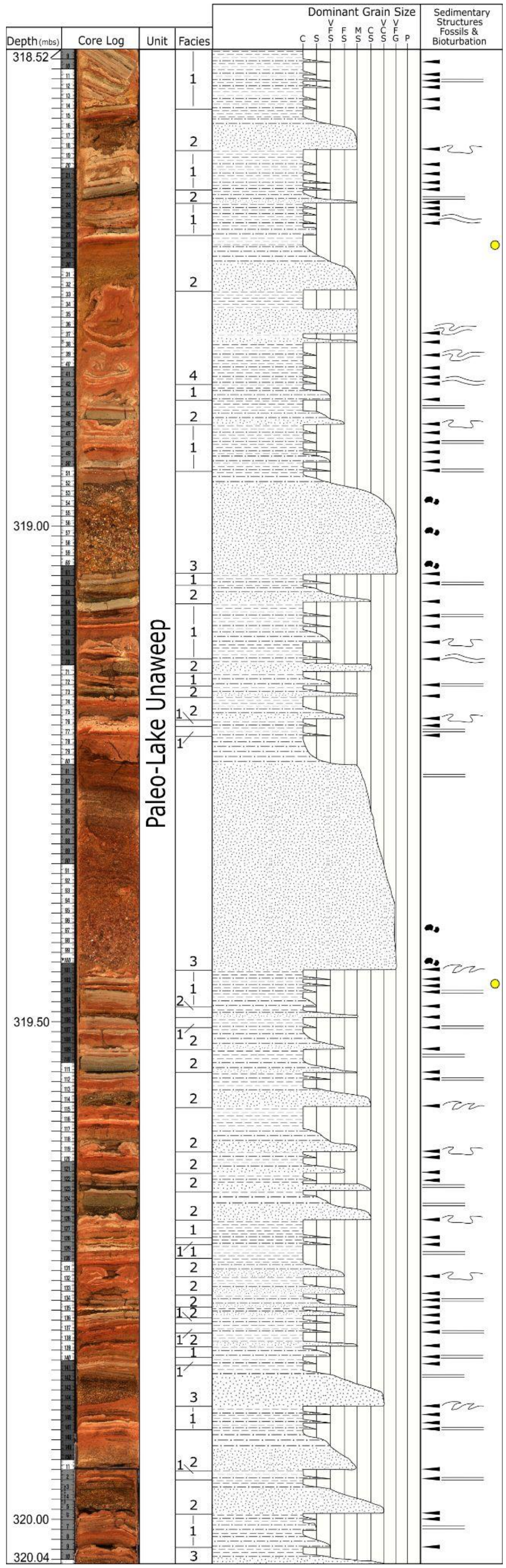

Depth (mbs)
Core Log
Unit
Facies
Dominant Grain Size
C S VFS FS MS CS VCS VFG P
Sedimentary Structures Fossils & Bioturbation
318.52
319.00
319.50
320.00
320.04
Paleo-Lake Unaweep

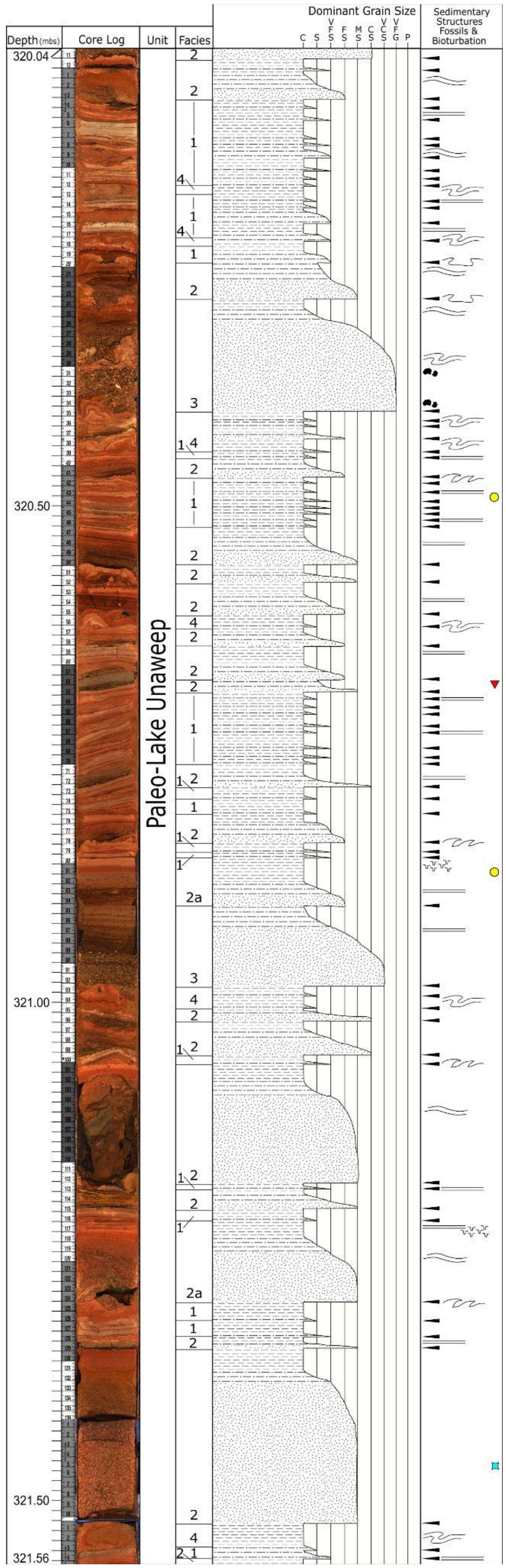
Depth (mbs)
Core Log
Unit
Facies
Dominant Grain Size
C S VFS FS MS CS VCS VFG P
Sedimentary Structures Fossils & Bioturbation
320.04
320.50
321.00
321.50
321.56
Paleo-Lake Unaweep

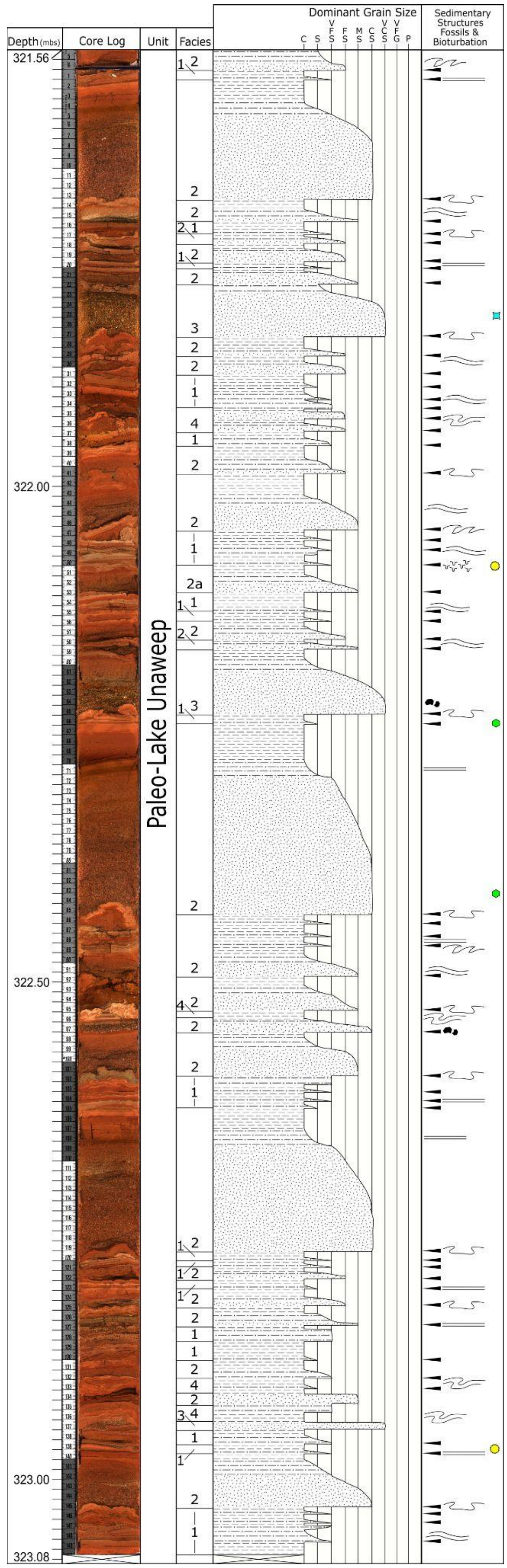
Depth (mbs)
Core Log
Unit
Facies
Dominant Grain Size
C S VFS FS MS CS VCS VFG P
Sedimentary Structures Fossils & Bioturbation
321.56
322.00
322.50
323.00
323.08
Paleo-Lake Unaweep

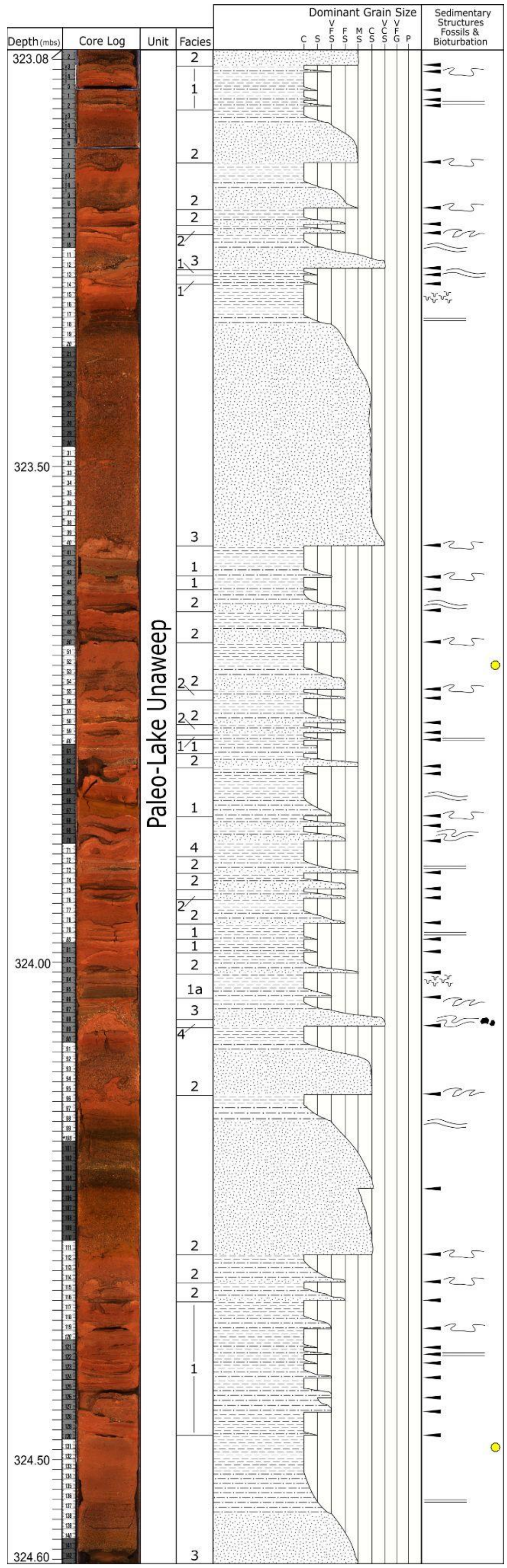
Depth (mbs)
Core Log
Unit
Facies
Dominant Grain Size
C S VFS FS MS CS VCS VFG P
Sedimentary Structures Fossils & Bioturbation
323.08
323.50
324.00
324.50
324.60
Paleo-Lake Unaweep

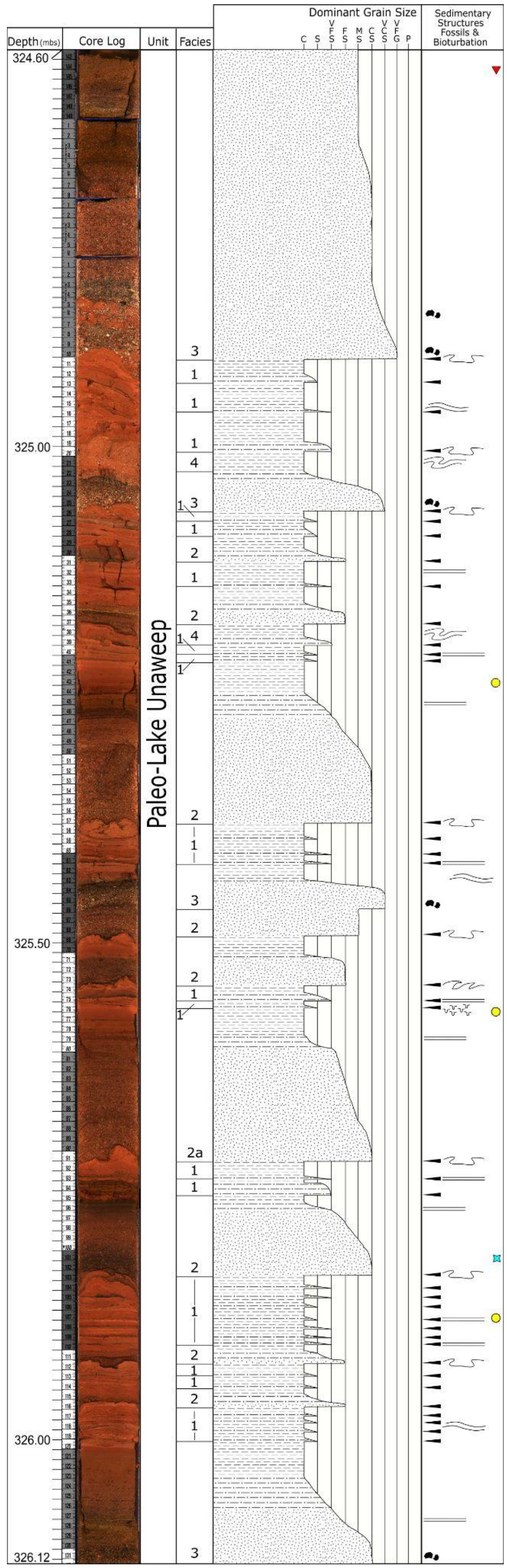
Depth (mbs)
Core Log
Unit
Facies
Dominant Grain Size
C S VFS FS MS CS VCS VFG P
Sedimentary Structures Fossils & Bioturbation
324.60
325.00
325.50
326.00
326.12
Paleo-Lake Unaweep
3
1
1
1
4
3
1
2
1
2
4
2
1
3
2
2
1
2a
1
1
2
1
2
1
1
2
1
3

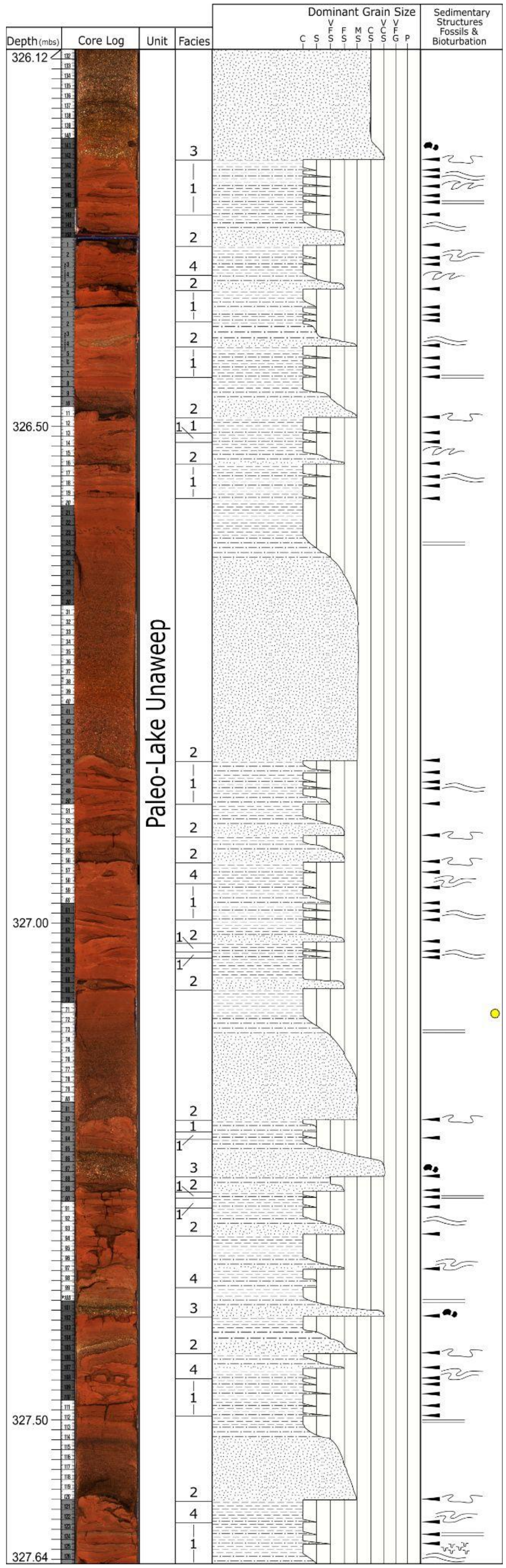
Depth (mbs)
Core Log
Unit
Facies
Dominant Grain Size
C S VFS FS MS CS VCS VFG P
Sedimentary Structures Fossils & Bioturbation
326.12
326.50
327.00
327.50
327.64
Paleo-Lake Unaweep

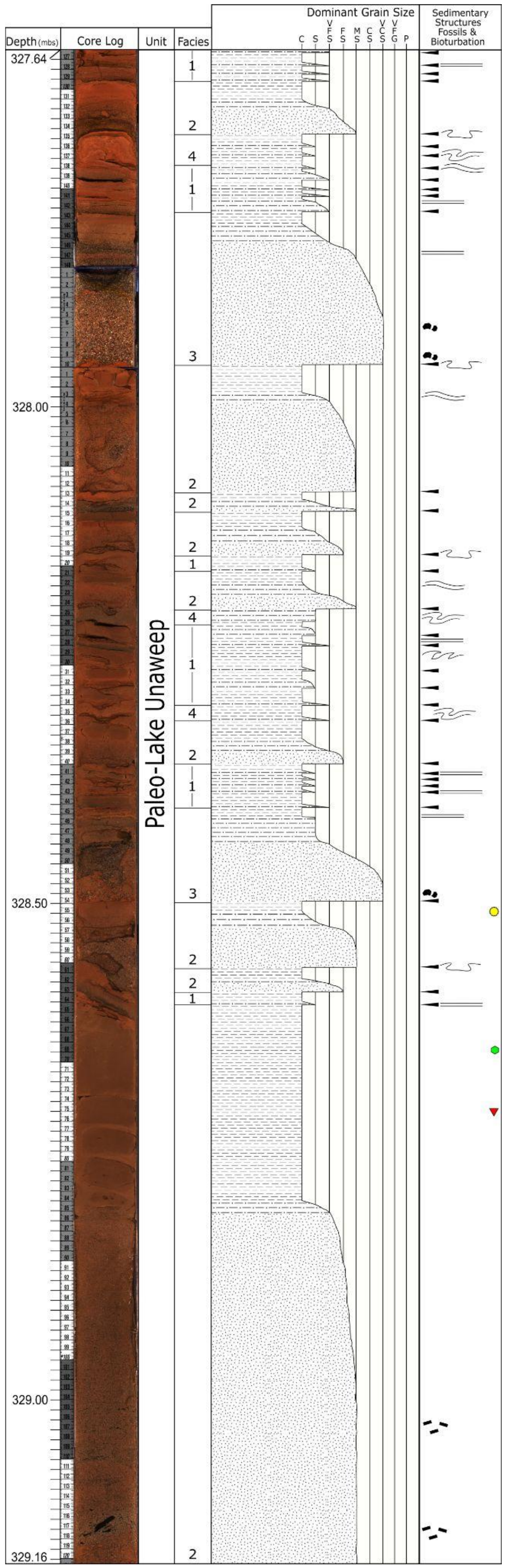
Depth (mbs)
Core Log
Unit
Facies
Dominant Grain Size
C S VFS FS MS CS VCS VFG P
Sedimentary Structures Fossils & Bioturbation
327.64
328.00
328.50
329.00
329.16
Paleo-Lake Unaweep
1
2
4
1
3
2
2
2
1
2
4
1
4
2
1
3
2
2
1
2

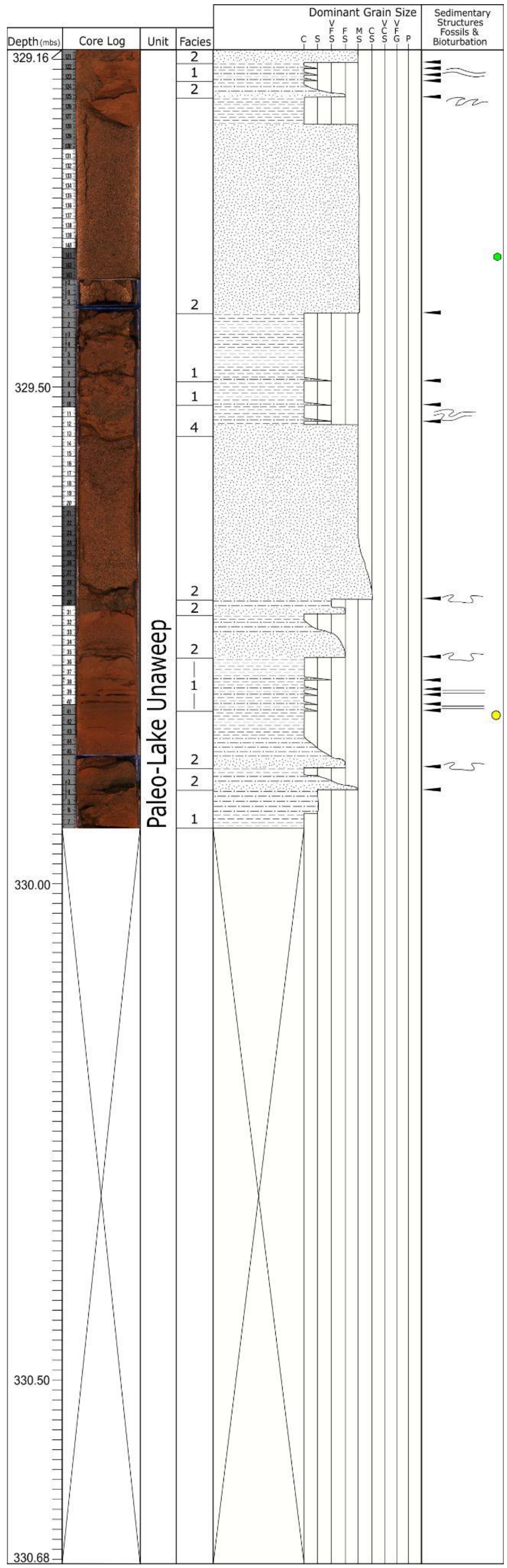

Depth (mbs)
Core Log
Unit
Facies
Dominant Grain Size
C S VFS FS MS CS VCS VFG P
Sedimentary Structures Fossils & Bioturbation
329.16
329.50
330.00
330.50
330.68
Paleo-Lake Unaweep
2
1
2
2
1
1
4
2
2
2
1
2
2
1

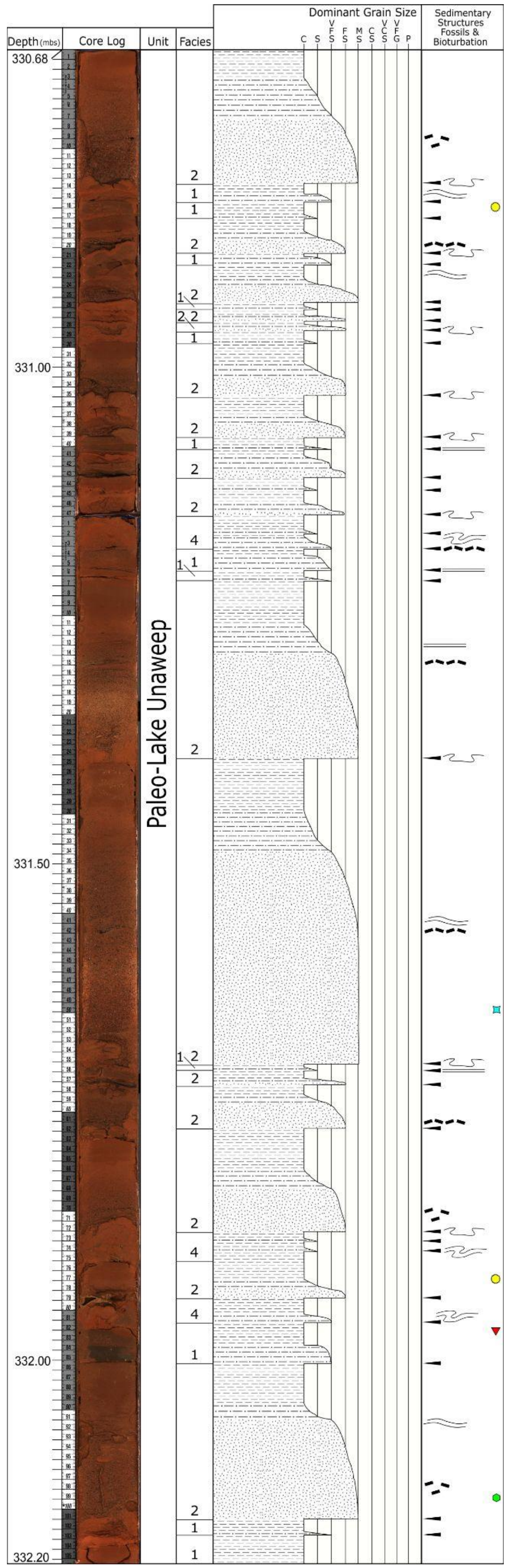
Depth (mbs)
Core Log
Unit
Facies
Dominant Grain Size
C S VFS FS MS CS VCS VFG P
Sedimentary Structures Fossils & Bioturbation
330.68
331.00
331.50
332.00
332.20
Paleo-Lake Unaweep

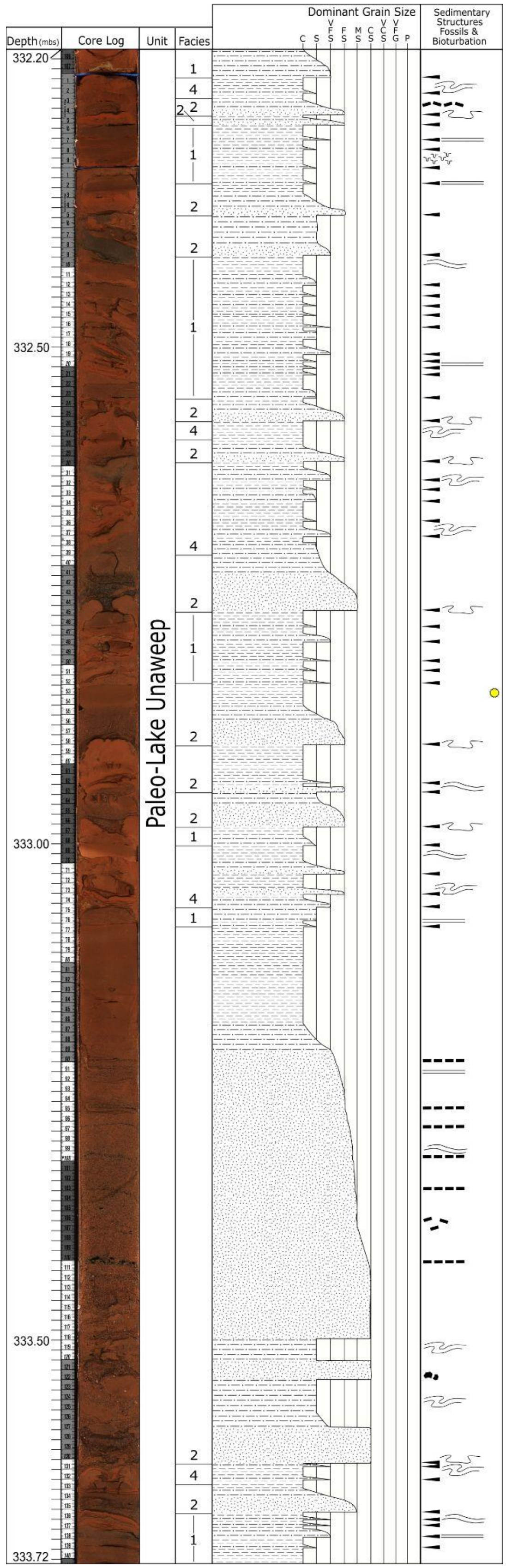
Depth (mbs)
Core Log
Unit
Facies
Dominant Grain Size
C S VFS FS MS CS VCS VFG P
Sedimentary Structures Fossils & Bioturbation
332.20
332.50
333.00
333.50
333.72
Paleo-Lake Unaweep
1
4
2
1
2
2
1
2
4
2
4
2
1
2
2
2
1
4
1
2
4
2
1

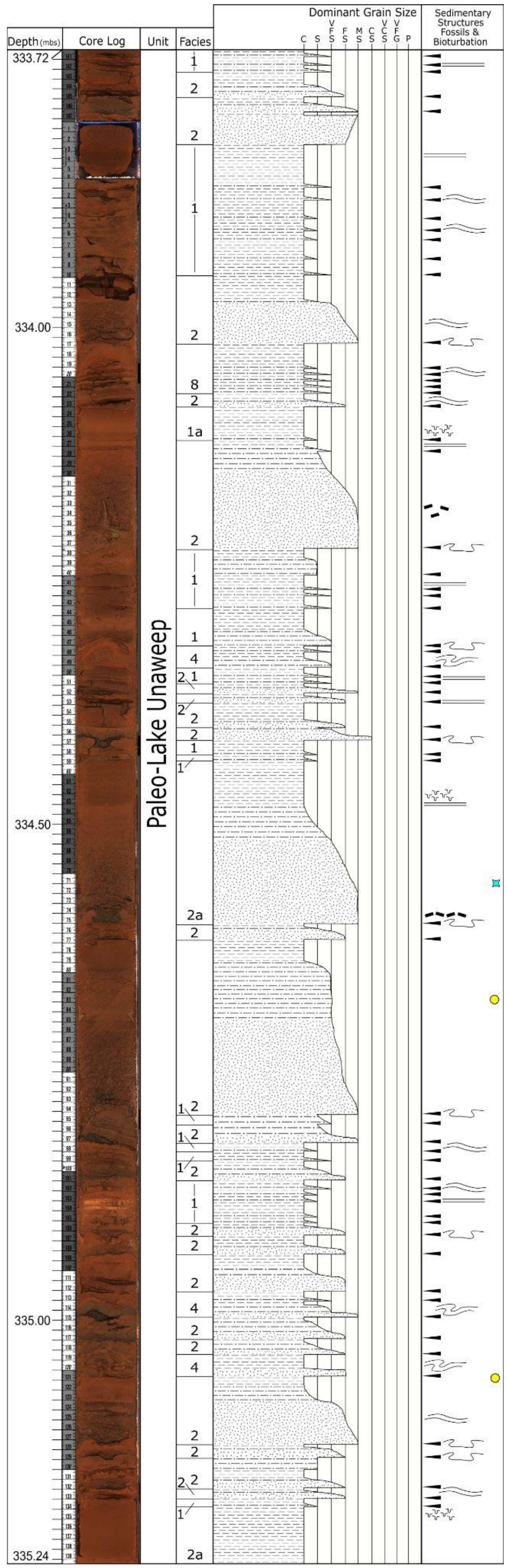

Depth (mbs)
Core Log
Unit
Facies
Dominant Grain Size
C S VFS FS MS CS VCS VFG P
Sedimentary Structures Fossils & Bioturbation
333.72
334.00
334.50
335.00
335.24
Paleo-Lake Unaweep

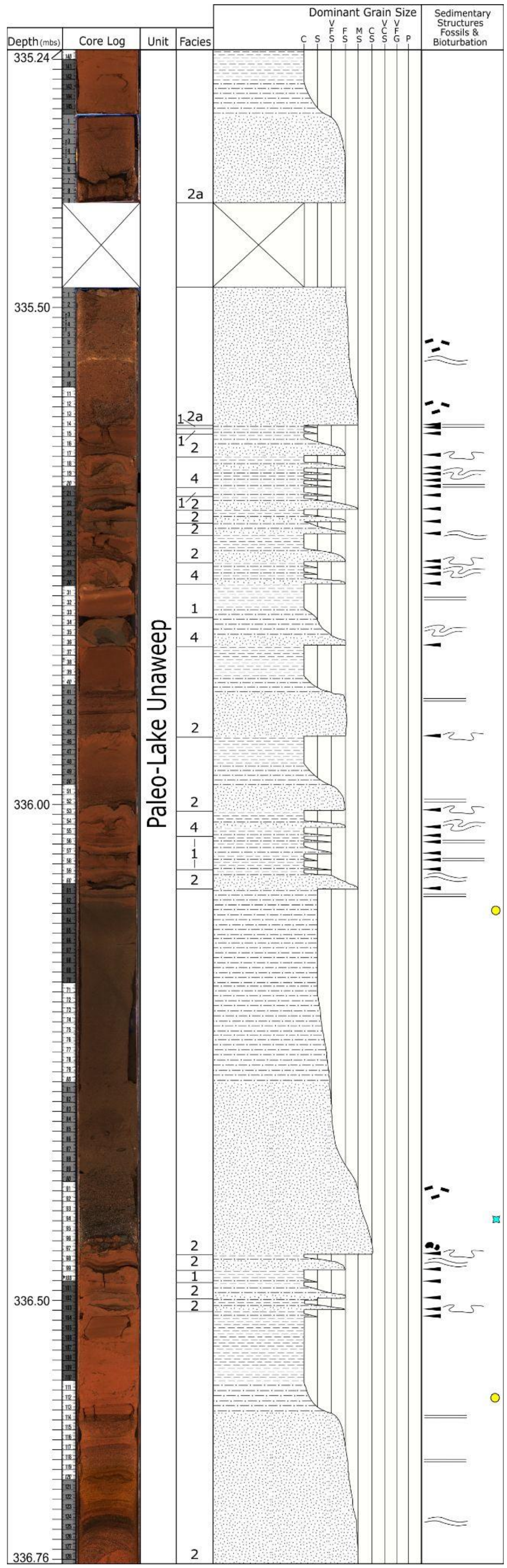
Depth (mbs)
Core Log
Unit
Facies
Dominant Grain Size
C S VFS FS MS CS VCS VFG P
Sedimentary Structures Fossils & Bioturbation
335.24
335.50
336.00
336.50
336.76
Paleo-Lake Unaweep
2a
1 2a
1
2
4
1
2
2
2
2
4
1
4
2
2
4
1
2
2
2
1
2
2
2

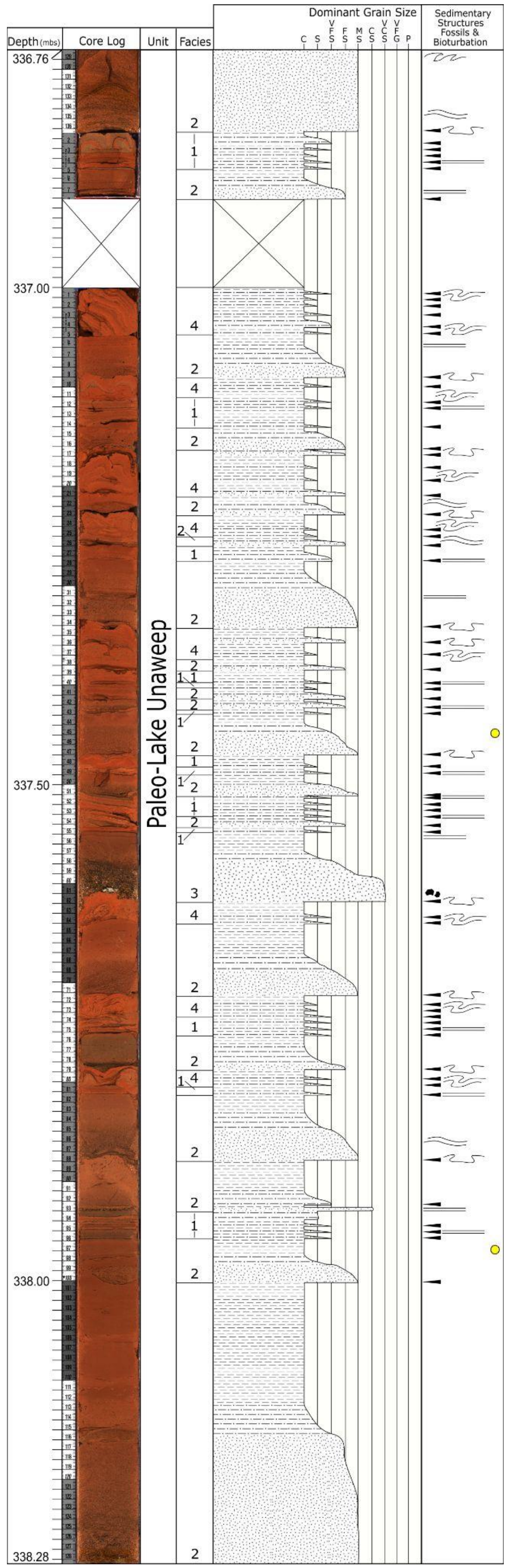
Depth (mbs)
Core Log
Unit
Facies
Dominant Grain Size
C S VFS FS MS CS VCS VFG P
Sedimentary Structures Fossils & Bioturbation
336.76
337.00
337.50
338.00
338.28
Paleo-Lake Unaweep

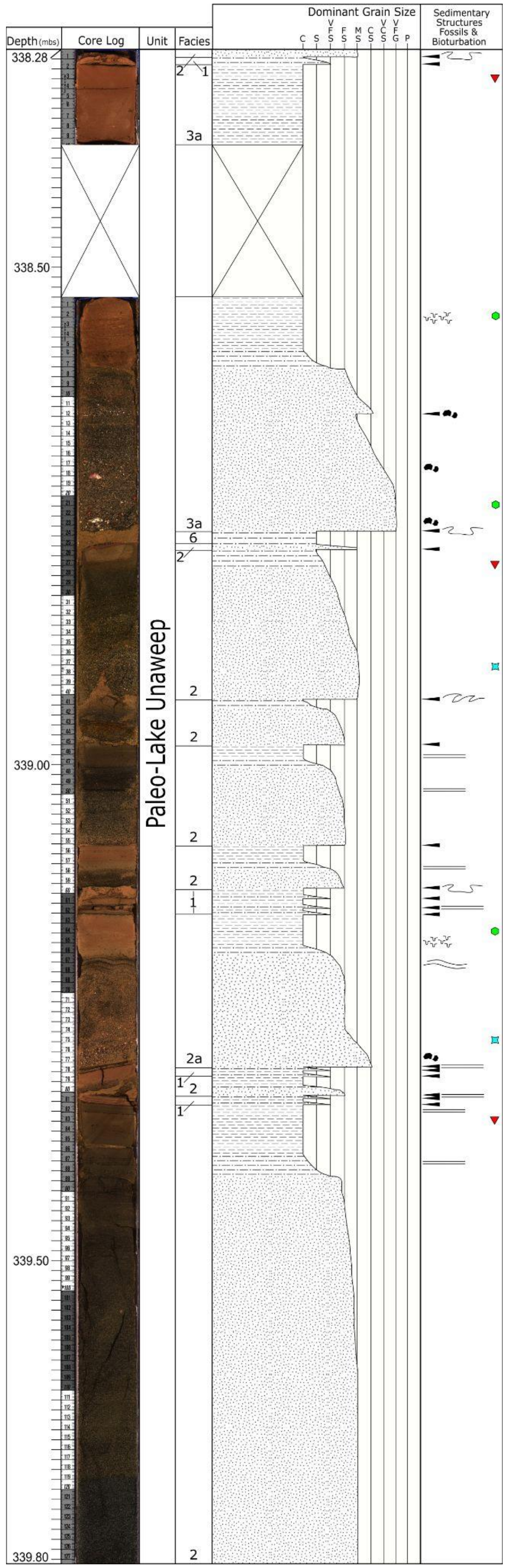

Depth (mbs)
Core Log
Unit
Facies
Dominant Grain Size
C S VFS FS MS CS VCS VFG P
Sedimentary Structures Fossils & Bioturbation
338.28
338.50
339.00
339.50
339.80
Paleo-Lake Unaweep
3a
6
2
2a
1

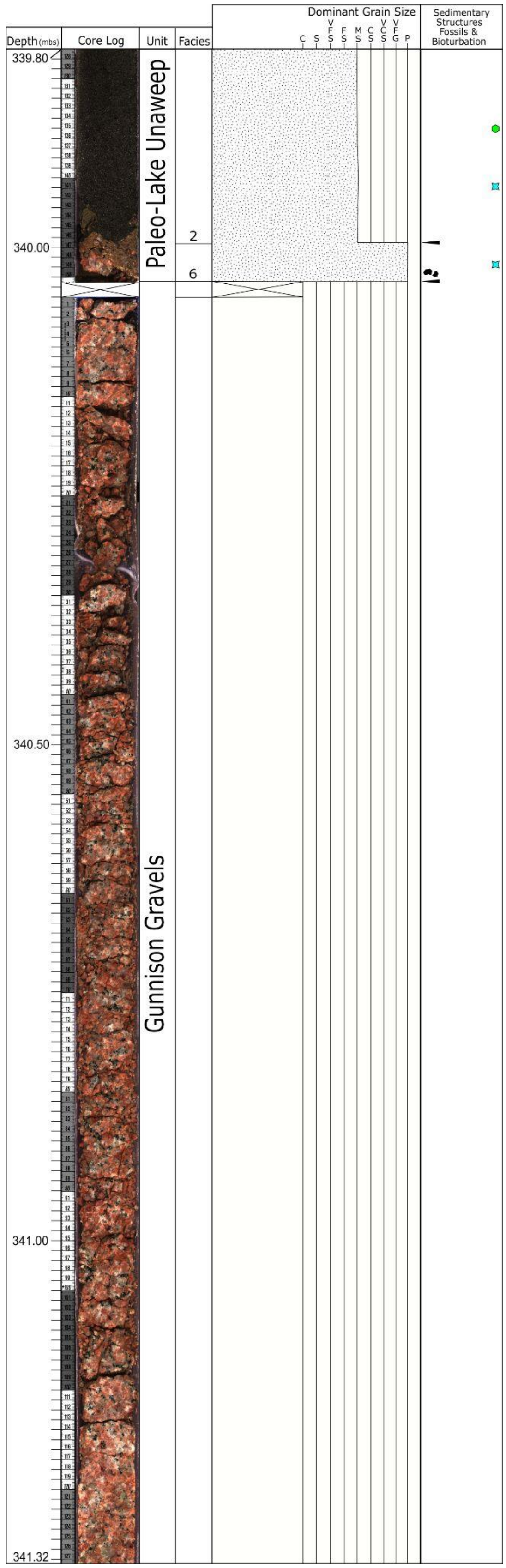

Depth (mbs)
Core Log
Unit
Facies
Dominant Grain Size
C S VFS FS MS CS VCS VFG P
Sedimentary Structures Fossils & Bioturbation
339.80
340.00
340.50
341.00
341.32
Paleo-Lake Unaweep
Gunnison Gravels
2
6

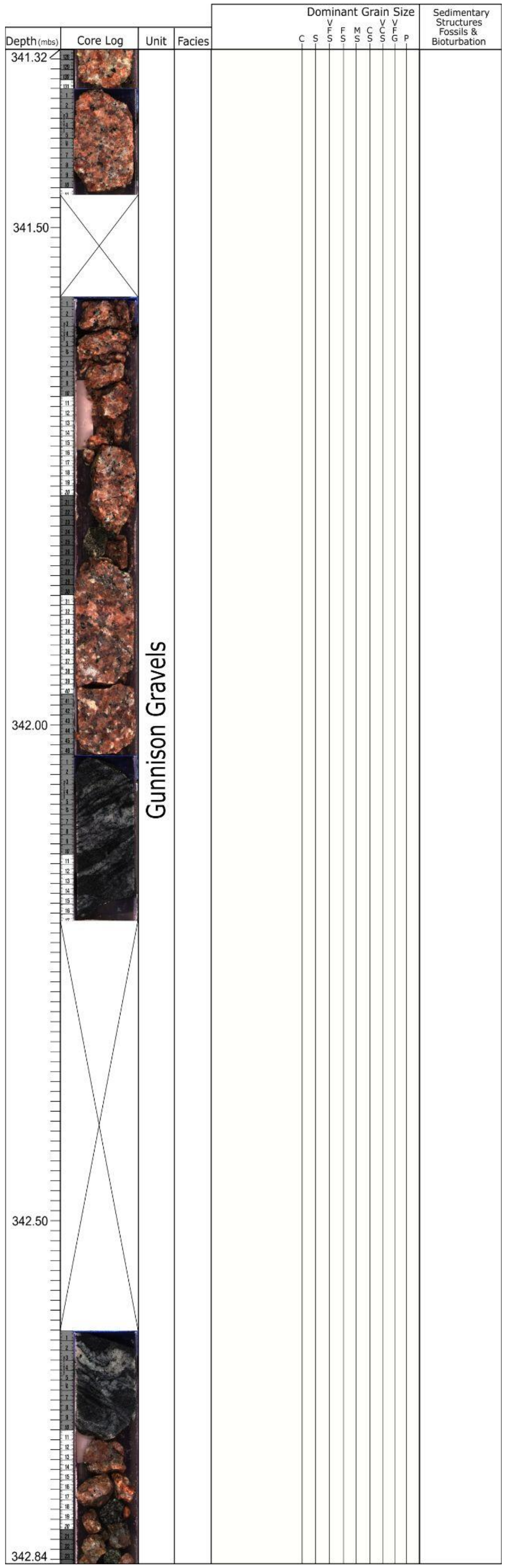
Depth (mbs)
Core Log
Unit
Facies
Dominant Grain Size
C S VFS FS MS CS VCS VFG P
Sedimentary Structures Fossils & Bioturbation
341.32
341.50
342.00
342.50
342.84
Gunnison Gravels

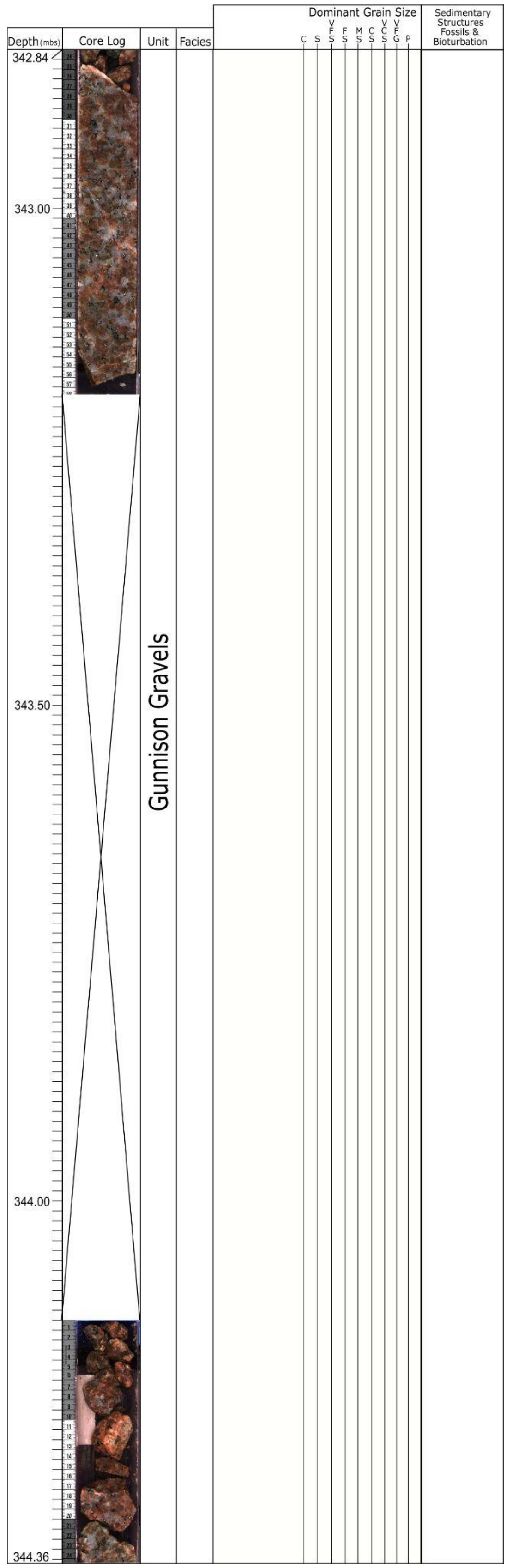
Depth (mbs)
Core Log
Unit
Facies
Dominant Grain Size
C S VFS FS MS CS VCS VFG P
Sedimentary Structures Fossils & Bioturbation
342.84
343.00
343.50
344.00
344.36
Gunnison Gravels

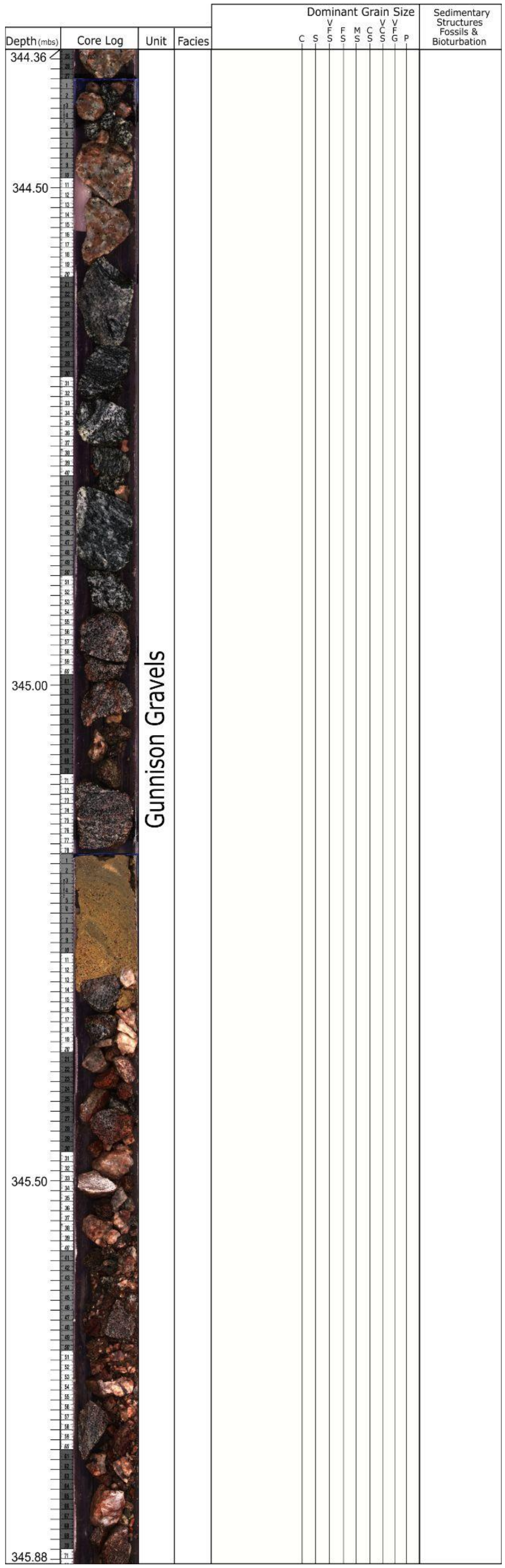
Depth (mbs)
Core Log
Unit
Facies
Dominant Grain Size
C S VFS FS MS CS VCS VFG P
Sedimentary Structures Fossils & Bioturbation
344.36
344.50
345.00
345.50
345.88
Gunnison Gravels

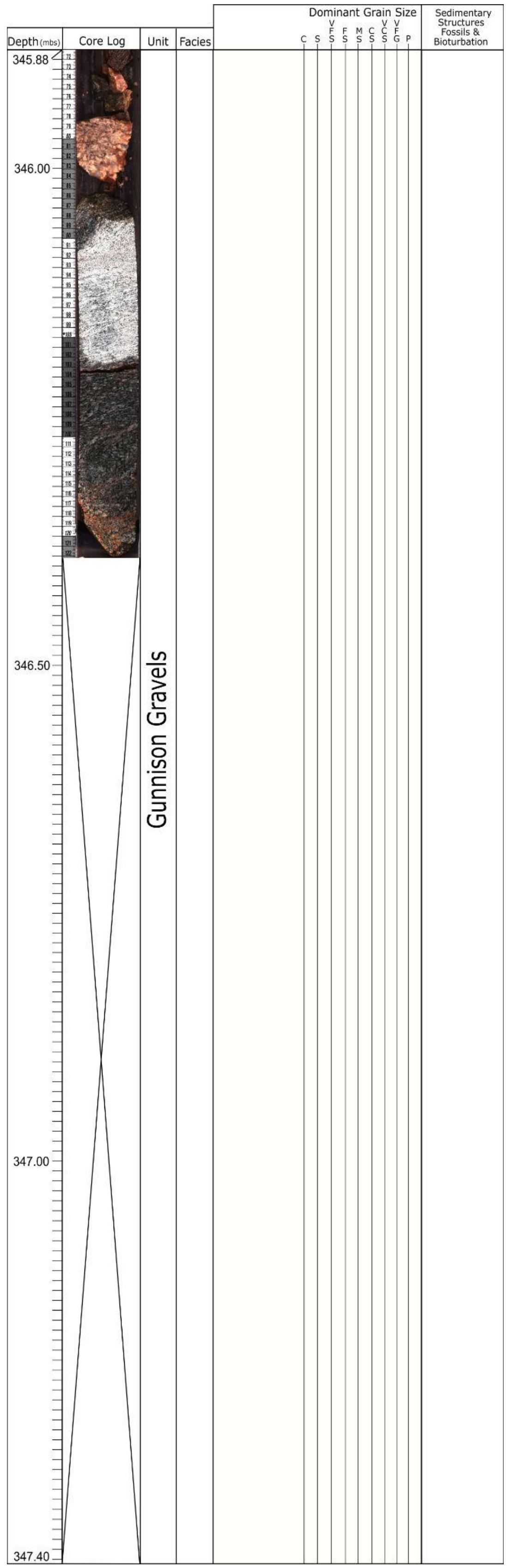
Depth (mbs)
Core Log
Unit
Facies
Dominant Grain Size
C S VFS FS MS CS VCS VFG P
Sedimentary Structures Fossils & Bioturbation
345.88
346.00
346.50
347.00
347.40
Gunnison Gravels

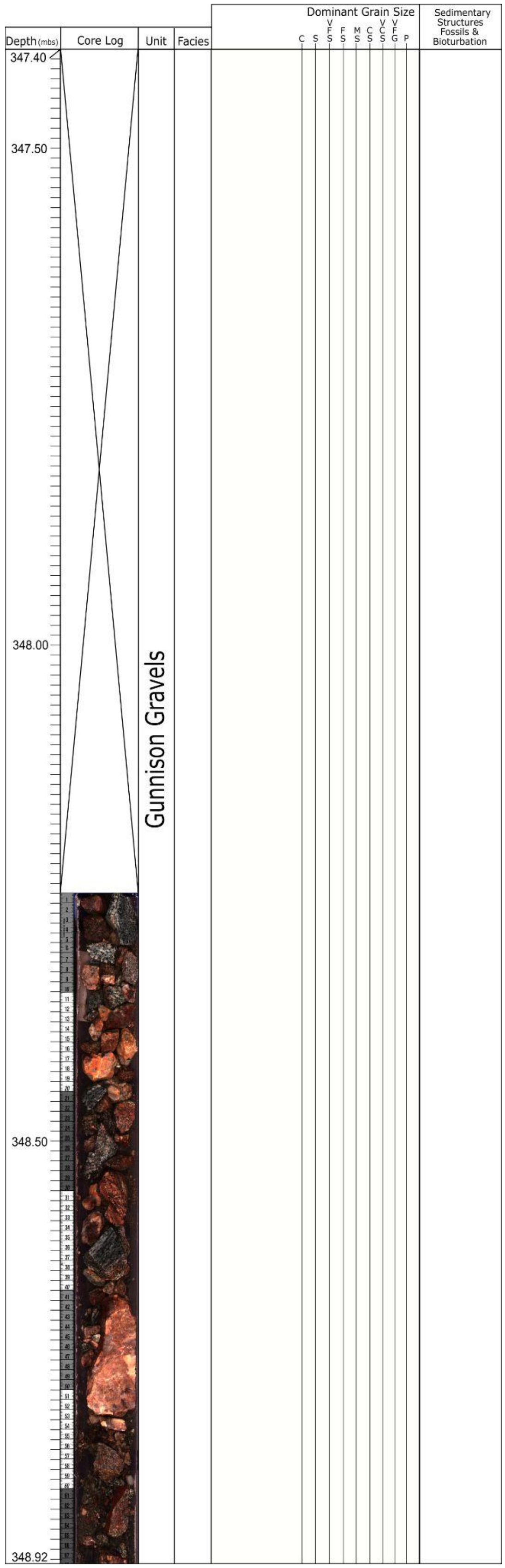
Depth (mbs)
Core Log
Unit
Facies
Dominant Grain Size
C S VFS FS MS CS VCS VFG P
Sedimentary Structures Fossils & Bioturbation
347.40
347.50
348.00
348.50
348.92
Gunnison Gravels

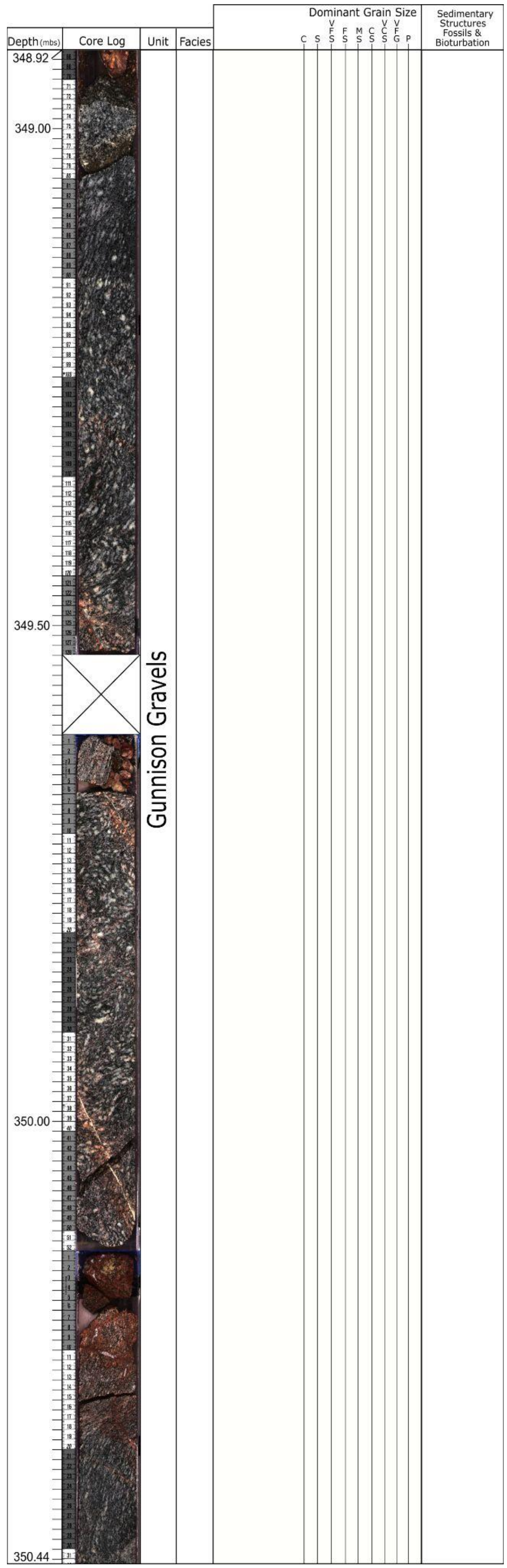

Depth (mbs)
Core Log
Unit
Facies
Dominant Grain Size
C S VFS FS MS CS VCS VFG P
Sedimentary Structures Fossils & Bioturbation
348.92
349.00
349.50
350.00
350.44
Gunnison Gravels

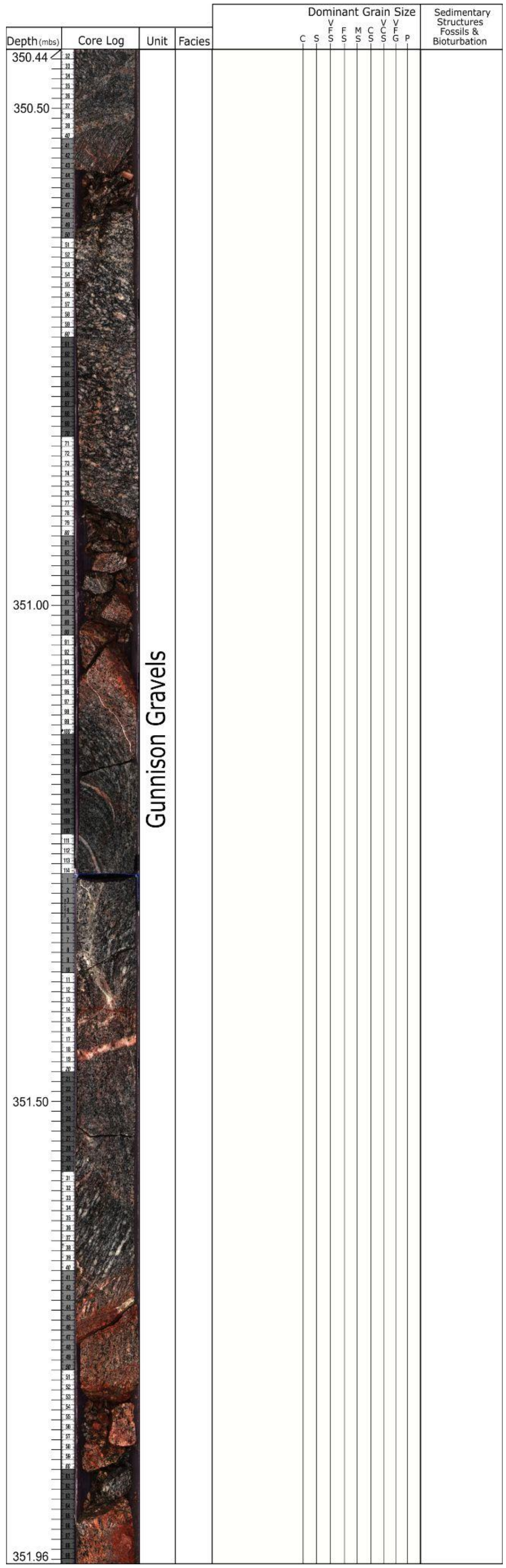
Depth (mbs)
Core Log
Unit
Facies
Dominant Grain Size
C S VFS FS MS CS VCS VFG P
Sedimentary Structures Fossils & Bioturbation
350.44
350.50
351.00
351.50
351.96
Gunnison Gravels

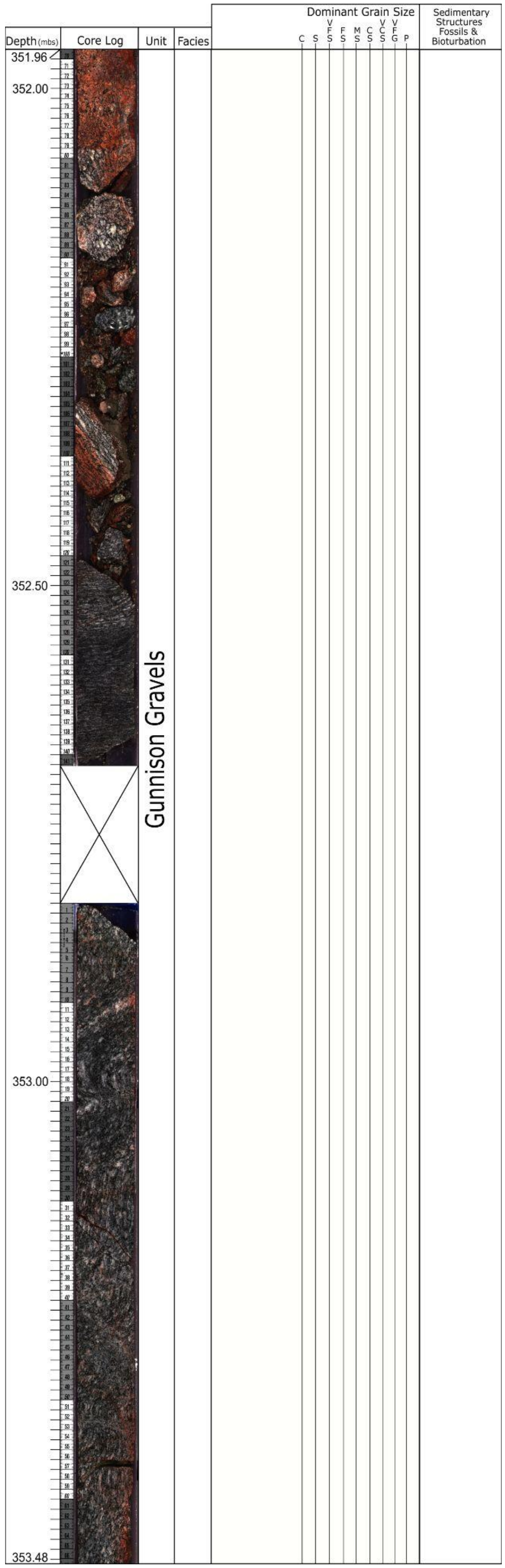
Depth (mbs)
Core Log
Unit
Facies
Dominant Grain Size
C S VFS FS MS CS VCS VFG P
Sedimentary Structures Fossils & Bioturbation
351.96
352.00
352.50
353.00
353.48
Gunnison Gravels

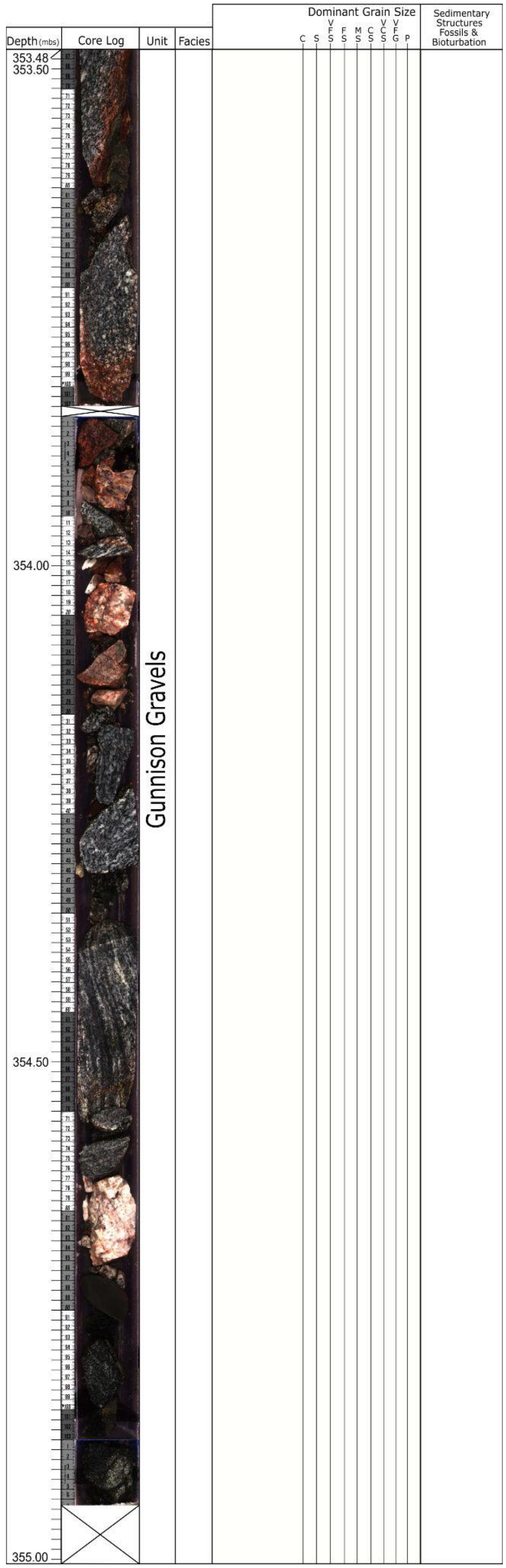
Depth (mbs)
Core Log
Unit
Facies
Dominant Grain Size
C S VFS FS MS CS VCS VFG P
Sedimentary Structures Fossils & Bioturbation
353.48
353.50
354.00
354.50
355.00
Gunnison Gravels

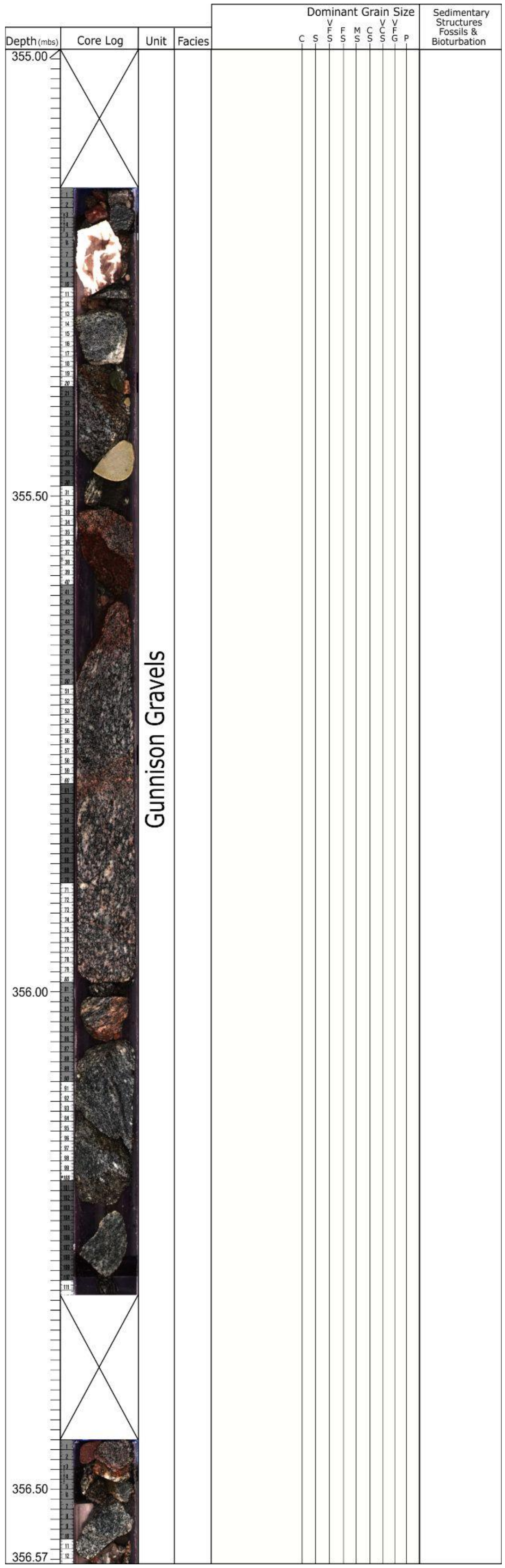
Depth (mbs)
Core Log
Unit
Facies
Dominant Grain Size
C S VFS FS MS CS VCS VFG P
Sedimentary Structures Fossils & Bioturbation
355.00
355.50
356.00
356.50
356.57
Gunnison Gravels

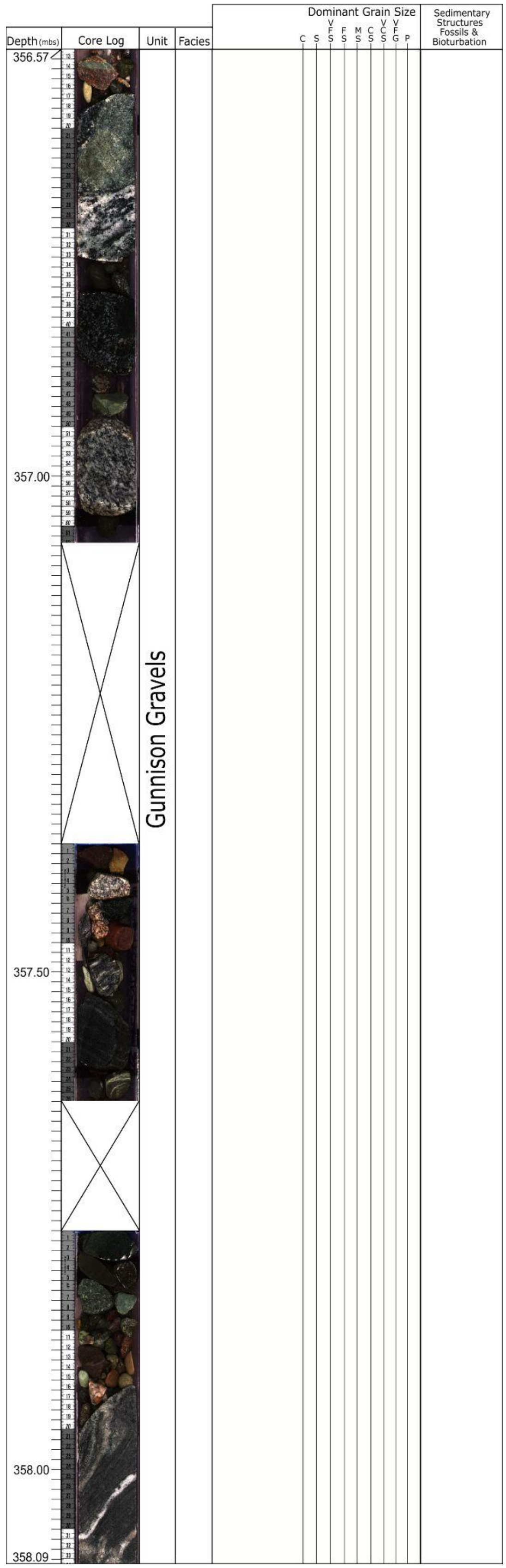
Depth (mbs)
Core Log
Unit
Facies
Dominant Grain Size
C S VFS FS MS CS VCS VFG P
Sedimentary Structures Fossils & Bioturbation
356.57
357.00
357.50
358.00
358.09
Gunnison Gravels

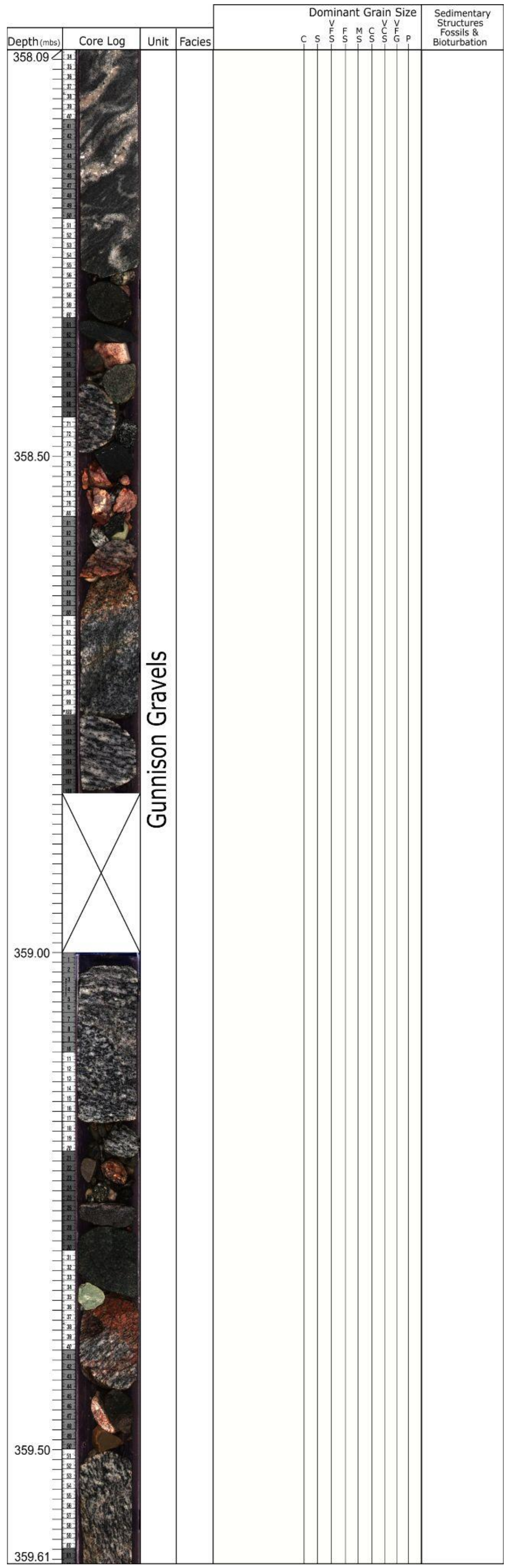
Depth (mbs)
Core Log
Unit
Facies
Dominant Grain Size
C S VFS FS MS CS VCS VFG P
Sedimentary Structures Fossils & Bioturbation
358.09
358.50
359.00
359.50
359.61
Gunnison Gravels

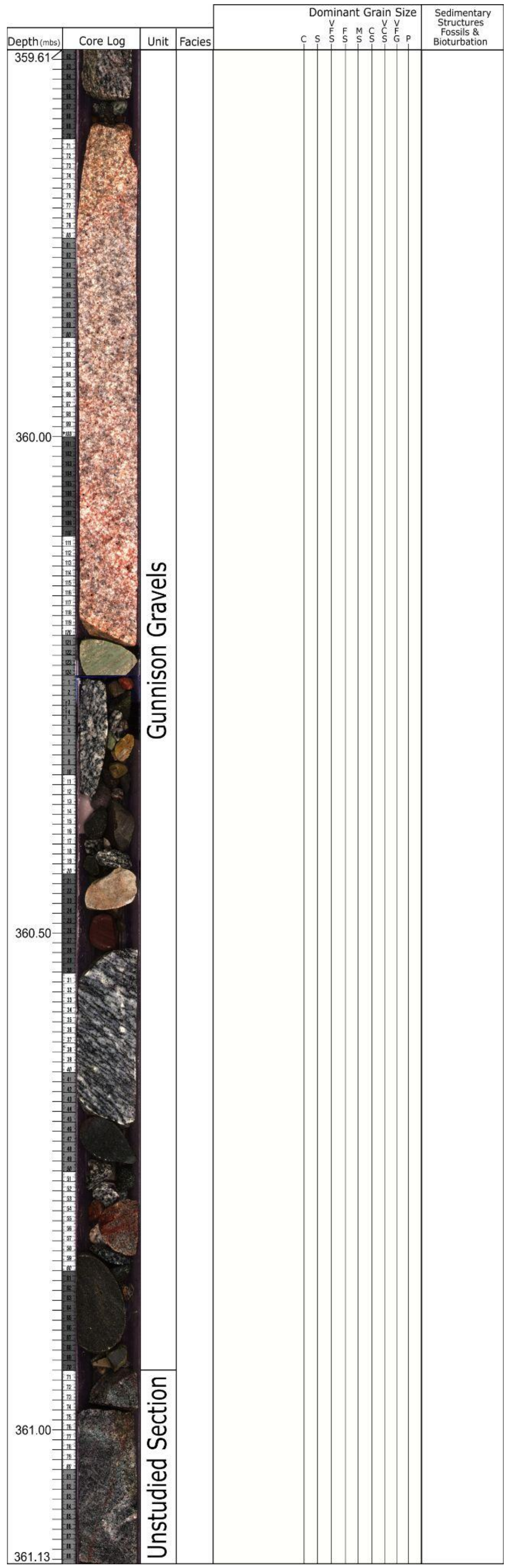
Depth (mbs)
Core Log
Unit
Facies
Dominant Grain Size
C S VFS FS MS CS VCS VFG P
Sedimentary Structures Fossils & Bioturbation
359.61
360.00
360.50
361.00
361.13
Gunnison Gravels
Unstudied Section

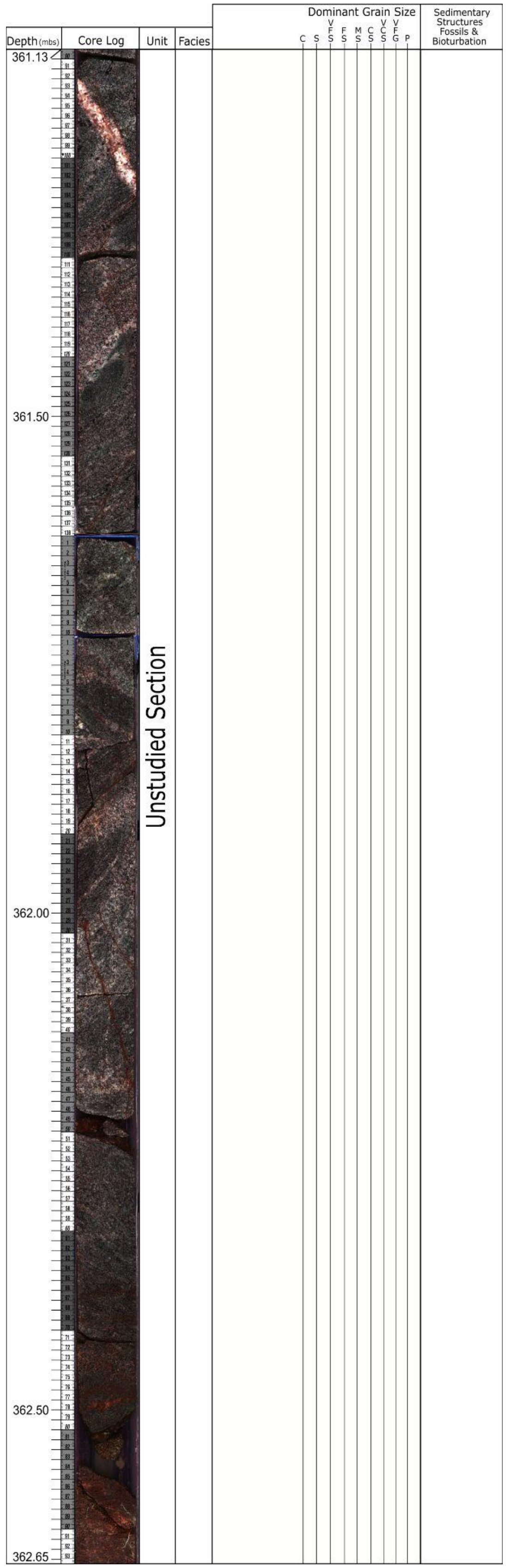
Depth (mbs)
Core Log
Unit
Facies
Dominant Grain Size
C S VFS FS MS CS VCS VFG P
Sedimentary Structures Fossils & Bioturbation
361.13
361.50
362.00
362.50
362.65
Unstudied Section

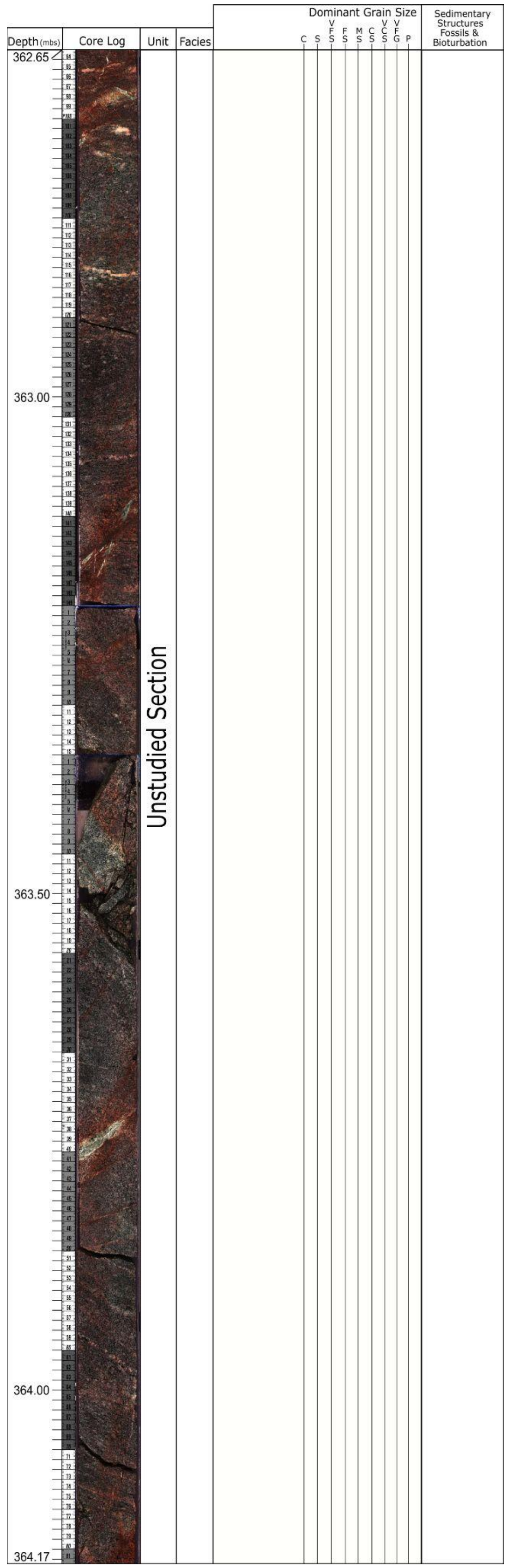
Depth (mbs)
Core Log
Unit
Facies
Dominant Grain Size
C S VFS FS MS CS VCS VFG P
Sedimentary Structures Fossils & Bioturbation
362.65
363.00
363.50
364.00
364.17
Unstudied Section

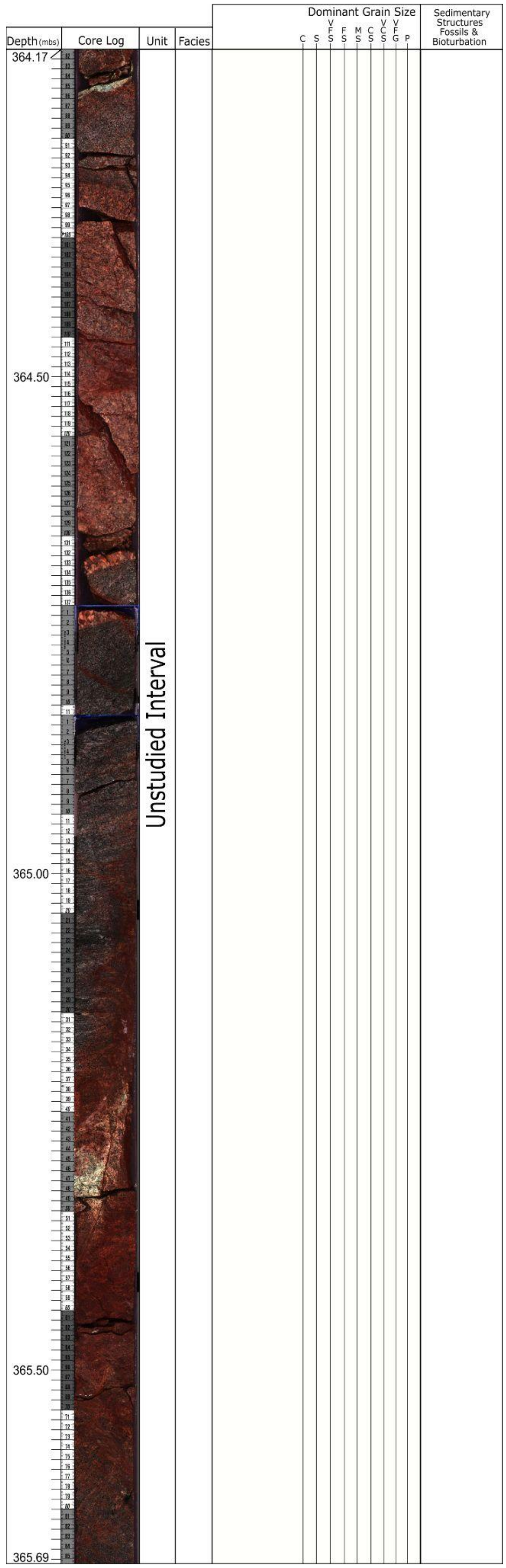
Depth (mbs)
Core Log
Unit
Facies
Dominant Grain Size
C S VFS FS MS CS VCS VFG P
Sedimentary Structures Fossils & Bioturbation
364.17
364.50
365.00
365.50
365.69
Unstudied Interval

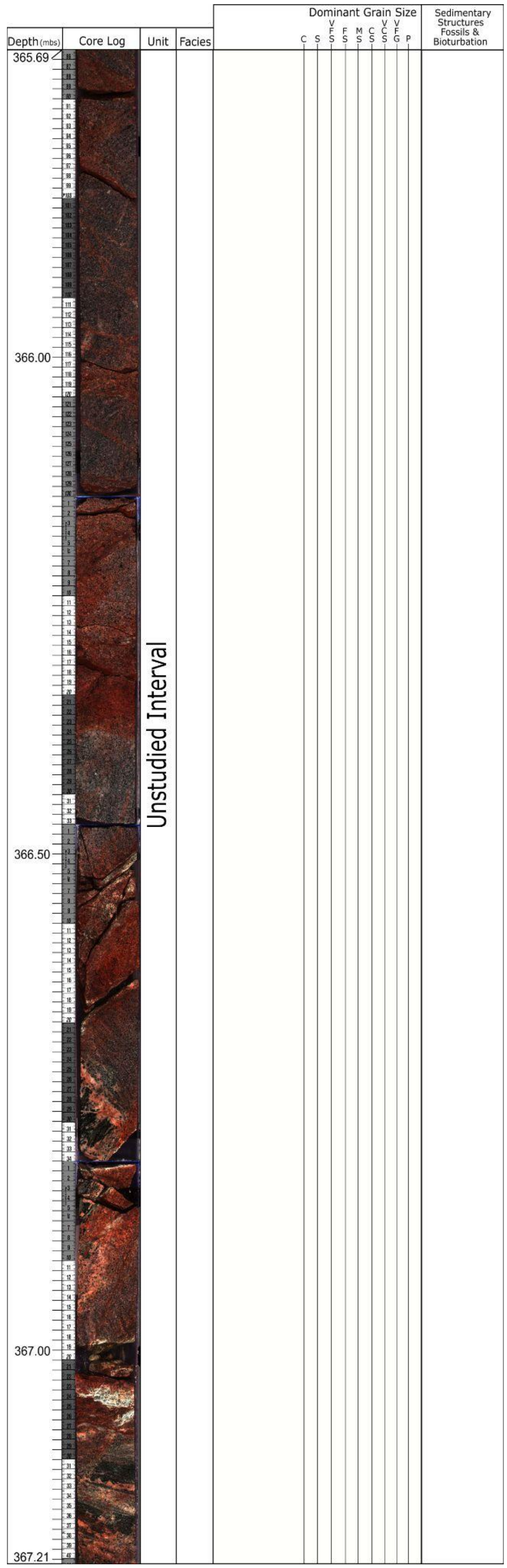
Depth (mbs)
Core Log
Unit
Facies
Dominant Grain Size
C S VFS FS MS CS VCS VFG P
Sedimentary Structures Fossils & Bioturbation
365.69
366.00
366.50
367.00
367.21
Unstudied Interval

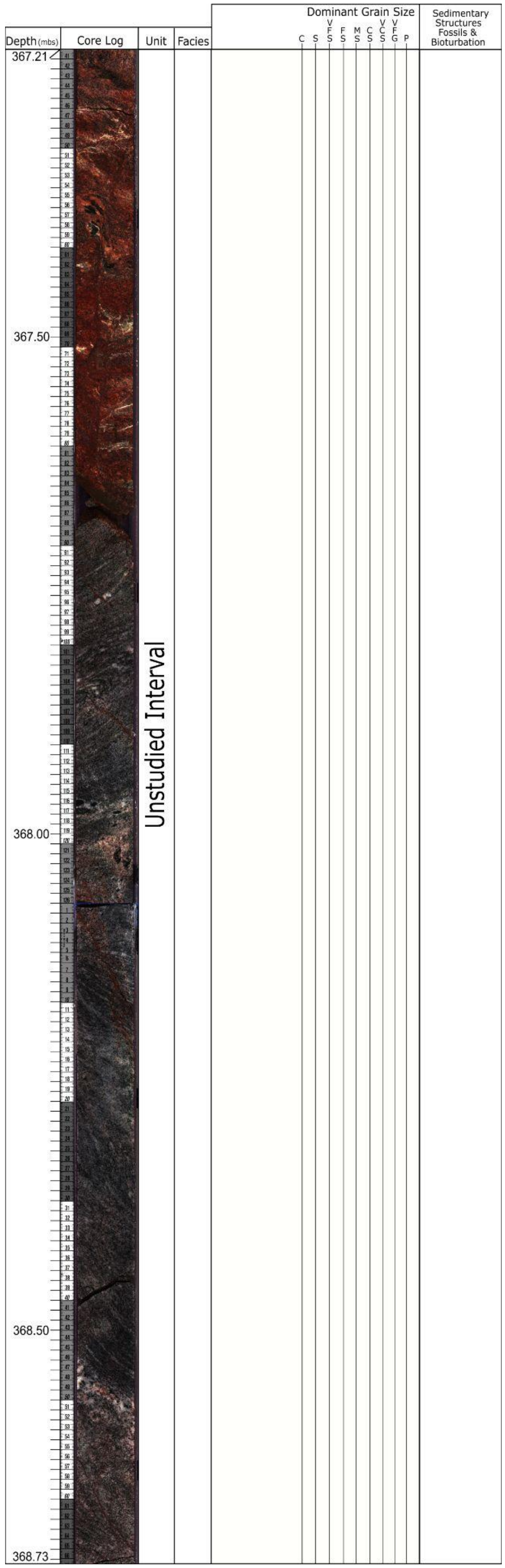
Depth (mbs)
Core Log
Unit
Facies
Dominant Grain Size
C S VFS FS MS CS VCS VFG P
Sedimentary Structures Fossils & Bioturbation
367.21
367.50
368.00
368.50
368.73
Unstudied Interval

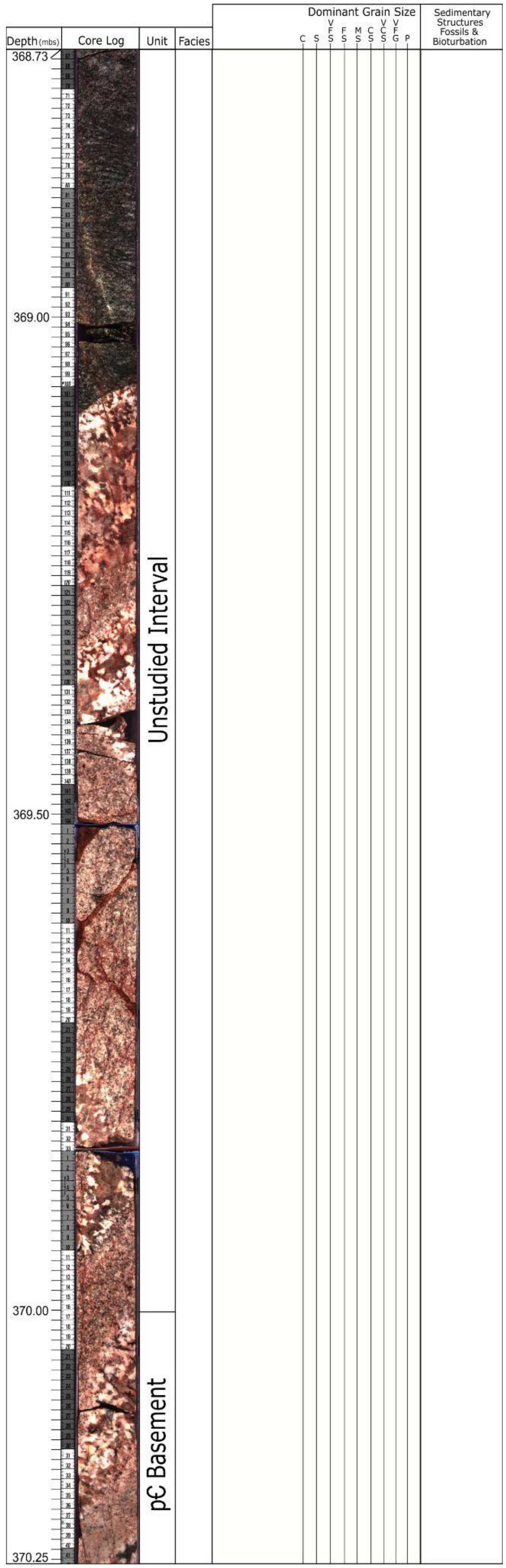
Depth (mbs)
Core Log
Unit
Facies
Dominant Grain Size
C S VFS FS MS CS VCS VFG P
Sedimentary Structures Fossils & Bioturbation
368.73
369.00
369.50
370.00
370.25
Unstudied Interval
p€ Basement

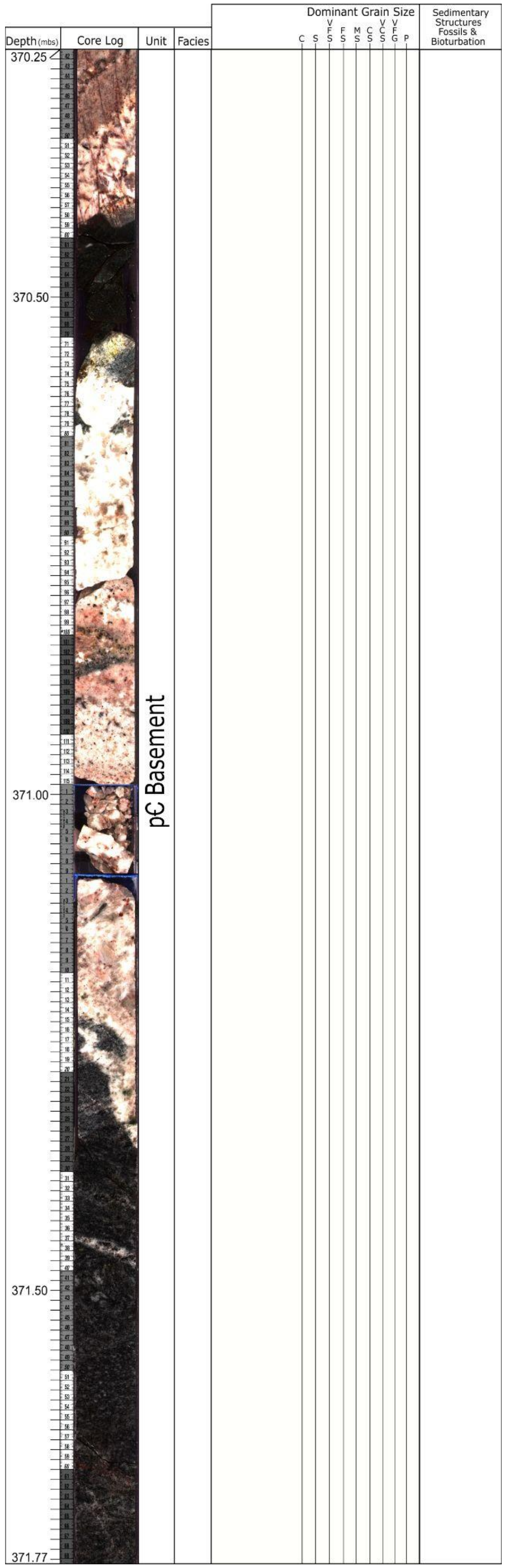

Depth (mbs)
Core Log
Unit
Facies
Dominant Grain Size
C
S
VFS
FS
MS
CS
VCS
VFG
P
Sedimentary Structures Fossils & Bioturbation
370.25
370.50
371.00
371.50
371.77
p€ Basement

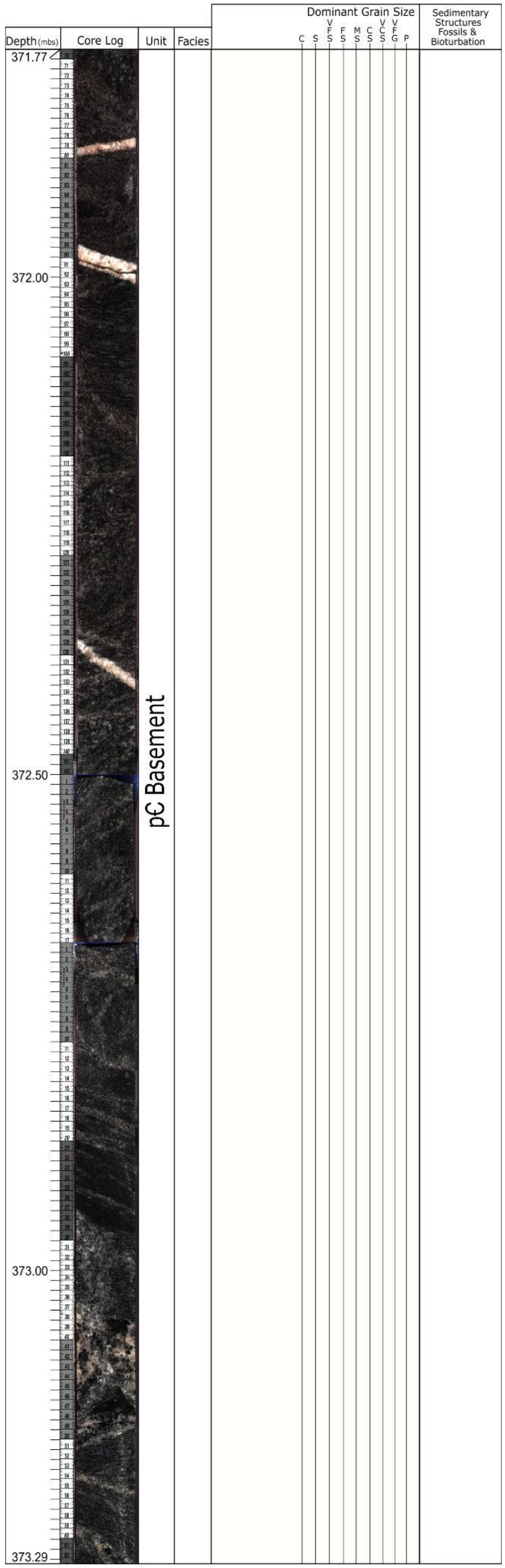
Depth (mbs)
Core Log
Unit
Facies
Dominant Grain Size
C S VFS FS MS CS VCS VFG P
Sedimentary Structures Fossils & Bioturbation
371.77
372.00
372.50
373.00
373.29
pЄ Basement

Depth (mbs)	Core Log	Unit	Facies	Dominant Grain Size: C S VFS FS MS CS VCS VFG P	Sedimentary Structures Fossils & Bioturbation
373.29 – 374.81		pЄ Basement			

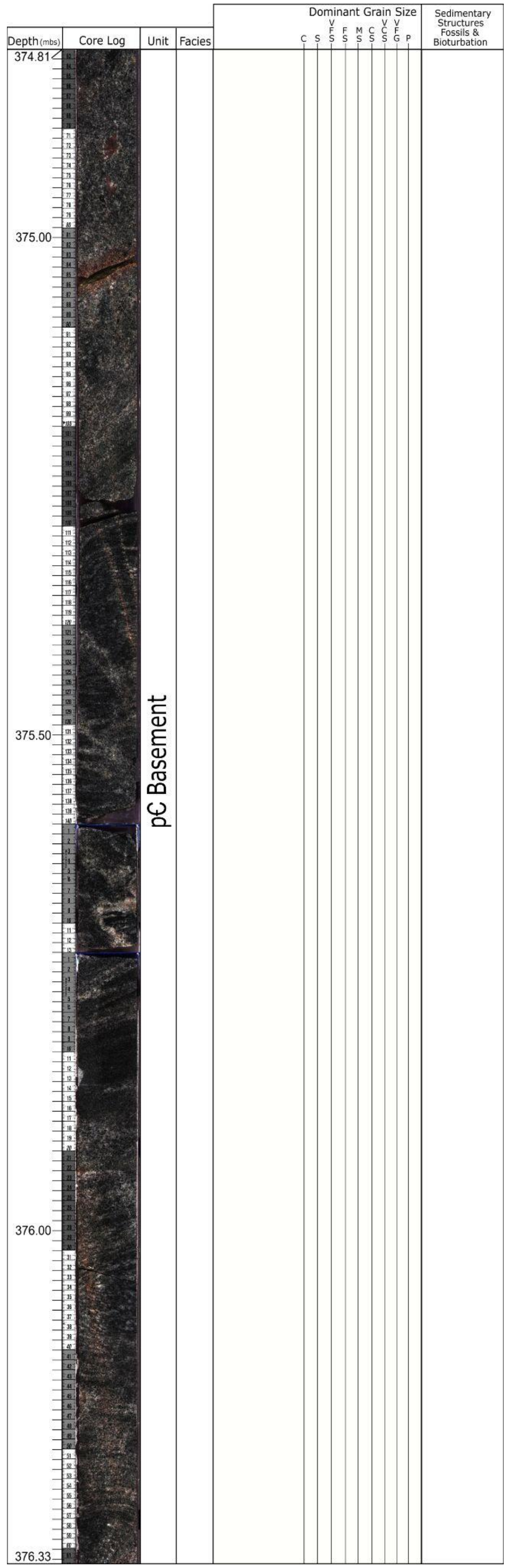
Depth (mbs)
Core Log
Unit
Facies
Dominant Grain Size
C S VFS FS MS CS VCS VFG P
Sedimentary Structures Fossils & Bioturbation
374.81
375.00
375.50
376.00
376.33
pЄ Basement

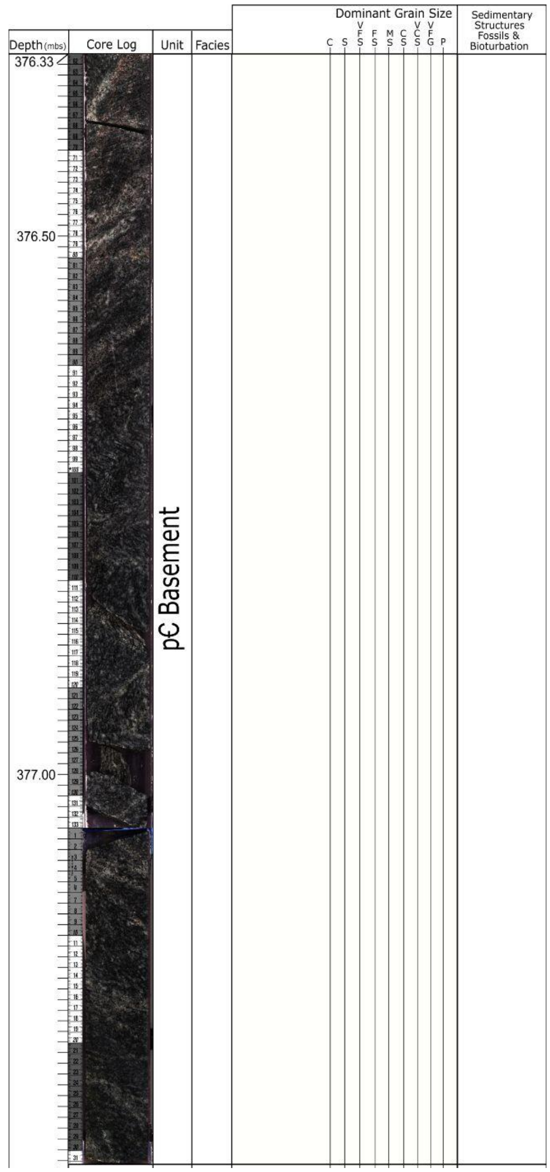
Depth (mbs)
Core Log
Unit
Facies
Dominant Grain Size
C S VFS FS MS CS VCS VFG P
Sedimentary Structures Fossils & Bioturbation
376.33
376.50
377.00
p€ Basement